The Influence of Constant Region Polymorphisms on Antibody Stability and Structural Dynamics

A thesis

submitted in fulfilment

of the requirements for the degree

of

Doctor of Philosophy in Molecular and Cellular Biology

at

The University of Waikato

by

Annmaree Keely Warrender

THE UNIVERSITY OF
WAIKATO
Te Whare Wānanga o Waikato

2023

Abstract

Antibodies are highly effective mediators of the adaptive immune response. Their unique structural architecture makes them ideally suited for the specific targeting of disease-causing agents and the subsequent activation of potent effector functions upon binding to immune cells. These properties have led to the extensive use of antibodies in the biomedical industry as diagnostics and therapeutics. Notably, the IgG class of human antibodies (defined by the sequence of the constant region) has dominated the pool of antibody-based therapeutics, largely due to exceptional stability and efficient immune activation. The constant region genes of human IgG harbour a surprising amount of genetic variation in the form of allelic sequences encoding nonsynonymous mutations. Many allelic sequences have only been uncovered within the last five years, yet a handful of studies have already identified links between specific amino acid polymorphisms and improved receptor binding affinities that lead to enhanced activation of effector functions. This thesis furthers our understanding of the evolutionary pressures driving this genetic diversification by investigating the influence of IgG constant region diversity on antibody structural dynamics, including stability and flexibility.

To analyse the structural effects in detail, I expressed a large panel of 35 trastuzumab-formatted antibodies with unique constant region allele sequences from subclasses IgG1, IgG2, and IgG3. Purified antibodies were confirmed to be of high purity and the composition of appended glycans was characterised for each variant. In this thesis, I compare the thermal stability properties of the unique IgG antibodies, measured by red edge excitation shift (REES) spectroscopy. Striking stability differences were resolved both between and within IgG subclasses, leading to new insights about the effect of specific amino acid positions on antibody stabilisation.

Following the stability analysis, I extensively evaluate the limitations of REES to measure antibody stability, with a particular emphasis on tryptophan content. Using the naturally occurring mutation of arginine to tryptophan present in three of the IgG3 alleles, I generated experimental data that demonstrates the relationship between the solvation state of local tryptophan environments and the REES effect. This analysis highlights the need for matched tryptophan content for robust comparison of antibody stability using a thermodynamic model of REES behaviour.

Finally, the effects of IgG3 hinge length polymorphisms on conformational flexibility are analysed. Here, I used small angle X-ray scattering to characterise the solution structures

of allelic variants encoding three distinct hinge lengths. This work provides the first report of X-ray scattering data for naturally occurring IgG3 antibodies with hinge lengths of 32 and 47 amino acids. Comparison of the scattering behaviour and predicted *ab initio* model structures reveal more compact conformations with reduced space between the Fab domains and the Fc domain when the hinge is truncated, thereby resulting in reduced overall flexibility of the full-length structure. This study highlights dynamic differences between the IgG3 variants tested, which are likely to translate into differences in biological functions.

Taken together, this data provides an important basis for future investigations into the functional roles of IgG allelic diversity. Moreover, the experimental schemes optimised throughout this thesis will enable the high-throughput screening of antibody constant region variants in the future, particularly as more genetic diversity comes to light.

Acknowledgements

First and foremost, I would like to acknowledge my Chief Supervisor Dr William Kelton. Thank you for your ongoing support throughout this PhD journey and for the numerous opportunities you have provided. Your passion for innovative science has driven this research and continues to inspire me for my own research going forward. A big thank you must also go to Prof Vic Arcus for his guidance as a secondary supervisor, along with Associate Prof Brett Langely.

Thank you to my colleagues and mentors in the C2 labs who have been amazing to work alongside for the past several years. A special thank you to Dr Judith Burrows (C2 lab mum). Your amazing efforts to keep the lab running smoothly whilst also taking care of everyone does not go unnoticed and makes the hard work that much easier. Thank you for always offering support through the tough times and for celebrating the successes, no matter how small. Thank you to Dr Joanna Hicks for continuing to be a point of call when needed, your mentorship is sincerely appreciated. To my fellow PhD candidates, Emma, Stacy, Kyrin, Liz, Jack, Carlin, and Keely, it has been amazing sharing this journey with you, and I will always be grateful for the morning tea and coffee breaks that have kept me sane. An extra thanks must go to Kyrin for continually helping me out with my many questions about technology and figure making, and to Emma and Keely for proofreading my thesis chapters.

To Prof Sai Reddy and Dr Eddie Irvine at the Department of Biosystems Science and Engineering at ETH Zürich (Basel, Switzerland), thank you for welcoming me into your lab and for allowing me to learn from you and the lab group. You were a pleasure to work with. I am also grateful to the Maurice Wilkins Centre who provide financial support for this visit.

Finally, I would like to acknowledge my parents, sister, grandparents, parents-in-law and sisters-in-law for your unwavering support throughout the highs and lows of my PhD journey and for always showing an interest in my work – even if you might not understand it all. Last but not least, thank you to my dearest partner, Gavin, who has been nothing but supportive through all the long hours and (many) stressful times. I couldn't have accomplished this huge achievement without you by my side.

Table of Contents

List of Figures

List of Tables

List of Abbreviations

ADCC	antibody-dependent cell-mediated cytotoxicity
ADCP	antibody-dependent cell-mediated phagocytosis
BLI	biolayer interferometry
CH1/2/3	heavy chain constant domain 1/2/3
CSM	centre of spectral mass
DSF	differential scanning fluorimetry
ELISA	enzyme-linked immunosorbent assay
FACS	fluorescence-activated cell sorting
FcR	Fc receptor
FcRn	neonatal Fc receptor
FcγR	Fc gamma receptor
GST	glutathione-S-transferase
HCV	hepatitis c virus
HEK293F	human embryonic kidney cell line 293F
HRP	horseradish peroxidase
Ig	immunoglobulin
IGHC	immunoglobulin heavy-chain constant
IGLC	immunoglobulin light-chain constant
IMGT	International Immunogenetics Information System®
ITAM	immunoreceptor tyrosine-based activation motif
ITIM	immunoreceptor tyrosine-based inhibitory motif
LC-MS	liquid chromatography mass spectrometry
mAb	monoclonal antibody
NK cells	natural killer cells
NSD	normalised spatial discrepancy
PCR	polymerase chain reaction
pmIG	population matched IG
PNGase F	Peptide -*N*-Glycosidase F
REES	red edge excitation shift
RMSD	root mean square deviation
RSV	respiratory syncytial virus
SASA	solvent accessible surface area
SAXS	small angle x-ray scattering
SNP	single nucleotide polymorphism
SPR	surface plasmon resonance
T_m	thermal melt transition temperature
TRIM21	tripartite motif 21
x *g*	times the force of gravity

Chapter One

Introduction

The human immune system plays a crucial role in safeguarding the body against harmful pathogens and diseases. Effective defence against potential threats is facilitated by two immune subsystems: the innate immune system and the adaptive immune system. The innate immune system provides rapid but non-specific protection as a first line of defence. The adaptive immune system generates a more targeted immune response and can provide long-lasting protection by storing a memory of the specific pathogen for effective response upon re-exposure. Within the adaptive immune system, antibodies are critical mediators of protective responses. They function by specifically binding to target antigens, via the variable domains, and subsequently directing precise immune effector functions, via the constant domains (Vidarsson et al., 2014). Fine control over the nature of the immune response is provided by the diversification of the constant region into five classes: IgM, IgD, IgG, IgA, and IgE. Each class engages unique patterns of antibody receptors on immune cell subsets to elicit distinct effector functions. IgG is the most common class of antibody in human serum and has been widely exploited as a highly effective therapeutic agent in modern medicine (e.g., for cancer therapy) (Lu et al., 2020). Yet, despite the ubiquitous use of antibodies in medicine and the Life Sciences, there is a wide array of genetic diversity present in the IgG constant region sequence of antibodies, which has only come to light in recent years due to large-scale genomic sequencing of diverse human populations. Evidence throughout the literature (discussed in *Chapter Two: Literature Review*) strongly suggests a link between constant region amino acid variation and IgG immune function. Nevertheless, the precise evolutionary drivers behind constant region diversification are still not fully understood, leaving significant gaps in our knowledge regarding the impact of this diversity on basic antibody properties, such as stability. Exploring this area in greater depth will contribute to understanding the driving forces behind immune variations among different human populations and may provide valuable insights for the advancement of antibody-based therapeutics.

This thesis aims to understand the influence of constant region polymorphic diversity on fundamental antibody properties underlying effective immune performance. With a focus on structural dynamics, this work encompasses a comparative analysis of the thermal stability of unique IgG variants, an in-depth evaluation of the fluorescent technique employed to resolve stability differences, and the characterisation of the flexibility of full-

length antibody structures. As part of this work, I generated a panel of 35 trastuzumab (Herceptin®) monoclonal IgG antibody variants spanning the IgG1, IgG2, and IgG3 subclasses. This antibody panel forms the basis of the research discussed in this thesis and has been made available to collaborators beyond the scope of work presented here.

This thesis comprises an in-depth literature review followed by three chapters addressing each of the research objectives and concludes with a discussion of future perspectives. The literature review chapter is adapted from a peer-reviewed Review Article published in *Frontiers in Immunology*:

Warrender, A. K., & Kelton, W. (2020). Beyond Allotypes: The Influence of Allelic Diversity in Antibody Constant Domains. *Frontiers in Immunology*, *11*(2016). https://doi.org/10.3389/fimmu.2020.02016

The subsequent research-focused chapters are presented as a combination of published manuscripts, submitted manuscripts, or manuscripts ready for submission, as outlined in *Section 1.1: Research Objectives*.

1.1 Research Objectives

To determine the effects of antibody genetic diversity on the fundamental biophysical properties of antibodies, the following objectives were explored in this doctoral thesis research:

Objective one:

Determine how naturally occurring constant region polymorphisms influence antibody stability by characterising the structural dynamics of 32 unique IgG antibodies using red edge excitation shift spectroscopy.

This research resulted in the following publication and is presented in Chapter Three as the final peer-reviewed manuscript:

Warrender, A. K., Pan, J., Pudney, C. R., Arcus, V. L., & Kelton, W. (2023). Constant Domain Polymorphisms Influence Monoclonal Antibody Stability and Dynamics. *Protein Science*, *32*(3), e4589. https://doi.org/10.1002/pro.4589

Objective two:

Explore the viability of red edge excitation shift spectroscopy for assessing the stability of antibody variants with tryptophan polymorphisms and evaluate the mechanisms by

which the local environments of tryptophan fluorophores translate to overall antibody stability.

This research led to the manuscript presented in Chapter Four. The completed manuscript has been submitted for publication.

Warrender, A. K., Pan, J., Pudney, C. R., Arcus, V. L., & Kelton, W. Red Edge Excitation Shift Spectroscopy is Highly Sensitive to Tryptophan Composition. *(Submitted)*

Objective three:

Evaluate the effect of naturally occurring diversity in the hinge length of IgG3 antibodies on structural conformations and flexibility using small angle X-ray scattering.

The research on this objective is presented as a complete manuscript that is ready for submission.

Warrender, A. K., Pan, J., Sethi, A., & Kelton, W. Antibody Hinge Length Governs Conformational Flexibility of IgG3 Allelic Variants. (*In Preparation*).

1.2 Acknowledgement of Funds

This research was funded by the Royal Society Te Apārangi (Marsden Fast Start grant; 19-FRI-002) and the New Zealand Synchrotron Group Limited (Capability Build Fund grant). Financial support for the duration of my PhD was provided by the University of Waikato Doctoral Scholarship and the Waikato Graduate Women Educational Trust Merit Award for Doctoral Study. An extended visit to work with international collaborators was funded by the Maurice Wilkins Centre (Flexible Research Funding - Category 4).

1.3 References

Lu, R.-M., Hwang, Y.-C., Liu, I.-J., Lee, C.-C., Tsai, H.-Z., Li, H.-J., & Wu, H.-C. (2020). Development of therapeutic antibodies for the treatment of diseases. *J Biomed Sci*, *27*(1), 1. https://doi.org/10.1186/s12929-019-0592-z

Vidarsson, G., Dekkers, G., & Rispens, T. (2014). IgG subclasses and allotypes: From structure to effector functions. *Front Immunol*, *5*, 520. https://doi.org/10.3389/fimmu.2014.00520

Chapter Two

Literature Review

2.1 Preface

An in-depth survey of the literature on the influence of constant region genetic diversity on human antibody function was published as a peer-reviewed Review Article in *Frontiers in Immunology*. The literature review highlights the critical functions orchestrated by antibody constant regions and explores previously established connections between genetic variation in these regions and immune function, shedding light on the implications for infection and disease. By examining these associations, it aims to enhance our understanding of how antibody constant domains contribute to immune responses and their relevance in various pathological conditions. The future perspectives section discusses current advances in technology that will be instrumental in uncovering more diversity and outlines the remaining knowledge gaps surrounding the effects of antibody constant region diversity.

The format of the published article has been modified for this thesis to allow for the inclusion of additional text to provide the most up-to-date review of the literature. All text added after the initial publication is presented in blue to differentiate it from the already published text.

Warrender, A. K., & Kelton, W. (2020). Beyond Allotypes: The Influence of Allelic Diversity in Antibody Constant Domains. *Frontiers in Immunology, 11*(2016). https://doi.org/10.3389/fimmu.2020.02016

2.1.1 Author contributions

The compilation of literature and writing of this manuscript was shared equally between myself and my Chief Supervisor, William Kelton.

Beyond Allotypes: The Influence of Allelic Diversity in Antibody Constant Domains.

Annmaree K. Warrender[a] and William Kelton[a]

[a]*Te Huataki Waiora School of Health, University of Waikato, Hamilton, New Zealand*

2.2 Abstract

Polymorphic diversity in antibody constant domains has long been defined by allotypic motifs that cross react with the sera of other individuals. Improvements in sequencing technologies have led to the discovery of a large number of new allelic sequences that underlie this diversity. Many of the point mutations lie outside traditional allotypic motifs suggesting they do not elicit immunogenic responses. As antibodies play an important role in immune defence and biotechnology, understanding how this newly resolved diversity influences the function of antibodies is important. This review investigates the current known diversity of antibody alleles at a protein level for each antibody isotype as well as the kappa and lambda light chains. We focus on evidence emerging for how these mutations perturb antibody interactions with antigens and Fc receptors that are critical for function, as well as the influence this might have on the use of antibodies as therapeutics and reagents.

2.3 Introduction

Antibodies play an essential role as frontline molecules of adaptive immunity in the fight against infection and disease. While pathogenic targets can be directly neutralised via binding of antibody variable domains, binding of the constant domain to specialised Fc receptors on the surface of immune cells dictates powerful inflammatory or anti-inflammatory responses (Bruhns et al., 2009). Together the remarkable affinity, exquisite specificity, and immune modulation potency of these interactions have seen antibodies adopted as indispensable reagents in medicine and as diagnostics.

The profile of Fc receptor engagement is, in part, governed by the heavy chain isotype of the antibody encountered. Immunoglobulin (Ig) isotypes are divided into classes and subclasses depending on the heavy chain they possess; IgM (μ), IgD (δ), IgG (γ) which encompasses subclasses IgG1, IgG2, IgG3, IgG4, IgA (α) which encompasses subclasses IgA1 and IgA2, and IgE (ε) (Vidarsson et al., 2014). Each isotype is paired with either a kappa (κ) or lambda (λ) light chain to create a tetrameric immunoglobulin complex capable of triggering unique effector functions. Adding a further level of complexity, and in spite of the 'constant' naming convention, genes of the immunoglobulin heavy-chain constant (IGHC) and light-chain constant (IGLC) loci are polymorphic, although to a far lesser extent than the immunoglobulin heavy-chain variable locus (Lefranc et al., 2014). IGHC/IGLC polymorphic diversity has historically been defined by amino-acid mutations in the polypeptide chain that are immunogenic. Termed allotypes, these mutations were first identified by *ex vivo* serological studies in which antibodies from donor sera were observed to trigger agglutination of erythrocytes treated with host serum (Grubb, 1956; Lefranc & Lefranc, 2012). Allotypes have been identified for IgG1, IgG2, IgG3, IgG4, IgA2 and IgE as well as the kappa light chain (Jefferis, 1998; Kunkel et al., 1969; van Loghem et al., 1984). Before the ready availability of genetic sequencing techniques, allotyping provided an excellent method to track genetic linkage between human populations and ethnic groups thus allowing deeper understanding of human migration patterns (Dugoujon et al., 2004), population genetics (Johnson et al., 1977), and providing tools in forensic medicine (Jefferis & Lefranc, 2009).

More recently, allotypes have been investigated for their potential role as immunogenic motifs in therapeutic antibodies. Surprisingly, it appears that allotypes act only as minor epitopes in monoclonal antibodies and do not appear to elicit acute rejection (Webster et al., 2016), although some studies have reported low levels of pre-existing circulating antibodies against allotypes of therapeutic monoclonals (Goldberg et al., 2020;

Tatarewicz et al., 2012). A key pitfall of serological detection of allotypes is the difficulty of evaluating immunogenic responses to immunoglobulin isotypes expressed at low levels in serum, such as IgE and IgM, signified by a lack of known allotypes for these classes (van Loghem et al., 1984). Furthermore, serological reagents used for allotype detection are of limited availability, and sourcing of anti-sera for rare motifs is difficult, meaning some motifs may be missed (Dard et al., 2001; Johnson et al., 1977).

While allotypes have long been the defining feature of Ig isotype diversity we argue that the richer diversity found at the allelic level is likely to have profound consequences for our use and understanding of antibodies. These mutations have largely been ignored due to a lack of immunogenic phenotype; however, they likely play a crucial role in host immunity or in the mechanism of monoclonal antibody drugs (Figure 2-1). This review summarises the current known natural diversity of human immunoglobulin constant regions, the implications for antibody function beyond what is known for historically defined antibody allotypes, and gaps in our current knowledge of IGHC/IGLC allele function.

2.4 The challenges of IGHC/IGLC allelic discovery

The extent of IGHC/IGLC allelic diversity has been overlooked for many years due to the technical inaccessibility of the highly homologous IGH genomic locus. Approaches requiring the assembly of short DNA sequencing reads and genome-wide association studies (GWAS) have struggled to resolve individual genes in this locus (Pandey, 2012; Robinson, 2015). These challenges have been compounded by the common practice of sampling circulating B cells that have undergone multiple instances of unique rearrangements, including class switch recombination, resulting in an IGH locus of inconsistent length and composition (Robinson, 2015). It is particularly notable that GWAS gene probes for detection of single nucleotide polymorphisms (SNPs) in this region are largely absent from modern arrays (Pandey, 2012) and any identified SNPs have been difficult to assign to the correct immunoglobulin domain (Pandey & Li, 2013). The result has been a slow and very manual accumulation of known IGHC/IGLC allelic sequence data over more than 30 years.

Recently, specifically targeted PCR approaches and the curation of high-quality sequencing data, such as the 1000 genomes project, have enhanced our ability to detect

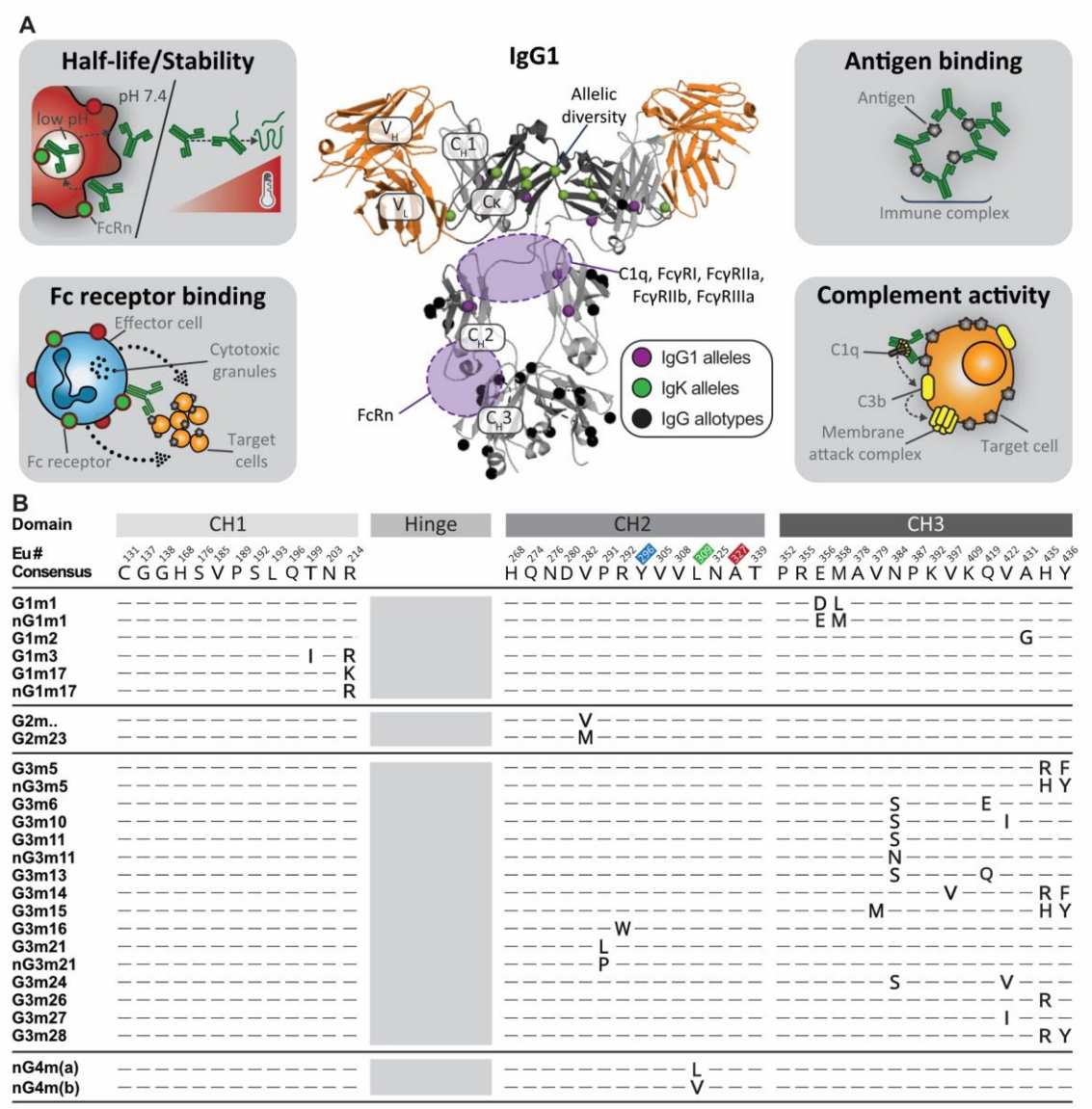

Figure 2-1. (A) The influence of antibody constant domain diversity on function. Amino acid differences in antibody alleles perturb interaction with Fc receptors, antigens, and complement proteins, as well as influencing intrinsic antibody stability. Shown in the centre is a crystal structure of full-length IgG1 (PDB: 1hzh (Saphire et al., 2001)) with mapped allotype locations (black), additional IgG1 point mutations coded by alleles (purple), and IgK point mutations coded by alleles (green). The light chain comprises the VL and Cκ domains whereas the heavy chain is made of the VH, CH1, CH2, and CH3 domains. Orange indicates the domains responsible for antigen binding. Key Fc receptor binding regions of the structure are shaded in purple. **(B) IgG allotype motifs.** Allotypes are motifs identified by serological cross reactivity between donors. These motifs are mapped to the same alignment shown in Figure 2-2 for all IGHG alleles. Residues known to directly interact with Fc receptors are highlighted in blue (FcγRI) (Lu et al., 2015), red (FcγRIIa & FcγRIII) (Ramsland et al., 2011; Sondermann et al., 2000), and green (FcRn) (Oganesyan et al., 2014).

variation in this region at the genomic level (Calonga-Solís et al., 2019; Khatri et al., 2021). In the past two years alone, more than 250 new IGHC/IGLC allelic variants have been discovered. Because a large proportion of the newly discovered diversity is protein coding and does not map to known allotypes (Figure 2-1B, Figure 2-2) the consequences for antibody function are unknown. There is agreement with allotype population data in that IGHC allelic prevalence is heavily biased toward different ethnicities as evidenced by the differential distribution of alleles between five superpopulations; Africans, Americans, East Asians, Europeans and South Asians (Khatri et al., 2021). Within each allele, variation is largely confined to certain nucleotide positions suggesting the functional consequences of these alleles may be driving evolutionary selection over time. It is likely some of this variation was introduced via admixture from archaic hominins (Browning et al., 2018). Nonetheless, it remains evident that the true breadth of constant domain allelic diversity can only be uncovered once many more populations are investigated.

2.5 Mechanisms by which constant domain diversity influences function

2.5.1 Antibody stability

Diversity in the constant domain is inherently linked to antibody function both *in vivo* and *ex vivo*. At a fundamental level, changes to the amino acid sequence can greatly influence both antibody assembly and stability. For example, the IgG4 subclass is well known to carry out Fab-arm exchange to create naturally bispecific antibodies which are thought to contribute to anti-inflammatory properties typical of IgG4 antibodies (Labrijn et al., 2011; Lewis et al., 2009). While most IgG4 alleles have arginine at position 409, IGHG4*03 has the non-allotypic polymorphism, K409 (Figure 2-2). This mutation inhibits Fab-arm exchange by stabilising CH3-CH3 interactions of the antibody (Labrijn et al., 2011; Rispens et al., 2014). Occurrence of this natural variant suggests there are benefits to remaining monospecific, however these have yet to be explored in detail.

Other IgG subclasses (IgG1, IgG2, IgG3) also have allelic variants that influence CH3-CH3 interaction stability, despite not carrying out Fab-arm exchange. These include variations at positions 392 and 397 which are situated at the edges of the CH3 dimerization interface (Rispens et al., 2014). Asparagine at position 392 significantly weakens CH3-CH3 interaction compared to K392 and the resulting IGHG3*03 allele dissociates significantly faster than IgG4 molecules. It is proposed these point mutations

influence antibody aggregation dynamics that may be important for the stability of mixed antibody populations in therapeutic formulations (Rispens et al., 2010). Mutations found in the CH3 domains of other subclasses and isotypes may also impact antibody stability but have yet to be investigated.

2.5.2 Fc receptor binding

A delicate balance of immune modulation is mediated by antibody interaction with Fc receptors. Disrupting or enhancing binding affinity for key activatory receptors (FcγRs (FcγRIII, FcγRIIa, FcγRI, TRIM21), FcαRs (FcαRI, Fcα/μR), FcεRs (FcεRI, FcεRII) and FcμRs (FcμR, Fcα/μR)) and inhibitory Fc receptors (FcγR (FcγRIIb)) can have significant consequence. These interactions are responsible for driving potent antibody-dependent cell-mediated actions, including cytotoxicity (ADCC), phagocytosis, trogocytosis, degranulation responses, antiviral responses, and cytokine release, all of which have been extensively reviewed elsewhere (Mkaddem et al., 2019; Nimmerjahn & Ravetch, 2008; Takai, 2002). As a general rule, the strength/pattern of binding to each receptor is correlated to the intensity of the immune response, with high affinity interactions directing stronger responses. Extensive mutational studies from antibody engineering have provided valuable insight into how Fc domain point mutations can alter antibody function (Lazar et al., 2006; Moore et al., 2010; Nordstrom et al., 2011; Stavenhagen et al., 2007). Not only can single heavy chain point mutations massively alter Fc receptor selectivity ratios (Richards et al., 2008), but these mutations do not need to be proximal to receptor binding sites (Jung et al., 2013).

Investigations into allotypes have long implicated a potential for perturbed interactions with Fc receptors. In particular, FcγRIII mediated NK cell cytotoxicity by clinical antibodies is diminished or enhanced by certain allotypes (Moraru et al., 2015; Pandey & Namboodiri, 2014). Very recently, a systematic study of Fc receptor binding to 27 unique IgG alleles found variation in the IgG3 class of antibodies contributed to altered Fc receptor binding (de Taeye et al., 2020). These effects were linked independently to both variation in the hinge length and to the presence of unique point mutations at positions 291, 292, and 296 in the CH2 domain. Differences in observed Fc receptor binding led to altered ADCC capacity thus highlighting the functional consequence of this diversity. Natural heavy chain variation is also proving to be beneficial for passive immunization strategies. A potent anti-HIV antibody response was linked to the expression of two

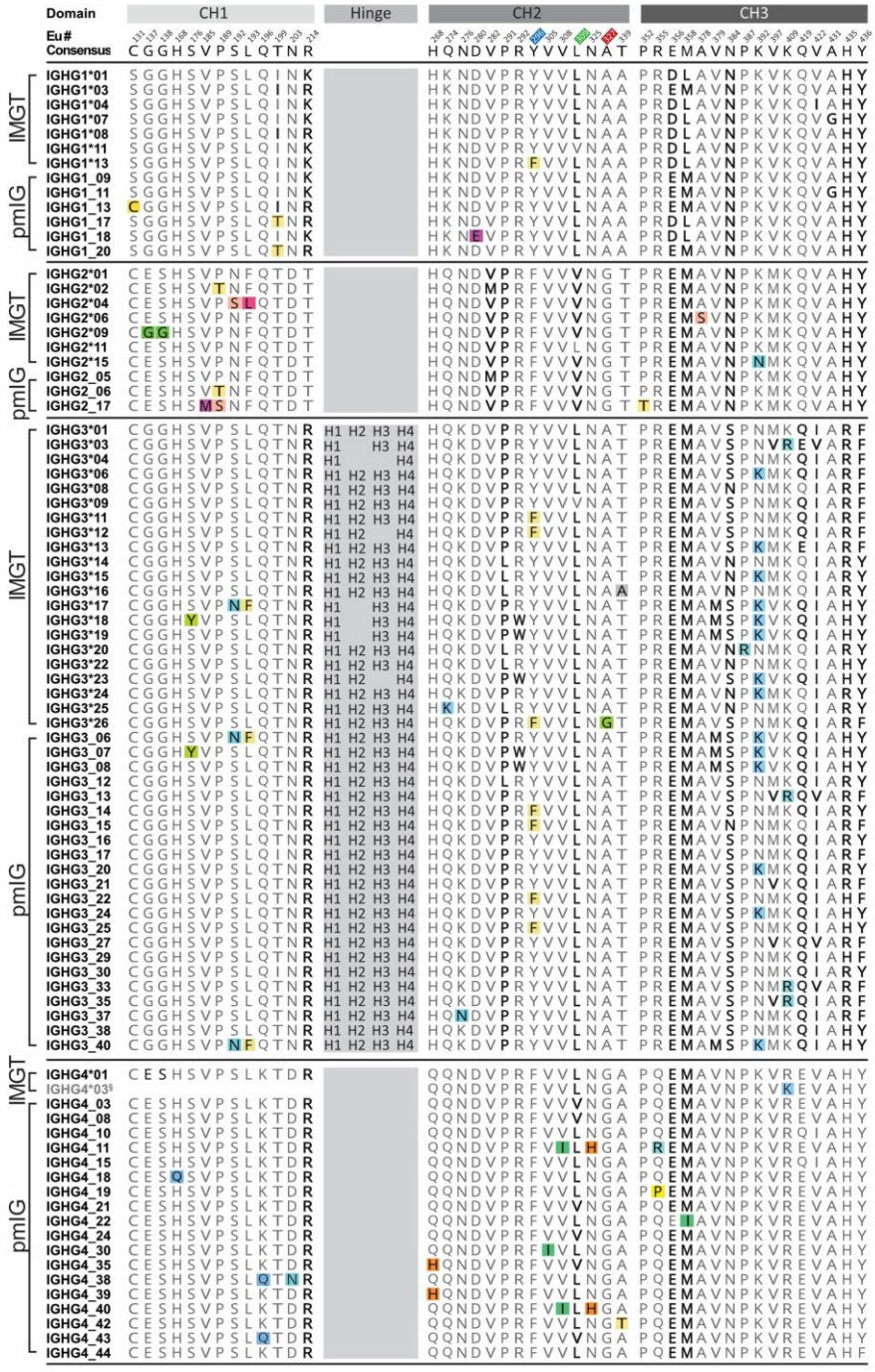

Figure 2-2. Unique amino acid mutations within IGHG constant alleles of all subclasses. IgG heavy chain alleles (IGHG) for all subclasses (IgG1, IgG2, IgG3, IgG4) were obtained from IMGT and pmIG databases, aligned, and corresponding allotype or isoallotype motifs mapped as indicated in bold (Khatri et al., 2021; Lefranc et al., 2014; Lefranc & Lefranc, 2012). Isoallotypes have only been reported in certain subclasses despite the often ubiquitous presence of these motifs. Residues are numbered according to the Eu numbering convention. Coloured boxes represent unique amino acid differences between alleles that are not associated with known allotypes and for which the functional impact is largely unknown. Residues known to directly interact with Fc receptors are highlighted in blue (FcγRI) (Lu et al., 2015), red (FcγRIIa & FcγRIII) (Ramsland et al., 2011; Sondermann et al., 2000), and green (FcRn) (Oganesyan et al., 2014). H1, H2, H3, H4 indicate amino acid sequences for each of the hinge exons in IGHG3 alleles. §Partial alleles where complete allele sequence information is missing.

IGHG3 alleles; IGHG3*01m (GenBank:MK679684) and IGHG3*17 (Richardson et al., 2019). Both alleles carry polymorphisms (E419 and K392, respectively) that do not define allotypes but are implicated in improved binding to FcγRIII and FcγRIIb receptors and enhanced ADCC responses.

2.5.3 FcRn binding

Neonatal receptor binding (FcRn) is important for enhancing the circulating half-life of antibodies in serum, the transfer of passive immunity to neonates, and in the uptake of exogenous antibody bound antigens (Dechavanne et al., 2017; Roopenian & Akilesh, 2007; Stapleton et al., 2011). Antibodies are recycled in a pH dependent manner with binding occurring at ~pH 6.5 within pinocytosed endosomes and released when returned to pH 7.4 at the cell surface. Altering the binding affinity of the CH2/CH3 domain interface at either of these pHs can have immense consequence and has been well established for allotypic variants of clinical antibodies (Ternant et al., 2016). In certain IgG3 alleles, a single amino acid change, R435, reduces binding to FcRn at low pH despite enhancing binding at neutral pH (Natsume et al., 2008; Shah et al., 2017). This results in out-competition by circulating IgG1 antibodies for FcRn binding sites and a greatly shortened half-life relative to other IgG subclasses.

2.5.4 Classical C1q-mediated complement

Binding of C1q to IgG or IgM is the first step in the classical complement-dependent cytotoxicity (CDC) cascade that culminates with the formation of a membrane attack complex that lyse target cells (Idusogie et al., 2000). As with FcγR binding, C1q interacts with amino acids in the CH2 domain so variants at or near this interface can influence binding and thus CDC immune response. Although allotypic effects have been reported to affect C1q binding in other species (Bastida-Corcuera et al., 1999), little effect has been reported in humans (Redpath et al., 1998). Instead, alterations to the length of the hinge region in IgG3, particularly truncations, have been shown to enhance C1q activity (Giuntini et al., 2016). A wide range of allelic hinge diversity is found in IgG3, but it is currently unknown how this might influence C1q binding.

2.5.5 Antigen binding

Selective antigen recognition underpins both the evolutionary and clinical success of antibodies. A longstanding dogma of immunology postulates antigen binding is determined by the variable domains of the heavy and light chains while effector function and isotype are determined by the constant domains alone (Torres & Casadevall, 2008).

However, there is growing evidence that this theory is oversimplified. Not only do B cell superantigens bind non-canonically to antibody domains (Zouali, 1995), but some antigen binding domains influence effector function and constant domain selection can affect antigen binding (Janda et al., 2016; Pandey & Li, 2013; Torres & Casadevall, 2008). Abundant evidence from isotype switched antibodies possessing identical variable domains indicates point modifications to the CH1 domain can affect the conformation of the antigen binding pocket and subsequent affinity (Pritsch et al., 1996; Torres et al., 2007). Several alleles (IGHG2*02, *04, *09 and IGHG3*17, *18) have amino acid substitutions in the CH1 domain, and diversity in light chain constant domains is well established, although to our knowledge the influence of these mutations on antigen binding have not been investigated. It is less intuitive to note mutation in the CH2/CH3 domains can also propagate allosteric changes to modulate antigen binding (Su et al., 2018). Differences in antigen binding have been found for different alleles with the same variable region, although without high resolution analysis to determine exactly which mutations are contributing to the effect (Cen et al., 2020).

2.6 Implications of constant domain diversity in disease

Immunoglobulin allotypes and haplotypes have long been associated with susceptibility to infections and diseases including breast cancer (Pandey et al., 2012), autoimmunity (Chen et al., 2018; Nakao et al., 1980), malaria (Dechavanne et al., 2017; Giha et al., 2009), herpes (Atherton et al., 2000; Pandey, 2012; Pandey et al., 2019) and hepatitis C (Namboodiri et al., 2008; Pandey et al., 2008). More recently, studies have even linked constant domain diversity to longevity observed in certain populations (Puca et al., 2018). Often allotypic diversity is linked with serum abundance of antibodies targeting the infectious agent. For instance, antibody titers against Hepatitis C virus E1E2 glycoproteins are, in part, determined by G1m1, G1m17, G3m5, and G3m13 motifs (Figure 2-1B) (Pandey et al., 2008) and are prognostic for faster recovery (Pandey et al., 2004). Similarly, breast cancer patients carrying the G2m23 (Pandey et al., 2012) or Km1 kappa allotypes (Pandey et al., 2014) tend to have higher levels of IgG antibodies, which can be associated with better patient outcomes. The focus on allotypic motifs in these studies means the exact allelic context is uncertain and therefore which amino acids may be contributing to the observed phenotypes remains unknown.

In recent years, high quality genomic datasets have provided evidence implicating non-allotypic IGHC diversity in human disease. In line with the observations from allotypic analyses, a key consequence of variation is marked differences in antibody serum

abundance. Jonsson et al., reported variant P189T (SNP:rs11627594) in the CH1 domain of IGHG2*02 decreases global expression of IgG molecules (Jonsson et al., 2017). Importantly, their evidence also extended to isotypes other than IgG for which less diversity has been discovered to date. The study found a novel variant of IGHA1, also reported by Khatri et al, (encoding P85.1S; IMGT numbering, SNP:rs117775520) is associated with high IgA concentration. In Alzheimer's disease, advances in the quality of exome sequencing have led to data reporting an association of three IGHG3 alleles with severity (Bis et al., 2018). One of these variants (Y296F) is non-allotypic and found in alleles IGHG3*11, IGHG3*12, IGHG3*26. The underlying mechanism for this association is yet to be explored. Similarly, SNP associations have been reported in IGHG3*18 (S176Y SNP:rs201430154) to increase the risk of inhibiting components of protein replacement therapies in hemophilia (Gorski et al., 2016). The importance of considering non-allotypic allelic variation is further highlighted by the discovery of a SNP in the cytoplasmic tail of IgG1 which is prevalent in cases of systemic lupus erythematosus (Chen et al., 2018). This variant has major implications for the humoral response upon infection or vaccination, and in autoimmune disorders, by enhancing IgG1 expression. Furthermore, allelic variants of the IgG2 and IgG3 subclasses have been linked to increased susceptibility to severe acute respiratory syndrome coronavirus (SARS-CoV2) and risk of mortality (Ligotti et al., 2023; López-Martínez et al., 2022). In a cohort study of Sicilian patients, the IGHG2*02 allele (allotype G2m23) was more prevalent in individuals infected with SARS-CoV2 compared to healthy individuals (Ligotti et al., 2023). In a similar but separate study, the risk of mortality in SARS-CoV2 patients was associated with IGHG3 alleles that had hinge length polymorphisms (López-Martínez et al., 2022). Individuals carrying IGHG3 alleles with the short hinge sequence had greater risk of mortality compared to those with alleles encoding the long hinge. Beyond these studies, the role of constant domain diversity in disease remains broadly underexplored, especially in light of new allele discoveries, and despite a critical antibody role in adaptive immune defence.

2.7 Potential implications for therapeutics and diagnostics

Analysis of anti-drug antibodies has suggested that unique variable region motifs rather than allotypes have greater immunogenic potential (Bartelds et al., 2010; Webster et al., 2016). Nonetheless genetic variation in antibody constant domains is considered critical to antibody design and most clinical antibodies are either of the G1m17 or G1m3 allotypes (Jefferis & Lefranc, 2009). We also note the emergence of therapeutic antibody

formats entirely lacking constant domains e.g Nanobodies or BiTEs (Bannas et al., 2017). As IGH allelic discovery accelerates, the choice of therapeutic backbones will become even wider and allogenic potential should not be discounted. Additional consideration needs to be given to the influence of allelic selection on immune effector function especially considering the polymorphisms present in several of the Fc receptor genes (FcγRIIa-R131H, FcγRIII-F156V) (Nagelkerke et al., 2019). More studies are required to determine the influence of new allelic diversity on potential effector functions. The influence of diversity in the constant domain also impacts antibody serum persistence, especially when in competition with natural allelic variants that may have vastly different FcRn binding affinities (Stapleton et al., 2011).

Both monoclonal and polyclonal antibodies continue to be essential reagents for rapid diagnostic testing and as probes in research despite contributing to a 'crisis of reproducibility' in the scientific literature (Bradbury & Plückthun, 2015). Constant domain diversity can introduce error in two primary ways. First, purification of these reagents from complex mixtures such as serum or culture media requires the use of chromatographic approaches. The commonly used Fc-binding protein, Protein A, can only bind to and purify certain allelic variants of IgG3 carrying H435 (Saito et al., 2019; Shah et al., 2017). Missing certain antibody subclasses could impact the functional composition of certain antibody preparations. Second, detection blind spots are created as common secondary detection-antibodies have incomplete reactivity to all antibody alleles or may even possess unwanted cross-reactivity to other isotypes (Cen et al., 2020; Howie et al., 2017). A key example is the discovery of an FDA approved anti-Kell monoclonal that fails to detect IgG3*03 and IgG3*13 antibodies, a false-negative result that could lead to hemolytic complications in new-borns.

2.8 Future perspectives

The discovery of large numbers of new alleles in recent years (Calonga-Solís et al., 2019; Jonsson et al., 2017; Khatri et al., 2021; Richardson et al., 2019) exemplifies the idea that much of the diversity within the constant region of antibodies has been technically inaccessible and therefore largely underestimated. It is probable the full extent of diversity is yet to be realised, as suggested by comparative genomics studies in non-human species (Ramesh et al., 2017), especially for antibody isotypes other than IgG and for kappa/lambda light chains. High quality genomic assemblies such as the upcoming 'All of Us' million genome project have the potential to provide rich haplotype information for the IgH region (Denny et al., 2019). We highlight the recent development of new

genomics tools and databases specifically aligned with diversity in this region. Rodriguez et al., report the use of a novel bioinformatics tool, called IGenotyper, used in conjunction with IGH-targeted long-read sequencing to characterise variation in the IGH locus in eight samples (Rodriguez et al., 2020). Since being established, IGenotyper has been implemented to validate a new sequencing approach that exceeds the resolution of previous Adaptive Immune Receptor Repertoire sequencing (AIRR-seq) methods (Ford et al., 2023). The new technique, termed full-length AIRR-seq (FLAIRR-seq), was able to identify class and subclass as well as more specific gene and allele usages. The proof-of-concept study also resulted in the identification of 11 novel IGHG allele sequences that had not previously been reported on the IMGT database (Ford et al., 2023). This technology can be readily multiplexed to enable population-scale analyses. Furthermore, a population matched IG (pmIG) database (https://github.com/InduKhatri/pmIG) has been released which compiles known immunoglobulin allelic variants from the 1000 Genomes project (Khatri et al., 2021).

Several questions are inevitably raised as new diversity is discovered. Key among these is how constant domain diversity influences the immune response with implications for identifying those at risk for disease, infection susceptibility, and in the design of more effective vaccine strategies. There is growing evidence that antibodies can interact with non-canonical Fc receptors (TRIM21, DC-SIGN) and display functions that are not typical of antibodies. This includes activities characteristic of proteins (enzymes, cytokines, or chaperones) and the use of atypical means to neutralise pathogens or regulate the immune system (Dimitrov & Lacroix-Desmazes, 2020). The role of constant domain diversity has not yet been investigated for these instances. Likewise, the influence of IGLC diversity on antibody function will be important to explore in greater depth. Together we expect this information will enhance the design and delivery of next generation antibody drugs and enable higher accuracy in diagnostic approaches.

2.9 References

Atherton, A., Armour, K. L., Bell, S., Minson, A. C., & Clark, M. R. (2000). The herpes simplex virus type 1 Fc receptor discriminates between IgG1 allotypes. *Eur J Immunol*, *30*(9), 2540–2547. https://doi.org/10.1002/1521-4141(200009)30:9<2540::AID-IMMU2540>3.0.CO;2-S

Bannas, P., Hambach, J., & Koch-Nolte, F. (2017). Nanobodies and Nanobody-Based Human Heavy Chain Antibodies As Antitumor Therapeutics. *Frontiers in Immunology*, *8*. https://www.frontiersin.org/articles/10.3389/fimmu.2017.01603

Bartelds, G. M., de Groot, E., Nurmohamed, M. T., Hart, M. H., van Eede, P. H., Wijbrandts, C. A., Crusius, J. B., Dijkmans, B. A., Tak, P. P., & Aarden, L. (2010). Surprising negative association between IgG1 allotype disparity and anti-adalimumab formation: A cohort study. *Arthritis Res Ther*, *12*(6), R221. https://doi.org/10.1186/ar3208

Bastida-Corcuera, F. D., Butler, J. E., Yahiro, S., & Corbeil, L. B. (1999). Differential complement activation by bovine IgG2 allotypes. *Vet Immunol Immunopathol*, *71*(2), 115–123. https://doi.org/10.1016/s0165-2427(99)00095-1

Bis, J. C., Jian, X., Kunkle, B. W., Chen, Y., Hamilton-Nelson, K. L., Bush, W. S., Salerno, W. J., Lancour, D., Ma, Y., Renton, A. E., Marcora, E., Farrell, J. J., Zhao, Y., Qu, L., Ahmad, S., Amin, N., Amouyel, P., Beecham, G. W., Below, J. E., … Farrer, L. A. (2018). Whole exome sequencing study identifies novel rare and common Alzheimer's-associated variants involved in immune response and transcriptional regulation. *Mol Psychiatry*, *25*, 1859–1875. https://doi.org/10.1038/s41380-018-0112-7

Bradbury, A., & Plückthun, A. (2015). Reproducibility: Standardize antibodies used in research. *Nature*, *518*(7537), 27–29. https://doi.org/10.1038/518027a

Browning, S. R., Browning, B. L., Zhou, Y., Tucci, S., & Akey, J. M. (2018). Analysis of human sequence data reveals two pulses of archaic Denisovan admixture. *Cell*, *173*(1), 53-61.e9. https://doi.org/10.1016/j.cell.2018.02.031

Bruhns, P., Iannascoli, B., England, P., Mancardi, D. A., Fernandez, N., Jorieux, S., & Daëron, M. (2009). Specificity and affinity of human Fcγ receptors and their polymorphic variants for human IgG subclasses. *Blood*, *113*(16), 3716–3725. https://doi.org/10.1182/blood-2008-09-179754

Calonga-Solís, V., Malheiros, D., Beltrame, M. H., Vargas, L. B., Dourado, R. M., Issler, H. C., Wassem, R., Petzl-Erler, M. L., & Augusto, D. G. (2019). Unveiling the diversity of immunoglobulin gamma heavy chain constant region (IGHG) gene segments in Brazilian populations reveals twenty-eight novel alleles and evidence of gene conversion and natural selection. *Front Immunol*, *10*, 1161. https://doi.org/10.3389/fimmu.2019.01161

Cen, S. Y., Holton, M. B., Binnington, B., Denomme, G. A., Howie, H. L., Lebedev, J. N., Zimring, J. C., & Branch, D. R. (2020). IgG3 anti-Kell allotypic variation results in differential antigen binding and phagocytosis. *Transfusion*, *60*(4), 688–693. https://doi.org/10.1111/trf.15663

Chen, X., Sun, X., Yang, W., Yang, B., Zhao, X., Chen, S., He, L., Chen, H., Yang, C., Xiao, L., Chang, Z., Guo, J., He, J., Zhang, F., Zheng, F., Hu, Z., Yang, Z., Lou, J., Zheng, W., … Liu, W. (2018). An autoimmune disease variant of IgG1 modulates B cell activation and differentiation. *Science*, *362*(6415), 700–705. https://doi.org/10.1126/science.aap9310

Dard, P., Lefranc, M. P., Osipova, L., & Sanchez-Mazas, A. (2001). DNA sequence variability of IGHG3 alleles associated to the main G3m haplotypes in human populations. *Eur J Hum Genet*, *9*(10), 765–772. https://doi.org/10.1038/sj.ejhg.5200700

de Taeye, S. W., Bentlage, A. E. H., Mebius, M. M., Meesters, J. I., Lissenberg-Thunnissen, S., Falck, D., Sénard, T., Salehi, N., Wuhrer, M., Schuurman, J., Labrijn, A. F., Rispens, T., & Vidarsson, G. (2020). FcγR binding and ADCC activity of human IgG allotypes. *Front Immunol*, *11*(740). https://doi.org/10.3389/fimmu.2020.00740

Dechavanne, C., Dechavanne, S., Sadissou, I., Lokossou, A. G., Alvarado, F., Dambrun, M., Moutairou, K., Courtin, D., Nuel, G., Garcia, A., Migot-Nabias, F., & King, C. L. (2017). Associations between an IgG3 polymorphism in the binding domain for FcRn, transplacental transfer of malaria-specific IgG3, and protection against Plasmodium falciparum malaria during infancy: A birth cohort study in Benin. *PLOS Medicine*, *14*(10), e1002403. https://doi.org/10.1371/journal.pmed.1002403

Denny, J. C., Rutter, J. L., Goldstein, D. B., Philippakis, A., Smoller, J. W., Jenkins, G., & Dishman, E. (2019). The "All of Us" Research Program. *N Engl J Med*, *381*(7), 668–676. https://doi.org/10.1056/NEJMsr1809937

Dimitrov, J. D., & Lacroix-Desmazes, S. (2020). Noncanonical functions of antibodies. *Trends Immunol*, *41*(5), 379–393. https://doi.org/10.1016/j.it.2020.03.006

Dugoujon, J.-M., Hazout, S., Loirat, F., Mourrieras, B., Crouau-Roy, B., & Sanchez-Mazas, A. (2004). GM haplotype diversity of 82 populations over the world suggests a centrifugal model of human migrations. *Am J Phys Anthropol*, *125*(2), 175–192. https://doi.org/10.1002/ajpa.10405

Ford, E. E., Tieri, D., Rodriguez, O. L., Francoeur, N. J., Soto, J., Kos, J. T., Peres, A., Gibson, W. S., Silver, C. A., Deikus, G., Hudson, E., Woolley, C. R., Beckmann, N., Charney, A., Mitchell, T. C., Yaari, G., Sebra, R. P., Watson, C. T., & Smith, M. L. (2023). FLAIRR-Seq: A Method for Single-Molecule Resolution of Near Full-Length Antibody H Chain Repertoires. *J Immunol*, ji2200825. https://doi.org/10.4049/jimmunol.2200825

Giha, H. A., Nasr, A., Iriemenam, N. C., Arnot, D., Troye-Blomberg, M., Theander, T. G., Berzins, K., ElGhazali, G., & Pandey, J. P. (2009). Antigen-specific influence of GM/KM allotypes on IgG isotypes and association of GM allotypes with susceptibility to Plasmodium falciparum malaria. *Malar J*, *8*(1), 306. https://doi.org/10.1186/1475-2875-8-306

Giuntini, S., Granoff, D. M., Beernink, P. T., Ihle, O., Bratlie, D., & Michaelsen, T. E. (2016). Human IgG1, IgG3, and IgG3 Hinge-Truncated Mutants Show Different Protection Capabilities against Meningococci Depending on the Target Antigen and Epitope Specificity. *Clin Vaccine Immunol*, *23*(8), 698–706. https://doi.org/10.1128/CVI.00193-16

Goldberg, J. L., Navid, F., Hank, J. A., Erbe, A. K., Santana, V., Gan, J., de Bie, F., Javaid, A. M., Hoefges, A., Merdler, M., Carmichael, L., Kim, K., Bishop, M. W., Meager, M. M., Gillies, S. D., Pandey, J. P., & Sondel, P. M. (2020). Pre-existing antitherapeutic antibodies against the Fc region of the hu14.18K322A mAb are associated with outcome in patients with relapsed neuroblastoma. *J Immunother Cancer*, *8*(1), e000590. https://doi.org/10.1136/jitc-2020-000590

Gorski, M. M., Blighe, K., Lotta, L. A., Pappalardo, E., Garagiola, I., Mancini, I., Mancuso, M. E., Fasulo, M. R., Santagostino, E., & Peyvandi, F. (2016). Whole-exome sequencing to identify genetic risk variants underlying inhibitor development in severe hemophilia A patients. *Blood*, *127*(23), 2924–2933. https://doi.org/10.1182/blood-2015-12-685735

Grubb, R. (1956). Agglutination of eryhtrocytes coated with "incomplete" anti-Rh by certain rheumatoid arthritic sera and some other sera: The existence of human serum groups. *APMIS*, *39*(3), 195–197. https://doi.org/10.1111/j.1699-0463.1956.tb03392.x

Howie, H. L., Delaney, M., Wang, X., Er, L. S., Kapp, L., Lebedev, J. N., & Zimring, J. C. (2017). Errors in data interpretation from genetic variation of human analytes. *JCI Insight*, *2*(13), 1–10. https://doi.org/10.1172/jci.insight.94532

Idusogie, E. E., Presta, L. G., Gazzano-Santoro, H., Totpal, K., Wong, P. Y., Ultsch, M., Meng, Y. G., & Mulkerrin, M. G. (2000). Mapping of the C1q binding site on rituxan, a chimeric antibody with a human IgG1 Fc. *J Immunol*, *164*(8), 4178–4184. https://doi.org/10.4049/jimmunol.164.8.4178

Janda, A., Bowen, A., Greenspan, N. S., & Casadevall, A. (2016). Ig constant region effects on variable region structure and function. *Front Microbiol*, *7*, 22. https://doi.org/10.3389/fmicb.2016.00022

Jefferis, R. (1998). Allotypes, Immunoglobulin. In P. J. Delves (Ed.), *Encyclopedia of Immunology* (2nd ed., pp. 74–77). Elsevier. https://doi.org/10.1006/rwei.1999.0021

Jefferis, R., & Lefranc, M.-P. (2009). Human immunoglobulin allotypes: Possible implications for immunogenicity. *MAbs*, *1*(4), 332–338. https://doi.org/10.4161/mabs.1.4.9122

Johnson, W. E., Kohn, P. H., & Steinberg, A. G. (1977). Population genetics of the human allotypes Gm, Inv, and A2m: An analytical review. *Clin Immunol Immunopathol*, *7*(1), 97–113. https://doi.org/10.1016/0090-1229(77)90034-4

Jonsson, S., Sveinbjornsson, G., de Lapuente Portilla, A. L., Swaminathan, B., Plomp, R., Dekkers, G., Ajore, R., Ali, M., Bentlage, A. E. H., Elmér, E., Eyjolfsson, G. I., Gudjonsson, S. A., Gullberg, U., Gylfason, A., Halldorsson, B. V., Hansson, M., Holm, H., Johansson, Å., Johnsson, E., … Stefansson, K. (2017). Identification of sequence variants influencing immunoglobulin levels. *Nat Genet*, *49*(8), 1182–1191. https://doi.org/10.1038/ng.3897

Jung, S. T., Kelton, W., Kang, T. H., Ng, D. T. W., Andersen, J. T., Sandlie, I., Sarkar, C. A., & Georgiou, G. (2013). Effective Phagocytosis of Low Her2 Tumor Cell Lines with Engineered, Aglycosylated IgG Displaying High FcγRIIa Affinity and Selectivity. *ACS Chemical Biology*, *8*(2), 368–375. https://doi.org/10.1021/cb300455f

Khatri, I., Berkowska, M. A., van den Akker, E. B., Teodosio, C., Reinders, M. J. T., & van Dongen, J. J. M. (2021). Population matched (pm) germline allelic variants of immunoglobulin (IG) loci: Relevance in infectious diseases and vaccination studies in human populations. *Genes Immun*, *22*(3), 172–186. https://doi.org/10.1038/s41435-021-00143-7

Kunkel, H. G., Smith, W. K., Joslin, F. G., Natvig, J. B., & Litwin, S. D. (1969). Genetic Marker of the γA2 Subgroup of γA Immunoglobulins. *Nature*, *223*(5212), 1247–1248. https://doi.org/10.1038/2231247a0

Labrijn, A. F., Rispens, T., Meesters, J., Rose, R. J., den Bleker, T. H., Loverix, S., van den Bremer, E. T. J., Neijssen, J., Vink, T., Lasters, I., Aalberse, R. C., Heck, A. J. R., van de Winkel, J. G. J., Schuurman, J., & Parren, P. W. H. I. (2011). Species-specific determinants in the IgG CH3 domain enable Fab-arm exchange by affecting the noncovalent CH3–CH3 interaction strength. *J Immunol*, *187*(6), 3238–3246. https://doi.org/10.4049/jimmunol.1003336

Lazar, G. A., Dang, W., Karki, S., Vafa, O., Peng, J. S., Hyun, L., Chan, C., Chung, H. S., Eivazi, A., & Yoder, S. C. (2006). Engineered antibody Fc variants with enhanced effector function. *Proc Natl Acad Sci U S A*, *103*(11), 4005–4010. https://doi.org/10.1073/pnas.0508123103

Lefranc, M.-P., Giudicelli, V., Duroux, P., Jabado-Michaloud, J., Folch, G., Aouinti, S., Carillon, E., Duvergey, H., Houles, A., Paysan-Lafosse, T., Hadi-Saljoqi, S., Sasorith, S., Lefranc, G., & Kossida, S. (2014). IMGT®, the international ImMunoGeneTics information system® 25 years on. *Nucleic Acids Res*, *43*(D1), D413–D422. https://doi.org/10.1093/nar/gku1056

Lefranc, M.-P., & Lefranc, G. (2012). Human Gm, Km, and Am allotypes and their molecular characterization: A remarkable demonstration of polymorphism. In J. M. Walker (Ed.), *Immunogenetics: Methods and Applications in Clinical Practice*. (Vol. 882, pp. 635–680). Humana Press. https://doi.org/10.1007/978-1-61779-842-9_34

Lewis, K. B., Meengs, B., Bondensgaard, K., Chin, L., Hughes, S. D., Kjær, B., Lund, S., & Wang, L. (2009). Comparison of the ability of wild type and stabilized human IgG4 to undergo Fab arm exchange with endogenous IgG4 in vitro and in vivo. *Mol Immunol*, *46*(16), 3488–3494. https://doi.org/10.1016/j.molimm.2009.07.009

Ligotti, M. E., Calabrò, A., Accardi, G., Aiello, A., Caruso, C., Colomba, C., Bona, D. D., Duro, G., Namboodiri, A. M., Tuttolomondo, A., Pandey, J. P., & Candore, G. (2023). GM allotypes and COVID-19. A pilot study performed on Sicilian patients. *Transl Med @ UniSa*, *24*(2). https://doi.org/10.37825/2239-9747.1039

López-Martínez, R., Albaiceta, G. M., Amado-Rodríguez, L., Gómez, J., Cuesta-Llavona, E., García-Clemente, M., Hermida-Valverde, T., Enríquez-Rodriguez, A. I., Hernández-González, C., Martínez-Borra, J., López-Larrea, C., Gil-Peña, H., Alvarez, V., & Coto, E. (2022). IGHG3 hinge length variation was associated with the risk of critical disease and death in a Spanish COVID-19 cohort. *Genes Immun*, *23*(6), 205–208. https://doi.org/10.1038/s41435-022-00179-3

Lu, J., Chu, J., Zou, Z., Hamacher, N. B., Rixon, M. W., & Sun, P. D. (2015). Structure of FcγRI in complex with Fc reveals the importance of glycan recognition for high-affinity IgG binding. *PNAS*, *112*(3), 833–838. https://doi.org/10.1073/pnas.1418812112

Mkaddem, S. B., Benhamou, M., & Monteiro, R. C. (2019). Understanding Fc receptor involvement in inflammatory diseases: From mechanisms to new therapeutic tools. *Front Immunol*, *10*, 811. https://doi.org/10.3389/fimmu.2019.00811

Moore, G. L., Chen, H., Karki, S., & A, G. (2010). Engineered Fc variant antibodies with enhanced ability to recruit complement and mediate effector functions. *MAbs*, *2*(2), 181–189.

Moraru, M., Black, L. E., Muntasell, A., Portero, F., López-Botet, M., Reyburn, H. T., Pandey, J. P., & Vilches, C. (2015). NK cell and Ig interplay in defense against Herpes Simplex Virus Type 1: Epistatic interaction of CD16A and IgG1 allotypes of variable affinities modulates antibody-dependent cellular cytotoxicity and susceptibility to clinical reactivation. *J Immunol*, *195*(4), 1676–1684. https://doi.org/10.4049/jimmunol.1500872

Nagelkerke, S. Q., Schmidt, D. E., de Haas, M., & Kuijpers, T. W. (2019). Genetic variation in low-to-medium-affinity Fcγ receptors: Functional consequences, disease associations, and opportunities for personalized medicine. *Front Immunol*, *10*(2237). https://doi.org/10.3389/fimmu.2019.02237

Nakao, Y., Matsumoto, H., Miyazaki, T., Nishitani, H., Takatsuki, K., Kasukawa, R., Nakayama, S., Izumi, S., Fujita, T., & Tsuji, K. (1980). IgG heavy chain allotypes (Gm) in autoimmune diseases. *Clin Exp Immunol*, *42*(1), 20–26. PMID: 6780255; PMCID: PMC1537060.

Namboodiri, A. M., Nietert, P. J., & Pandey, J. P. (2008). Hepatitis C virus core protein discriminates between the two IgG2 allotypes. *Viral Immunol*, *21*(2), 273–276. https://doi.org/10.1089/vim.2008.0008

Natsume, A., In, M., Takamura, H., Nakagawa, T., Shimizu, Y., Kitajima, K., Wakitani, M., Ohta, S., Satoh, M., Shitara, K., & Niwa, R. (2008). Engineered Antibodies of IgG1/IgG3 Mixed Isotype with Enhanced Cytotoxic Activities. *Cancer Res*, *68*(10), 3863–3872. https://doi.org/10.1158/0008-5472.CAN-07-6297

Nimmerjahn, F., & Ravetch, J. V. (2008). Fcγ receptors as regulators of immune responses. *Nat Rev Immunol*, *8*(1), 34. https://doi.org/10.1038/nri2206

Nordstrom, J. L., Gorlatov, S., Zhang, W., Yang, Y., Huang, L., Burke, S., Li, H., Ciccarone, V., Zhang, T., & Stavenhagen, J. (2011). Anti-tumor activity and toxicokinetics analysis of MGAH22, an anti-

HER2 monoclonal antibody with enhanced Fcγ receptor binding properties. *Breast Cancer Res*, *13*(6), R123. https://doi.org/10.1186/bcr3069

Oganesyan, V., Damschroder, M. M., Cook, K. E., Li, Q., Gao, C., Wu, H., & Dall'Acqua, W. F. (2014). Structural insights into neonatal Fc receptor-based recycling mechanisms. *J Biol Chem*, *289*(11), 7812–7824. https://doi.org/10.1074/jbc.M113.537563

Pandey, J. P. (2012). Immunoglobulin genes and immunity to herpes simplex virus type 1. *J Infect Dis*, *206*(1), 143–144. https://doi.org/10.1093/infdis/jis317

Pandey, J. P., Astemborski, J., & Thomas, D. L. (2004). Epistatic effects of immunoglobulin GM and KM allotypes on outcome of infection with hepatitis C virus. *J Virol*, *78*(9), 4561–4565. https://doi.org/10.1128/JVI.78.9.4561-4565.2004

Pandey, J. P., Kistner-Griffin, E., Black, L., Namboodiri, A. M., Iwasaki, M., Kasuga, Y., Hamada, G. S., & Tsugane, S. (2014). IGKC and FcγR genotypes and humoral immunity to HER2 in breast cancer. *Immunobiology*, *219*(2), 113–117. https://doi.org/10.1016/j.imbio.2013.08.005

Pandey, J. P., Kistner-Griffin, E., Iwasaki, M., Bu, S., Deepe, R., Black, L., Kasuga, Y., Hamada, G. S., & Tsugane, S. (2012). Genetic markers of immunoglobulin G and susceptibility to breast cancer. *Hum Immunol*, *73*(11), 1155–1158. https://doi.org/10.1016/j.humimm.2012.07.340

Pandey, J. P., Kothera, R. T., Liu, S., Costa, A. S., Mancuso, R., & Agostini, S. (2019). Immunoglobulin genes and immunity to HSV1 in Alzheimer's disease. *J Alzheimers Dis*, *70*, 917–924. https://doi.org/10.3233/JAD-190265

Pandey, J. P., & Li, Z. (2013). The forgotten tale of immunoglobulin allotypes in cancer risk and treatment. *Exp Hematol Oncol*, *2*(1), 6. https://doi.org/10.1186/2162-3619-2-6

Pandey, J. P., Luo, Y., Elston, R. C., Wu, Y., Philp, F. H., Astemborski, J., Thomas, D. L., & Netski, D. M. (2008). Immunoglobulin allotypes influence IgG antibody responses to hepatitis C virus envelope proteins E1 and E2. *Hum Immunol*, *69*(3), 158–164. https://doi.org/10.1016/j.humimm.2008.01.019

Pandey, J. P., & Namboodiri, A. M. (2014). Genetic variants of IgG1 antibodies and FcγRIIIa receptors influence the magnitude of antibody-dependent cell-mediated cytotoxicity against prostate cancer cells. *OncoImmunology*, *3*(1), e27317-3. https://doi.org/10.4161/onci.27317

Pritsch, O., Hudry-Clergeon, G., Buckle, M., Petillot, Y., Bouvet, J. P., Gagnon, J., & Dighiero, G. (1996). Can immunoglobulin C(H)1 constant region domain modulate antigen binding affinity of antibodies? *J Clin Invest*, *98*(10), 2235–2243. https://doi.org/10.1172/JCI119033

Puca, A. A., Ferrario, A., Maciag, A., Accardi, G., Aiello, A., Gambino, C. M., Candore, G., Caruso, C., Namboodiri, A. M., & Pandey, J. P. (2018). Association of immunoglobulin GM allotypes with longevity in long-living individuals from Southern Italy. *Immun Ageing*, *15*(1), 26. https://doi.org/10.1186/s12979-018-0134-7

Ramesh, A., Darko, S., Hua, A., Overman, G., Ransier, A., Francica, J. R., Trama, A., Tomaras, G. D., Haynes, B. F., Douek, D. C., & Kepler, T. B. (2017). Structure and diversity of the rhesus macaque immunoglobulin loci through multiple de novo genome assemblies. *Front Immunol*, *8*(1407). https://doi.org/10.3389/fimmu.2017.01407

Ramsland, P. A., Farrugia, W., Bradford, T. M., Sardjono, C. T., Esparon, S., Trist, H. M., Powell, M. S., Tan, P. S., Cendron, A. C., Wines, B. D., Scott, A. M., & Hogarth, P. M. (2011). Structural Basis for FcγRIIa Recognition of Human IgG and Formation of Inflammatory Signaling Complexes. *J. Immun.*, *187*(6), 3208–3217. https://doi.org/10.4049/jimmunol.1101467

Redpath, Michaelsen, Sandlie, & Clark. (1998). Activation of complement by human IgG1 and human IgG3 antibodies against the human leucocyte antigen CD52. *Immunology*, *93*(4), 595–600. https://doi.org/10.1046/j.1365-2567.1998.00472.x

Richards, J. O., Karki, S., Lazar, G. A., Chen, H., Dang, W., & Desjarlais, J. R. (2008). Optimization of antibody binding to FcgammaRIIa enhances macrophage phagocytosis of tumor cells. *Mol Cancer Ther*, *7*(8), 2517–2527. https://doi.org/10.1158/1535-7163.Mct-08-0201

Richardson, S. I., Lambson, B. E., Crowley, A. R., Bashirova, A., Scheepers, C., Garrett, N., Karim, S. A., Mkhize, N. N., Carrington, M., Ackerman, M. E., Moore, P. L., & Morris, L. (2019). IgG3 enhances neutralization potency and Fc effector function of an HIV V2-specific broadly neutralizing antibody. *PLOS Pathogens*, *15*(12), e1008064. https://doi.org/10.1371/journal.ppat.1008064

Rispens, T., Davies, A. M., Ooijevaar-de Heer, P., Absalah, S., Bende, O., Sutton, B. J., Vidarsson, G., & Aalberse, R. C. (2014). Dynamics of inter-heavy chain interactions in human immunoglobulin G (IgG) subclasses studied by kinetic Fab arm exchange. *J Biol Chem*, *289*(9), 6098–6109. https://doi.org/10.1074/jbc.M113.541813

Rispens, T., Himly, M., Ooievaar-De Heer, P., den Bleker, T. H., & Aalberse, R. C. (2010). Traces of pFc' in IVIG interact with human IgG Fc domains and counteract aggregation. *Eur J Pharm Sci*, *40*(1), 62–68. https://doi.org/10.1016/j.ejps.2010.03.001

Robinson, W. H. (2015). Sequencing the functional antibody repertoire—Diagnostic and therapeutic discovery. *Nat Rev Rheumatol*, *11*(3), 171–182. https://doi.org/10.1038/nrrheum.2014.220

Rodriguez, O. L., Gibson, W. S., Parks, T., Emery, M., Powell, J., Strahl, M., Deikus, G., Auckland, K., Eichler, E. E., Marasco, W. A., Sebra, R., Sharp, A. J., Smith, M. L., Bashir, A., & Watson, C. T. (2020). A Novel Framework for Characterizing Genomic Haplotype Diversity in the Human Immunoglobulin Heavy Chain Locus. *Front Immunol*, *11*. https://www.frontiersin.org/articles/10.3389/fimmu.2020.02136

Roopenian, D. C., & Akilesh, S. (2007). FcRn: The neonatal Fc receptor comes of age. *Nat Rev Immunol*, *7*(9), 715–725. https://doi.org/10.1038/nri2155

Saito, S., Namisaki, H., Hiraishi, K., Takahashi, N., & Iida, S. (2019). A stable engineered human IgG3 antibody with decreased aggregation during antibody expression and low pH stress. *Protein Sci.*, *28*(5), 900–909. https://doi.org/10.1002/pro.3598

Saphire, E. O., Parren, P. W. H. I., Pantophlet, R., Zwick, M. B., Morris, G. M., Rudd, P. M., Dwek, R. A., Stanfield, R. L., Burton, D. R., & Wilson, I. A. (2001). Crystal Structure of a Neutralizing Human IgG Against HIV-1: A Template for Vaccine Design. *Science*, *293*(5532), 1155–1159. https://doi.org/10.1126/science.1061692

Shah, I. S., Lovell, S., Mehzabeen, N., Battaile, K. P., & Tolbert, T. J. (2017). Structural characterization of the Man5 glycoform of human IgG3 Fc. *Mol Immunol*, *92*, 28–37. https://doi.org/10.1016/j.molimm.2017.10.001

Sondermann, P., Huber, R., Oosthuizen, V., & Jacob, U. (2000). The 3.2-A crystal structure of the human IgG1 Fc fragment-Fc gammaRIII complex. *Nature*, *406*(6793), 267–273. https://doi.org/10.1038/35018508

Stapleton, N. M., Andersen, J. T., Stemerding, A. M., Bjarnarson, S. P., Verheul, R. C., Gerritsen, J., Zhao, Y., Kleijer, M., Sandlie, I., de Haas, M., Jonsdottir, I., van der Schoot, C. E., & Vidarsson, G. (2011). Competition for FcRn-mediated transport gives rise to short half-life of human IgG3 and offers therapeutic potential. *Nat Commun*, *2*, 599–599. https://doi.org/10.1038/ncomms1608

Stavenhagen, J. B., Gorlatov, S., Tuaillon, N., Rankin, C. T., Li, H., Burke, S., Huang, L., Johnson, S., Bonvini, E., & Koenig, S. (2007). Fc optimization of therapeutic antibodies enhances their ability to kill tumor cells in vitro and controls tumor expansion in vivo via low-affinity activating Fcγ receptors. *Cancer Res*, *67*(18), 8882. https://doi.org/10.1158/0008-5472.CAN-07-0696

Su, C. T.-T., Lua, W.-H., Ling, W.-L., & Gan, S. K.-E. (2018). Allosteric effects between the antibody constant and variable regions: A study of IgA Fc mutations on antigen binding. *Antibodies (Basel)*, *7*(2), 20. https://doi.org/10.3390/antib7020020

Takai, T. (2002). Roles of Fc receptors in autoimmunity. *Nat Rev Immunol*, *2*(8), 580–592. https://doi.org/10.1038/nri856

Tatarewicz, S. M., Juan, G., Swanson, S. J., & Moxness, M. S. (2012). Epitope characterization of pre-existing and developing antibodies to an aglycosylated monoclonal antibody therapeutic of G1m17,1 allotype. *J Immunol Methods*, *382*(1–2), 93–100. https://doi.org/10.1016/j.jim.2012.05.009

Ternant, D., Arnoult, C., Pugnière, M., Dhommée, C., Drocourt, D., Perouzel, E., Passot, C., Baroukh, N., Mulleman, D., Tiraby, G., Watier, H., Paintaud, G., & Gouilleux-Gruart, V. (2016). IgG1 allotypes influence the pharmacokinetics of therapeutic monoclonal antibodies through FcRn binding. *J Immunol*, *196*(2), 607–613. https://doi.org/10.4049/jimmunol.1501780

Torres, M., & Casadevall, A. (2008). The immunoglobulin constant region contributes to affinity and specificity. *Trends Immunol*, *29*(2), 91–97.

Torres, M., Fernández-Fuentes, N., Fiser, A., & Casadevall, A. (2007). The immunoglobulin heavy chain constant region affects kinetic and thermodynamic parameters of antibody variable region interactions with antigen. *J Biol Chem*, *282*(18), 13917–13927. https://doi.org/10.1074/jbc.M700661200

van Loghem, E., Aalberse, R., & Matsumoto, H. (1984). A genetic marker of human IgE heavy chains, Em (1). *Vox Sang*, *46*(4), 195–206. https://doi.org/10.1111/j.1423-0410.1984.tb00075.x

Vidarsson, G., Dekkers, G., & Rispens, T. (2014). IgG subclasses and allotypes: From structure to effector functions. *Front Immunol*, *5*, 520. https://doi.org/10.3389/fimmu.2014.00520

Webster, C. I., Bryson, C. J., Cloake, E. A., Jones, T. D., Austin, M. J., Karle, A. C., Spindeldreher, S., Lowe, D. C., & Baker, M. P. (2016). A comparison of the ability of the human IgG1 allotypes G1m3 and G1m1,17 to stimulate T-cell responses from allotype matched and mismatched donors. *MAbs*, *8*(2), 253–263. https://doi.org/10.1080/19420862.2015.1128605

Zouali, M. (1995). B-cell superantigens: Implications for selection of the human antibody repertoire. *Immunol Today*, *16*(8), 399–405. https://doi.org/10.1016/0167-5699(95)80009-3

Chapter Three

Constant Domain Polymorphisms Influence Monoclonal Antibody Stability and Dynamics

3.1 Preface

Stability is a fundamental property of antibodies governing effective immune function and biopharmaceutical developability. This chapter assesses the influence of naturally occurring amino acid polymorphisms in the constant domains of IgG antibodies on thermal stability. A fluorescence spectroscopy-based technique, termed red edge excitation shift, was used to screen the local structural dynamics of 32 unique IgG antibodies as a measure of stability.

This research is presented in this chapter as a published, peer-reviewed Research Article. The format has been modified to fit with the theme of this thesis. Supplementary material associated with this manuscript is presented in Appendix A:.

Warrender, A. K., Pan, J., Pudney, C. R., Arcus, V. L., & Kelton, W. (2023). Constant Domain Polymorphisms Influence Monoclonal Antibody Stability and Dynamics. *Protein Science*, *32*(3), e4589. https://doi.org/10.1002/pro.4589

3.1.1 Author contributions

As the first author, I led the experimental work involved with this research (including production of the antibodies, glycan characterisation, and stability experiments), conducted the data analysis, and contributed to writing and editing the manuscript from draft to submission, including figure design. Jolyn Pan assisted with producing some of the antibodies used in the experiments. Vickery Arcus contributed to the experimental conceptualisation, provided expert advice around data interpretation, and offered feedback on the draft manuscript. Chris Pudney assisted with data analysis, provided expert advice around data interpretation, and offered feedback on the draft manuscript. William Kelton conceptualised the research, assisted with experimental work involving glycan characterisation, provided guidance with data interpretation, contributed to writing and editing the manuscript and collated the manuscript for submission.

Constant Domain Polymorphisms Influence Monoclonal Antibody Stability and Dynamics

Annmaree K. Warrender[a], Jolyn Pan[b], Chris R. Pudney[c], Vickery L. Arcus[b] and William Kelton[a]

[a]Te Huataki Waiora School of Health, University of Waikato, Hamilton, New Zealand; [b]Te Aka Mātuatua School of Science, University of Waikato, Hamilton, New Zealand; [c]Department of Biology and Biochemistry, University of Bath, Bath, UK

3.2 Abstract

The constant regions of clinical monoclonal antibodies are derived from a select number of allotypes found in IgG subclasses. Despite a long-term acknowledgement that this diversity may impact both antibody function and developability, there is a lack of data on the stability of variants carrying these mutations. Here, we generated a panel of IgG1, IgG2, and IgG3 antibodies with 32 unique constant region alleles and performed a systematic comparison of stability using red edge excitation shift (REES). This technique exploits the fluorescent properties of tryptophan residues to measure antibody structural dynamics which predict flexibility and the propensity to unfold. Our REES measurements revealed broad stability differences between subclasses with IgG3 possessing the poorest overall stability. Further interrogation of differences between variants within each subclass enabled the high-resolution profiling of individual allotype stabilities. Crucially, these observed differences were not found to be linked to N297-linked glycan heterogeneity. Our work demonstrates diverse stabilities (and dynamics) for a range of naturally occurring constant domain alleles and the utility of REES as a method for rapid and sensitive antibody stability profiling, requiring only laboratory spectrophotometry equipment.

3.3 Introduction

In the 25 years since the first approval of humanised daclizumab with an IgG1 backbone, the diversity of clinically approved antibodies has grown to encompass both IgG2 and IgG4 subclasses (Kaplon et al., 2020). The majority of clinical monoclonal antibodies (mAbs) within each of these subclasses are based on a small number of allotypes encoded by constant region alleles (Jefferis & Lefranc, 2009). This is despite the long-standing recognition that human populations exhibit significant constant region diversity (Vidarsson et al., 2014; Warrender & Kelton, 2020). Recent targeted sequencing approaches, and the mining of high-resolution genome sequences, have further increased known constant region diversity with potential implications for the design of next generation monoclonal drugs (Calonga-Solís et al., 2019; Khatri et al., 2021).

The constant region of antibodies directly contributes to antibody mediated effector function, immunogenicity, and stability. Antibody engagement of Fc receptors via the constant region mediates potent effector responses, such as antibody-dependent cellular cytotoxicity (ADCC) and antibody-dependent cellular phagocytosis (ADCP). Engineered constant region sequences that modulate immune function have been very successful clinically with more than 21 modified mAb drugs approved in the US to date (The Antibody Society, 2022). Moreover, naturally occurring polymorphisms (specifically in the CH2 and hinge domains) have been demonstrated to alter Fc receptor binding and subsequently influence in vitro effector function (de Taeye et al., 2020). Given that this diversity potentially creates new epitopes, it is surprising to find long standing immunogenicity concerns around patient constant region polymorphic disparity with mAb drugs have largely not manifested clinically (Bartelds et al., 2010). There are a few notable exceptions and some reports have highlighted T cell epitope driven mechanisms may account for instances of elevated antidrug antibody levels (Benucci et al., 2018; Stickler et al., 2011).

Alongside low immunogenicity, high stability is fundamental to the developability of reliable mAbs and is inherently linked to dynamic flexibility of the protein structure (Feige et al., 2004; Karshikoff et al., 2015). The relationship between flexibility and stability encompasses a wide range of phenomena (e.g. local unfolding vs loop motions) over a wide range of timescales (ranging from ns to ms). Entropic and enthalpic contributions are unique to each situation and are also heavily influenced by the surrounding solvent. Typically, mAbs exhibiting greater intradomain flexibility have

poorer stability than more rigid counterparts although even small environmental perturbations (e.g. temperature increases) are liable to enable conformations predisposed to unfolding or aggregation. Post-translational glycosylation can further influence antibody stability through interactions with CH2 domain residues (Aoyama et al., 2019; Higel et al., 2016; Krapp et al., 2003). Within the IgG isotype, subclass stability differences are well established, with IgG1 ranked the most stable subclass, followed by IgG2 and IgG4, and finally IgG3 being the least thermally stable and most prone to aggregation (Ito & Tsumoto, 2013). Resolving stability differences at the single point mutation level, however, is significantly more challenging and has not been systematically investigated for mutations in antibody constant regions. Traditional methods used to measure protein stability (e.g., differential scanning fluorimetry, differential scanning calorimetry, or circular dichroism) have been successfully deployed but require the careful preparation of samples to avoid aggregates and the results can be dependent on heating rates and incubation times (Lin et al., 2015; Vermeer & Norde, 2000). Alternative nuclear magnetic resonance (Arbogast et al., 2015; Brinson et al., 2019; Nokwe et al., 2014) and hydrogen/deuterium exchange mass spectrometry (Houde & Engen, 2013; Majumdar et al., 2015; More et al., 2018) approaches are also excellent for the interrogation of antibody dynamics at high resolution but remain confined to specialist facilities.

The recent development of red edge excitation shift (REES) spectroscopy for high resolution antibody stability analysis offers a rapid and accessible technique using common laboratory equipment (Knight et al., 2020; Thakkar et al., 2012). This highly sensitive approach detects distinct flexibility profiles for structurally identical proteins harboring single point mutation differences (Jones et al., 2017). The underlying principles of REES have been thoroughly discussed in several publications (Catici et al., 2016; Haldar et al., 2011; Kwok et al., 2021). In brief, REES exploits the fluorescent properties of tryptophan (Trp) residues as highly sensitive reporters of the local protein environment (Figure 3-1). In particular, the fluorescent emission profile of Trp is greatly influenced by the degree of interaction with surrounding water molecules. In stable, folded structures Trp residues are often buried within the structure where solvent molecules are excluded and as a result retain a higher energy of emission with minimal red shift. In contrast, Trp residues in more flexible or partially unfolded proteins can become exposed to solvents, giving rise to a red shift in emission. This creates a unique population of Trp residues that fluoresce at low emission energies regardless of excitation wavelength. Across

sequentially lower excitation energies, the emission energy of Trp residues in folded, rigid proteins decreases relative to the excitation wavelength shifting toward the "red-edge" (The REES phenomenon). REES can therefore be used to interrogate the structural dynamics of antibodies and the changes in flexibility imparted by thermal stress as a means to rapidly quantify mAb stability.

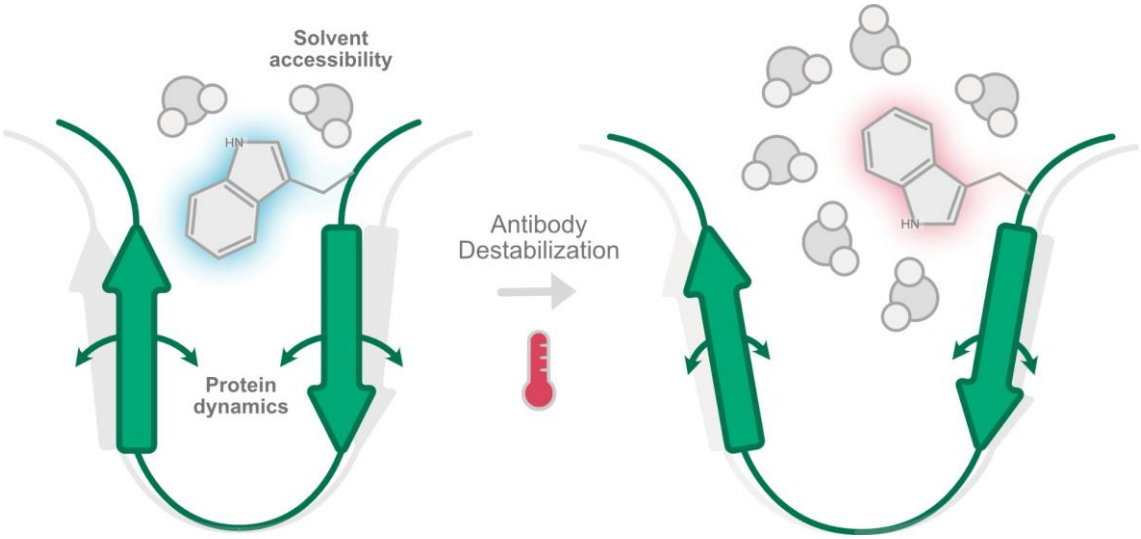

Figure 3-1. Graphical depiction of the REES effect as determined by the solvent-accessibility of tryptophan residues. Tryptophan residues in a rigid/folded protein structure typically have limited solvent access causing blue-shifted fluorescent emission profiles. Destabilisation causes the protein structure to become more flexible, increasing the solvent accessibility to tryptophan and causing a red-shifted fluorescent emission profile.

Here, we have used REES to establish relative stability profiles for a panel of 32 IgG1, IgG2, and IgG3 constant region polymorphisms formatted with trastuzumab variable domains. We report broad differences in stability between the subclasses with IgG1 and IgG2 allelic variants displaying greater thermal stability than IgG3 alleles. Importantly, REES also enables high-resolution discrimination of differences in stability at the allelic/point mutation level. The present work leads us to expect a broader utility of this technique for the high-throughput screening of potential mAb candidates with enhanced stability.

3.4 Materials and Methods

Selection and expression of antibody variants

Exon sequences for 32 human IGHG1, IGHG2, and IGHG3 genes were obtained from the International Immunogenetics Information System® (IMGT) database (Giudicelli et al., 2006). For the purposes of this study, IGHG allele sequences were taken from the IMGT database alone as alleles published on other databases are yet to be robustly verified (Collins et al., 2021). Only allelic sequences with non-synonymous mutations were selected (Table A-1). To meet the requirements of the REES technique (Knight et al., 2020; Kwok et al., 2021), we selected alleles within each subclass containing equal numbers of tryptophan residues. IGHG4 alleles were excluded from analysis due to incomplete sequence information in the CH1 domain or the presence of synonymous mutations.

For each allele, expression constructs were designed, synthesised, and cloned into pTwist CMV BetaGlobulin WPRE Neo vectors (Twist Biosciences). Briefly, constant region allelic sequences were appended to trastuzumab variable heavy sequences with a rabbit IGHG endoplasmic reticulum signal sequence to create full-length heavy chains. Similarly, a universal light chain was created by joining the trastuzumab variable light sequence to the IGKC*01 kappa constant allele with a rabbit IGKC signal peptide.

Antibodies were expressed by transient transfection using the Expi293 expression system according to the manufacturer's instructions for 25 mL cultures (Thermo Fisher). Expi293 cells were maintained at 37°C, 8% CO_2 with shaking at 125 rpm for the duration of the experiment. Plasmid DNA was transfected at a 2:1 ratio of light chain to heavy chain, respectively. Expressed antibodies were harvested by collecting supernatants six days after transfection by centrifugation at 5000 x *g* for 20 min at 4°C. Supernatants were passed through 0.22 µm filters prior to purification. Gravity flow columns were packed with Protein G sepharose (Thermo Fisher) to a final bed volume of 1 mL. Antibody supernatants were passed through the column three times and washed with 50 mM sodium phosphate buffer, pH 7.5. Antibodies were eluted at pH 2.5 with 4 x 1 mL volumes of formic acid directly into 10 kDa Amicon® Ultra-15 filter units (Merck Millipore) containing 500 µL of 1 M Ammonium Carbonate pH 8.0. The filter units were centrifuged at 5000 x *g* for 15 min at 4°C and buffer exchanged into 50 mM sodium phosphate pH 7.5. Antibody purity was determined by SDS-PAGE using 12% cross-linked acrylamide gels under reducing conditions.

Homology modelling

Homology models of IgG1 allelic variants were built using the Robetta protein structure prediction service (https://robetta.bakerlab.org/) with the comparative modelling setting (Song et al., 2013). The crystal structure of full-length IgG1 anti-gp120 mAb [PDB: 1hzh] was retrieved from the PDB and used as the template. The full trastuzumab sequence of each IgG1 constant region allele was threaded onto 1hzh template. Homology models were aligned using PYMOL software and the quality of alignment was determined by calculating the root mean square deviation from 1hzh.

REES Analysis

Antibody stability was assessed using the method established by Knight *et al*., (2020) with some minor adaptations. Antibodies were diluted to 150 μg mL^{-1} in 50 mM Tris-HCl buffered saline pH 8.0. Fluorescent measurements were performed using a Hitachi F-7000 fluorescent spectrometer connected to a circulating water bath set to 10°C. Samples were analysed in triplicate in a 200 μL micro-cuvette with a magnetic cuvette stirrer. Dry compressed air was supplied to the chamber to prevent condensation. All samples were equilibrated to 10°C for 5 min prior to measurement. Both excitation and emission slit widths were set to 5 nm. A 3D scan was run with excitation wavelengths from 290 - 310 nm in 1 nm steps and emission wavelengths monitored from 325 – 500 nm in 1 nm steps. A control sample containing only 50 mM Tris-HCl buffered saline pH 8.0 was used for background subtraction and removal of solvent-induced Raman scattering. Immediately following fluorescent scanning, samples were incubated at 65°C in an Eppendorf thermomixer for 5 h, transferred back to 10°C and allowed to equilibrate for 5 min before repeating the 3D fluorescent scan.

Data processing and analyses were undertaken using R software. Control sample fluorescent scans were averaged to determine the background fluorescence and subtracted from each individual antibody allele scan. The centre of spectral mass (CSM) was calculated for each scan using Equation 1:

Equation 1 $$CSM = \frac{\Sigma(f_i \lambda_{Em})}{\Sigma(f_i)}$$

Where f_i is the measured fluorescence intensity and λ_{Em} is the emission wavelength (Knight et al., 2020). The CSM data was then fit with a thermodynamic model of REES behaviour that describes a two-state transition of tryptophan fluorophores from an excited to a relaxed state (Kwok et al., 2021) (Equation 2):

Equation 2 $$CSM(\lambda_{Ex}) = \frac{CSM(\lambda_{Ex}^{Fc}) + CSM(\lambda_{Ex}^{R}) e^{\left(\frac{\Delta Gm(\lambda_{Ex} - \lambda_{Ex}^{50\%})}{RT}\right)}}{1 + e^{\left(\frac{\Delta Gm(\lambda_{Ex} - \lambda_{Ex}^{50\%})}{RT}\right)}}$$

Where $CSM(\lambda_{Ex}^{Fc})$ is the centre of spectral mass for collective tryptophan emission in an excited state (also known as the Franck-Condon state), $CSM(\lambda_{Ex}^{R})$ the centre of spectral mass for the fully relaxed tryptophan state, λ_{Ex} the excitation wavelength, $\lambda_{Ex}^{50\%}$ the excitation wavelength at half the maximal CSM between the excited and relaxed states, and ΔG_m is the gradient of the slope describing the change in free energy (ΔG) of the solvent-fluorophore interaction states sampled during tryptophan relaxation. *R* is the gas constant of 8.3145 J mol^{-1} K^{-1} and *T* is temperature of the fluorescent measurement in K (283.15 K as experiments were conducted at 10°C). The CSM of the relaxed state, $CSM(\lambda_{Ex}^{R})$, is the maximum wavelength of emission in which the antibodies would be fully solvated and will be the same for all antibodies given the same number of tryptophan residues. This variable was globally fit to all antibody variants and constrained between 387 and 440 nm, a practical range of $CSM(\lambda_{Ex}^{R})$ values determined by Kwok *et al.* (2021). Statistical testing for comparative analyses were performed using one-way ANOVA with Tukey Post-Hoc multiple comparisons tests and the p-adjusted values used to determine significance with a p-value (*p*) cut-off of 0.05.

Differential scanning fluorimetry

Differential scanning fluorimetry (DSF) was used to determine the temperature of unfolding for a subset of antibody alleles (IgG1*01, *11, IgG2*04, *09, IgG3*03, *09, *16, *17). SYPRO orange protein gel stain (Invitrogen) was prepared at 25X concentration with phosphate buffered saline (PBS) pH 7.4. Samples were prepared with 300 μg mL^{-1} antibody, 2.5X final concentration SYPRO orange dye and PBS to a final volume of 25 μL in 0.2 mL optically clear tubes. A buffer only control was prepared with SYPRO orange dye and PBS only. All samples were run in triplicate on a Rotor-Gene 6000 real-time PCR cycler with 36-tube ring and Rotor-Gene Q series software. The temperature was held at 25°C for 1.5 min before beginning the thermal ramp from 25°C to 99°C in 0.2°C increments with a 5 s hold at each step. Excitation was set at 470 nm and emission detected at 555 nm with autogain enabled. Each antibody scan was corrected for background fluorescence by subtracting absorbance from the buffer-only control. The first derivate was calculated and the maximum value of each first derivative peak was determined to be the thermal melting transition (T_m), equivalent to the inflection point of the DSF curves.

Glycan analysis

To characterise the glycan profiles of each allelic variant, glycans were analysed by modifying the method reported by Segu *et al.,* (2020). Antibodies (50 µg) were immobilised on Protein G sepharose resin and treated with PNGase F Rapid (NEB). Enzymatic release was performed at 45°C for 45 min. Released glycans were collected from the supernatant after centrifugation at 4000 x *g* for 2 min and labelled with InstantPC dye (Agilent). The PC dye was prepared following the manufacturer's protocol, added to the glycan sample, and left at room temperature away from light for 10 min. Labelled samples were washed three times with 950 µL acetone and centrifuged at 18,000 x *g* for 5 min. Samples were dried using a centrifugal vacuum evaporator for 20 min at ambient temperature and subsequently stored dry at -20°C before use.

HPLC

Glycans were resuspended in 25 µL ddH_2O and transferred to glass vials where 75 µL of acetonitrile was added. Samples were centrifuged at max speed for one hour at 4°C to remove precipitant. HPLC was carried out using Thermo Scientific™ Ultimate™ 3000 UPLC systems with a 1.7 µm 2.1 x 150 mm AQUITY UPLC BEH Amide column (Waters) and fluorescence detection (excitation at 285 nm and emission at 345 nm). The flow rate was 0.5 mL min^{-1}. Mobile phase A was 100 mM ammonium formate, pH 4.4 and mobile phase B was 100% acetonitrile. Labeled glycans were separated at 60°C using a gradient elution. After an initial hold of 23% A for up to 25 min to remove the dye front, phase A was increased gradually from 23% to 39% over 42 to 48 min. The column was cleaned and reequilibrated between each run by rapidly increasing A from 39% to 90% over 1 min, holding at 90% A for 5 mins, rapidly decreasing A from 90% to 23% over 1 min, and finally holding at 23% A for 6 mins. HPLC data was processed using Thermo Fisher Chromeleon software.

Mass spectrometry

LC-MS was performed on a Thermo Scientific Q Exactive Orbitrap mass spectrometer with liquid chromatography conditions as described above. The electrospray ionization voltage was set at 3.5 kV and the capillary maintained at 350°C. The maximum injection time was 100 ms. Sheath gas and auxiliary gas flow rates were held at 25 mL min^{-1} and 10 mL min^{-1} respectively. Full MS was performed at a resolution of 70,000 and a scan range of 500–2500 m/z was used to detect glycan species. Mass spectrometry spectral

data were processed using Thermo XCalibur FreeStyle software. Glycoforms were assigned to MS peaks manually based on expected mass-to-charge ratios of IgG glycoforms (Table A-3) (Bereman et al., 2009), taking into account the mass of the conjugated dye (262.3 Da).

3.5 Results

Stability profiling of IgG subclasses by REES shows broad differences

Thirty-two trastuzumab variants each possessing a unique constant region allele (Figure 3-2A, B) containing equal numbers of tryptophan (Trp) residues were isolated at high purity following expression (Figure A-1). Homology modelling of IgG1 allelic variants, using template based Robetta software, predicted only minor structural differences despite the known influences of these mutations on antibody function (Table A-2, Figure A-2). We therefore concluded the contributions of allelic variation to variant structure and stability would be better captured by REES analysis of dynamic antibody flexibility. Fluorescent spectra were obtained before and after heating in a pH 8 buffer designed to induce destabilisation over a timescale amenable to analysis in a single day (Cheng et al., 2012) (Figure 3-3A). A recently developed thermodynamic model for REES was then fitted to the fluorescent data to extract values for $CSM(\lambda_{Ex}^{Fc})$ and ΔG_m that allow for biologically relevant insights to be drawn from the data (Figure 3-3B, Figure A-3) (Kwok et al., 2021). Specifically, $CSM(\lambda_{Ex}^{Fc})$ provides information about the degree of tryptophan residue exposure to the surrounding solvent (a measure of protein foldedness) and ΔG_m describes the rigidity of the protein, which is linked to the aggregation state.

Values of $CSM(\lambda_{Ex}^{Fc})$ and ΔG_m were calculated for the pre-heated samples to set a baseline for initial stability characteristics of each individual antibody. Subsequent increases in

$CSM(\lambda_{Ex}^{Fc})$ following heating are indicative of increased Trp exposure to the surrounding buffer and were observed for all variants tested. When assessed in conjunction with values of ΔG_m, insights into antibody unfolding dynamics and aggregation propensity are obtained. Associated decreases in ΔG_m suggest greater flexibility indicating partial unfolding whereas increases in ΔG_m indicate loss of flexibility due to aggregation.

A

	Domain	CH1						Hinge				CH2							CH3												
	EU#	137	138	189	192	193	214					274	282	291	296	309	327	339	356	358	378	379	384	387	392	397	409	419	422	431	435	436
IgG1	1*01	G	G	P	S	L	K					K	V	P	Y	L	A	A	D	L	A	V	N	P	K	V	K	Q	V	A	H	Y
	1*03	G	G	P	S	L	R					K	V	P	Y	L	A	A	E	M	A	V	N	P	K	V	K	Q	V	A	H	Y
	1*04	G	G	P	S	L	K					K	V	P	Y	L	A	A	D	L	A	V	N	P	K	V	K	Q	I	A	H	Y
	1*07	G	G	P	S	L	K					K	V	P	Y	L	A	A	D	L	A	V	N	P	K	V	K	Q	V	G	H	Y
	1*08	G	G	P	S	L	R					K	V	P	Y	L	A	A	D	L	A	V	N	P	K	V	K	Q	V	A	H	Y
	1*11	G	G	P	S	L	K					K	V	P	Y	V	A	A	D	L	A	V	N	P	K	V	K	Q	V	A	H	Y
	1*13	G	G	P	S	L	K					K	V	P	F	L	A	A	D	L	A	V	N	P	K	V	K	Q	V	A	H	Y
IgG2	2*01	E	S	P	N	F	T					Q	V	P	F	V	G	T	E	M	A	V	N	P	K	M	K	Q	V	A	H	Y
	2*02	E	S	T	N	F	T					Q	M	P	F	V	G	T	E	M	A	V	N	P	K	M	K	Q	V	A	H	Y
	2*04	E	S	P	S	L	T					Q	V	P	F	V	G	T	E	M	A	V	N	P	K	M	K	Q	V	A	H	Y
	2*06	E	S	P	N	F	T					Q	V	P	F	V	G	T	E	M	S	V	N	P	K	M	K	Q	V	A	H	Y
	2*09	G	G	P	N	F	T					Q	V	P	F	V	G	T	E	M	A	V	N	P	K	M	K	Q	V	A	H	Y
	2*11	E	S	P	N	F	T					Q	V	P	F	L	G	T	E	M	A	V	N	P	K	M	K	Q	V	A	H	Y
	2*15	E	S	P	N	F	T					Q	V	P	F	V	G	T	E	M	A	V	N	P	N	M	K	Q	V	A	H	Y
IgG3	3*01	G	G	P	S	L	R	H1	H2	H3	H4	Q	V	P	Y	L	A	T	E	M	A	V	S	P	N	M	K	Q	I	A	R	F
	3*03	G	G	P	S	L	R	H1		H3	H4	Q	V	P	Y	L	A	T	E	M	A	V	S	P	N	V	R	E	V	A	R	F
	3*04	G	G	P	S	L	R	H1			H4	Q	V	P	Y	L	A	T	E	M	A	V	S	P	N	M	K	Q	I	A	R	F
	3*06	G	G	P	S	L	R	H1	H2	H3	H4	Q	V	P	Y	L	A	T	E	M	A	V	S	P	K	M	K	Q	I	A	R	F
	3*08	G	G	P	S	L	R	H1	H2	H3	H4	Q	V	P	Y	L	A	T	E	M	A	V	N	P	N	M	K	Q	I	A	R	F
	3*09	G	G	P	S	L	R	H1	H2	H3	H4	Q	V	P	Y	V	A	T	E	M	A	V	S	P	N	M	K	Q	I	A	R	F
	3*11	G	G	P	S	L	R	H1	H2	H3	H4	Q	V	P	F	L	A	T	E	M	A	V	S	P	N	M	K	Q	I	A	R	F
	3*12	G	G	P	S	L	R	H1	H2		H4	Q	V	P	F	L	A	T	E	M	A	V	S	P	N	M	K	Q	I	A	R	F
	3*13	G	G	P	S	L	R	H1	H2	H3	H4	Q	V	P	Y	L	A	T	E	M	A	V	S	P	K	M	K	E	I	A	R	F
	3*14	G	G	P	S	L	R	H1	H2	H3	H4	Q	V	L	Y	L	A	T	E	M	A	V	N	P	N	M	K	Q	I	A	R	Y
	3*15	G	G	P	S	L	R	H1	H2	H3	H4	Q	V	L	Y	L	A	T	E	M	A	V	N	P	K	M	K	Q	I	A	R	Y
	3*16	G	G	P	S	L	R	H1	H2	H3	H4	Q	V	L	Y	L	A	A	E	M	A	V	N	P	N	M	K	Q	I	A	R	Y
	3*17	G	G	P	N	F	R	H1		H3	H4	Q	V	P	Y	L	A	T	E	M	A	M	S	P	K	V	K	Q	I	A	H	Y
	3*20	G	G	P	S	L	R	H1	H2	H3	H4	Q	V	L	Y	L	A	T	E	M	A	V	N	R	N	M	K	Q	I	A	R	Y
	3*22	G	G	P	S	L	R	H1	H2	H3	H4	Q	V	L	Y	L	A	T	E	M	A	V	N	P	N	M	K	Q	I	A	H	Y
	3*24	G	G	P	S	L	R	H1	H2	H3	H4	Q	V	P	Y	L	A	T	E	M	A	V	N	P	K	M	K	Q	I	A	R	Y
	3*25	G	G	P	S	L	R	H1	H2	H3	H4	K	V	L	Y	L	A	T	E	M	A	V	N	P	N	M	K	Q	I	A	R	Y
	3*26	G	G	P	S	L	R	H1	H2	H3	H4	Q	V	P	F	L	G	T	E	M	A	V	S	P	N	M	K	Q	I	A	R	F

B

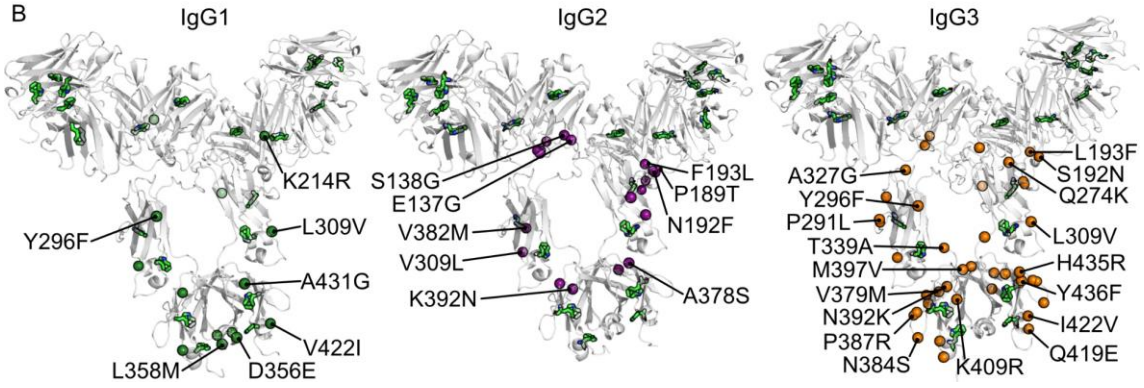

Figure 3-2. Amino acid polymorphisms in IgG1, IgG2 and IgG3 constant heavy chain alleles. (A) Amino acid position is given based on the EU numbering and divided into the three constant domains and hinge. The hinge sequence is identical for IgG1 and IgG2 alleles. The number of hinge exons differs for IgG3 alleles; H1-4 denotes what exon is present in each allele. Allelic variations are highlighted yellow. (B) Allele polymorphisms are mapped onto representative models of full-length IgG1, IgG2, and IgG3 generated using Robetta structural prediction software. Tryptophan residues are distributed throughout the structure and are highlighted in green.

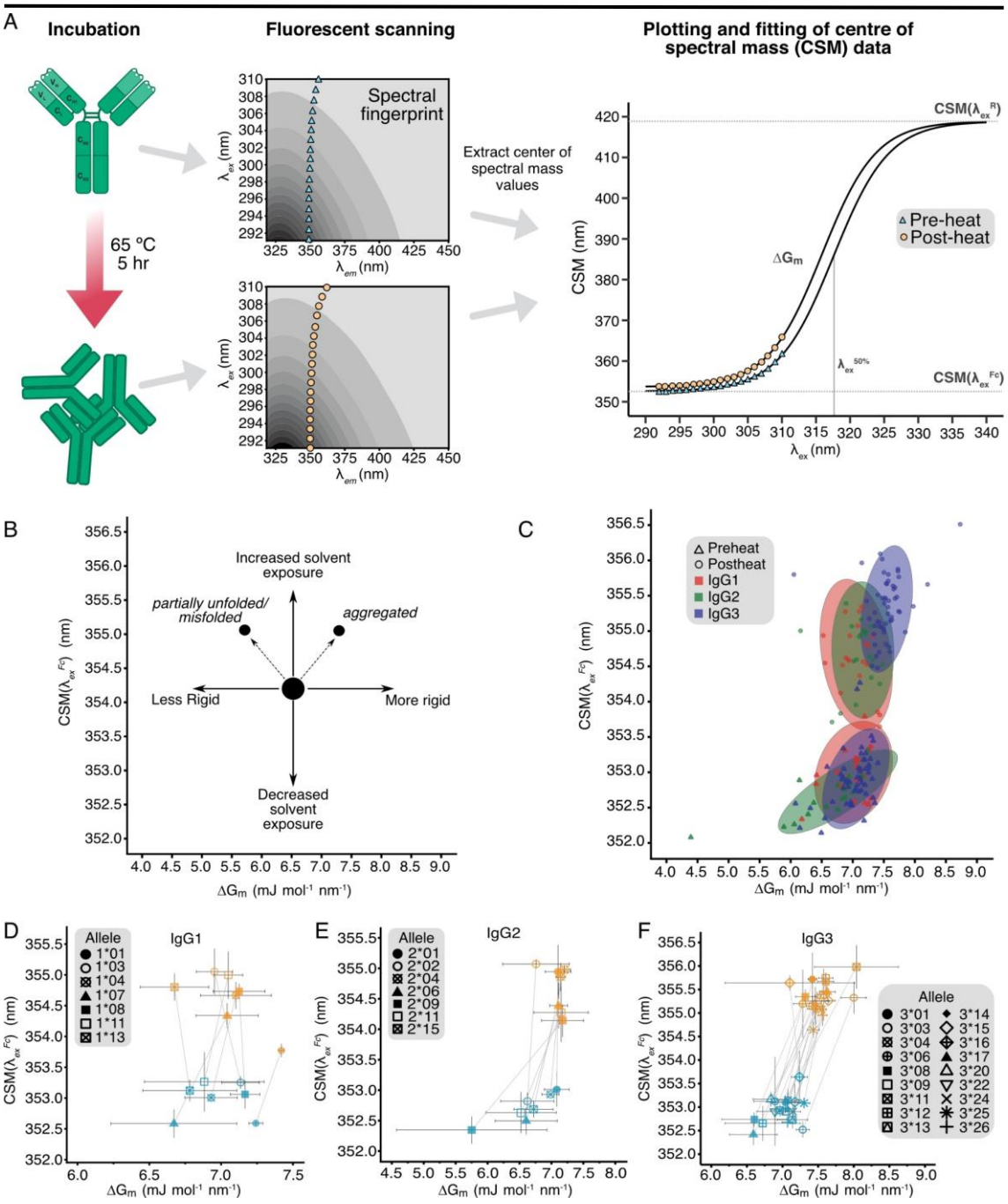

Figure 3-3. REES analysis of 32 trastuzumab constant region variants. (A) Overview of the REES method: (left) depiction of the state of the antibody measured in each condition, (middle) examples of the emission/excitation matrices of tryptophan residues in the pre- and post-heat samples, contoured from high (black) to low (light grey) fluorescent intensity, (right) model fitting to obtain $\boldsymbol{CSM}(\boldsymbol{\lambda_{Ex}^{Fc}})$ and ΔG_m values from the centre of spectral mass data. (B) Description of the physical state of the antibody given a corresponding directional shift in $\boldsymbol{CSM}(\boldsymbol{\lambda_{Ex}^{Fc}})$ and ΔG_m values from the native state. (C) $\boldsymbol{CSM}(\boldsymbol{\lambda_{Ex}^{Fc}})$ verses ΔG_m for native (circle) and heat stressed (triangle) antibodies from all subclasses; IgG1 (red), IgG2 (green) and IgG3 (blue). Datapoints are of each triplicate measurement for each antibody sample. The coloured ellipses show the clustering of 95% of the data for a given subclass and condition. (D-F) $\boldsymbol{CSM}(\boldsymbol{\lambda_{Ex}^{Fc}})$ verses ΔG_m plots of antibodies in subclasses IgG1-3, respectively. For each allele, the native antibody state (blue) is connected to the heat stressed state (orange).

The value of the centre of spectral mass (CSM) of the completely relaxed state of emission ($CSM(\lambda_{Ex}^{R})$) was obtained by global fitting of data collected between λ_{Ex} = 292 - 310 nm (Kwok et al., 2021) and was 418.9 ± 3 nm for our trastuzumab variants. Individual variant fits all displayed regression p-values of less than 0.05 (Figure A-3). Within individual subclasses, IgG1 and IgG2 variants shared similar structural dynamics with post-heat $CSM(\lambda_{Ex}^{Fc})$ values clustered around 354.6 ± 0.5 and 354. 7 ± 0. 5 nm, respectively, while IgG3 variants exhibited larger post-heat $CSM(\lambda_{Ex}^{Fc})$ values centred around 355.3 ± 0.4 nm ($p < 0.001$) (Figure 3-3C). This trend was likewise consistent for post-heat ΔG_m values; IgG1 and IgG2 variants had average post-heat ΔG_m values of 7.1 ± 0.3 and 7.1 ± 0.3 mJ mol^{-1} nm^{-1}, significantly lower than ΔG_m = 7.5 ± 0.3 mJ mol^{-1} nm^{-1} ($p < 0.001$) for IgG3 variants.

Subclass stability rankings were supported by differential scanning fluorimetry (DSF) for a subset of the antibody alleles measured. DSF curves for each variant showed two unfolding transitions characteristic of IgG antibodies (Figure A-4) (Damelang et al., 2019; Ito & Tsumoto, 2013; Richardson et al., 2019). On average, the first transition (T_m1) of IgG3 variants was 66.3 ± 1.5 °C, significantly lower than 69.7 ± 0.5 and 69 ± 0.5 °C for IgG1 and IgG2 variants respectively ($p < 0.001$, Table 3-1). Similarly, the second transition (T_m2) for IgG3 variations (76.8 ± 0.7°C) was significantly lower ($p = 0.016$) than IgG1 T_m2 (79.7 ± 0.1°C). The average T_m2 values for IgG2 and IgG3 variants fell within the margin of error. Within each subclass, only differences in T_m1 values were distinguishable between allelic variants. IgG1 variant 1*01 had the highest T_m1 of 70.1 ± 0.2°C, significantly higher than the T_m1 = 69.3 ± 0.1°C for 1*11 ($p = 0.0079$). Likewise, 3*17 exhibited the highest T_m1 of 68.5 ± 0.1°C, significantly higher ($p < 0.01$) than all other IgG3 variants tested. There were no discernible differences between the IgG2 variants tested, nor for three of the IgG3 variants (3*03, 3*09, 3*16).

Table 3-1. Differential scanning fluorimetry measurements using SYPRO orange dye of melting transitions of eight unique variants. Reported as the average and standard deviation of triplicate measurements. Measurements were averaged across each subclass to determine average melting transition data per subclass.

Allele	Tm1		Tm2	
1*01	70.1	± 0.2	79.7	± 0.1
1*11	69.3	± 0.1	79.7	± 0.1
2*04	69.3	± 0.3	74.9	± 3.4
2*09	68.6	± 1.2	79.6	± 0.0
3*03	65.4	± 0.2	75.8	± 2.2
3*09	65.5	± 0.2	76.7	± 1.0
3*16	65.9	± 1.0	77.3	± 0.5
3*17	68.5	± 0.1	77.3	± 1.3
IgG1 average	69.7	± 0.5	79.7	± 0.1
IgG2 average	69.0	± 0.5	77.2	± 3.4
IgG3 average	66.3	± 1.5	76.8	± 0.7

REES analysis reveals individual allelic stability fingerprints

IgG1 allelic variation

Having identified trends in stability at the subclass level, we profiled the relative stabilities of individual antibody constant region alleles. Within the panel of IgG1 variants, significant differences were evident in the pre-heated $CSM(\lambda_{Ex}^{Fc})$ values indicating differing levels of Trp exposure in the native state (Figure 3-3D). Variants 1*07 and 1*01 had respective pre-heated $CSM(\lambda_{Ex}^{Fc})$ values of 352.6 ± 0.5 and 352.6 ± 0 nm, the lowest of all the IgG1 variants. These values were distinct from variants 1*03 and 1*11 which had respective $CSM(\lambda_{Ex}^{Fc})$ values of 353.3 ± 0.1 and 353.3 ± 0.5 nm ($p < 0.05$). However, ΔG_m was not significantly different between any of these variants. After heating, 1*01 had the smallest increase in $CSM(\lambda_{Ex}^{Fc})$ of all antibody alleles ($\Delta CSM(\lambda_{Ex}^{Fc})$ = 1.2 ± 0.1 nm) and only a slight increase in ΔG_m ($\Delta\Delta G_m$ = 0.2 ± 0.1 mJ mol^{-1} nm^{-1}) (Figure 3-4). Together these values suggest a high tolerance to temperature induced unfolding and aggregation and indicate 1*01 is the most stable of the tested alleles. By comparison, 1*03 had a much larger increase in $CSM(\lambda_{Ex}^{Fc})$ of 1.8 ± 0.4 nm ($p = 0.051$) and a decrease in ΔG_m of 0.2 ± 0.2 mJ mol^{-1} nm^{-1} indicating greater solvent exposure of Trp after heating likely due to unfolding.

IgG2 allelic variation

Compared to IgG1, IgG2 variants exhibited more variation in the measured REES profiles (Figure 3-3E and Figure 3-4). The native IgG2 variants all displayed similar $CSM(\lambda_{Ex}^{Fc})$ and ΔG_m profiles with the exception of 2*09 which had a pre-heated $CSM(\lambda_{Ex}^{Fc})$ of 352.3 ± 0.2 nm that was significantly lower than 2*01 ($CSM(\lambda_{Ex}^{Fc})$ = 353.0 ± 0.3 nm, $p = 0.034$). Despite similar pre-heat REES profiles, differences in the magnitude of change for $CSM(\lambda_{Ex}^{Fc})$ suggested unique thermostability fingerprints for IgG2 variants. After heating, 2*11 had the smallest $\Delta CSM(\lambda_{Ex}^{Fc})$ of 1.6 ± 0.2 nm relative to 2*02 ($\Delta CSM(\lambda_{Ex}^{Fc})$ = 2.3 ± 0.2 nm, $p = 0.0091$) and 2*15 variants ($\Delta CSM(\lambda_{Ex}^{Fc})$ = 2.3 ± 0.1 nm, $p = 0.0053$). However, there were no significant differences between the changes in ΔG_m for these variants. We also note 2*09 and 2*01 variants showed similar increases in $CSM(\lambda_{Ex}^{Fc})$ of 1.8 ± 0.1 and 2 ± 0.2 nm, respectively, despite differences in pre-heat values. The increase in ΔG_m for 2*09 after heating was 1.4 ± 0.9 mJ mol^{-1} nm^{-1} which was significantly larger than 2*01 ($\Delta\Delta G_m$ = 0.02 ± 0.4 mJ mol^{-1} nm^{-1}, $p = 0.012$), 2*02 ($\Delta\Delta G_m$ = 0.1 ± 0.1 mJ mol^{-1} nm^{-1}, $p = 0.023$) and 2*04 ($\Delta\Delta G_m$ = 0.2 ± 0.1 mJ mol^{-1} nm^{-1}, $p = 0.026$).

IgG3 allelic variation

IgG3 variants in the native, pre-heated state exhibited similar $CSM(\lambda_{Ex}^{Fc})$ and ΔG_m values to each other with a few exceptions (Figure 3-3F). Variant 3*16 had the highest pre-heated $CSM(\lambda_{Ex}^{Fc})$ value of 353.6 ± 0.6 nm, illustrating a state of Trp solvent exposure distinct from variants 3*17 and 3*03 ($CSM(\lambda_{Ex}^{Fc})$ = 352.4 ± 0.2, $p = 0.0075$ and 352.5 ± 0.2 nm, p = *0.021*, respectively*)*. The structural rigidity represented by ΔG_m, however, appeared to be within the margin of error between these alleles. After heating, the magnitude of change for $CSM(\lambda_{Ex}^{Fc})$ and ΔG_m differed between variants (Figure 3-4). IgG3*24 showed the smallest shift in $CSM(\lambda_{Ex}^{Fc})$, increasing by only 1.7 ± 0.04 nm to 352.9 ± 0.2 nm. This was significantly smaller than eight other IgG3 variants (3*01, *03, *04, *08, *09, *11, *13, and *17, $p < 0.05$*).* Variants 3*11 and 3*17 appeared to be the least stable, with values of $CSM(\lambda_{Ex}^{Fc})$ increasing by 3.1 ± 0.4 and 3.0 ± 0.2 nm, respectively. This increase was significantly greater than eight other IgG3 alleles (3*06, *14, *15, *16, *20, *22, *24 and *25, $p < 0.05$*).* The values of ΔG_m for 3*11 and 3*17 increased by 1.1 ± 0.7 and 1.0 ± 0.4 mJ mol^{-1} nm^{-1}, respectively, distinctly larger increases than the most stable IgG3 variant, 3*16 ($\Delta\Delta G_m$ = -0.1 ± 0.8 mJ mol^{-1} nm^{-1}, $p = 0.011$ *and 0.016*, respectively).

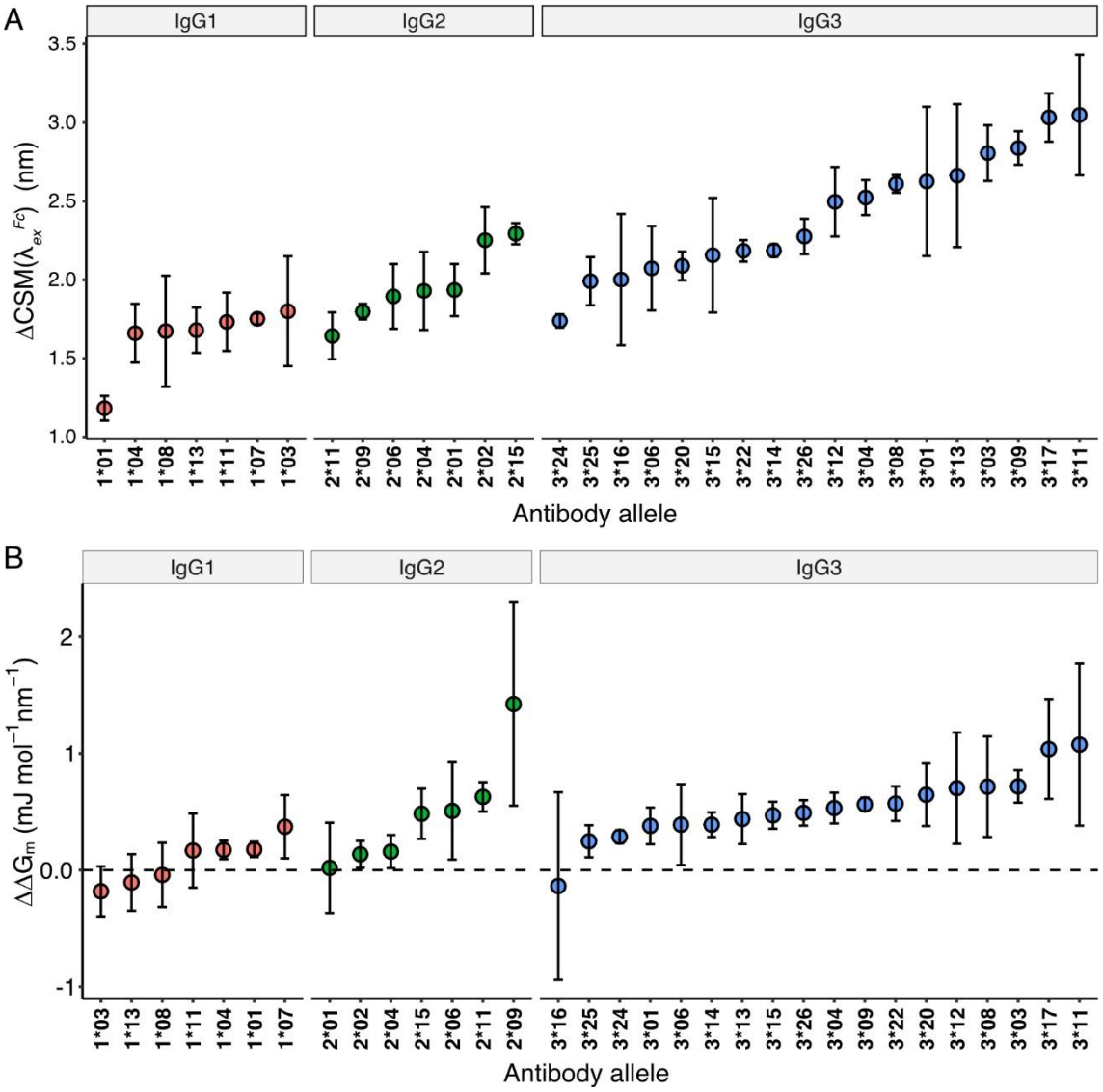

Figure 3-4. The magnitude of change in (A) $CSM(\lambda_{Ex}^{Fc})$ and (B) ΔG_m values for each allele after heating. Data is presented in ascending order of change within each subclass.

Specific amino acid substitutions explain differences in REES profiles

Specific amino acid mutations are known to play a direct role in antibody domain stabilisation (Saito et al., 2019; Teplyakov et al., 2013). We therefore undertook a systematic analysis to correlate REES stability metrics with amino acid substitutions present in the IgG3 variant panel (possessing the greatest number of individual alleles with shared mutations) (Figure 3-2A). Polymorphisms at positions 192, 193, 291, 379, 384 and 397 (Figure 3-5A) were significantly correlated to changes in both $CSM(\lambda_{Ex}^{Fc})$ and ΔG_m, (Figure 3-5B, C, Figure A-5). Of particular interest is residue 397 as it is located

at the interface between the CH3 domains (Figure A-6), suggesting a possible role in stabilising the antibody structure (Rispens et al., 2014). IgG3 alleles harbor a methionine (Met) or valine (Val) at this position. Variants with Met-397 had an average increase in $CSM(\lambda_{Ex}^{Fc})$ of 2.3 ± 0.4 nm, a smaller increase compared to variants with Val-397 ($\Delta CSM(\lambda_{Ex}^{Fc})$= 2.9 ± 0.2 nm, $p = 0.00136$). Met-397 variants also had a smaller increase in $\Delta\Delta G_m$ of 0.5 ± 0.4 mJ mol^{-1} nm^{-1} compared to 0.9 ± 0.3 mJ mol^{-1} nm^{-1}, $p = 0.02$ (Figure 3-5B, C).

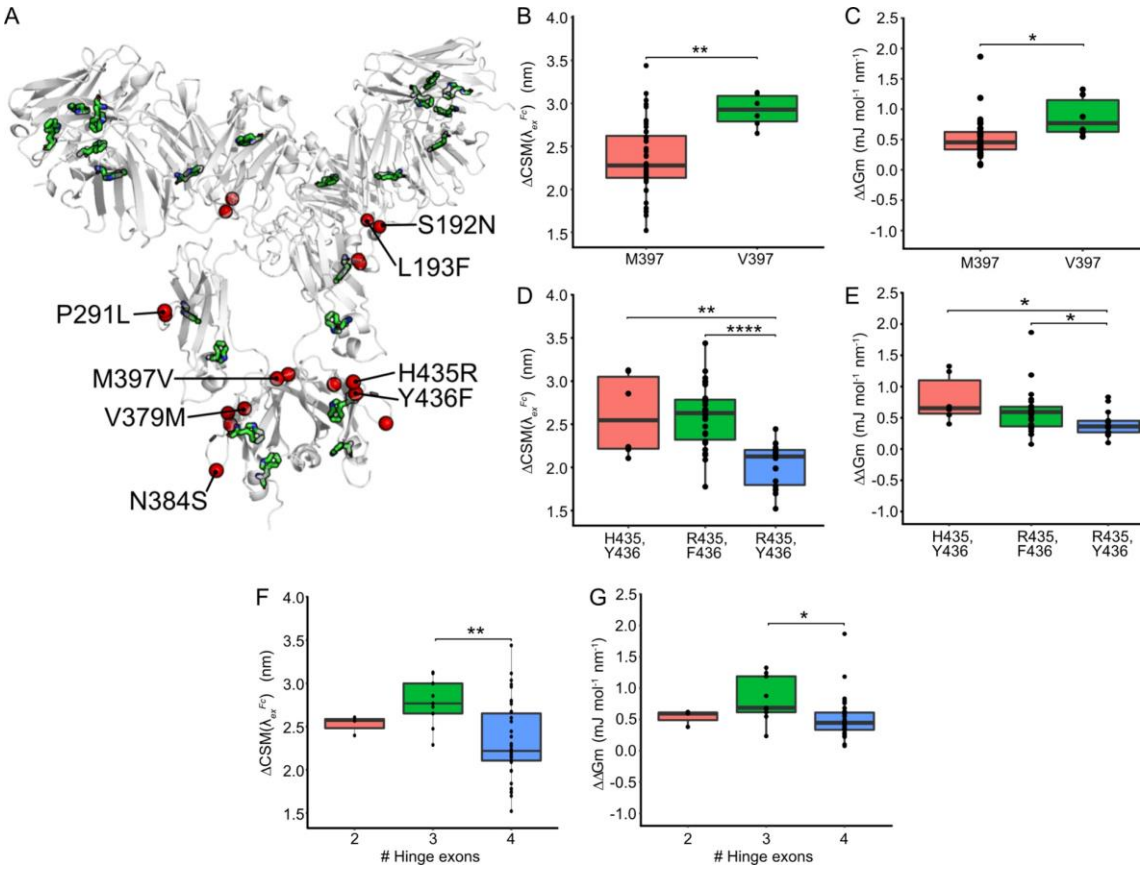

Figure 3-5. Effect of allelic variation on stability. Data is for IgG3 alleles only. (A) Structural map of amino acid substitutions found in IgG3 alleles (red spheres) that significantly correlated to stability. The location of Trp residues are also shown (green sticks). (B-G) The magnitude of change in $\boldsymbol{CSM(\lambda_{Ex}^{Fc})}$ and ΔG_m for amino acid variants at position 397 (B, C), positions 435 and 436 combined (D, E) and hinge length variants (F, G) as measured using REES. Statistical significance was tested by one-way ANOVA with Tukey posthoc multiple comparison testing. * $p < 0.05$, ** $p < 0.01$, *** $p < 0.001$, **** $p < 0.0001$.

We further interrogated the influence of combinations of allelic mutations. This analysis revealed the influence of amino acid mutations at positions 435 and 436 of the IgG3 CH3

domain. Three combinations of alleles are observed within the IgG3 subclass; His-435 and Tyr-436, Arg-435 and Tyr-436, or Arg-435 and Phe-436. Upon exposure to heat, Arg-435/Tyr-436 variants exhibited the smallest change in both $CSM(\lambda_{Ex}^{Fc})$ (2.0 ± 0.3 nm) and ΔG_m (0.3 ± 0.4 J mol^{-1} nm^{-1}) compared to His-435/Tyr-436 ($\Delta CSM(\lambda_{Ex}^{Fc})$ = 2.6± 0.5 nm, $p = 0.0018$, $\Delta\Delta G_m$ = 0.8 ± 0.4 J mol^{-1} nm^{-1}, $p = 0.018$) and Arg-435/Phe-436 ($\Delta CSM(\lambda_{Ex}^{Fc})$ = 2.6 ± 0.4 nm, $p < 0.001$, $\Delta\Delta G_m$ = 0.6 ± 0.4 J mol^{-1} nm^{-1}, $p = 0.032$) variants (Figure 3-5D, E). These small differences in REES parameters suggest the Arg-435/Tyr-436 variant is significantly more resistant to heat induced aggregation than either His-435/Tyr-436 and Arg-435/Phe-436 variants, indicating these mutations likely confer greater stability.

Finally, we investigated the influence of IgG3 hinge length on stability. The hinge length of IgG3 alleles varies significantly depending on the number of hinge exons present (H1-4) (Figure 3-2A). Differences in stability were evident between variants with three hinge exons and those with four. Four-exon variants had significantly smaller changes in REES parameters ($\Delta CSM(\lambda_{Ex}^{Fc})$ = 2.3 ± 0.4 nm and $\Delta\Delta G_m$ = 0.5 ± 0.4 mJ mol^{-1} nm^{-1}) compared to variants with three exons ($\Delta CSM(\lambda_{Ex}^{Fc})$ = 2.9 ± 0.3 nm, $p = 0.0084$ and $\Delta\Delta G_m$ = 0.8 ± 0.4 mJ mol^{-1} nm^{-1}, $p = 0.037$) (Figure 3-5F, G). Variants with two hinge exons reported values in between ($\Delta CSM(\lambda_{Ex}^{Fc})$ = 2.5 ± 0.1 nm and $\Delta\Delta G_m$ = 0.5 ± 0.1 mJ mol^{-1} nm^{-1}).

Antibody variants share heterogenous glycosylation patterns regardless of sequence

To confirm that observed stability differences were a result of allelic point mutations and not glycan structural differences, we performed high-resolution glycosylation analysis for each variant. Mass spectrometry revealed individual variants from all subclasses shared largely similar heterogeneous glycan profiles consistent with those reported for clinical trastuzumab antibodies (Figure A-7A) (Segu et al., 2020). The glycan profiles were dominated by core-fucosylation (fucose attached to the main chain of the glycan structure, e.g. G0 F, G1 F) and varying degrees of terminal galactosylation (galactose appended to the antennae of the glycan, e.g. G0, G1, G2) (Figure 3-6, Table A-3). In some cases, G0 F structures were present at up to 57.5% of the total glycan content. We also observed a varying degree of mannosylation (e.g. M5, M6, M7) with some bias towards higher levels in IgG2 antibodies. The five most prevalent glycoforms across all of the antibody alleles, in order of decreasing abundance, were G0 F > G1 Fa ≥ M5 > G1 Fb > G2 F. G1 F is present in two isoforms that differ in the position of the terminal galactose residue (G1 Fa (a (1,6)) and G1 Fb (b (1,3))). We detected differences in the ratio of G1 Fa: G1 Fb

isoforms between antibody variants. Variants with Phe-296 (all IgG2 variants, 1*13, 3*11, 3*12, and 3*26) had an equal abundance of each G1 F isoform whereas all variants with Tyr-296 had three to four times more G1 Fa compared to G1 Fb. Despite variation in the abundance of G1 F isoforms and minor variation between other glycan species, no significant correlations were detected between glycosylation patterns and the $\Delta CSM(\lambda_{Ex}^{Fc})$ and $\Delta\Delta G_m$ values measured by REES (Figure A-7B).

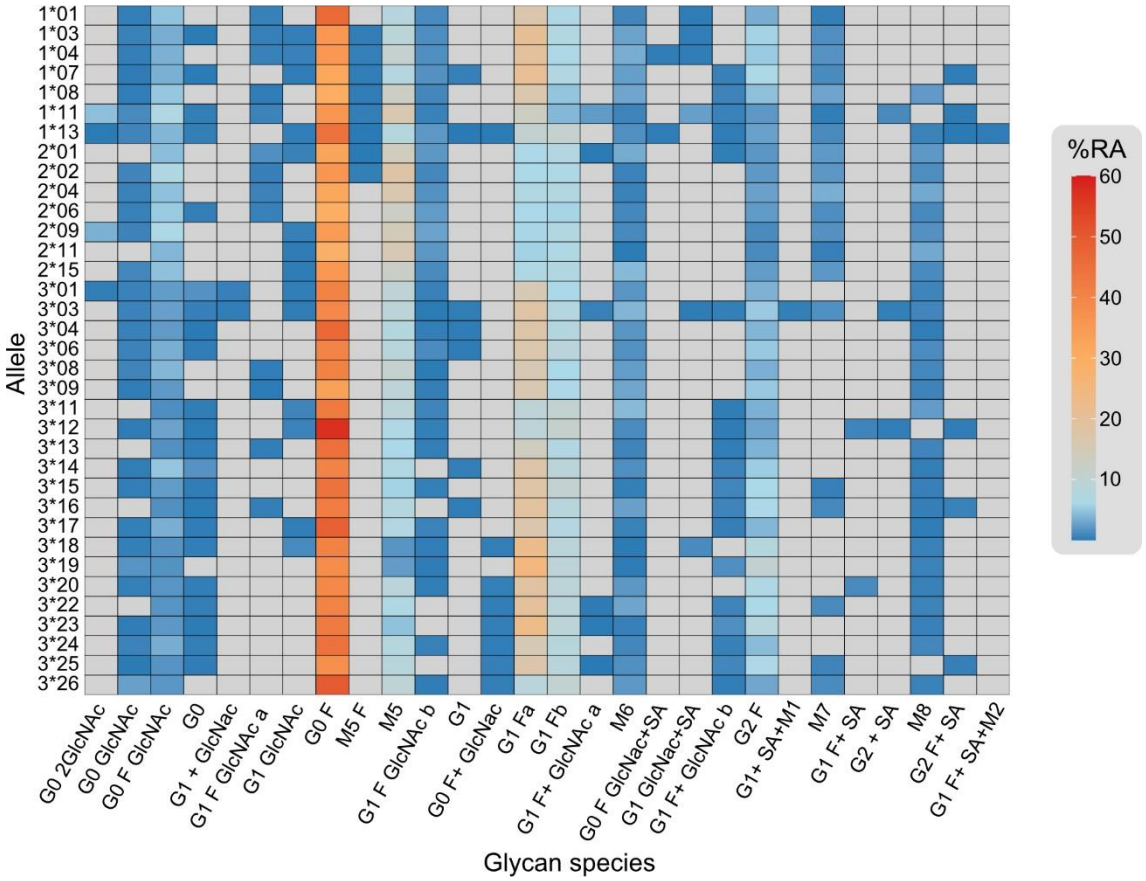

Figure 3-6. Heatmap showing the relative abundance (RA) of each glycoform appended to each unique antibody. The colour scale (right) shows the relative abundance as a percentage. Grey cells are present where the glycoform was not detected or had less than 0.05% RA. Actual RA percentages are shown in Table A-3.

3.6 Discussion

Recent high-resolution interrogation of the constant region locus has revealed significant population-linked allelic diversity within antibody subclasses. As therapeutic mAb designs are increasingly exploring alternative antibody constant region scaffolds, we report here the relative thermal stability of 32 constant region alleles from IgG1, IgG2, and IgG3 subclasses, which is one key determinant of mAb developability. We used red edge excitation shift spectroscopy to provide information about antibody structural dynamics and found broad differences between each antibody subclass that were supported by differential scanning fluorimetry (DSF) measurements. In addition, we describe striking differences between certain individual alleles of the same subclass (Figure 3-3D-F). These differences were not contingent on glycan pattern differences between each antibody. Further analysis of our REES data resolved the significant contribution of specific groups of point mutations to overall stability including at positions 435/436 which are known to contribute to antibody half-life.

While REES has been used for broad profiling of clinical mAb stabilities (Knight et al., 2020), there have been limited reports on the resolution of differences at the point mutation level. Other techniques offer potentially higher resolution for stability analysis but few are as accessible and high-throughput as REES. Despite these advantages, REES remains unsuitable for the comparative analysis of proteins with different tryptophan content. In this study, three IgG3 allelic variants were excluded from the analysis due to extra tryptophan residues arising from an Arg>Trp mutation in the CH2 domains. Care should also be taken to ensure high quality spectra are obtained from buffer blank samples to eliminate confounding Raman scattering effects.

Nonetheless, the results of our REES analysis show clear differences in stability between the subclasses, with IgG3 exhibiting poorer stability than IgG1 and IgG2 isotypes in alignment with other studies (Garber & Demarest, 2007). The REES data suggests IgG3 antibodies have greater hydrophobic residue exposure to the surrounding aqueous environment and a loss of structural flexibility following heat stress, indicative of aggregation. Our findings confirm existing concerns around the stability of IgG3 antibodies, which alongside poor half-life, have hindered their utility as therapeutic mAbs despite offering strong neutralisation activity against pathogens and eliciting potent ADCP and ADCC effector functions (Bruhns et al., 2009; Damelang et al., 2019; Richardson et al., 2019; Tay et al., 2016). Variants belonging to the IgG1 and IgG2

subclasses had relatively similar stability profiles and showed greater resistance to aggregation compared to IgG3. The development of antibody-products with reduced effector function, such as where neutralisation is desired, has led to a rise in the prevalence of IgG2 mAbs (Andualem et al., 2020; Doñate et al., 2016). IgG4 mAbs are also increasing in clinical popularity but this subclass was not tested in this study due to a lack of complete allelic sequences in the IMGT database. As the number of alleles continues to increase, future REES studies will help to illuminate the relative stability and profile the unique heavy chain exchange dynamics of this isotype.

Despite a relatively large uncertainty in certain variant measurements, REES nonetheless provided sufficient resolution to allow us to rapidly identify differences in stability between individual allelic variants, particularly where no discernible differences were detected by DSF. Crucially, these differences were not due to glycan heterogeneity between alleles and glycan species proportions closely matched those previously reported (Chen & Flynn, 2007; Raju & Jordan, 2012; Segu et al., 2020). Within the IgG1 subclass, allelic variant 1*01 was the most stable of all the IgG1 variants and already the allele of choice for the majority of clinical mAbs alongside 1*03, 1*07 and 1*08 (Brader et al., 2015; Rispens et al., 2014). Clinically approved IgG2 mAbs predominantly use 2*01 allele scaffolds (e.g. evolocumab, tezepelumab) although we note crizanlizumab and gevokizumab use the 2*02 allele (Poiron et al., 2010; Wilkinson & Hale, 2022). These IgG2 allelic variants possessed unique REES profiles showing evidence of unfolding (increased hydrophobic residue exposure) accompanied by only small changes in structural rigidity, potentially suggesting minimal aggregate formation. Further investigation is required to elucidate the nature of structural changes occurring to produce these REES profiles. Clinical approval for IgG3 antibodies has remained elusive, with the vast genetic diversity between alleles a major concern for stability and potential immunogenicity in therapeutic settings (Jefferis, 2007; Salfeld, 2007). Our results show a diverse profile of conformational stability between IgG3 allelic variants with 3*11 and 3*17 exhibiting the greatest aggregation propensities and longer hinge region variants demonstrating improved thermal stability (Figure 3-5F, G). While the first transition temperature for 3*17 was measured to be the highest of the IgG3 variants tested by DSF, we note that the relationship between conformational stability and aggregation propensity is highly complex for multi-domain antibody structures and transition temperatures do not always align with aggregation rates depending on experimental conditions (Brader et al., 2015). Embracing this naturally occurring sequence variation, particularly within the

IgG3 subclass, could aid targeted mAb therapies (Richardson et al., 2019; Rispens et al., 2014; Stapleton et al., 2011) and potentially unlock mAbs that exploit unique functional capabilities (Tay et al., 2016). Despite the presence of allelic mutations distal to the CH1-VH interface (Figure 3-2B), further studies using variable domains from clinical antibodies beyond trastuzumab will improve our understanding of variant influence on stability, especially since several reports indicate possible variable domain influence on constant region function (Tang et al., 2021).

Analysis exploiting the conservation of mutations across multiple alleles within the IgG3 subclass provided insights into potential mechanisms behind variant stability rankings. For example, position 435 within IgG3 alleles harbors either a histidine or an arginine and is known to influence binding to the neonatal Fc receptor (DeLano et al., 2000; Stapleton et al., 2011). This position is closely linked to the adjacent position 436 which varies as either a tyrosine or a phenylalanine. Our observation of greater stability of variants with Arg-435/Tyr-436 mutations compared to those possessing Arg-435/Phe-436 or His-435/Tyr-436 mutations is likely due to a combination of factors. First, Arg-435 interacts with both Leu-251 and Ile-253 (Figure A-6), rather than Leu-251 alone, which could limit the motion of CH2 relative to the CH3 domain and thus create a more rigid structure than variants containing His-435 (Shah et al., 2017; Teplyakov et al., 2013). Second, we suggest that the hydroxyl group of Tyr-436 offers the potential for stabilising hydrogen bonds to form with Ser-426 and Gln-438; an interaction not available to Phe-436. The influence of other mutations on stability was less clear. For instance, IgG3*17 has valine at position 397 located in the CH3 dimerization interface (Figure A-6) which has been linked to altered C1q binding, fab-arm exchange, and propensity to aggregate (Natsume et al., 2008; Rispens et al., 2014). This mutation in combination with Lys-392 has been previously reported to reduce aggregation in IgG3 structures, albeit in different allelic backgrounds (Saito et al., 2019), in contrast to our observations of higher aggregation propensity. Given these differences it is likely that single point mutations significantly contribute to overall constant region stability.

To the best of our knowledge, this study represents the first comprehensive interrogation of constant region allelic stability for IgG1, IgG2, and IgG3. We expect further improvements can be made to enhance the resolution of the technique through improvements to spectrophotometers that can perform time-resolved REES measurements at faster timescales. More broadly, we anticipate REES having utility as a

rapid stability screening tool for antibody variants containing either natural or engineered diversity.

3.7 Supplementary Material

Supplementary Tables A-1 – A-4 and Figures A-1 – A-7 supporting this manuscript can be found in Appendix A: Supplementary Material for Chapter Three.

3.8 References

Andualem, H., Kiros, M., Getu, S., & Hailemichael, W. (2020). Immunoglobulin G2 Antibody as a Potential Target for COVID-19 Vaccine. *ImmunoTargets Ther*, *9*, 143–149. https://doi.org/10.2147/ITT.S274746

Aoyama, M., Hashii, N., Tsukimura, W., Osumi, K., Harazono, A., Tada, M., Kiyoshi, M., Matsuda, A., & Ishii-Watabe, A. (2019). Effects of terminal galactose residues in mannose α1-6 arm of Fc-glycan on the effector functions of therapeutic monoclonal antibodies. *MAbs*, *11*(5), 826–836. https://doi.org/10.1080/19420862.2019.1608143

Arbogast, L. W., Brinson, R. G., & Marino, J. P. (2015). Mapping Monoclonal Antibody Structure by 2D 13C NMR at Natural Abundance. *Anal Chem*, *87*(7), 3556–3561. https://doi.org/10.1021/ac504804m

Bartelds, G. M., de Groot, E., Nurmohamed, M. T., Hart, M. H., van Eede, P. H., Wijbrandts, C. A., Crusius, J. B., Dijkmans, B. A., Tak, P. P., & Aarden, L. (2010). Surprising negative association between IgG1 allotype disparity and anti-adalimumab formation: A cohort study. *Arthritis Res Ther*, *12*(6), R221. https://doi.org/10.1186/ar3208

Benucci, M., Damiani, A., Li Gobbi, F., Bandinelli, F., Infantino, M., Grossi, V., Manfredi, M., Noguier, G., & Meacci, F. (2018). Correlation between HLA haplotypes and the development of antidrug antibodies in a cohort of patients with rheumatic diseases. *Biol: Targets Ther*, *12*, 37–41. https://doi.org/10.2147/BTT.S145941

Bereman, M. S., Young, D. D., Deiters, A., & Muddiman, D. C. (2009). Development of a Robust and High Throughput Method for Profiling N-Linked Glycans Derived from Plasma Glycoproteins by NanoLC−FTICR Mass Spectrometry. *J Proteome Res*, *8*(7), 3764–3770. https://doi.org/10.1021/pr9002323

Brader, M. L., Estey, T., Bai, S., Alston, R. W., Lucas, K. K., Lantz, S., Landsman, P., & Maloney, K. M. (2015). Examination of Thermal Unfolding and Aggregation Profiles of a Series of Developable Therapeutic Monoclonal Antibodies. *Mol Pharmaceutics*, *12*(4), 1005–1017. https://doi.org/10.1021/mp400666b

Brinson, R. G., Marino, J. P., Delaglio, F., Arbogast, L. W., Evans, R. M., Kearsley, A., Gingras, G., Ghasriani, H., Aubin, Y., Pierens, G. K., Jia, X., Mobli, M., Grant, H. G., Keizer, D. W., Schweimer, K., Ståhle, J., Widmalm, G., Zartler, E. R., Lawrence, C. W., … Wikström, M. (2019). Enabling adoption of 2D-NMR for the higher order structure assessment of monoclonal antibody therapeutics. *MAbs*, *11*(1), 94–105. https://doi.org/10.1080/19420862.2018.1544454

Bruhns, P., Iannascoli, B., England, P., Mancardi, D. A., Fernandez, N., Jorieux, S., & Daëron, M. (2009). Specificity and affinity of human Fcγ receptors and their polymorphic variants for human IgG subclasses. *Blood*, *113*(16), 3716–3725. https://doi.org/10.1182/blood-2008-09-179754

Calonga-Solís, V., Malheiros, D., Beltrame, M. H., Vargas, L. B., Dourado, R. M., Issler, H. C., Wassem, R., Petzl-Erler, M. L., & Augusto, D. G. (2019). Unveiling the diversity of immunoglobulin gamma heavy chain constant region (IGHG) gene segments in Brazilian populations reveals twenty-eight novel alleles and evidence of gene conversion and natural selection. *Front Immunol*, *10*, 1161. https://doi.org/10.3389/fimmu.2019.01161

Catici, D. A., Amos, H. E., Yang, Y., van den Elsen, J. M., & Pudney, C. R. (2016). The red edge excitation shift phenomenon can be used to unmask protein structural ensembles: Implications for NEMO-ubiquitin interactions. *The FEBS J*, *283*(12), 2272–2284. https://doi.org/10.1111/febs.13724

Chen, X., & Flynn, G. C. (2007). Analysis of N-glycans from recombinant immunoglobulin G by on-line reversed-phase high-performance liquid chromatography/mass spectrometry. *Anal Biochem*, *370*(2), 147–161. https://doi.org/10.1016/j.ab.2007.08.012

Cheng, W., Joshi, S. B., He, F., Brems, D. N., He, B., Kerwin, B. A., Volkin, D. B., & Middaugh, C. R. (2012). Comparison of High-Throughput Biophysical Methods to Identify Stabilizing Excipients for a Model IgG2 Monoclonal Antibody: Conformational Stability and Kinetic Aggregation Measurements. *J Pharm Sci*, *101*(5), 1701–1720. https://doi.org/10.1002/jps.23076

Collins, A. M., Peres, A., Corcoran, M. M., Watson, C. T., Yaari, G., Lees, W. D., & Ohlin, M. (2021). Commentary on Population matched (pm) germline allelic variants of immunoglobulin (IG) loci: Relevance in infectious diseases and vaccination studies in human populations. *Genes Immun*, *22*(7), 7. https://doi.org/10.1038/s41435-021-00152-6

Damelang, T., Rogerson, S. J., Kent, S. J., & Chung, A. W. (2019). Role of IgG3 in infectious diseases. *Trends Immunol*, *40*(3), 197–211. https://doi.org/10.1016/j.it.2019.01.005

de Taeye, S. W., Bentlage, A. E. H., Mebius, M. M., Meesters, J. I., Lissenberg-Thunnissen, S., Falck, D., Sénard, T., Salehi, N., Wuhrer, M., Schuurman, J., Labrijn, A. F., Rispens, T., & Vidarsson, G. (2020). FcγR binding and ADCC activity of human IgG allotypes. *Front Immunol*, *11*(740). https://doi.org/10.3389/fimmu.2020.00740

DeLano, W. L., Ultsch, M. H., de, A. M., Vos, & Wells, J. A. (2000). Convergent Solutions to Binding at a Protein-Protein Interface. *Science*, *287*(5456), 1279–1283. https://doi.org/10.1126/science.287.5456.1279

Doñate, F., Raitano, A., Morrison, K., An, Z., Capo, L., Aviña, H., Karki, S., Morrison, K., Yang, P., Ou, J., Moriya, R., Shostak, Y., Malik, F., Nadell, R., Liu, W., Satpayev, D., Atkinson, J., Joseph, I. B. J., Pereira, D. S., … Stover, D. R. (2016). AGS16F Is a Novel Antibody Drug Conjugate Directed against ENPP3 for the Treatment of Renal Cell Carcinoma. *Clin Cancer Res*, *22*(8), 1989–1999. https://doi.org/10.1158/1078-0432.CCR-15-1542

Feige, M. J., Walter, S., & Buchner, J. (2004). Folding Mechanism of the CH2 Antibody Domain. *J Mol Biol*, *344*(1), 107–118. https://doi.org/10.1016/j.jmb.2004.09.033

Garber, E., & Demarest, S. J. (2007). A broad range of Fab stabilities within a host of therapeutic IgGs. *Biochem Biophys Res Commun*, *355*(3), 751–757. https://doi.org/10.1016/j.bbrc.2007.02.042

Giudicelli, V., Duroux, P., Ginestoux, C., Folch, G., Jabado-Michaloud, J., Chaume, D., & Lefranc, M.-P. (2006). IMGT/LIGM-DB, the IMGT® comprehensive database of immunoglobulin and T cell receptor nucleotide sequences. *Nucleic Acids Res*, *34*(suppl_1), D781–D784. https://doi.org/10.1093/nar/gkj088

Haldar, S., Chaudhuri, A., & Chattopadhyay, A. (2011). Organization and dynamics of membrane probes and proteins utilizing the red edge excitation shift. *J Phys Chem B*, *115*(19), 5693–5706. https://doi.org/10.1021/jp200255e

Higel, F., Seidl, A., Sörgel, F., & Friess, W. (2016). N-glycosylation heterogeneity and the influence on structure, function and pharmacokinetics of monoclonal antibodies and Fc fusion proteins. *Eur J Pharm Biopharm*, *100*, 94–100. https://doi.org/10.1016/j.ejpb.2016.01.005

Houde, D., & Engen, J. R. (2013). Conformational Analysis of Recombinant Monoclonal Antibodies with Hydrogen/Deuterium Exchange Mass Spectrometry. *Methods Mol Biol (Clifton, N.J.)*, *988*, 269. https://doi.org/10.1007/978-1-62703-327-5_17

Ito, T., & Tsumoto, K. (2013). Effects of subclass change on the structural stability of chimeric, humanized, and human antibodies under thermal stress. *Prot Sci*, *22*(11), 1542–1551. https://doi.org/10.1002/pro.2340

Jefferis, R. (2007). Antibody therapeutics: Isotype and glycoform selection. *Expert Opin Biol Ther*, *7*(9), 1401–1413. https://doi.org/10.1517/14712598.7.9.1401

Jefferis, R., & Lefranc, M.-P. (2009). Human immunoglobulin allotypes: Possible implications for immunogenicity. *MAbs*, *1*(4), 332–338. https://doi.org/10.4161/mabs.1.4.9122

Jones, H. B. L., Wells, S. A., Prentice, E. J., Kwok, A., Liang, L. L., Arcus, V. L., & Pudney, C. R. (2017). A complete thermodynamic analysis of enzyme turnover links the free energy landscape to enzyme catalysis. *FEBS J*, *284*(17), 2829–2842. https://doi.org/10.1111/febs.14152

Kaplon, H., Muralidharan, M., Schneider, Z., & Reichert, J. M. (2020). Antibodies to watch in 2020. *MAbs*, *12*(1), 1703531. https://doi.org/10.1080/19420862.2019.1703531

Karshikoff, A., Nilsson, L., & Ladenstein, R. (2015). Rigidity versus flexibility: The dilemma of understanding protein thermal stability. *FEBS J*, *282*(20), 3899–3917. https://doi.org/10.1111/febs.13343

Khatri, I., Berkowska, M. A., van den Akker, E. B., Teodosio, C., Reinders, M. J. T., & van Dongen, J. J. M. (2021). Population matched (pm) germline allelic variants of immunoglobulin (IG) loci: Relevance in infectious diseases and vaccination studies in human populations. *Genes Immun*, *22*(3), 172–186. https://doi.org/10.1038/s41435-021-00143-7

Knight, M. J., Woolley, R. E., Kwok, A., Parsons, S., Jones, H. B. L., Gulácsy, C. E., Phaal, P., Kassaar, O., Dawkins, K., Rodriguez, E., Marques, A., Bowsher, L., Wells, S. A., Watts, A., van den Elsen, J. M. H., Turner, A., O'Hara, J., & Pudney, C. R. (2020). Monoclonal antibody stability can be usefully monitored using the excitation-energy-dependent fluorescence edge-shift. *Biochem J*, *477*(18), 3599–3612. https://doi.org/10.1042/BCJ20200580

Krapp, S., Mimura, Y., Jefferis, R., Huber, R., & Sondermann, P. (2003). Structural Analysis of Human IgG-Fc Glycoforms Reveals a Correlation Between Glycosylation and Structural Integrity. *J Mol Biol*, *325*(5), 979–989. https://doi.org/10.1016/S0022-2836(02)01250-0

Kwok, A., Camacho, I. S., Winter, S., Knight, M., Meade, R. M., Van der Kamp, M. W., Turner, A., O'Hara, J., Mason, J. M., Jones, A. R., Arcus, V. L., & Pudney, C. R. (2021). A thermodynamic model for interpreting tryptophan excitation-energy-dependent fluorescence spectra provides insight into protein conformational sampling and stability. *Front Mol Biosci*, *8*, 778244. https://doi.org/10.3389/fmolb.2021.778244

Lin, J. C., Glover, Z. K., & Sreedhara, A. (2015). Assessing the Utility of Circular Dichroism and FTIR Spectroscopy in Monoclonal-Antibody Comparability Studies. *J Pharm Sci*, *104*(12), 4459–4466. https://doi.org/10.1002/jps.24683

Majumdar, R., Esfandiary, R., Bishop, S. M., Samra, H. S., Middaugh, C. R., Volkin, D. B., & Weis, D. D. (2015). Correlations between changes in conformational dynamics and physical stability in a mutant

IgG1 mAb engineered for extended serum half-life. *MAbs*, *7*(1), 84–95. https://doi.org/10.4161/19420862.2014.985494

More, A. S., Toth, R. T. th, Okbazghi, S. Z., Middaugh, C. R., Joshi, S. B., Tolbert, T. J., Volkin, D. B., & Weis, D. D. (2018). Impact of Glycosylation on the Local Backbone Flexibility of Well-Defined IgG1-Fc Glycoforms Using Hydrogen Exchange-Mass Spectrometry. *J Pharm Sci*, *107*(9), 2315–2324. https://doi.org/10.1016/j.xphs.2018.04.026

Natsume, A., In, M., Takamura, H., Nakagawa, T., Shimizu, Y., Kitajima, K., Wakitani, M., Ohta, S., Satoh, M., Shitara, K., & Niwa, R. (2008). Engineered Antibodies of IgG1/IgG3 Mixed Isotype with Enhanced Cytotoxic Activities. *Cancer Res*, *68*(10), 3863–3872. https://doi.org/10.1158/0008-5472.CAN-07-6297

Nokwe, C. N., Zacharias, M., Yagi, H., Hora, M., Reif, B., Goto, Y., & Buchner, J. (2014). A Residue-specific Shift in Stability and Amyloidogenicity of Antibody Variable Domains. *J Biol Chem*, *289*(39), 26829–26846. https://doi.org/10.1074/jbc.M114.582247

Poiron, C., Wu, Y., Ginestoux, C., Ehrenmann, F., Duroux, P., & Lefranc, M. P. (2010). IMGT/mAb-DB: the IMGT® database for therapeutic monoclonal antibodies. *Poster No101*, *11*.

Raju, T. S., & Jordan, R. (2012). Galactosylation variations in marketed therapeutic antibodies. *MAbs*, *4*(3), 385–391. https://doi.org/10.4161/mabs.19868

Richardson, S. I., Lambson, B. E., Crowley, A. R., Bashirova, A., Scheepers, C., Garrett, N., Karim, S. A., Mkhize, N. N., Carrington, M., Ackerman, M. E., Moore, P. L., & Morris, L. (2019). IgG3 enhances neutralization potency and Fc effector function of an HIV V2-specific broadly neutralizing antibody. *PLOS Pathogens*, *15*(12), e1008064. https://doi.org/10.1371/journal.ppat.1008064

Rispens, T., Davies, A. M., Ooijevaar-de Heer, P., Absalah, S., Bende, O., Sutton, B. J., Vidarsson, G., & Aalberse, R. C. (2014). Dynamics of inter-heavy chain interactions in human immunoglobulin G (IgG) subclasses studied by kinetic Fab arm exchange. *J Biol Chem*, *289*(9), 6098–6109. https://doi.org/10.1074/jbc.M113.541813

Saito, S., Namisaki, H., Hiraishi, K., Takahashi, N., & Iida, S. (2019). A stable engineered human IgG3 antibody with decreased aggregation during antibody expression and low pH stress. *Prot Sci*, *28*(5), 900–909. https://doi.org/10.1002/pro.3598

Salfeld, J. G. (2007). Isotype selection in antibody engineering. *Nature Biotech*, *25*(12), 12. https://doi.org/10.1038/nbt1207-1369

Segu, Z., Stone, T., Berdugo, C., Roberts, A., Doud, E., & Li, Y. (2020). A rapid method for relative quantification of N-glycans from a therapeutic monoclonal antibody during trastuzumab biosimilar development. *MAbs*, *12*(1), 1750794. https://doi.org/10.1080/19420862.2020.1750794

Shah, I. S., Lovell, S., Mehzabeen, N., Battaile, K. P., & Tolbert, T. J. (2017). Structural characterization of the Man5 glycoform of human IgG3 Fc. *Mol Immunol*, *92*, 28–37. https://doi.org/10.1016/j.molimm.2017.10.001

Song, Y., DiMaio, F., Wang, R. Y.-R., Kim, D., Miles, C., Brunette, T., Thompson, J., & Baker, D. (2013). High resolution comparative modeling with RosettaCM. *Structure (London, England : 1993)*, *21*(10), 10.1016/j.str.2013.08.005. https://doi.org/10.1016/j.str.2013.08.005

Stapleton, N. M., Andersen, J. T., Stemerding, A. M., Bjarnarson, S. P., Verheul, R. C., Gerritsen, J., Zhao, Y., Kleijer, M., Sandlie, I., de Haas, M., Jonsdottir, I., van der Schoot, C. E., & Vidarsson, G. (2011). Competition for FcRn-mediated transport gives rise to short half-life of human IgG3 and offers therapeutic potential. *Nat Commun*, *2*, 599–599. https://doi.org/10.1038/ncomms1608

Stickler, M. M., Reddy, A., Xiong, J. M., Hinton, P. R., DuBridge, R., & Harding, F. A. (2011). The human G1m1 allotype associates with CD4+ T-cell responsiveness to a highly conserved IgG1 constant region peptide and confers an asparaginyl endopeptidase cleavage site. *Genes Immun*, *12*(3), 213–221. https://doi.org/10.1038/gene.2010.68

Tang, Y., Cain, P., Anguiano, V., Shih, J. J., Chai, Q., & Feng, Y. (2021). Impact of IgG subclass on molecular properties of monoclonal antibodies. *MAbs*, *13*(1), 1993768. https://doi.org/10.1080/19420862.2021.1993768

Tay, M. Z., Liu, P., Williams, L. D., McRaven, M. D., Sawant, S., Gurley, T. C., Xu, T. T., Dennison, S. M., Liao, H.-X., Chenine, A.-L., Alam, S. M., Moody, M. A., Hope, T. J., Haynes, B. F., & Tomaras, G. D. (2016). Antibody-Mediated Internalization of Infectious HIV-1 Virions Differs among Antibody Isotypes and Subclasses. *PLOS Pathogens*, *12*(8), e1005817. https://doi.org/10.1371/journal.ppat.1005817

Teplyakov, A., Zhao, Y., Malia, T. J., Obmolova, G., & Gilliland, G. L. (2013). IgG2 Fc structure and the dynamic features of the IgG CH2–CH3 interface. *Mol Immunol*, *56*(1), 131–139. https://doi.org/10.1016/j.molimm.2013.03.018

Thakkar, S. V., Kim, J. H., Samra, H. S., Sathish, H. A., Bishop, S. M., Joshi, S. B., Volkin, D. B., & Middaugh, C. R. (2012). Local dynamics and their alteration by excipients modulate the global conformational stability of an lgG1 monoclonal antibody. *J Pharm Sci*, *101*(12), 4444–4457. https://doi.org/10.1002/jps.23332

The Antibody Society. (2022). *Therapeutic monoclonal antibodies approved or in regulatory review.* The Antibody Society. https://www.antibodysociety.org/antibody-therapeutics-product-data/

Vermeer, A. W., & Norde, W. (2000). The thermal stability of immunoglobulin: Unfolding and aggregation of a multi-domain protein. *Biophys J*, *78*(1), 394–404. https://doi.org/10.1016/S0006-3495(00)76602-1

Vidarsson, G., Dekkers, G., & Rispens, T. (2014). IgG subclasses and allotypes: From structure to effector functions. *Front Immunol*, *5*, 520. https://doi.org/10.3389/fimmu.2014.00520

Warrender, A. K., & Kelton, W. (2020). Beyond allotypes: The influence of allelic diversity in antibody constant domains. *Front Immunol*, *11*(2016). https://doi.org/10.3389/fimmu.2020.02016

Wilkinson, I., & Hale, G. (2022). Systematic analysis of the varied designs of 819 therapeutic antibodies and Fc fusion proteins assigned international nonproprietary names. *MAbs*, *14*(1), 2123299. https://doi.org/10.1080/19420862.2022.2123299

Chapter Four

Red Edge Excitation Shift Spectroscopy is Highly Sensitive to Tryptophan Composition

4.1 Preface

Resolving subtle differences in the stability of antibody variants with as little as single amino acid changes can be difficult using conventional laboratory techniques. In the previous chapter, we assessed the stability of a panel of IgG allelic variants using the highly sensitive technique of red edge excitation shift (REES) spectroscopy. This approach offers several advantages over other techniques: i) measurements are performed on a standard fluorescent spectrophotometer, ii) the intrinsic fluorescence of tryptophan residues is used as the fluorescent probe so no additional modifications to the antibodies were required, and iii) only a small amount of sample (~200 μL at 0.15 mg mL^{-1}) was required for each measurement. While the REES analysis effectively resolved differences between most variants, this technique is not without limitations. It has also long been proposed that proteins evaluated by REES must have equal numbers of tryptophan residues in equivalent positions within the structures for stability outputs to be directly comparable. Despite little direct experimental evidence to support this requirement, we excluded three of the IgG3 allelic variants from the analysis in Chapter Three as they contained two additional tryptophan residues (arising from arginine to tryptophan polymorphisms in the CH2 domains).

This chapter expands our prior stability analyses to include these three IgG3 allelic variants with additional tryptophan content. The naturally occurring tryptophan variation among the IgG3 alleles proved a valuable tool to deconvolute the complexities of REES data interpretation, which arise from an amalgamation of structural dynamics occurring over vastly different timescales. Additionally, this analysis provided experimental evidence to confirm that matched tryptophan content is an essential prerequisite for comparative analysis of antibody variants.

The manuscript presented in this chapter has been submitted for publication. Supplementary material associated with this work is presented in Appendix B:.

Warrender, A. K., Pan, J., Pudney, C. R., Arcus, V. L., & Kelton, W. Red Edge Excitation Shift Spectroscopy is Highly Sensitive to Tryptophan Composition. *(Submitted)*

4.1.1 Author contributions

As the first author, I led the experimental work, conducted the data analysis, and contributed to all aspects of manuscript writing, editing and figure production. Jolyn Pan assisted with producing some of the antibodies used in the experiments. Vickery Arcus and Chris Pudney contributed to conceptualising the research, provided advice around data interpretation, and offered feedback on the draft manuscript. William Kelton conceptualised the research, assisted with data analysis, contributed to writing and editing the manuscript, and collated the manuscript for submission.

Red Edge Excitation Shift Spectroscopy is Highly Sensitive to Tryptophan Composition

Annmaree K. Warrender[a], Jolyn Pan[b], Chris R. Pudney[c], Vickery L. Arcus[b] and William Kelton[a]

[a]Te Huataki Waiora School of Health, University of Waikato, Hamilton, New Zealand;

[b]Te Aka Mātuatua School of Science, University of Waikato, Hamilton, New Zealand; [c]Department of Biology and Biochemistry, University of Bath, Bath, UK

4.2 Abstract

Red edge excitation shift (REES) spectroscopy relies on the unique fluorescence properties of tryptophan-solvent interactions to profile protein molecular dynamics. Recently, we reported the use of REES to compare the stability of 32 polymorphic IgG antibodies. Here, we expand on this work to investigate the sensitivity of REES to variations in tryptophan content using a subset of IgG3 antibodies containing arginine to tryptophan polymorphisms. Structural analysis revealed that the additional tryptophan residues were situated in highly solvated environments. Subsequently, REES showed clear differences in fluorescence emission profiles when compared to the unmutated variants, thereby limiting direct comparison of their structural dynamics. These findings highlight the exquisite sensitivity of REES to minor variations in protein structure and tryptophan composition.

4.3 Introduction

The intrinsic red shift properties of tryptophan (Trp) fluorescence have proven useful for evaluating protein structural dynamics and stability. Termed red-edge excitation shift (REES), it has been nearly 40 years since the correlation was first made between Trp fluorescence emission spectra and the local solvation environment within proteins (Demchenko, 1988, 2002; Demchenko & Ladokhin, 1988; Mukherjee & Chattopadhyay, 1995). Since then, a number of models have been proposed to relate the REES effect to protein molecular dynamics. These models have been useful for monitoring protein stability and plasticity (Chakraborty & Chattopadhyay, 2017; Chattopadhyay et al., 2003; Kelkar et al., 2010; Knight et al., 2020; Thakkar et al., 2012), understanding mechanism of ligand binding (Catici et al., 2016; Kabir et al., 2021), and linking enzyme kinetics to conformational flexibility (Jones et al., 2017).

Measurement of the REES effect via spectroscopy involves the quantification of Trp emission at progressively longer excitation wavelengths, sampling unique Trp microstates with each step (Haldar et al., 2011). The overall change in maximum emission energy across excitation energies is dependent on the ensemble of Trp microenvironments, which are affected by the physical and structural parameters of the sample such as polarity, packing density, solvent accessibility, and exciplex formation (Demchenko, 1988; Demchenko & Ladokhin, 1988; Reshetnyak et al., 2001; Reshetnyak & Burstein, 2001). In proteins, changes to the microenvironments occur due to subtle fluctuations in the folded structure or from larger structural rearrangements during unfolding or aggregation events (Brooks et al., 1998; Karshikoff et al., 2015). Interactions between Trp and surrounding molecules during fluorescent excitation influence the timescale of fluorescent relaxation and emission (Maglia et al., 2008; Mukherjee & Chattopadhyay, 1995; Reshetnyak et al., 2001). While the technique is experimentally simple, requiring only a laboratory-grade spectrophotometer, the mechanistic underpinnings are less so and it is worth taking time to understand the REES phenomena to support interpretation of the resulting spectra.

REES is underpinned by the interaction of polar solvent molecules (water) with Trp as they are excited by light within the UV range of the spectrum (Demchenko, 1988; Demchenko & Ladokhin, 1988; Itoh & Azumi, 1975; Vivian & Callis, 2001; Weber, 1960). The absorption of a photon by Trp induces a high energy state as a result of energy transfer to both the electronic and vibrational degrees of freedom of the fluorophore

(Figure 4-1). This process is accompanied by a characteristic change in the dipole moment of Trp. The surrounding polar solvent molecules reorientate to accommodate the altered dipole moment and reach an energetically favourable state. These timescales are heavily dependent on the polarity of the surrounding solvent and the number of possible discrete solvent orientation states to be sampled (Demchenko, 1988; Demchenko & Ladokhin, 1988; Haldar et al., 2011; Vivian & Callis, 2001). In any given protein with multiple Trp residues, each position will contribute differently to the fluorescent emission profile.

For highly flexible or unstructured protein regions, where Trp solvent accessibility is high, the reorientation of the water molecules occurs relatively quickly compared to Trp fluorescence lifetime (Haldar et al., 2011). There are few interactions with the surrounding protein environment to impede the movement of water molecules surrounding the fluorophore. Therefore, the observed fluorescence emission occurs entirely from a low energy solvent relaxed state and does so independently of the excitation wavelength (Chattopadhyay et al., 2003; Cushing et al., 2014; Haldar et al., 2011; Mitra et al., 2015). Only a minimal red-edge effect is observed in this case (Figure 4-1). In rigid and structured regions of proteins with buried Trp residues, there can be significant interaction with the surrounding protein microenvironment. As a result, reorganisation of water molecules around a recently excited Trp are significantly slower than in unstructured protein regions (Galley & Purkey, 1970). In this instance, the time taken for surrounding solvent molecules to reorientate to the more favourable, lower energy state exceeds the fluorescent lifetime, resulting in emission from the excited, high-energy state (Cushing et al., 2014; Reshetnyak et al., 2001). In systems with multiple Trp residues, excitation with progressively lower energy quanta (longer excitation wavelengths) specifically selects for the subpopulation of Trp residues requiring less energy to excite (Galley & Purkey, 1970; Haldar et al., 2011). As shown in Figure 4-1, this population of Trp residues have a higher energy ground state (as the solvent molecules have not yet reorientated to the Franck-Condon (FC) ground state) and a corresponding lower energy excited state. It is the specific excitation of these Trp residues that gives rise to the REES effect and provides an overall estimate of the solvent accessibility within a protein (Demchenko & Ladokhin, 1988; Vivian & Callis, 2001).

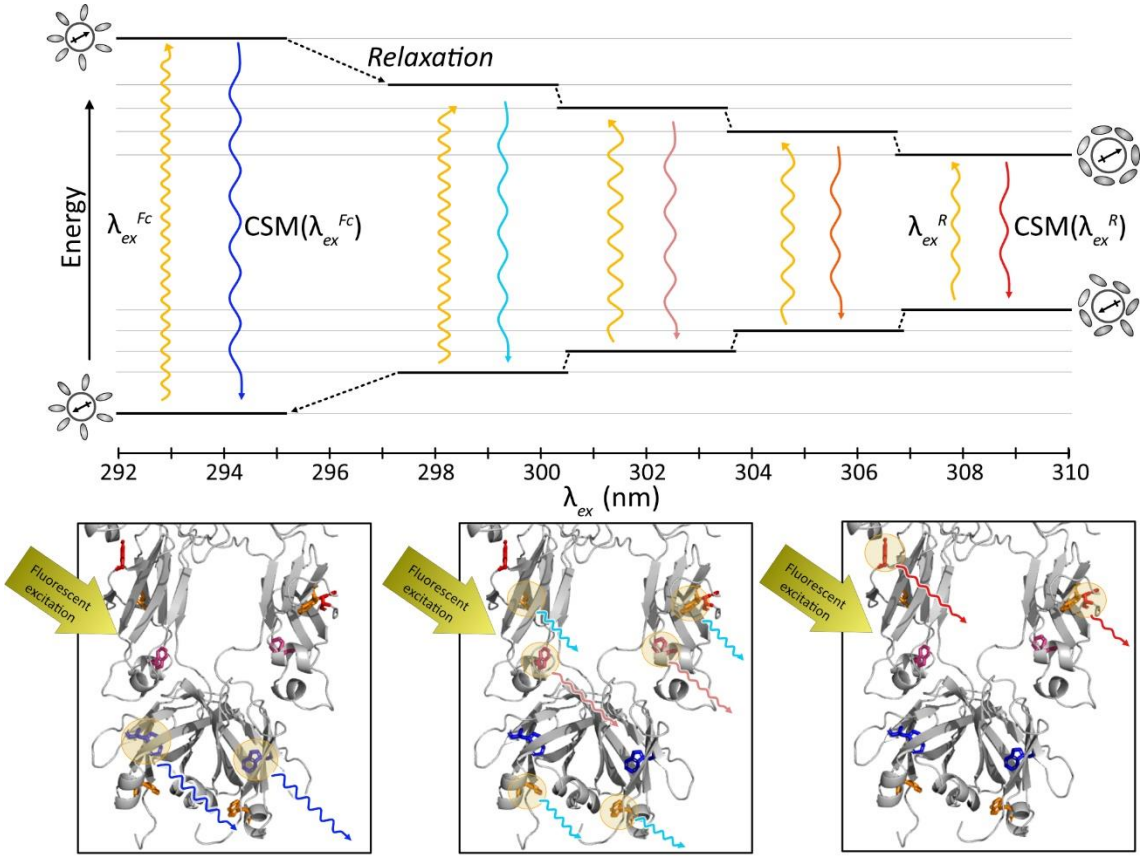

Figure 4-1. Depiction of the REES phenomenon in relation to excitation and emission energies. (Top) A Jablonski diagram showing energy transitions between the excited and relaxed states of tryptophan (Trp) and the corresponding energy of emission. The circles containing arrows represent the dipole moment of Trp with orientation of the surrounding solvent molecules depicted by ovals. As Trp is excited, the dipole moment changes and the energy increases. As the solvent molecules reorientate around the new dipole moment, the energy decreases. The rate of relaxation relative to the fluorescence lifetime determines the transition state energy at which fluorescence emission occurs. As energy of emission decreases, the ground state is higher energy which is readily excited by the subsequent lower excitation energies. (Bottom) Trp residues with unique solvation states are represented in part of the antibody structure to demonstrate the contribution of different Trp to emission energy. From left-to-right, blue Trp (low solvent exposure, rigid environment) emit from high energy, orange Trp (mid-range solvent exposure) emit from slightly lower energy, pink Trp (some solvent exposure) emit from low energy, and red Trp (highly solvent exposed, flexible environment) have the most red-shifted emission.

One complication arising from the use of the Trp REES effect to predict protein flexibility is the occurrence of three excited rotamer states available to Trp sidechains that exert unique red-edge effects of emission (Catici et al., 2016; Maglia et al., 2008; Pan et al., 2006; Royer, 2006). The excited dipole moment can exist in unique orientations that hold different interaction energies with the surrounding molecules which affect the relaxation time and fluorescent emission energies (Itoh & Azumi, 1975; Xu et al., 2009).

Contributions from each Trp residue in each rotamer formation will influence the overall REES effect. Therefore, to implement REES for the biophysical comparison of multiple proteins, the number and position of Trp residues must be considered. To ensure differences can be attributed to the structural behaviour of the protein backbone, it has been suggested that proteins should have the same number of Trp residues positioned in similar microenvironments (Catici et al., 2016; Knight et al., 2020). However, there has been little experimental data gathered to determine how influential such differences might be on REES spectra.

Here, we have extended a prior REES analysis of 32 highly similar monoclonal antibodies to include Trp variation (Warrender et al., 2023) and demonstrated the technique is highly sensitive to Trp residue content and sequence position. We measured IgG3 antibodies with identical Fab domains and unique Fc sequences containing human allele-encoded amino acid polymorphisms (Warrender & Kelton, 2020). While most of the Trp residues are highly conserved throughout the Fc sequences, three of the variants carry an arginine (Arg) to Trp mutation at position 292 resulting in two additional Trp residues (given that antibody heavy chains are homodimers) located on the outer edge of the antibody structure (Figure 4-2). We found a significant difference in REES effect between the IgG3-Arg292 variants compared to IgG3-Trp292 variants. Our study demonstrates the importance of considering Trp content and positioning within the protein structure when using REES for comparative analysis.

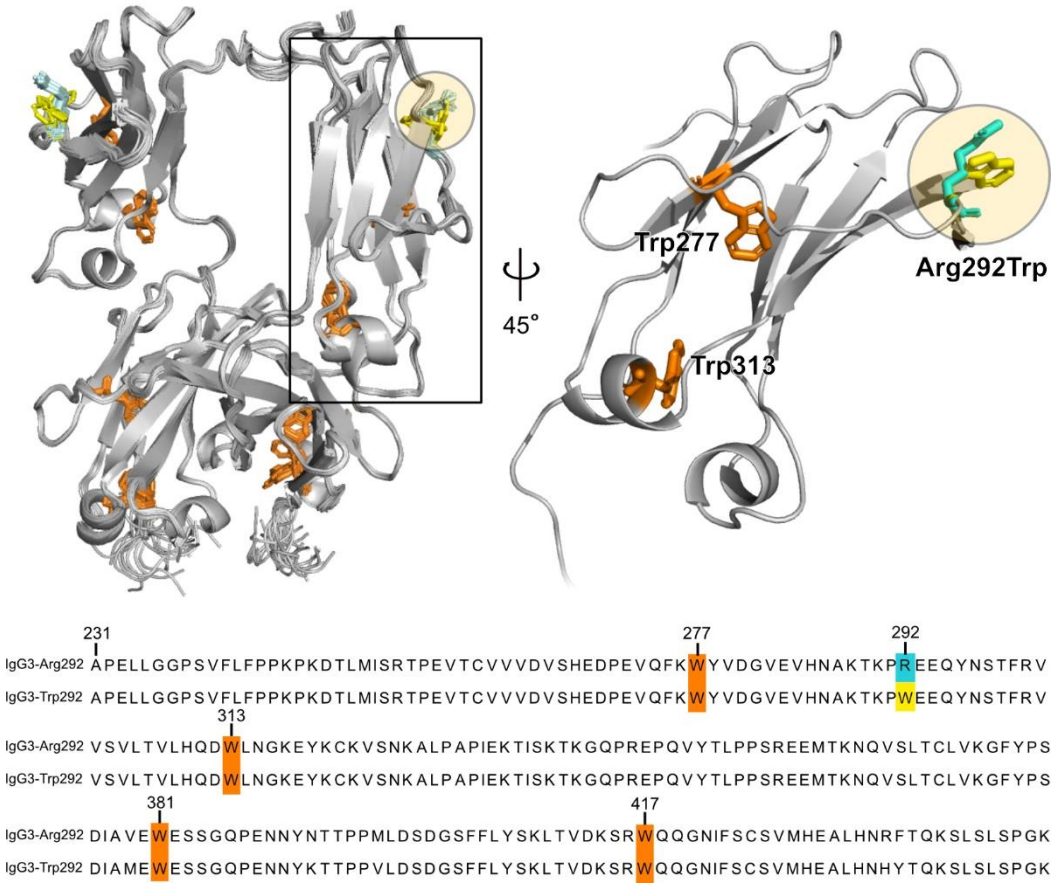

Figure 4-2. Structure and sequence alignment of IgG3 variants. (Top left) Overlaid structures of the Fc region (CH2-CH3) of all IgG3 alleles showing the location of conserved Trp (orange sticks), Arg292 (cyan sticks) and Trp292 (yellow sticks). (Top right) A single CH2 domain highlighting the position of the Arg292Trp polymorphism. (Bottom) Sequence alignment of IgG3-Arg292 and IgG3-Trp292 Fc region to highlighting the conserved Trp (W, orange), Arg292 (R, cyan), and Trp292 (yellow). Sequences given are for IgG3*01 and IgG3*18 alleles, respectively, as representative sequences. Amino acid positions are shown above the sequences using EU numbering.

4.4 Methods

4.4.1 Antibody selection and expression

Antibodies were cloned, expressed, and purified as described previously (Warrender et al., 2023). In brief, trastuzumab (Herceptin®) variable domain sequences were used for the heavy and light chain variable domains (Table B-1). The constant domain sequences were obtained from the Immunogenetics Information System® (IMGT) database (Giudicelli et al., 2006). For the light chain of all antibodies, the IGKC*01 kappa constant allele was selected and appended to the trastuzumab light chain variable domain sequence with a rabbit IGKC signal peptide in the expression vector, pTwist CMV BetaGlobulin WPRE Neo (Twist Biosciences). The heavy chain constant domain sequences for each human IgG3 allele were appended to the trastuzumab heavy chain variable sequence with a rabbit IGHG signal sequence. Antibodies were expressed using the Expi293 expression system (Thermo Fisher) and purified using Protein G Sepharose (Thermo Fisher).

4.4.2 Homology modelling and solvent accessibility calculations

Homology models of the antibodies were generated using Robetta (https://robetta.bakerlab.org/), a Rosetta-based protein structure prediction software. Sequences of each of the IgG3 anti-HER2 antibodies were threaded onto the template structure of full-length IgG1 anti-gp120 mAb (PDB: 1hzh). The homology models were used to calculate the relative percentage of solvent accessibility of each Trp residue for each structure in PyMOL. The total solvent accessible surface area (SASA) was calculated for all Trp residues within a structure and divided by the number of Trp residues (22 for IgG3-Arg292 variants, 24 for IgG3-Trp292 variants) to give the average SASA per Trp across the molecule, in Angstrom squared ($Å^2$).

4.4.3 Red Edge Excitation Shift Analysis

REES data collection and analysis were performed using the methods reported by Warrender *et al.* (Warrender et al., 2023). Antibody samples were diluted to 0.15 mg ml^{-1} with 50 mM Tris-HCl buffered saline pH 8.0. Samples were measured in triplicate in magnetically stirred cuvettes at 10°C in a temperature-controlled chamber in a Hitachi F-7000 fluorescent spectrometer. Fluorescent scans were performed by exciting at wavelengths from 292 - 310 nm and monitoring emission wavelengths between 325 – 500 nm, increasing in 1 nm steps. Slit widths were set to 5 nm.

Fluorescent data was processed by first applying Equation 1 to determine the centre of spectral mass (CSM) for each sample. Where *fi* is the measured fluorescence intensity and λ_{Em} is the emission wavelength.

Equation 1 $$CSM = \frac{\Sigma(f_i \lambda_{Em})}{\Sigma(f_i)}$$

Subsequently, the CSM data was modelled using Equation 2 (Kwok et al., 2021).

Equation 2 $$CSM(\lambda_{Ex}) = \frac{CSM(\lambda_{Ex}^{Fc}) + CSM(\lambda_{Ex}^{R}) e^{\left(\frac{m(\lambda_{Ex} - \lambda_{Ex}^{50\%})}{RT}\right)}}{1 + e^{\left(\frac{m(\lambda_{Ex} - \lambda_{Ex}^{50\%})}{RT}\right)}}$$

The CSM of the relaxed state, $CSM(\lambda_{Ex}^{R})$, is a theoretical measure of the emission wavelength if the antibodies were fully solvated. This is dependent on the number of tryptophan residues and therefore would be the same for each antibody provided the tryptophan content is the same (Kwok et al., 2021). The antibodies tested were classified into two groups, denoted IgG3-Arg292 and IgG3-Trp292, based on the number of tryptophan residues contained within the sequence (22 or 24, respectively) and treated separately for the model fitting process. $CSM(\lambda_{Ex}^{R})$ was globally fit within each group, with constraints set between 387 and 440 nm to align with a practical range determined previously (Kwok et al., 2021). The constant variables, R (gas constant, 8.3145 J mol^{-1} K^{-1}), T (temperature, 283.15 K), and λ_{Ex} (excitation wavelength, 292-310 nm) were kept the same for each sample, regardless of Trp content. The remaining variables were unique to each sample and determined using a non-linear regression. For context, $CSM(\lambda_{Ex}^{Fc})$ is the maximum wavelength of emission from a fully excited (Franck-Condon) state, $\lambda_{Ex}^{50\%}$ is the excitation wavelength at the CSM halfway between $CSM(\lambda_{Ex}^{Fc})$ and $CSM(\lambda_{Ex}^{R})$ (the inflection point of the sigmoid), and *m* is the gradient of the slope, reflecting the change in Gibbs-free energy (ΔG) as a function of λ_{Ex}. In the text, the value of *m* is referred to as ΔG_m with units of J mol^{-1} nm^{-1}.

Statistical analyses were performed using one-way ANOVA testing and Tukey Post-Hoc multiple comparisons tests. The p-adjusted values are reported with a significance cut-off of $p = 0.05$.

4.5 Results

4.5.1 IgG Fc variants with differences in the number of tryptophan residues exhibit differing REES effects

REES data was collected for 21 trastuzumab-formatted antibodies with unique IgG3 constant domains. Of these variants, 18 contained 22 Trp residues (IgG3-Arg292 variants) and three contained 24 Trp residues (IgG3-Trp292 variants).

REES parameters were derived from the fluorescence emission profiles by fitting the data with a recently established thermodynamic model (Kwok et al., 2021)(Equation 2, Figure B-1). Using this model, the solvation state of the ensemble of tryptophans (described by $CSM(\lambda_{Ex}^{Fc})$) and the overall flexibility of the globular protein structure (described by $\Delta G m$) can be inferred (Figure 4-3A). Higher values of $CSM(\lambda_{Ex}^{Fc})$ (the centre of spectral mass of the fully excited Franck–Condon state) indicate more Trp residues are in a solvent exposed state and therefore emitting at a lower energy. Likewise, higher values of $\Delta G m$ (related to the number of solvent-fluorophore interactions) indicate greater protein rigidity. Finally, the model derives $CSM(\lambda_{Ex}^{R})$ (the centre of spectral mass of the completely relaxed state), which is assumed to be similar for highly similar protein structures with the same number of Trp residues and represents the predicted fluorescence of Trp in a completely unfolded state with full solvent access. It is not possible to measure $CSM(\lambda_{Ex}^{R})$ experimentally using conventional spectrophotometers as there is generally insufficient UV light intensity at longer, low energy wavelengths (λ_{Ex} > 310 nm) to generate signal above the noise. To accurately derive this value from the model, $CSM(\lambda_{Ex}^{R})$ was fit globally for antibody samples of the same group (IgG3-Arg292 or IgG3-Trp292), resulting in values of 418.9 ± 2.9 nm for IgG3-Arg292 variants and 423.3 ± 16.2 nm for IgG3-Trp292 variants (Figure 4-3A, Table 4-1).

The values of $CSM(\lambda_{Ex}^{Fc})$ and $\Delta G m$ were determined for each individual sample and subsequently grouped for data analysis (Table 4-1). The $CSM(\lambda_{Ex}^{Fc})$ values of IgG3-Arg292 variants varied between 352.4 and 353.6 nm with an average of 352.9 ± 0.3 nm (Figure 4-3B). The values for IgG3-Trp292 variants were significantly higher ($p < 0.001$) with a minimum $CSM(\lambda_{Ex}^{Fc})$ of 353.7 nm, maximum of 354.2 nm and average of 353.9 ± 0.3 nm. The same trend was evident for $\Delta G m$, for which IgG3-Trp292 variants exhibited significantly higher ($p < 0.001$) values between 7.7 and 8.0 mJ mol-1 nm-1 with an average of 7.8 ± 0.2 mJ mol-1 nm-1 while IgG3-Arg292 variants had $\Delta G m$ values

between 6.6 and 7.3 mJ mol-1 nm-1 with an average of 7.0 ± 0.2 mJ mol-1 nm-1 (Figure 4-3B, Table 4-1).

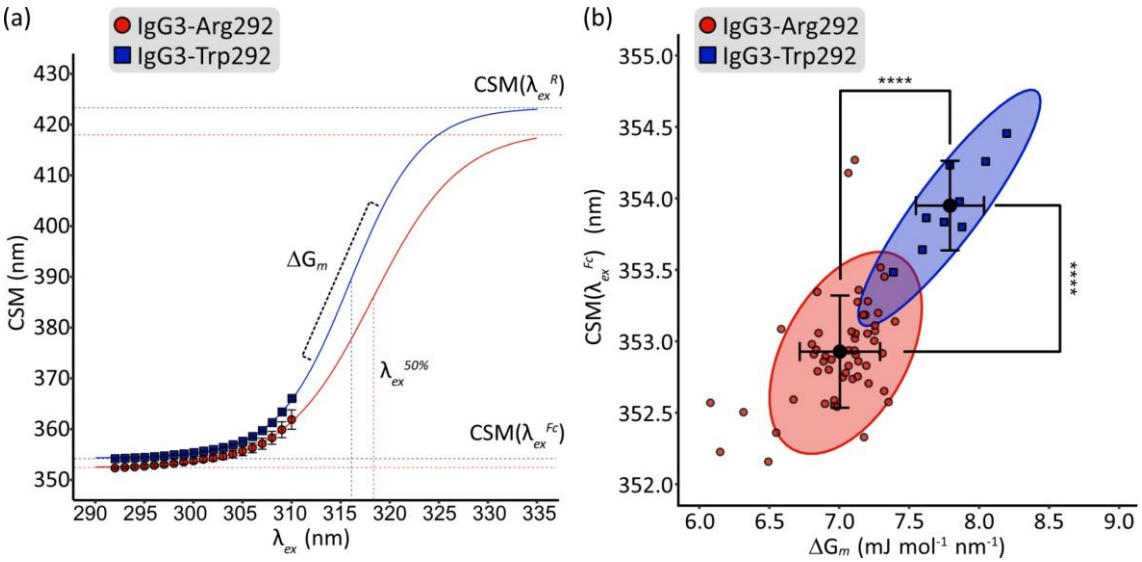

Figure 4-3. Processed REES data comparing antibody groups. (A) Centre of spectral mass (CSM) profiles for IgG3-Arg292 (variant IgG3*17, red circles) and IgG3-Trp292 (variant IgG3*19, blue squares) fitted with the sigmoidal REES model from Equation 2. The data points represent the average of three replicate measurements with error bars showing standard deviation. Dotted lines show the values of $CSM(\lambda_{Ex}^{R})$, $CSM(\lambda_{Ex}^{Fc})$, ΔG_m, and $(\lambda_{Ex}^{50\%})$ derived from the model. (B) Derived REES values of $CSM(\lambda_{Ex}^{Fc})$ vs ΔG_m for all IgG3 variants. Data points representing each replicate measured of IgG3-Arg292 variants (red circles) and IgG3-Trp292 variants (blue squares). A 95% data ellipse shows the spread of data for each group. The black circle in the centre of each ellipse represents the mean for each group with error bars showing the standard deviation. Significance levels were tested using one-way ANOVA with Tukey Post-hoc multiple comparison testing, The difference between $CSM(\lambda_{Ex}^{Fc})$ (top) and ΔG_m (right side) between the antibody groups is shown to be of high significance. **** $p < 0.0001$.

Table 4-1. Values of $CSM(\lambda_{Ex}^{Fc})$, ΔG_m and $CSM(\lambda_{Ex}^{R})$ derived from fitting the fluorescence emission centre of spectral mass profiles with the sigmoidal REES model. Values given are the average (Avg) of triplicate measurements with standard deviations (sd). Average solvent accessible surface area (SASA) per tryptophan (Trp) calculated using PyMOL is given for each variant. The group averages for IgG3-Arg292 and IgG3-Trp292 are shown in the bottom section.

	Allele	$CSM(\lambda_{Ex}^{Fc})$		ΔG_m		$CSM(\lambda_{Ex}^{R})$		Average SASA per Trp (Å^2)	
		Avg	sd	Avg	sd	Avg	sd	Avg	sd
IgG3-Arg292	**3*01**	353.1	± 0.2	7.0	± 0.2	418.9	±2.9	4.89	
	3*03	352.5	± 0.2	7.3	± 0.1	418.9	±2.9	4.75	
	3*04	353.1	± 0.2	7.1	± 0.2	418.9	±2.9	7.12	
	3*06	353.1	± 0.9	6.9	± 0.3	418.9	±2.9	6.87	
	3*08	352.7	± 0.2	6.6	± 0.5	418.9	±2.9	6.85	
	3*09	352.9	± 0.0	7.0	± 0.1	418.9	±2.9	10.73	
	3*11	352.9	± 0.1	7.0	± 0.1	418.9	±2.9	6.63	
	3*12	352.7	± 0.4	6.7	± 0.5	418.9	±2.9	8.69	
	3*13	352.7	± 0.2	7.1	± 0.2	418.9	±2.9	10.52	
	3*14	353.0	± 0.4	7.1	± 0.1	418.9	±2.9	8.67	
	3*15	353.1	± 0.4	7.2	± 0.1	418.9	±2.9	8.86	
	3*16	353.6	± 0.6	7.2	± 0.1	418.9	±2.9	11.49	
	3*17	352.4	± 0.2	6.6	± 0.3	418.9	±2.9	8.86	
	3*20	353.2	± 0.2	6.8	± 0.3	418.9	±2.9	8.45	
	3*22	352.9	± 0.3	6.9	± 0.3	418.9	±2.9	7.07	
	3*24	352.9	± 0.2	7.1	± 0.1	418.9	±2.9	6.93	
	3*25	353.1	± 0.1	7.3	± 0.1	418.9	±2.9	8.06	
	3*26	352.7	± 0.1	7.1	± 0.1	418.9	±2.9	8.75	
IgG3-Trp292	**3*18**	353.7	± 0.2	7.7	± 0.3	423.3	± 16.2	21.27	
	3*19	354.2	± 0.2	8.0	± 0.2	423.3	± 16.2	15.91	
	3*23	353.9	± 0.3	7.7	± 0.1	423.3	± 16.2	19.24	
IgG3-Arg292		352.9	± 0.3	7.0	± 0.2	418.9	±2.9	8.01	± 1.77
IgG3-Trp292		353.9	± 0.3	7.8	± 0.2	423.3	± 16.2	18.81	± 2.21

4.5.2 Arg292Trp mutations in antibody constant regions significantly increase the average solvent accessible surface area of tryptophan residues

To characterise the solvent accessibility of the Trp microenvironments within the antibody structures, PyMOL was used to predict the percentage of relative solvent exposure of each Trp residue. In this analysis, 0% indicates a residue with complete solvent inaccessibility (such as for Trp located tightly within the protein folds) and 100%, a fully solvent exposed residue. It should be noted antibody heavy chains are homodimeric and therefore the Arg292Trp mutation results in a net increase of two Trp per molecule. Despite this heavy chain symmetry, the estimated percentage of solvent exposure was not necessarily equal for each copy of Trp residue (Table B-2). This can be attributed to the homology modelled structures capturing Trp sidechains in different rotamer states on each chain. The additional Trp residues in IgG3-Trp292 variants had predicted levels of solvent exposure between 33% and 62%. This was substantially greater than the highest exposed Trp found in IgG3-Arg292 variants, with an estimated solvent exposure of 29%.

Subsequently, we estimated the solvent accessible surface area (SASA) for each Trp residue and calculated the average SASA per Trp for each antibody variant (Table 4-1). We observed a higher average SASA per Trp of 18.8 ± 2.2 $Å^2$ for IgG3-Trp292 variants compared to just 8.0 ± 1.8 $Å^2$ for IgG3-Arg292 variants.

4.5.3 Relationship between SASA and the REES effect

Pearson correlation coefficients were determined to analyse the relationship between the REES parameter for solvent exposure, $CSM(\lambda_{Ex}^{Fc})$, and the average SASA per Trp residue. A positive correlation was observed with a coefficient of r = 0.7345 ($p < 0.001$) (Figure 4-4A). We repeated this analysis with the REES parameter for protein rigidity, ΔG_m, and also found a strong correlation of r = 0.7030 ($p < 0.001$) (Figure 4-4B).

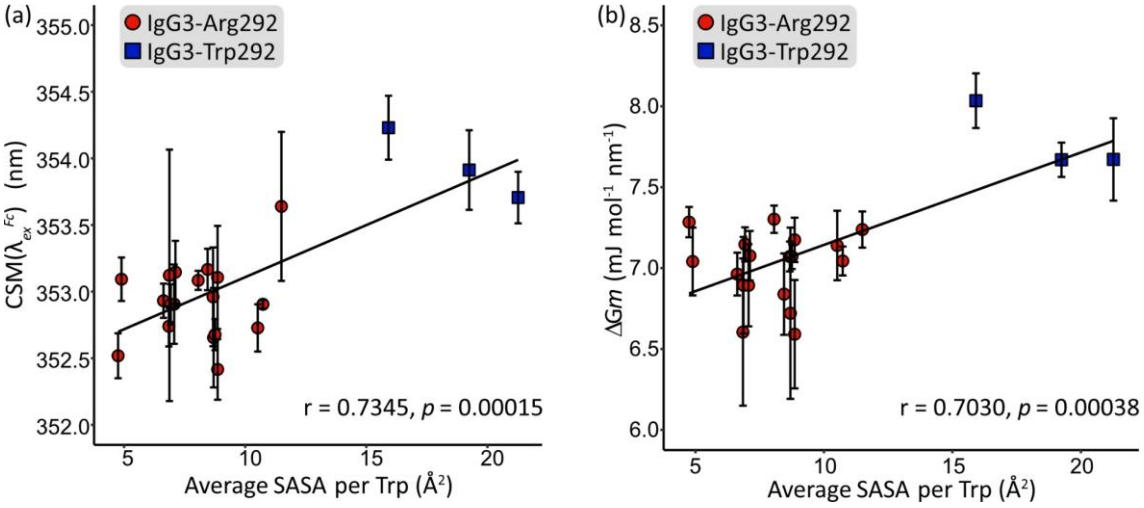

Figure 4-4. Correlation between average solvent accessible surface area (SASA) per Trp and (A) $CSM(\lambda_{Ex}^{Fc})$ (B) ΔG_m. Data points represent the average of triplicate measurements for IgG3-Arg292 (red circles) and IgG3-Trp292 (blue squares) variants with error bars to show standard deviation. Solid line shows the line of correlation corresponding with the Pearson's correlation coefficient (r) and p-value.

4.6 Discussion

Red edge excitation shift (REES) spectroscopy exploits the intrinsic properties of Trp amino acids to assess the structural rigidity and stability of highly similar proteins. We have shown previously that REES is sensitive enough to detect subtle differences in stability between human IgG antibodies with single amino acid differences in the heavy chain (Warrender et al., 2023). Here, we have expanded upon this analysis to demonstrate the sensitivity of the REES technique to Trp content. Moreover, we provide experimental evidence to support previous suggestions that equivalent Trp content is a prerequisite for comparing protein stability using REES.

A key advantage of the REES technique is the ability to sample a wide range of dynamic protein conformational states in solution to characterise protein flexibility and unfolding, while only requiring conventional laboratory spectrophotometry equipment. Yet, beneath the simplicity of data collection lies the more intricate task of interpreting the acquired data. This analysis is primarily complicated by the fact that REES signal stems from the average fluorescence emission arising from the ensemble of Trp residues throughout the structure. Specifically, Trp residues in different positions can result in unique emission profiles regardless of structural flexibility differences. We used a panel of 21 human IgG3 antibodies which possessed minor differences in Trp composition (22 or 24 Trp residues)

alongside additional amino acid polymorphisms (as many as eight mutations between variants). To detangle the influence of Trp composition changes we compared the relative solvent exposure of each Trp residue within the antibody structures. It was evident that the additional two Trp residues present in the IgG3 variants carrying the Arg292Trp mutation had a much larger degree of solvation compared to all other Trp. This subsequently increased the SASA per Trp when averaged across all the Trp residues within the structures. We acknowledge that the estimated SASA values are calculated from homology models predicted by threading onto a static IgG1 crystal structure and therefore may differ from dynamic SASA values of these proteins in solution. Nonetheless, our finding of a positive correlation between the increased SASA per Trp and an increase in $CSM(\lambda_{Ex}^{Fc})$ value aligns with previously published data (Kwok et al., 2021). The disparity observed in $CSM(\lambda_{Ex}^{Fc})$ between the antibody groups with varying Trp content was significantly larger than the variability between variants with an equal number of Trp residues. This finding strongly suggests that the additional Trp residues are likely responsible for the distinct REES profiles observed.

Perhaps counterintuitively, we also report a positive correlation between SASA per Trp and ΔG_m (a measure of structural rigidity). When interpreting REES profiles, it is expected that a greater value of ΔG_m is indicative of higher structural rigidity. Kwok *et al.* (2021) undertook a REES analysis of several engineered α-synuclein protein variants containing single Trp residues at specific locations. They proposed that differences in ΔG_m between variants arose from local structural arrangements or from flanking amino acids contributing to solvent-fluorophore interaction energies (Kwok et al., 2021). In these scenarios, a change in ΔG_m will be the result of local microenvironment changes rather than global structural rigidity differences. We suggest this phenomenon explains why we see such an unexpected increase in ΔG_m for IgG3-Trp292 variants compared to the IgG3-Arg292 variants.

These results highlight the remarkable sensitivity of REES spectroscopy to fine alterations in Trp solvation states. Although currently underutilised, REES has applications in protein biochemistry and biotechnology, not least of which is the rapid interrogation of large numbers of antibody variants as demonstrated here. However, caution must be taken to ensure the number of Trp residues remains consistent among the proteins being compared. Additional emission signals from extra Trp residues can

confound the results and mask any effects stemming from structural disparities in the proteins.

4.7 Supplementary Material

Supplementary Tables B-1 – B-2 and Figure B-1 supporting this manuscript can be found in Appendix B: Supplementary Material for Chapter Four.

4.8 References

Brooks, C. L., Gruebele, M., Onuchic, J. N., & Wolynes, P. G. (1998). Chemical physics of protein folding. *PNAS U.S.A*, *95*(19), 11037–11038.

Catici, D. A., Amos, H. E., Yang, Y., van den Elsen, J. M., & Pudney, C. R. (2016). The red edge excitation shift phenomenon can be used to unmask protein structural ensembles: Implications for NEMO-ubiquitin interactions. *FEBS J*, *283*(12), 2272–2284. https://doi.org/10.1111/febs.13724

Chakraborty, H., & Chattopadhyay, A. (2017). Sensing tryptophan microenvironment of amyloid protein utilizing wavelength-selective fluorescence approach. *J Fluoresc*, *27*(6), 1995–2000. https://doi.org/10.1007/s10895-017-2138-7

Chattopadhyay, A., Rawat, S. S., Kelkar, D. A., Ray, S., & Chakrabarti, A. (2003). Organization and dynamics of tryptophan residues in erythroid spectrin: Novel structural features of denatured spectrin revealed by the wavelength-selective fluorescence approach. *Prot Sci*, *12*(11), 2389–2403. https://doi.org/10.1110/ps.03302003

Cushing, S. K., Li, M., Huang, F., & Wu, N. (2014). Origin of strong excitation wavelength dependent fluorescence of graphene oxide. *ACS Nano*, *8*(1), 1002–1013. https://doi.org/10.1021/nn405843d

Demchenko, A. P. (1988). Red-edge-excitation fluorescence spectroscopy of single-tryptophan proteins. *Eur Biophys J*, *16*(2), 121–129. https://doi.org/10.1007/BF00255522

Demchenko, A. P. (2002). The red-edge effects: 30 years of exploration. *Luminescence*, *17*(1), 19–42. https://doi.org/10.1002/bio.671

Demchenko, A. P., & Ladokhin, A. S. (1988). Red-edge-excitation fluorescence spectroscopy of indole and tryptophan. *Eur Biophys J*, *15*(6), 369–379. https://doi.org/10.1007/BF00254724

Galley, W. C., & Purkey, R. M. (1970). Role of heterogeneity of the solvation site in electronic spectra in solution. *PNAS U.S.A*, *67*(3), 1116–1121.

Giudicelli, V., Duroux, P., Ginestoux, C., Folch, G., Jabado-Michaloud, J., Chaume, D., & Lefranc, M.-P. (2006). IMGT/LIGM-DB, the IMGT® comprehensive database of immunoglobulin and T cell receptor nucleotide sequences. *Nucleic Acids Res*, *34*(suppl_1), D781–D784. https://doi.org/10.1093/nar/gkj088

Haldar, S., Chaudhuri, A., & Chattopadhyay, A. (2011). Organization and dynamics of membrane probes and proteins utilizing the red edge excitation shift. *J Phys Chem B*, *115*(19), 5693–5706. https://doi.org/10.1021/jp200255e

Itoh, K., & Azumi, T. (1975). Shift of the emission band upon excitation at the long wavelength absorption edge. II. Importance of the solute–solvent interaction and the solvent reorientation relaxation process. *J Chem Phys*, *62*(9), 3431–3438. https://doi.org/10.1063/1.430977

Jones, H. B. L., Wells, S. A., Prentice, E. J., Kwok, A., Liang, L. L., Arcus, V. L., & Pudney, C. R. (2017). A complete thermodynamic analysis of enzyme turnover links the free energy landscape to enzyme catalysis. *FEBS J*, *284*(17), 2829–2842. https://doi.org/10.1111/febs.14152

Kabir, M. L., Wang, F., & Clayton, A. H. A. (2021). Red-edge excitation shift spectroscopy (REES): Application to hidden bound states of ligands in protein–ligand complexes. *Int J Mol Sci*, *22*(5), 5. https://doi.org/10.3390/ijms22052582

Karshikoff, A., Nilsson, L., & Ladenstein, R. (2015). Rigidity versus flexibility: The dilemma of understanding protein thermal stability. *FEBS J*, *282*(20), 3899–3917. https://doi.org/10.1111/febs.13343

Kelkar, D., Chaudhuri, A., Haldar, S., & Chattopadhyay, A. (2010). Exploring tryptophan dynamics in acid-induced molten globule state of bovine α-lactalbumin: A wavelength-selective fluorescence approach. *Eur Biophys J*, *39*, 1453–1463. https://doi.org/10.1007/s00249-010-0603-1

Knight, M. J., Woolley, R. E., Kwok, A., Parsons, S., Jones, H. B. L., Gulácsy, C. E., Phaal, P., Kassaar, O., Dawkins, K., Rodriguez, E., Marques, A., Bowsher, L., Wells, S. A., Watts, A., van den Elsen, J. M. H., Turner, A., O'Hara, J., & Pudney, C. R. (2020). Monoclonal antibody stability can be usefully monitored using the excitation-energy-dependent fluorescence edge-shift. *Biochem J*, *477*(18), 3599–3612. https://doi.org/10.1042/BCJ20200580

Kwok, A., Camacho, I. S., Winter, S., Knight, M., Meade, R. M., Van der Kamp, M. W., Turner, A., O'Hara, J., Mason, J. M., Jones, A. R., Arcus, V. L., & Pudney, C. R. (2021). A thermodynamic model for interpreting tryptophan excitation-energy-dependent fluorescence spectra provides insight into protein conformational sampling and stability. *Front Mol Biosci*, *8*, 778244. https://doi.org/10.3389/fmolb.2021.778244

Maglia, G., Jonckheer, A., De Maeyer, M., Frère, J.-M., & Engelborghs, Y. (2008). An unusual red-edge excitation and time-dependent Stokes shift in the single tryptophan mutant protein DD-carboxypeptidase from Streptomyces: The role of dynamics and tryptophan rotamers. *Prot Sci*, *17*(2), 352–361. https://doi.org/10.1110/ps.073147608

Mitra, M., Chaudhuri, A., Patra, M., Mukhopadhyay, C., Chakrabarti, A., & Chattopadhyay, A. (2015). Organization and dynamics of tryptophan residues in brain spectrin: Novel insight into conformational flexibility. *J Fluoresc*, *25*(3), 707–717. https://doi.org/10.1007/s10895-015-1556-7

Mukherjee, S., & Chattopadhyay, A. (1995). Wavelength-selective fluorescence as a novel tool to study organization and dynamics in complex biological systems. *J Fluoresc*, *5*(3), 237–246. https://doi.org/10.1007/BF00723895

Pan, C.-Pin., Callis, P. R., & Barkley, M. D. (2006). Dependence of tryptophan emission wavelength on conformation in cyclic hexapeptides. *J Phys Chem B*, *110*(13), 7009–7016. https://doi.org/10.1021/jp056164p

Reshetnyak, Y. K., & Burstein, E. A. (2001). Decomposition of protein tryptophan fluorescence spectra into log-normal components. II. The statistical proof of discreteness of tryptophan classes in proteins. *Biophys J*, *81*(3), 1710–1734.

Reshetnyak, Y. K., Koshevnik, Y., & Burstein, E. A. (2001). Decomposition of protein tryptophan fluorescence spectra into log-normal components. III. Correlation between fluorescence and microenvironment parameters of individual tryptophan residues. *Biophys J*, *81*(3), 1735–1758. https://doi.org/10.1016/S0006-3495(01)75825-0

Royer, C. A. (2006). Probing protein folding and conformational transitions with fluorescence. *Chem Rev*, *106*(5), 1769–1784. https://doi.org/10.1021/cr0404390

Thakkar, S. V., Kim, J. H., Samra, H. S., Sathish, H. A., Bishop, S. M., Joshi, S. B., Volkin, D. B., & Middaugh, C. R. (2012). Local dynamics and their alteration by excipients modulate the global conformational stability of an lgG1 monoclonal antibody. *J Pharm Sci*, *101*(12), 4444–4457. https://doi.org/10.1002/jps.23332

Vivian, J. T., & Callis, P. R. (2001). Mechanisms of tryptophan fluorescence shifts in proteins. *Biophys J*, *80*(5), 2093–2109.

Warrender, A. K., & Kelton, W. (2020). Beyond allotypes: The influence of allelic diversity in antibody constant domains. *Front Immunol*, *11*(2016). https://doi.org/10.3389/fimmu.2020.02016

Warrender, A. K., Pan, J., Pudney, C. R., Arcus, V. L., & Kelton, W. (2023). Constant domain polymorphisms influence monoclonal antibody stability and dynamics. *Prot Sci*, *32*(3), e4589. https://doi.org/10.1002/pro.4589

Weber, G. (1960). Fluorescence-polarization spectrum and electronic-energy transfer in tyrosine, tryptophan and related compounds. *Biochem J*, *75*(2), 335–345.

Xu, J., Chen, J., Toptygin, D., Tcherkasskaya, O., Callis, P., King, J., Brand, L., & Knutson, J. R. (2009). Femtosecond fluorescence spectra of tryptophan in human γ-crystallin mutants: Site-dependent ultrafast quenching. *J Am Chem Soc*, *131*(46), 16751–16757. https://doi.org/10.1021/ja904857t

Chapter Five

Antibody Hinge Length Governs Protein Flexibility of IgG3 Allelic variants

5.1 Preface

A key dynamic element that contributes to antibody function is the motility of the two Fab domains and the Fc domain, which are connected by a flexible linker region termed the hinge domain. The length of the hinge domain governs the degree to which the Fab domains can move in relation to the Fc which has implications for antigen and Fc receptor binding. Intriguingly, the hinge length of IgG3 antibodies varies substantially between allelic sequences within a range of 32 to 62 amino acids. This chapter aims to characterise the structural flexibility of IgG3 allelic variants with different hinge lengths for the first time using small angle X-ray scattering (SAXS). This analysis has important implications for understanding the mechanistic underpinnings of functional differences between the variants (Crowley et al., 2022; de Taeye et al., 2020) and may allude to the evolutionary drivers behind IgG3 hinge length diversity.

Chapter Five is presented as a completed manuscript prepared for submission. A discussion of additional experimental work that has been planned to support the SAXS analysis presented here is discussed in *Section 5.7: Future Directions* and is not part of the manuscript itself. Supplementary Material associated with this manuscript is presented in Appendix C: Supplementary Material for Chapter Five.

Warrender, A. K., Pan, J., Sethi, A., & Kelton, W. Antibody Hinge Length Governs Conformational Flexibility of IgG3 Allelic Variants. (*In Preparation*).

5.1.1 Author contributions

As the first author of this manuscript, I contributed to all aspects of experimental design, data collection and analysis, manuscript writing, figure generation and editing. Jolyn Pan assisted with antibody production and preparing the samples for analysis. Ashish Sethi was the SAXS Beamline Scientist at the ANSTO Australian Synchrotron and provided guidance with experimental design and data analysis. William Kelton conceived the concept for this research, assisted with experimental design and data collection and edited the manuscript.

Antibody Hinge Length Governs Conformational Flexibility of IgG3 Allelic Variants

Annmaree K. Warrender[a], Jolyn Pan[b], Ashish Sethi[c], William Kelton[a,b]

[a]Te Huataki Waiora School of Health, University of Waikato, Hamilton, New Zealand;
[b]Te Aka Mātuatua School of Science, University of Waikato, Hamilton, New Zealand;
[c]Australian Nuclear Science Technology Organisation, The Australian Synchrotron, 800 Blackburn Rd, Clayton, VIC 3168, Australia

5.2 Abstract

The increased conformational flexibility of IgG3 antibodies, relative to the other IgG subclasses, has often been attributed to the substantially longer hinge domains. Naturally occurring polymorphisms in the IgG3 genes have given rise to allelic variation with diverse hinge lengths, ranging from 32 to 62 amino acids. This natural variation has been shown to alter binding affinities to Fc receptors and influence the potency of effector functions. However, the underlying differences in flexibility that might drive this behaviour have not been thoroughly characterised. Here, we analysed small angle X-ray scattering data collected from IgG3 allelic variants with varying hinge lengths and identical variable domains. The scattering data were systematically compared between IgG3 variants, as well as with data collected from IgG1 and IgG2 antibodies. *Ab initio* bead models generated from the X-ray scattering datasets uncovered differences in the length of each variant structure, in which structural elongation correlated positively with hinge length. This is the first study to provide a solution-based structural characterisation of IgG3 encoded by constant-region alleles containing hinge length polymorphisms. The resolved structural disparities provide strong rationale for further analysis of the natural variants using higher resolution techniques to complement the X-ray scattering data.

5.3 Introduction

The pool of clinically approved monoclonal antibodies is dominated by immunoglobulin gamma (IgG) backbones, which exhibit superior pharmacokinetics and effector functions compared to other antibody classes, such as IgA or IgM (Carter, 2006; Kaplon et al., 2022). Within the IgG class, IgG3 antibodies have largely been avoided in the clinic despite suggestions of a greater neutralisation potential and the ability to elicit more potent effector functions than achievable with IgG1 backbones (Chu et al., 2020; Dangl et al., 1988; Foss et al., 2022; Izadi et al., 2023; Kallolimath et al., 2021; Kober et al., 2022; Richardson et al., 2019; Scharf et al., 2001). This hesitance is largely attributed to concerns regarding immunogenicity and stability, stemming from the broad genetic diversity associated with IgG3.

A distinctive difference between the IgG subclasses (IgG1, IgG2, IgG3, and IgG4) is the length of the hinge region (Figure 5-1). IgG3 antibodies have a particularly long hinge region of up to 62 amino acids, in stark contrast to the shorter hinge lengths of IgG1, IgG2, and IgG4, which range between 12 and 15 amino acids. This flexible hinge region links the Fab domains on each of the paired heavy chains to the Fc domain in fully assembled antibody structures and is primarily constrained by two or more interchain-disulphide bonds (Figure 5-1A) (H. Liu & May, 2012). While the Fab and Fc domains are rigid globular-like structures, the hinge region allows for the movement of the Fab domains relative to each other and to the Fc (Roux et al., 1997). These dynamics influence not only antigen binding but also immune activation. Hinge length is therefore critical to antibody function. The extended hinge of IgG3 allows for broader conformational changes and reduces steric hindrance around Fc receptor binding sites resulting in enhanced binding by immune cell receptors (Canfield & Morrison, 1991; Lu et al., 2007). Subsequently, effector function potencies, including phagocytosis and intracellular neutralisation, are enhanced by antibodies with a long hinge (Foss et al., 2022; Richardson et al., 2019). It is currently thought coevolution of the immune system alongside broad classes of pathogens (e.g., malaria parasites, meningococci, and human immunodeficiency virus) may have led to the large degree of subclass diversity (Chu et al., 2020; Giuntini et al., 2016; Kyei-Baafour et al., 2022; Scharf et al., 2001). In particular, the expression density of surface antigens by invading pathogens is linked to the neutralisation potential of IgG3 antibodies. The long IgG3 hinge facilitates avidity binding to high density epitopes where antigen pairs are presented within close proximity on the cell surface, subsequently

improving neutralisation (Cooper et al., 1994; D'Eall et al., 2019; Scharf et al., 2001; Shaw et al., 2019). One possible explanation for this behaviour is that the flexibility of the long hinge allows the Fab domains to orientate closer together to accommodate binding of antigens at different densities (X. Liu et al., 2019; Ryazantsev et al., 1990).

The hinge length of IgG3 is encoded by constant region alleles with polymorphisms in sequence length. In contrast to the other IgG subclasses, IgG3 hinge is uniquely formed from multiple exons (Figure 5-1B). Allelic variants have the upper-hinge exon (H1, 17 amino acids long) followed by a middle-hinge exon (H2/3/4, 15 amino acids long) that is repeated up to three times due to past genomic duplication events (Roux et al., 1997, 1998). As a result, allelic variants have short (32 amino acids), medium (47 amino acids) and long (62 amino acids) hinge lengths (Giudicelli et al., 2006; Lefranc & Lefranc, 2019). The continual discovery of novel allelic diversity among IgG sequences suggests the full extent of sequence variation is yet to be realised (Bashirova et al., 2021; Calonga-Solís et al., 2019; Ford et al., 2023; Khatri et al., 2021) and, while it seems unlikely even longer hinge structures will be discovered, one study has reported a rare IgG3 allele encoding five hinge exons (Bashirova et al., 2021). Considering many of the unique properties observed for IgG3 antibodies have been attributed to the particularly long hinge length, it is curious that such significant variation within the IgG3 hinge has evolved. The determination of correlations between IgG3 hinge diversity and antibody properties will shed light on the evolutionary drivers behind the diversification and provide insight into how the naturally occurring variation could be harnessed to improve the design of future IgG3 therapeutics.

A

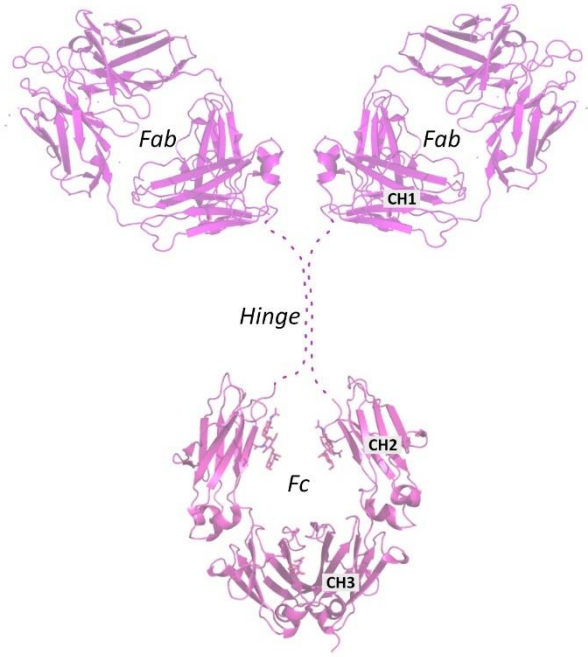

B

```
                CH1
                ASTKGPSVFPLAPCSRSTSGGTAALGCLVKDYFPEPVTVSWNSGALTSGVHTFPAVLQSSGLYSLSSVVTVPSSSLGTQTYTCNVNHKPSNTKVD
IgG1*01-15mer   .............S.K.....................................................................I..... 95
IgG2*02-12mer   ...................ES.....................................................T..NF.........D..... 95
IgG3*04-32mer   ..................................................................................... 95
IgG3*03-47mer   ..................................................................................... 95
IgG3*12-47mer   ..................................................................................... 95
IgG3*01-62mer   ..................................................................................... 95
IgG3*08-62mer   ..................................................................................... 95
                   H1                H2              H3              H4              CH2
                KRV----------------------------------------------------------APELLGGPSVFLFPPKPKDTLMISRTPEVT
IgG1*01-15mer   .K.EPKSCDKTHTCPPCP-------------------------------------------..... 143
IgG2*02-12mer   .T.ERKCCVECPPCP-----------------------------------------..P-VA..... 139
IgG3*04-32mer   ...ELKTPLGDTTHTCPRCPEPKSCDTPPPCPRCP---------------------------..... 190
IgG3*03-47mer   ...ELKTPLGDTTHTCPRCPEPKSCDTPPPCPRCPEPKSCDTPPPCPRCP--------------..... 175
IgG3*12-47mer   ...ELKTPLGDTTHTCPRCPEPKSCDTPPPCPRCPEPKSCDTPPPCPRCP--------------..... 160
IgG3*01-62mer   ...ELKTPLGDTTHTCPRCPEPKSCDTPPPCPRCPEPKSCDTPPPCPRCPEPKSCDTPPPCPRCP..... 190
IgG3*08-62mer   ...ELKTPLGDTTHTCPRCPEPKSCDTPPPCPRCPEPKSCDTPPPCPRCPEPKSCDTPPPCPRCP..... 175
                                                                                  CH3
                CVVVDVSHEDPEVQFKWYVDGVEVHNAKTKPREEQYNSTFRVVSVLTVLHQDWLNGKEYKCKVSNKALPAPIEKTISKTKGQPREPQVYTLPPSR
IgG1*01-15mer   .............K.N.....................Y.....................................A..... 238
IgG2*02-12mer   ..............N.....M.............F............V.................G..... 234
IgG3*04-32mer   ..................................................................... 285
IgG3*03-47mer   ..................................................................... 270
IgG3*12-47mer   ................................F..... 255
IgG3*01-62mer   ..................................................................... 285
IgG3*08-62mer   ..................................................................... 270

                EEMTKNQVSLTCLVKGFYPSDIAVEWESSGQPENNYNTTPPMLDSDGSFFLYSKLTVDKSRWQQGNIFSCSVMHEALHNRFTQKSLSLSPGK
IgG1*01-15mer   D.L.........................N.......K....V.........................V............HY.....  330
IgG2*02-12mer   ............................N.......K.............................V............HY.....  326
IgG3*04-32mer   ..................................................................  377
IgG3*03-47mer   ....................................V...........R.........E..V.....................  362
IgG3*12-47mer   ..................................................................  347
IgG3*01-62mer   ..................................................................  377
IgG3*08-62mer   ............................N.....................................................  362
```

Figure 5-1. Antibody structure and constant region sequence alignment. (A) Labelled antibody structure generated in PyMOL using Fab domains from anti-gp120 IgG1 [PDB: 1hzh (Saphire, Parren, Pantophlet, et al., 2001)] and human IgG3 Fc domain [PDB: 5w38 (Shah et al., 2017)]. The hinge region is depicted as dotted lines to represent the polymorphic nature of length. (B) Sequences of the constant domain alleles. The beginning of each domain or hinge exon is labelled above the consensus sequence (CH1, Hinge: H1-4, CH2 and CH3). The consensus sequence shown above each allele sequence represents the most common amino acid at each position. Polymorphisms are shown with the amino acid single-letter code within the row of the corresponding allele. Dots indicate the sequence is the same as the consensus. The amino acid number at the end of each row is the count from the start of the CH1 domain. Dashes indicate no amino acid is present in the sequence and are used to highlight the differences between the hinge sequences.

There has been only a handful of studies comparing functional differences between alleles within the IgG3 subclass. Nonetheless, allelic hinge length variation has been linked to differences in stability (Warrender et al., 2023) and effector function (Chu et al., 2020; de Taeye et al., 2020), and has shown clinical associations with human disease. Shorter hinge length variants reportedly drive stronger natural killer cell-mediated cytotoxicity, potentially due to the closer proximity between effector and target cells compared to the longer hinge variants (de Taeye et al., 2020). On the other hand, longer hinge variants trigger greater phagocytic activity (Chu et al., 2020). In a cohort study of SARS-CoV-2 patients, the prevalence of IgG3 short-hinge variants was correlated with increased disease severity as well as higher mortality rates (López-Martínez et al., 2022). This finding is consistent with reports that the longer IgG3 hinge corresponds to stronger neutralisation against SARS-CoV-2 as a result of effective cross-linking of the spike protein on the virion surface (Kallolimath et al., 2021). Furthermore, an association between the medium hinge polymorphism and the occurrence of Cerebral Malaria has been reported, possibly due to a lower efficiency to clear parasites (Kyei-Baafour et al., 2022). These studies provide a snapshot of the influence of IgG3 hinge length variation on antibody function.

One avenue to gain a deeper understanding of the impacts of hinge length on antibody function involves defining the structural conformations and dynamic properties of different antibody variants. Structural prediction by high-resolution techniques, such as X-ray crystallography, has proven exceedingly challenging for full-length antibodies. This is largely due to the highly flexible hinge linker region hindering crystal packing and electron density resolution. As a result, only a handful of full-length structures have been resolved by crystallography to date, including murine IgG2a (Harris et al., 1992, 1997; Larson et al., 1991), murine IgG1 (Harris et al., 1998) and human IgG1 anti-gp120 (Saphire et al., 2002; Saphire, Parren, Barbas, et al., 2001; Saphire, Parren, Pantophlet, et al., 2001). There remains no high-resolution structure of IgG3 with an extended hinge, although partial X-ray crystallography structures of individual Fc domains have been resolved (Krapp et al., 2003; Shah et al., 2017; Teplyakov et al., 2013).

To overcome structural limitations, solution-based approaches have been implemented in combination with computational simulations to characterise full-length IgG3 structures. Early studies using fluorescence emission anisotropy kinetics (Dangl et al., 1988; Tan et al., 1990) and electron microscopy imaging (Ryazantsev et al., 1990) show the long hinge of IgG3 promotes a more elongated conformation compared to the other IgG subclasses

and enables greater movement of the Fab domains in relation to each other, and to the Fc domain. In more recent work, small angle neutron scattering (SANS) and small angle X-ray scattering (SAXS) have been used in combination with analytical ultracentrifugation and computational modelling to compare antibody flexibility in more detail and predict ensembles of structural conformations sampled by each subclass in solution (Ashish et al., 2010; Belviso et al., 2022; Eryilmaz et al., 2013; Furtado et al., 2004; Gregory et al., 1987; Hui et al., 2015, 2019; X. Liu et al., 2019; Lu et al., 2007; Spiteri, Doutch, et al., 2021; Spiteri, Goodall, et al., 2021; X. Tian et al., 2014, 2015). Predictions of IgG3 conformations from SAXS data using ensemble optimisation modelling resolved conformations with a range of motion unique to the subclass and domain orientations highly distinguishable from IgG1, IgG2, and IgG4 (X. Liu et al., 2019). Molecular dynamics and Monte Carlo simulations have since been implemented to produce molecular structures of a full-length IgG3 antibody (with the long hinge) in solution that comply with physically realistic structural arrangements (Spiteri, Goodall, et al., 2021).

Here, we assess whether the differences in molecular flexibility observed between IgG3 and the other subclasses are mirrored by IgG3 allelic variants with hinge length polymorphisms. Five, trastuzumab-formatted IgG3 antibodies with unique Fc allele sequences were selected to represent the allelic hinge variation. Using SAXS, the structural conformations and corresponding flexibilities sampled by each IgG3 hinge variant in solution were assessed. Comparison of the SAXS scattering profiles revealed longer hinge regions were significantly elongated and had greater flexibility than shorter hinge regions. These results have important implications for the behaviour of IgG3 antibodies in solution, in terms of both antigen engagement and the promotion of effector functions. We also highlight that allelic variation should be considered in studies where IgG3 is being compared to other subclasses, as the 62 amino acid hinge is but one possible hinge length and not necessarily representative of the subclass.

5.4 Methods

5.4.1 Antibody selection

IgG allelic variants were selected to represent all naturally occurring hinge lengths (except the five-exon allele reported by Bashirova *et al.* (2021)). Amino acid polymorphisms present elsewhere in the IgG sequences were considered by selecting variants with the highest sequence similarities to reduce possible confounding effects of point mutations. Two of each of the long and medium hinge allelic variants were included

to test the replicability of the observed scattering (IgG3*01 and IgG3*08, IgG3*03 and IgG3*12, respectively). At the time of conducting this study, there was only one verified IgG allele sequence with a short hinge (IgG3*04). Single alleles were used to represent IgG1 (IgG1*01) and IgG2 (IgG2*02) subclasses.

5.4.2 Antibody production

The antibodies were formatted with Ig kappa (κ) light chain constant domains, trastuzumab (Herceptin®) light and heavy chain variable domains, and IgG heavy chain constant domain allele sequences (Warrender et al., 2023). Each of the heavy and light chain genes were cloned into the mammalian expression vector, pTwist CMV BetaGlobulin WPRE Neo vector (Twist Biosciences) with a rabbit IGKC signal peptide.

The Expi293 Expression System (Thermo Fisher), optimised for expression of glycosylated, mammalian proteins, was used to express the antibodies. Following the manufacturer's instructions, cells were transfected with light chain and heavy chain plasmid DNA at a 2:1 ratio. Upon expression, antibodies were secreted into the supernatant which was collected after six days by centrifugation at 5000 x *g* for 20 min at 4°C. Antibodies were purified by gravity flow through a column packed with 2 mL Protein G Sepharose (Thermo Fisher). The supernatant was passed through the column three times to ensure association of the antibody. The column was washed with a minimum of 10 column volumes (~20 mL) of 50 mM sodium phosphate buffer, pH 7.5. Antibodies were eluted with 4 mL of formic acid, pH 2.5, directly into 500 µL 1 M ammonium bicarbonate, pH 8.0. Eluted antibodies were buffer exchanged into 50 mM sodium phosphate, pH 7.5, using Amicon® Ultra-4 Centrifugal Filter Units. Purified antibodies were stored at 4°C until used experimentally.

5.4.3 SAXS instrument set up and data collection

Experiments were conducted at the Australian Synchrotron SAXS/WAXS beamline equipped with a Pilatus detector (Dectris Ltd) coupled to size exclusion chromatography (SEC) with a co-flow set up (SEC-SAXS). Antibody samples were prepared for SEC-SAXS in Phosphate Buffered Saline (PBS), pH 7.4, to final concentrations between 4 - 7.5 mg mL^{-1}. Samples were concentrated using Amicon® Ultra-0.5 Centrifugal Filter Units with 10 kDa molecular weight cut-off with centrifugation at 4°C and 13,000 x *g*. Immediately prior to processing the samples on the SAXS beamline, the solutions were centrifuged again for 15 min to remove insoluble aggregates. A 3.2 mL Superdex S200

5/150 (Cytiva) size exclusion column was used and equilibrated with PBS, pH 7.4 prior to sample loading.

For data collection, the X-ray wavelength (λ) was set to 1.033 Å, the sample detector Z position was 2200 mm and the flow cell was set to 22°C (Table 5-1). Scattering intensity was measured as a function of momentum transfer (q), where $q = 4\pi\sin(\theta)/\lambda$ and 2θ is the scattering angle in Å. Samples (50 µL) were flowed through the size exclusion column at a flow rate of 0.2-0.4 mL min^{-1} and immediately into a 1.5 mm thin-walled glass capillary where scattering data was collected in 1 s intervals. SAXS data was collected for each antibody at two concentrations (either 4 or 4.5 mg mL^{-1} and 6 or 7.5 mg mL^{-1}).

Table 5-1. SEC-SAXS beamline setup and data collection parameters

Instrument	Australian Synchrotron SAXS/WAXS beamline with a Pilatus detector (Dectris Ltd)
Size Exclusion column	Superdex S200 5/150 3.2 mL (Cytiva)
Flow cell temp (°C)	22
Detector Z position (mm)	2200
Detector cover position (mm)	250
X-ray Wavelength (Å)	1.033
***q* range ($Å^{-1}$)**	0.005 – 0.500
Exposure time (s)	1.00
Concentration range (mg mL^{-1})	4 – 7.5

5.4.4 Data processing

Normalisation of the beamline intensity and data reduction was performed using scatterBrain (version 2.71) software at the Australian Synchrotron. All downstream data processing was performed using software from the ATSAS program suite (version 3.0.4) (Manalastas-Cantos et al., 2021), unless stated otherwise. The scattering files were aligned with the inline SEC data using CHROMIXS (Panjkovich & Svergun, 2018). The region of buffer-scattering was selected from the size exclusion chromatograph, upstream of the first elution peak. The region of sample-scattering was selected from the largest peak which corresponded to monomeric antibody in all the samples. The buffer-scattering was subtracted from the sample-scattering and the processed scattering curves were exported to a format (*.dat) readable by other programmes in the ATSAS package.

Analysis of the subtracted scattering data was performed using the PRIMUSqt software (Manalastas-Cantos et al., 2021). The radius of gyration (R_g) and relative intensity (or forward scattering intensity, I(0)) for each sample were calculated using both the "Radius of Gyration" and the "Distance Distribution" analysis functions. The "Radius of Gyration" function determined reciprocal space values using the Guinier Approximation of low-resolution scattering data (low-*q* region). The fitted range was kept below $qR_g = 1.3$ to meet the standard criteria for globular proteins (Kikhney & Svergun, 2015; Putnam, 2016). The quality of fit was assessed based on the fidelity value (1.0 being the highest, 0.0 being the lowest) and a random distribution of residuals that averaged around zero. The presence of aggregates was evaluated based on the linearity of the Guinier plot. The real-space R_g, I(0), and the maximum particle dimensions (D_{max}) were calculated from the pair distance distribution function (*P(r)*) from the "Distance Distribution" analysis function. This function uses GNOM (Svergun, 1992) to calculate the distribution of interatomic distances (r). The value of r where the *P(r)* curve reaches zero was used to define D_{max}. The data was fit to a maximum *q* of approximately 0.2 $Å^{-1}$ (Table 5-2, Table C-1) and D_{max} was adjusted manually to obtain the lowest D_{max} that produced a smooth curve, with *P(r)* greater than zero and a random distribution of residuals around zero.

The Porod volume (V_p) was determined using the "Porod Volume" function in PRIMUSqt, with reciprocal space values determined from the "Radius of Gyration" function and a *q*-range limited to the Porod-Debye region only. The upper limit of the Porod-Debye region was defined by the scattering data that reached and maintained a plateau in the Porod plot (Figure C-1) (Rambo & Tainer, 2011). The V_p was determined from this defined subset of scattering data for each concentration. An average V_p across both concentrations for each sample was calculated and used for subsequent analysis to eliminate potential concentration effects. The calculated values of V_p were used in combination with the molecular weights (MW) to determine the particle densities ($d_{particle}$) of each variant. The MW was determined from the protein sequence with the addition of glycan mass. We have previously determined the N-linked glycan composition of these antibodies (Warrender et al., 2023). While heterogeneous, the N-glycan G0 F makes up over 50% of the glycosylation and therefore this mass (1,500 Da) was used to approximate appended glycans. To account for two glycan attachment sites (on each of the CH2 domains), 3,000 Da was added to the total MW. The particle density was calculated using the following formula: $d_{particle} = (MW/V_p) \times 1.66$ (Rambo & Tainer, 2011). The average $d_{particle}$ was calculated across both high and low concentrations.

Dimensionless Kratky plots were generated by multiplying R_g (from the *P(r)* distribution) by *q*. To aid in comparing the antibodies and remove confounding effects of concentration on intensity, the intensity was normalised by dividing by I(0).

5.4.5 *Ab initio* bead modelling

Ab initio models were generated using GASBOR online (Version 2.3p) (Petoukhov et al., 2012; Svergun et al., 2001). Model calculations were performed with default parameters and no symmetry (P1) for all the antibody variants. The number of dummy residues were defined by the number of residues present in each antibody sequence. Datasets from both measured concentrations were used for modelling. The scattering behaviour of the predicted model was aligned to experimental data to generate a chi-squared value. For each variant, the model with the lowest chi-squared values was used for comparison.

The orientation of the *ab initio* models was determined by aligning with the C_α coordinates to full-length structures using the ATSAS SUPCOMB tool in BioXTAS RAW v.2.2.0 (Hopkins et al., 2017; Kozin & Svergun, 2001). IgG1*01-15mer model was aligned to full-length anti-gp120 IgG1 X-ray crystal structure [PDB: 1hzh (Saphire, Parren, Pantophlet, et al., 2001)]. IgG2*02-12mer was aligned to full-length anti-canine murine IgG2a X-ray crystal structure [PDB: 1igt (Harris et al., 1997)]. All IgG3 variants were aligned to the full-length solution structure of human myeloma IgG3 antibody [SASDBD reference code SASDLZ2 (Spiteri, Goodall, et al., 2021)]. Alignment was performed by minimising dissimilarities between the reference and target structures. The quality of alignment was assessed based on the normalised spatial discrepancy (NSD) criterion (Kozin & Svergun, 2001). For the purposes of orientating the *ab initio* models, a NSD score over 1 (but below 2) was considered acceptable.

5.5 Results

5.5.1 IgG3 variants show a greater propensity for aggregation than IgG1 or IgG2

The quality of each antibody sample was assessed prior to analysing the SAXS scattering data. As samples were run through a size exclusion column immediately before entering the SAXS capillary, aggregated antibody (high molecular weight species (HMWS)) and fractionated antibody (low molecular weight species (LMWS)) were separated out from monomeric antibody. This was important as IgG3 has a high propensity to form insoluble aggregates (Warrender et al., 2023). The size exclusion chromatograms were evaluated to assess the prevalence of HMWS and LMWS relative to monomeric antibody (Figure

C-2). The IgG1 and IgG2 antibodies eluted as a single peak containing monomeric antibody with only a minor increase in absorbance just prior to elution suggesting a small amount of HMWS were present. In comparison, all the IgG3 samples appeared to contain more HMWS due to the presence of at least two elution peaks in the size exclusion chromatograms. We suspect the HMWS consisted of dimers and trimers given elution times close to that of the monomeric antibody. Samples IgG3*04-32mer and IgG3*12-47mer both appeared to have LMWS present that eluted after the monomeric fractions suggesting some degradation of these antibodies in solution. Despite multiple peaks, the monomeric form of IgG3 antibodies was still the most prevalent in solution, eluting with more than double the absorbance signal of the HMWS and LMWS. This provided us with confidence that the antibody samples were of sufficient quality to collect scattering data of the antibodies as monomers. Using SAXS analysis software, the specific scattering data frames corresponding to the antibodies eluting in the monomeric fraction could be extracted from the other scattering frames. This allowed us to ensure the scattering data being analysed was in fact from antibodies in their simplest, monomeric form.

The scattering data was further checked for aggregation by assessing the scattering profiles (log(I) vs q) and particularly focusing on the linearity of the Guinier plot at low q (Figure 5-2A-G). The Guinier regions of IgG1*01-15mer and IgG2*02-12mer were linear indicating good quality SAXS data with no aggregation. The IgG3 variants differed slightly in sample quality, particularly at the higher concentrations. IgG3*03-47mer, IgG3*12-47mer, and IgG3*08-62mer exhibited some increased curvature at low q for the high concentration samples suggesting minor aggregation. The low concentration samples, however, did not display this scattering behaviour and the Guinier regions were linear. The remainder of the samples showed linear Guinier regions regardless of concentration. For consistency, the low concentration samples of all variants were used for subsequent comparison of the SAXS data.

5.5.2 IgG hinge length variants exhibit unique and distinguishable scattering patterns

Distinct differences in scattering behaviour of IgG with different hinge lengths were apparent (Figure 5-2H, Figure C-3). At values of $q < 0.03$ Å^{-1}, the scattering of antibodies with longer hinge regions showed a more rapid decrease in intensity relative to variants with shorter hinge lengths. This behaviour is typical of particles with increased size (Makowski et al., 2020). While the scattering patterns of IgG1*01-15mer and IgG2*02-

12mer were almost identical, the gradient of the slope at low *q* became steeper as the hinge length increased. That is, IgG3*04-32mer had a relatively shallow gradient (although steeper than IgG1*01-15mer and IgG2*02-12mer) while the gradients slightly increased for IgG3*03-47mer and IgG3*12-47mer and were the steepest for IgG3*01-62mer and IgG3*08-62mer. The scattering profiles of allelic variants with the same hinge length consistently overlaid with one another instilling confidence that scattering differences arose from different hinge lengths.

The overall dimensions of each antibody variant structure were compared using the radius of gyration (R_g) values and interparticle distance values calculated from the scattering data (Table 5-2, Table C-1). R_g provides a measure of the average radii between atoms within the structure and is therefore a measure of the effective size of the antibody structures (Makowski et al., 2020; Putnam, 2016). The R_g values were calculated in reciprocal space by Guinier analysis and in real space using the pair distance distribution function (*P(r)*). The calculated values from both approaches were in close agreement (± 2 Å) for each variant (Table 5-2, Table C-1), indicating high quality data. The values calculated by the pair distance distribution function was used for comparative analysis (Figure 5-3A), as opposed to the Guinier analysis tool, in which calculations assume globular shaped proteins rather than elongated (Eryilmaz et al., 2013). Nevertheless, the trends identified from the pair distance distribution function held true for both sets of calculations.

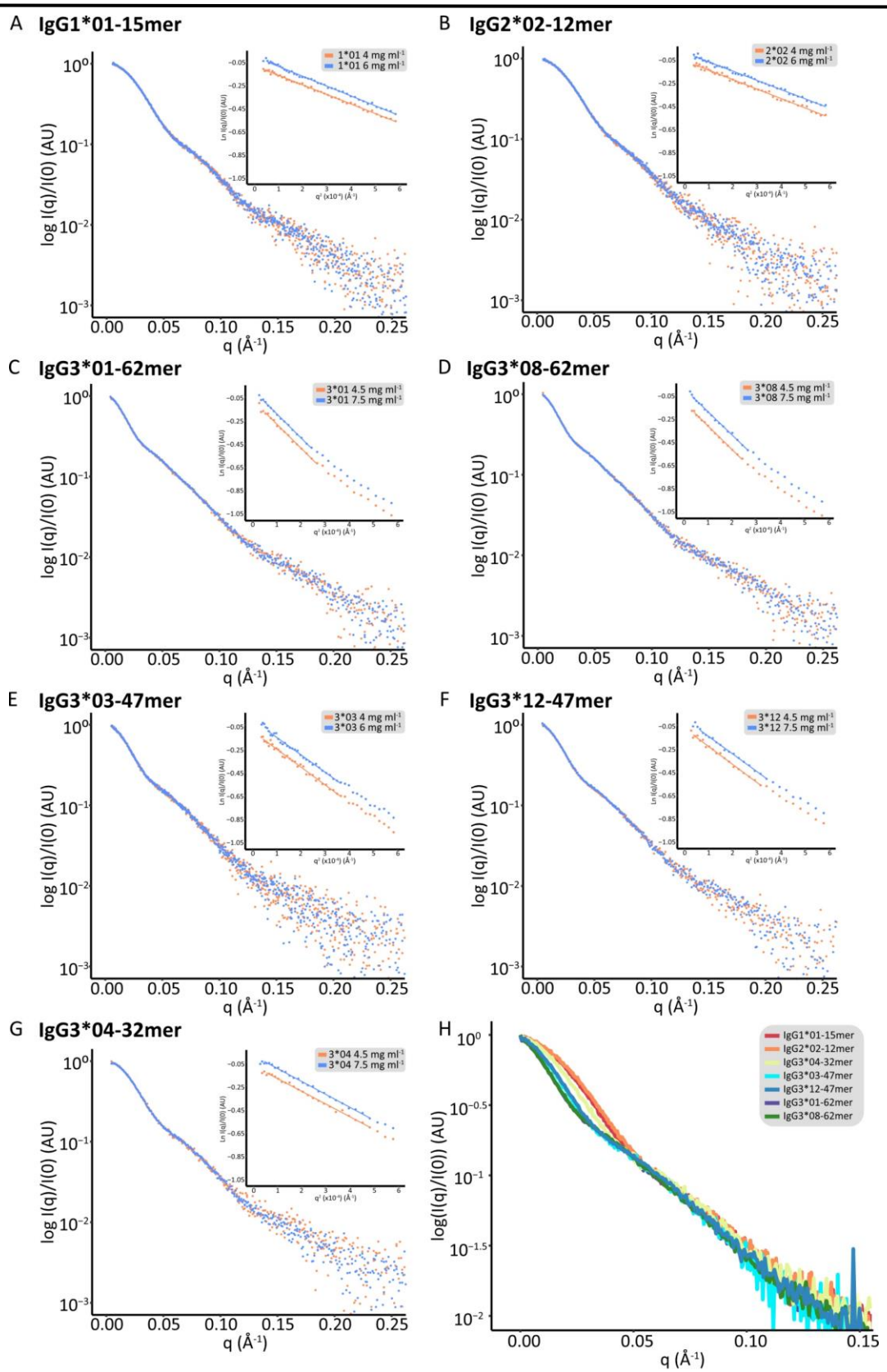

Figure 5-2. Comparison of the SAXS scattering curves at different concentrations. (A-G) Scattering intensity as log I(*q*)/I(0) of each antibody variant, at low and high concentrations. Inset plots show the Guinier region fit with the Guinier Approximation linear model. (H) Scattering plots of all low concentration datasets overlaid on a single plot. Intensity is scaled by the relative intensity for ease of comparison.

The maximum particle dimensions (D_{max}) and R_g values showed a positive correlation with hinge length (Figure 5-3A, C, Table 5-2, Table C-1). IgG2*02-12mer had the smallest values of D_{max} = 156.9 Å and R_g = 49.49 ± 0.23 Å. Values for IgG1*01-15mer were very similar at D_{max} = 158.6 Å and R_g = 50.93 ± 0.23 Å. Overall, IgG3 antibodies had larger D_{max} and R_g values compared to both IgG1 and IgG2 antibodies, and variation among the IgG3 variants was evident. IgG3*04-32mer had a D_{max} of 179.8 Å and an R_g of 58.62 ± 0.74 Å while the variants with slightly longer hinge lengths (IgG3*03-47mer and IgG3*12-47mer) had D_{max} values of 240 Å and 234 Å, and R_g values of 69.04 ± 0.55 and 67.6 ± 0.57 Å, respectively. The measurements for the longest hinge variants (IgG3*01-62mer and IgG3*08-62mer) were the largest, with D_{max} of 249 Å and 242 Å and R_g of 79.05 ± 0.63 Å and 78.48 ± 0.64 Å, respectively.

The unique curvature of the *P(r)* distributions for each IgG3 hinge length polymorphism indicated conformational sampling differences. The *P(r)* distributions represent the frequency at which interatomic distances (r) are present within the structure as it samples various conformations. As expected for monoclonal antibodies, each variant had a *P(r)* distribution containing two or three peaks (Figure 5-3A, D) (Belviso et al., 2022; X. Liu et al., 2019; Lu et al., 2007; Spiteri, Goodall, et al., 2021; X. Tian et al., 2015). This represents multiple interatomic distances that occur frequently in the conformations sampled by the antibody (Figure 5-3B). The first peak (peak 1) seen in all the variants has a maximum at r = 38 - 40 Å. This most likely corresponds to the width across the Fc domain or a single Fab domain (Figure 5-3B) as these are similar in all the IgG variants (regardless of hinge length) and the values of r align approximately to the widths across each domain as estimated from X-ray crystallography structures (Lu et al., 2007; Padlan, 1996; Saphire, Parren, Pantophlet, et al., 2001; Shah et al., 2017).

The second peak (peak 2) has a maximum r that varies between variants with different hinge lengths (Figure 5-3A, D). In previous studies, this peak has been attributed to the distance between each Fab domain (Fab-Fab) and, in some cases, the distance between the Fab and Fc domains (Fab-Fc) (Belviso et al., 2022; Lu et al., 2007). IgG2*02-12mer has the narrowest *P(r)* distribution although the presence of a broad single peak was suggestive of a hidden second maximum at r = 74 Å. This peak may be less pronounced due to the Fab-Fab and Fab-Fc distances being similar to the distance across the individual Fab or Fc domains (so the *P(r)* distribution is closer to a globular protein-type shape). IgG1*01-15mer has a slightly broader distribution with two distinct peaks. The maximum of peak 2 was at approximately r = 77 Å for IgG1*01-15mer.

The *P(r)* distributions of IgG3 variants with identical hinge lengths shared very similar curvature, indicating any differences resolved from the SAXS data could be attributed to hinge length variation rather than single amino acid polymorphisms located elsewhere in the constant domains (Figure 5-1B, Figure 5-3A). The *P(r)* distribution for IgG3*04-32mer was much narrower in comparison to medium and long IgG3 hinge variants and had two distinct peaks (with maxima at r = 38 and 87 Å). The medium hinge variants showed a slightly broader distribution of distances with a slightly right-shifted second peak maximum (r = 100 Å), suggesting a less compact structure. The *P(r)* distributions of the longest hinge variants (IgG3*01-62mer and IgG3*08-62mer) were uniquely distinguishable due to the presence of a third peak, which had a maximum of r = 150 Å (Figure 5-3A, D). Interestingly, the maximum of the second peak of the long hinge variants appeared to be at a lower value of r (r = 94 Å) compared to IgG3*03-47mer and IgG3*12-47mer (r = 100 Å). It is likely that a third interparticle distance is present in the structural conformations of IgG3*03-47mer and IgG3*12-47mer but the peak maximum is masked by broadening of the second peak. Therefore, we observe a general increase in r for the maximum of peak 2 as the hinge length increases. Based on this, we suggest that the distance (r) corresponding to the maximum of the most right-shifted peak in any *P(r)* curve is attributed to the distance from the Fc to the Fab domain (Figure 5-3B).

5.5.3 Hinge region variation contributes to differences in structural flexibility

The macromolecular volumes and particle density were calculated to characterise the dynamic properties of each variant. The Porod-Debye law was applied to data at low *q* to determine the particle Porod volume (V_p) of each variant (Brosey & Tainer, 2019; Rambo & Tainer, 2011). Porod-Debye plots for each variant displayed plateaus that defined the upper value of *q* used for V_p calculations (Figure 5-4A, Figure C-1). The density of the structure in combination with the volume provides a quantitative measure of how compact each structure was (X. Tian et al., 2015). As the hinge length increased between variants, there was a clear trend of V_p increasing and $d_{particle}$ decreasing (Table 5-2, Table C-1). Out of all the IgG3 variants, IgG3*04-32mer exhibited the smallest V_p of 325,981.5 $Å^3$ and the greatest $d_{particle}$ of 0.782 g cm^{-3}. In contrast, IgG3*01-62mer and IgG3*08-62mer had the largest V_p values of 593,009.5 and 517,815 $Å^3$, respectively, and the smallest $d_{particle}$ of 0.45 and 0.52 g cm^{-3}, respectively. IgG3*03-47mer and IgG3*12-47mer had V_p and $d_{particle}$ values in between these extremes. In accordance with their relative hinge lengths, IgG1*01-15mer and IgG2*02-12mer exhibited reduced volumes and increased particle densities (Table 5-2).

Table 5-2. Calculated SAXS parameters for low concentration samples.

	IgG1*01	IgG2*02	IgG3*01	IgG3*03	IgG3*04	IgG3*08	IgG3*12
Concentration (mg mL^{-1})	4	4	4.5	4	4.5	4.5	4.5
Hinge length (amino acids)	15	12	62	47	32	62	47
Radius of gyration analysis							
Data point range	2 – 49	2 – 50	4 – 18	2 – 33	4 – 27	3 – 18	2 – 20
I(0) (cm-1) [from Guinier]	0.04 ± 0.0002	0.038 ± 0.0002	0.26 ± 0.0029	0.031 ± 0.0004	0.12 ± 0.0013	0.3 ± 0.0031	0.2 ± 0.0021
Rg (Å) [from Guinier]	49.72 ± 0.47	48.92 ± 0.51	77.84 ± 1.26	67.25 ± 1.37	56.93 ± 0.98	77.17 ± 1.21	67.92 ± 1.2
*q*Rg limits	0.3 – 1.28	0.3 – 1.28	0.52 – 1.28	0.41 – 1.29	0.38 – 1.29	0.46 – 1.26	0.36 – 1.21
Fidelity	1	1	1	1	1	1	0.99
Distance distribution analysis							
q range ($Å^{-1}$)	0.0061 – 0.2018	0.0061 – 0.1997	0.0073 – 0.1941	0.0061 – 0.1997	0.0073 – 0.1983	0.0059 – 0.2004	0.0073 – 0.2004
P(r) total quality estimate	0.83	0.8378	0.63	0.72	0.71	0.63	0.72
Rg (Å) [from Guinier]	50.91	49.18	78.68	68.92	58.53	78.25	67.43
I(0) (cm^{-1}) [from Guinier]	0.043	0.03749	0.2593	0.03067	0.1193	0.2985	0.1934
Rg (Å) [from P(r)]	50.93 ± 0.23	49.19 ± 0.23	79.05 ± 0.63	69.04 ± 0.55	58.62 ± 0.74	78.48 ± 0.64	67.6 ± 0.57
I(0) (cm^{-1}) [from P(r)]	0.04023 ± 0.0002	0.03749 ± 0.0002	0.2593 ± 0.002	0.03067 ± 0.0003	0.1193 ± 0.001	0.2985 ± 0.002	0.1934 ± 0.002
Dmax (Å)	153.34	145.94	243.66	210.66	190	239	210
Points	153	154	93	131	110	94	102
Alpha	4.512	7.673	2.153	3.34	0.9138	0.8201	1.949
Porod volume analysis – average values across all sample concentrations							
MW (kDa)	149.6	149.2	159.9	156.7	153.5	156.8	156.7
Porod volume estimate ($Å^3$)	292468	246457	593009	451019	325981	517815	433568
$p_{density}$ (g cm^{-3})	0.85	1.00	0.45	0.58	0.78	0.51	0.60

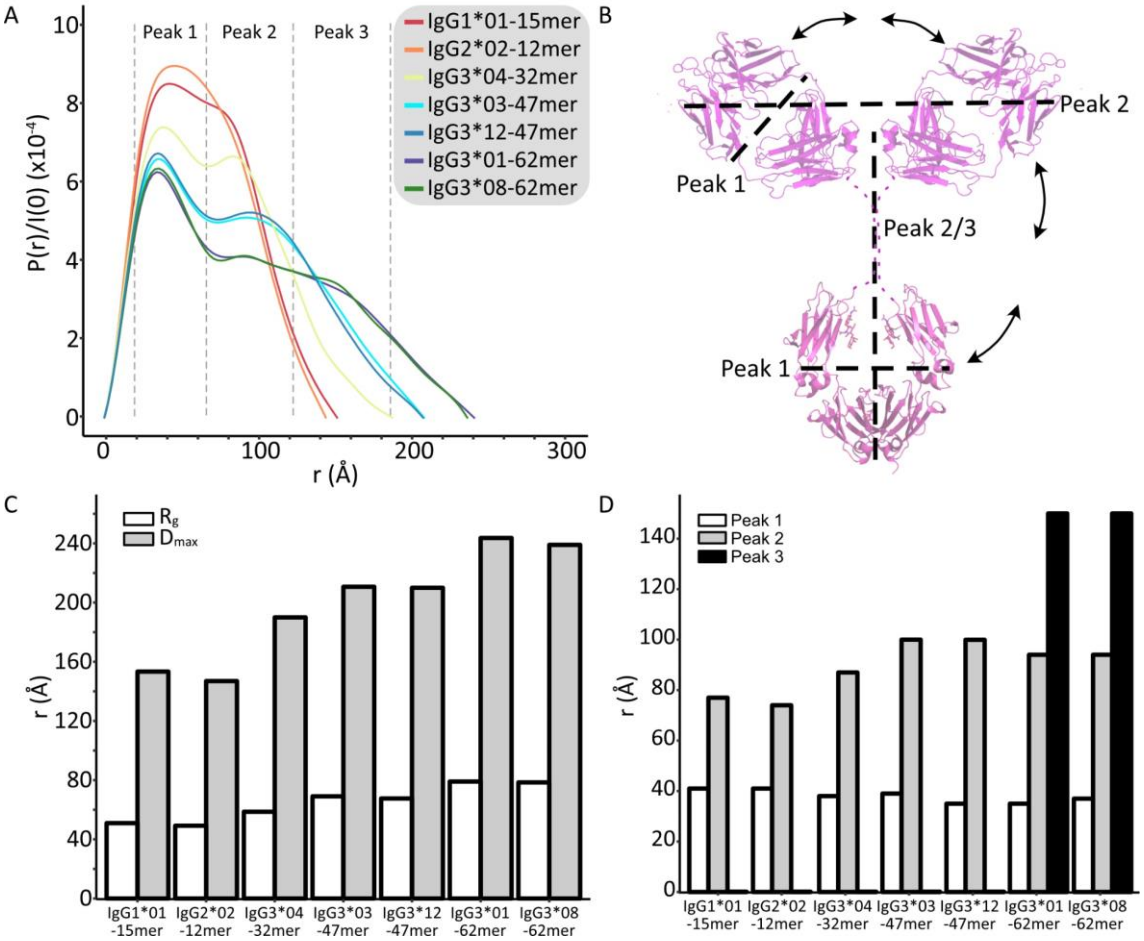

Figure 5-3. Pair distance distribution function (*P(r)*) analysis. (A) *P(r)* plot of each variant at the lowest measured concentration. The *P(r)* values are normalised by relative intensity for comparison of all antibody plots on the same scale. The areas of each peak, numbered across the top, are indicated by the dashed lines. (B) Antibody structure demonstrating the inter-particle distances within a single structure that correlate to each peak in the *P(r)* plot. Arrows indicate the potential range of motion exhibited by the antibody domains. The structure is representative only and was generated using PyMOL with Fab domains from anti-gp120 IgG1 [PDB: 1hzh (Saphire, Parren, Pantophlet, et al., 2001)] and the Fc domain from human IgG3 [PDB: 5w38 (Shah et al., 2017)]. Dashed lines arbitrarily represent the hinge. (C) Bar chart showing radius of gyration (R_g) and maximum inter-particle distance (D_{max}) values calculated from the *P(r)* distributions. (D) Bar chart showing the inter-particle distances (r) corresponding to the maxima of each peak in the *P(r)* distribution.

Dimensionless Kratky plots were used to further assess flexibility, independent of concentration and particle size effects (Figure 5-4B). Regardless of hinge length, the Kratky plot of each variant displayed an eventual downward curvature toward zero. This behaviour is characteristic of extended structures with relatively well-ordered domains (Fab and Fc) tethered by a flexible linker region (the hinge) (Receveur-Bréchot & Durand,

2012). If the structures were fully disordered and unfolded, one would expect the intensity to continue to increase as a function of *q*. Each Kratky plot was asymmetric with two peaks indicating a combination of globular and non-globular protein states. For ordered, globular proteins, one would expect a normal distribution with a peak maximum of 1.104 at $qR_g = \sqrt{3}$ in a *q* range of 0.05 – 0.1 $Å^{-1}$ (Makowski et al., 2020; Receveur-Bréchot & Durand, 2012). This peak was present for all the variants, although became sequentially less obvious for the IgG3 variants as the hinge length increased and the breadth of the second peak increased. To the best of our knowledge, this is the first report of Kratky plots for IgG3 antibodies that show two peaks. For IgG1*01-15mer, the two peaks were of similar intensities but for IgG2*02-12mer the second peak was less pronounced compared to the first peak. The maxima of the second peak increased with hinge length, such that IgG3*01-62mer and IgG3*08-62mer had a significantly larger second peak with a maximum that was slightly right-shifted compared to IgG3*03-47mer, IgG3*12-47mer and IgG3*04-32mer. Ultimately, the maxima of the second peak in the Kratky plots correlated with hinge length.

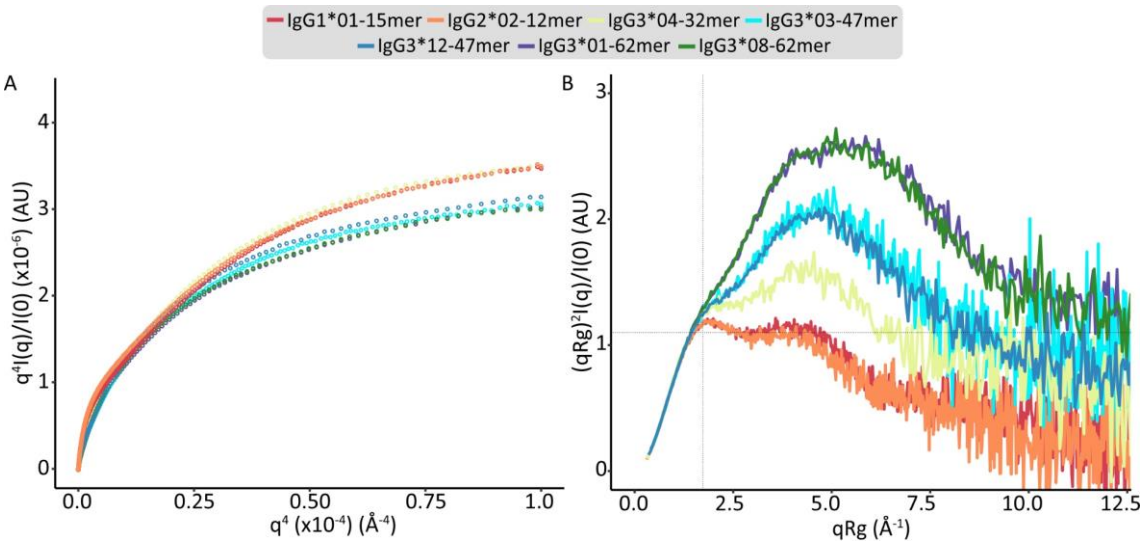

Figure 5-4. Comparison of antibody size and flexibility. (A) Porod-Debye plot of each antibody variant at low concentration, transformed as $q^4I(q)/I(0)$ vs q^4, normalised with I(0) for ease of comparison. (B) Dimensionless Kratky plot of each variant at low concentration. Intensity is normalised and *q* is multiplied by R_g to remove effects of protein size and molecular weight. The grey dashed lines represent the expected peak maxima for folded, globular proteins, where $(qRg)^2I(q)/I(0) = 1.104$ in a *q* range of 0.05 – 0.1 $Å^{-1}$ (Makowski et al., 2020; Receveur-Bréchot & Durand, 2012).

5.5.4 *Ab initio* models reveal distinctive differences between IgG3 antibody structures

Ab initio models produced using GASBOR revealed distinct structural envelopes for each antibody sampled (Figure 5-5A, Figure C-4,Figure C-5). Multiple models were generated for each variant at both concentrations. Model predictions for the same IgG variant consistently produced structural envelopes of similar size but with slight variance in the shape, likely corresponding to variation in Fab domain orientations (Figure C-4B, E, Figure C-5A-E). All of the predicted models had scattering profiles that fit well with the experimental SAXS data, indicated by chi-squared values between 0.23 and 0.5 (Figure 5-5B, Figure C-4C, F, Figure C-5F-J). The models with the lowest chi-squared values were selected as representative models for aligning with reference structures and comparing across variants (Figure 5-5A, C).

Alignment of the *ab initio* models of IgG1*01-15mer and IgG2*02-12mer to the corresponding X-ray crystal structures (PDB: 1hzh and 1igt, respectively) showed good agreement with the exception of some variation in the orientation of the Fab and Fc domains (NSD = 0.9421 and 1.1543, respectively) (Figure C-4A, D). The *ab initio* models of each of the IgG3 variants appeared to have at least two distinct conformational spaces separated by a region where the density of the model narrows (Figure 5-5A, C). This separation was not as defined in the IgG1*01-15mer and IgG2*02-12mer models. The IgG3 *ab initio* models were superimposed onto the full-length solution structure of human myeloma IgG3 antibody (Spiteri, Goodall, et al., 2021). The regions where the modelled envelope was more of a globular shape aligned well to the Fab and Fc domains, and the narrower regions corresponded closely to the hinge domain. The modelled density of the hinge domain was distinctly different between the IgG3 variants. For IgG3*04-32mer, this region was not as well defined in comparison to the other IgG3 variants, and the space between the Fc domain and the Fab domains was distinctly shorter. The model of IgG3*04-32mer overlaid on the myeloma IgG3 structure clearly demonstrated this size discrepancy in the hinge (NSD = 1.5151). The models of IgG3*01-62mer and IgG3*08-62mer showed improved alignment with the full-length myeloma IgG3 structure (NSD = 1.1275 and 1.4631, respectively). Differences in the orientation of the hinge may explain the NSD values above 1. The model of IgG3*12-47mer also showed a relatively good alignment with the full-length structure (NSD = 1.2276), despite having one less hinge exon. We suspect this was aided by the orientations of the hinge domains matching between the aligned structures. Nevertheless, differences between the overall

length and positions of the Fab domains were evident. Similarly, the *ab initio* model of IgG3*03-47mer showed moderate agreement with the myeloma IgG3 structure (NSD = 1.2409) but a clear difference in overall size was evident. Superimposition of all five IgG3 *ab initio* models further emphasized the size differences between variants (Figure 5-5C). The shape of each model appeared to be similar between the variants with a Fab domain orientated above the Fc and the second Fab domain more outstretched. The *ab initio* models of IgG3*01-62mer and IgG3*08-62mer were considerably longer than the other IgG3 variants, from the bottom of the Fc space to the top of the Fab space.

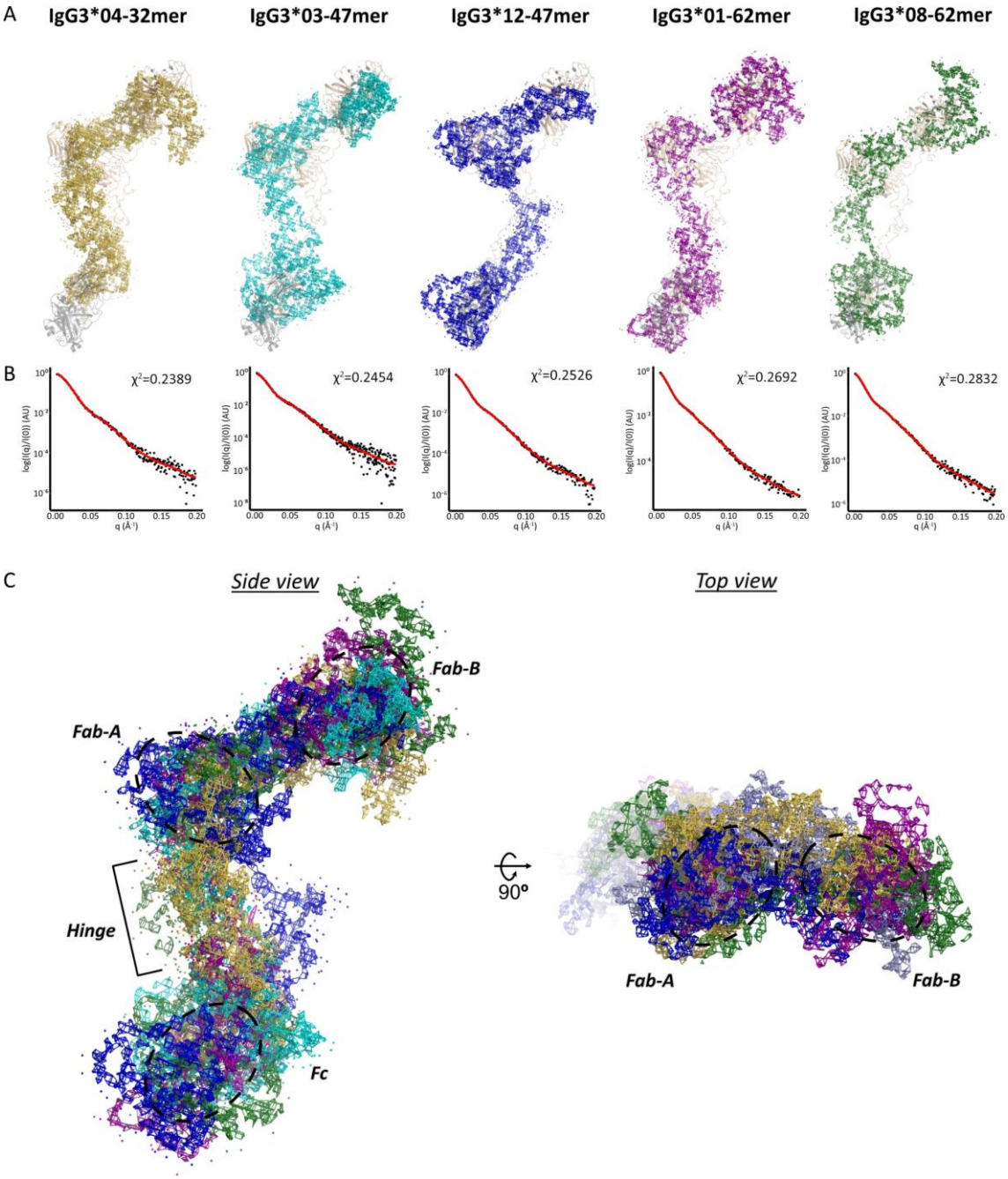

Figure 5-5. Bead models of IgG3 variants. (A) *Ab initio* bead models of each IgG3 variant, represented by the predicted model with the lowest chi-squared value. All other models are presented in Figure C-4, Figure C-5. Structures were generated in PyMOL. Mesh structural envelopes are shown overlaid onto human myeloma IgG3 solution structure (SASDBD reference SASDLZ2 (Spiteri, Goodall, et al., 2021)), presented in order of increasing hinge length (left-to-right): IgG3*04-32mer (yellow), IgG3*03-47mer (cyan), IgG3*12-47mer (blue), IgG3*01-62mer (purple) and IgG3*08-62mer (green). (B) Scattering curves of the predicted models (red line) fit to the experimental scattering data (black dots), with chi-squared values of the fits. (C) Alignment of the representative *ab initio* models for each variant in their respective colours. Left: the side view of the antibody orientated with Fc on the bottom. Right: view from the top of the structures looking down.

5.6 Discussion

Distinct conformational dynamics of naturally occurring IgG3 hinge length variants were characterised in this study using SEC-SAXS. Solution scattering profiles revealed differences in flexibility of IgG3 variants that correlated with the size of the hinge, such that the most common, long hinge polymorphism conferred the greatest flexibility. From the SAXS data, low-resolution bead models of full-length IgG3 allelic variants were resolved, highlighting distinctive structural variations specific to the hinge lengths. Previous publications comparing solution-based structures of all four IgG subclasses have reported similar links between hinge length and flexibility however the structures of IgG3 are limited to the long, 62 amino acid hinge sequence (Eryilmaz et al., 2013; X. Liu et al., 2019; Spiteri, Goodall, et al., 2021). In comparison to those studies, this study involves the naturally occurring diversity present among the human IgG3 allele sequences, providing unique insight into how allelic variation affects antibody structure.

Size differences between the IgG3 hinge length variants were evident from the SAXS scattering behaviour. The R_g and D_{max} determined from the SAXS data for IgG3*01-62mer and IgG3*08-62mer were the largest of all the variants, in accordance with previous comparative studies (Eryilmaz et al., 2013; X. Liu et al., 2019; Spiteri, Goodall, et al., 2021). In comparison to the other IgG3 variants, R_g and D_{max} were reduced for IgG3*03-47mer and IgG3*12-47mer, and further reduced for IgG3*04-32mer. These size differences were visible in the *ab initio* models where the structures appeared to be more elongated for the longer hinge variants. The globular-shaped regions of the structural envelopes, occupied by the Fab and Fc domains, were positioned further apart in the models with longer hinge sequences, and the narrow region of the envelopes was lengthened (Figure 5-5). These characteristics indicate the hinge adopts an extended, rather than compact, conformation when in solution, similar to the solution structures of human myeloma IgG3 (Ryazantsev et al., 1990; Spiteri, Goodall, et al., 2021). The presence of three interchain disulphide bonds within each lower hinge exon (H2-H4) restricts movement of the heavy chains away from each other and causes the hinge to retain an ordered elongated structure. Thus, as the sequence length increases, the structure progressively lengthens and separates the Fab domains further from the Fc.

The *P(r)* distribution analysis further confirmed the role of the hinge in extending the antibody structure. IgG1*01-15mer and IgG2*02-12mer had *P(r)* distributions with two peaks which is characteristic for these IgG subclasses. On the other hand, *P(r)* distributions with three peaks are thought to be typical of the IgG3 subclass (X. Liu et al.,

2019; Lu et al., 2007; Spiteri, Goodall, et al., 2021). Among the variants tested here, only IgG3*01-62mer and IgG3*08-62mer exhibited three distinct peaks (Figure 5-3A). IgG3*03-47mer, IgG3*12-47mer, and IgG3*04-32mer each displayed only two distinct peaks with slight shifts in r of the maxima of the second peak. There was a clear trend between the hinge length and the magnitude of r corresponding to the second peak maxima (Figure 5-3D). For IgG3 variants, the maxima of the second peak occurred at slightly higher r values as the hinge length increased. Assuming that this maximum is the widest distance between the Fab domains, this suggests the longer hinge length enables the Fab domains to orientate further apart from one another. Several studies suggest that it is only the "upper hinge" (hinge exon H1) that governs the Fab-Fab motions due to the long stretch of amino acids without inter-chain disulphide bonds (Dangl et al., 1988; Roux et al., 1998; Tan et al., 1990). As all the IgG3 variants analysed in this study have the same H1 exon, one would expect the distances sampled between the Fab domains to be very similar. Rather, we concluded that the interatomic distance between the furthest point on the Fc to a Fab domain was similar in length to the Fab-Fab distance, causing overlap of these peaks in the *P(r)* distribution. This hypothesis was supported by the presence of a third peak for the longest hinge variants, IgG3*01-62mer and IgG3*08-62mer, only. Having defined what each frequently sampled distance shown in the *P(r)* distributions corresponded to, we were able to confirm that the change in overall size of the structures was attributed to the hinge sequence length.

Having confirmed a longer hinge length corresponded to a more elongated molecule, our subsequent analysis investigated how this elongated state influenced the movement of the three independent domains (two Fab and a single Fc) as a measurement of overall molecule flexibility. Collectively, the Dimensionless Kratky plots and the Porod volume analyses suggested hinge length was correlated with overall flexibility. The presence of a broad peak in the Kratky plots, particularly for the longest hinge variants, is consistent with a large separation of the Fab and Fc domains causing the three regions to show independent scattering (X. Liu et al., 2019; Spiteri, Goodall, et al., 2021). The breadth of this peak was reduced for the other variants, suggesting allelic variants possessing the short IgG3 hinge are less flexible with structural features in between that of the long hinge variants and IgG1. This was also in accordance with the Porod volume and particle density analysis, in which the longest hinge variants, took up the largest volume but had the smallest particle density indicating the greatest flexibility. While low-resolution structures were predicted with good agreement to the scattering intensity curves, such a large degree of flexibility is difficult to capture by *ab initio* bead modelling alone. To

address this limitation in the future, molecular dynamic simulations would complement the structural insights presented here and enable profiling of the full assortment of conformations sampled by IgG3.

The structural differences identified using SAXS are likely of high biological relevance and suggest a potential structural basis for differences in Fc receptor (FcR) binding by IgG3 hinge length variants (de Taeye et al., 2020) or links to disease severity (López-Martínez et al., 2022). The orientation of the Fab domains in relation to the Fc has been shown to be important for accessibility of the FcR and C1q binding sites, preventing steric hindrance from interfering with the interactions (Lu et al., 2007; Rayner et al., 2015). It has also been proposed that the flexibility governed by the long hinge assists with bivalent antigen binding, which improves FcR and C1q binding affinity (Spiteri, Goodall, et al., 2021). The differences resolved between the IgG3 variants in the SAXS analysis highlight the value of future experimental work to determine how FcR/C1q accessibility to these sites differs between variants. We note that even the shortest hinge length variant of IgG3 has greater flexibility than either IgG1 or IgG2 subclasses, meaning effects on receptor binding may be universally observed across the IgG3 subclass. Alongside effector function, the long hinge makes IgG3 particularly susceptible to protease degradation which is a major concern for therapeutic development (Morell et al., 1970). As our results suggest a slightly more compact structure for IgG3 with shorter hinge sequences, an investigation into the protease resistance of these alleles is warranted. Improved protease resistance conferred by a short hinge would be therapeutically desirable for the enhancement of serum half-life, while potentially still enabling access to functionality offered by a hinge that is more flexible than that of other IgG subclasses.

Comparison of the SAXS profiles of the naturally occurring IgG3 hinge length variants elucidated distinguishable differences in conformational shape and flexibility. The models generated from the SAXS data showed asymmetric structures across all three subclasses and demonstrated differences in elongation of the hinge region between IgG3 variants. Often, emphasis is placed on the extended IgG3 hinge when comparing the subclasses. This study highlights for the first time that even within the IgG3 subclass there is variation in the hinge length that significantly alters antibody structural dynamics. It may, therefore, be beneficial to consider this variation when making generalised conclusions about IgG3 as a subclass. Further investigation into the functional effects of this diversity will be valuable to understanding the driving forces behind this variation and may help guide protein engineering efforts for therapeutic antibody development.

5.7 Future Directions†

This study provides an initial insight into differences between the hinge length variation in IgG3 antibodies. Although low-resolution in comparison to X-ray crystal structures, the creation of *ab initio* bead models provides evidence of distinct structural differences between the variants. These findings strongly support the further investigation of conformational dynamics at higher resolution than presented here.

For instance, the application of complementary analytical techniques and molecular dynamic (MD) simulations will provide further insight into the conformational dynamics of each variant. MD is a useful tool to produce an ensemble of structural models that represent the range of conformations assumed by each antibody in solution. SAXS data can be used as an input into MD simulations to generate models that satisfy specific spatial restraints but still account for the highly flexible nature of antibodies (Belviso et al., 2022; Kralj et al., 2021; Perkins et al., 2016; Spiteri, Goodall, et al., 2021; X. Zhang et al., 2015). For example, the structure of IgG1 mouse chimera mAb, rituximab, was modelled by MD simulations with biologically relevant constraints defined by the experimental SAXS data (Belviso et al., 2022). An assortment of structures was generated that captured the flexibility of the antibody in solution. Of particular relevance to the analysis of IgG3 performed in our study, are the MD simulations performed following SAXS analysis of glycosylated and deglycosylated human myeloma IgG3 antibodies, in which models were generated that shared excellent agreement with experimental SAXS data (Spiteri, Goodall, et al., 2021).

High-resolution analytical techniques such as hydrogen/deuterium exchange-mass spectrometry (HDX-MS) and negative stain electron microscopy (EM) are useful tools to complement experimental SAXS data and require relatively small amounts of sample (Gallagher et al., 2019; Huang & Chen, 2014; Wei et al., 2014). Negative stain EM has been implemented to generate and compare three-dimensional (3D) structures of MET-antibodies with backbones of subclass IgG1, IgG2, and IgG4 (Chen et al., 2017). The assortment of antibodies in different conformations are visualised by negative stain EM and can be averaged to evaluate the flexibility of the structures. Reconstruction of the negative stain EM structures in 3D or MD models can provide useful structural information to support SAXS data analysis along with interpretation of HDX-MS data, especially in lieu of X-ray crystal structures.

†The Future Directions section is not part of the manuscript that will be submitted for publication. This section is written for the thesis only to advise on future work intended to expand these studies.

HDX-MS is used to evaluate the structural dynamics of proteins in solution by tracking the exchange of hydrogen in the backbone for deuterium ions in solution over time. Hydrogens that are surface exposed or involved in weak hydrogen bonds will exchange more readily than those involved with stabilising the protein structure (Wales & Engen, 2006). Mass spectrometry is used to monitor the uptake of deuterium by measuring the change in mass of the peptide over time. HDX-MS data can be combined with broader structural information obtained from negative stain EM or SAXS, for instance, to gain insight into dynamic conformational changes (Engen & Komives, 2020; D. Houde & Engen, 2013; A. Zhang et al., 2015). This technique has been applied to assess antibody conformational dynamics. For example, HDX-MS coupled with X-ray crystallography data revealed conformational changes occurred at Fc receptor binding regions when glycans were removed from a full-length IgG1 mAb (D. Houde et al., 2009). More recently, the structural impact of phase separation and protein concentration of an IgG4 mAb was directly measured by HDX-MS (Y. Tian et al., 2019).

Work is currently underway to further evaluate the structural dynamics of IgG3 hinge length variants using the complementary techniques discussed above. The SAXS analysis presented in the manuscript is essential for informing the design of these subsequent experiments, specifically for defining parameters of MD simulations. Alignment of the SAXS data with flexibility data from HDX-MS and negative stain EM will provide a comprehensive understanding of the influence of IgG3 constant region diversity on antibody dynamics.

5.8 Supplementary Material

Supplementary Table C-1 and Figures C-1 – C-5 can be found via Appendix C: Supplementary Material for Chapter Five.

†The Future Directions section is not part of the manuscript that will be submitted for publication. This section is written for the thesis only to advise on future work intended to expand these studies.

5.9 References

Ashish, Solanki, A. K., Boone, C. D., & Krueger, J. K. (2010). Global structure of HIV-1 neutralizing antibody IgG1 b12 is asymmetric. *Biochem Biophys Res Comm*, *391*(1), 947–951. https://doi.org/10.1016/j.bbrc.2009.11.170

Bashirova, A. A., Zheng, W., Akdag, M., Augusto, D. G., Vince, N., Dong, K. L., O'hUigin, C., & Carrington, M. (2021). Population-specific diversity of the immunoglobulin constant heavy G chain (IGHG) genes. *Genes Immun*, *22*(7–8), 327–334. https://doi.org/10.1038/s41435-021-00156-2

Belviso, B. D., Mangiatordi, G. F., Alberga, D., Mangini, V., Carrozzini, B., & Caliandro, R. (2022). Structural Characterization of the Full-Length Anti-CD20 Antibody Rituximab. *Front Mol Biosci*, *9*. https://www.frontiersin.org/articles/10.3389/fmolb.2022.823174

Brosey, C. A., & Tainer, J. A. (2019). Evolving SAXS versatility: Solution X-ray scattering for macromolecular architecture, functional landscapes, and integrative structural biology. *Curr Opin Struct Biol*, *58*, 197–213. https://doi.org/10.1016/j.sbi.2019.04.004

Calonga-Solís, V., Malheiros, D., Beltrame, M. H., Vargas, L. B., Dourado, R. M., Issler, H. C., Wassem, R., Petzl-Erler, M. L., & Augusto, D. G. (2019). Unveiling the diversity of immunoglobulin gamma heavy chain constant region (IGHG) gene segments in Brazilian populations reveals twenty-eight novel alleles and evidence of gene conversion and natural selection. *Front Immunol*, *10*, 1161. https://doi.org/10.3389/fimmu.2019.01161

Canfield, S. M., & Morrison, S. L. (1991). The binding affinity of human IgG for its high affinity Fc receptor is determined by multiple amino acids in the CH2 domain and is modulated by the hinge region. *J Exp Med*, *173*(6), 1483–1491.

Carter, P. J. (2006). Potent antibody therapeutics by design. *Nat Rev Immunol*, *6*(5), 5. https://doi.org/10.1038/nri1837

Chen, Q., Vieth, M., Timm, D. E., Humblet, C., Schneidman-Duhovny, D., Chemmama, I. E., Sali, A., Zeng, W., Lu, J., & Liu, L. (2017). Reconstruction of 3D structures of MET antibodies from electron microscopy 2D class averages. *PLoS ONE*, *12*(4), e0175758. https://doi.org/10.1371/journal.pone.0175758

Chu, T. H., Crowley, A. R., Backes, I., Chang, C., Tay, M., Broge, T., Tuyishime, M., Ferrari, G., Seaman, M. S., Richardson, S. I., Tomaras, G. D., Alter, G., Leib, D., & Ackerman, M. E. (2020). Hinge length contributes to the phagocytic activity of HIV-specific IgG1 and IgG3 antibodies. *PLOS Pathogens*, *16*(2), e1008083. https://doi.org/10.1371/journal.ppat.1008083

Cooper, L. J., Robertson, D., Granzow, R., & Greenspan, N. S. (1994). Variable domain-identical antibodies exhibit IgG subclass-related differences in affinity and kinetic constants as determined by surface plasmon resonance. *Mol Immunol*, *31*(8), 577–584. https://doi.org/10.1016/0161-5890(94)90165-1

Crowley, A. R., Richardson, S. I., Tuyishime, M., Jennewein, M., Bailey, M. J., Lee, J., Alter, G., Ferrari, G., Morris, L., & Ackerman, M. E. (2022). Functional consequences of allotypic polymorphisms in human immunoglobulin G subclasses. *Immunogenetics*. https://doi.org/10.1007/s00251-022-01272-7

Dangl, J. L., Wensel, T. G., Morrison, S. L., Stryer, L., Herzenberg, L. A., & Oi, V. T. (1988). Segmental flexibility and complement fixation of genetically engineered chimeric human, rabbit and mouse antibodies. *The EMBO J*, *7*(7), 1989–1994.

de Taeye, S. W., Bentlage, A. E. H., Mebius, M. M., Meesters, J. I., Lissenberg-Thunnissen, S., Falck, D., Sénard, T., Salehi, N., Wuhrer, M., Schuurman, J., Labrijn, A. F., Rispens, T., & Vidarsson, G. (2020). FcγR binding and ADCC activity of human IgG allotypes. *Front Immunol*, *11*(740). https://doi.org/10.3389/fimmu.2020.00740

D'Eall, C., Pon, R. A., Rossotti, M. A., Krahn, N., Spearman, M., Callaghan, D., van Faassen, H., Hussack, G., Stetefeld, J., Butler, M., Durocher, Y., Zhang, J., Henry, K. A., & Tanha, J. (2019). Modulating antibody-dependent cellular cytotoxicity of epidermal growth factor receptor-specific heavy-chain antibodies through hinge engineering. *Immunol Cell Biol*, *97*(6), 526–537. https://doi.org/10.1111/imcb.12238

Engen, J. R., & Komives, E. A. (2020). Complementarity of Hydrogen/Deuterium Exchange Mass Spectrometry and Cryo-Electron Microscopy. *Trends Biochem Sci*, *45*(10), 906–918. https://doi.org/10.1016/j.tibs.2020.05.005

Eryilmaz, E., Janda, A., Kim, J., Cordero, R. J. B., Cowburn, D., & Casadevall, A. (2013). Global structures of IgG isotypes expressing identical variable regions. *Mol Immunology*, *56*(4), 588–598. https://doi.org/10.1016/j.molimm.2013.06.006

Ford, E. E., Tieri, D., Rodriguez, O. L., Francoeur, N. J., Soto, J., Kos, J. T., Peres, A., Gibson, W. S., Silver, C. A., Deikus, G., Hudson, E., Woolley, C. R., Beckmann, N., Charney, A., Mitchell, T. C., Yaari, G., Sebra, R. P., Watson, C. T., & Smith, M. L. (2023). FLAIRR-Seq: A Method for Single-Molecule Resolution of Near Full-Length Antibody H Chain Repertoires. *J Immunol*, ji2200825. https://doi.org/10.4049/jimmunol.2200825

Foss, S., Jonsson, A., Bottermann, M., Watkinson, R., Lode, H. E., McAdam, M. B., Michaelsen, T. E., Sandlie, I., James, L. C., & Andersen, J. T. (2022). Potent TRIM21 and complement-dependent intracellular antiviral immunity requires the IgG3 hinge. *Sci Immun*, *7*(70), eabj1640. https://doi.org/10.1126/sciimmunol.abj1640

Furtado, P. B., Whitty, P. W., Robertson, A., Eaton, J. T., Almogren, A., Kerr, M. A., Woof, J. M., & Perkins, S. J. (2004). Solution Structure Determination of Monomeric Human IgA2 by X-ray and Neutron Scattering, Analytical Ultracentrifugation and Constrained Modelling: A Comparison with Monomeric Human IgA1. *J Mol Biol*, *338*(5), 921–941. https://doi.org/10.1016/j.jmb.2004.03.007

Gallagher, J. R., Kim, A. J., Gulati, N. M., & Harris, A. K. (2019). Negative-Stain Transmission Electron Microscopy of Molecular Complexes for Image Analysis by 2D Class Averaging. *Curr Protoc Microbiol*, *54*(1), e90. https://doi.org/10.1002/cpmc.90

Giudicelli, V., Duroux, P., Ginestoux, C., Folch, G., Jabado-Michaloud, J., Chaume, D., & Lefranc, M.-P. (2006). IMGT/LIGM-DB, the IMGT® comprehensive database of immunoglobulin and T cell receptor nucleotide sequences. *Nucleic Acids Res*, *34*(suppl_1), D781–D784. https://doi.org/10.1093/nar/gkj088

Giuntini, S., Granoff, D. M., Beernink, P. T., Ihle, O., Bratlie, D., & Michaelsen, T. E. (2016). Human IgG1, IgG3, and IgG3 Hinge-Truncated Mutants Show Different Protection Capabilities against Meningococci Depending on the Target Antigen and Epitope Specificity. *Clin Vaccine Immunol*, *23*(8), 698–706. https://doi.org/10.1128/CVI.00193-16

Gregory, L., Davis, K. G., Sheth, B., Boyd, J., Jefferis, R., Nave, C., & Burton, D. R. (1987). The solution conformations of the subclasses of human IgG deduced from sedimentation and small angle X-ray scattering studies. *Mol Immunol*, *24*(8), 821–829. https://doi.org/10.1016/0161-5890(87)90184-2

Harris, L. J., Larson, S. B., Hasel, K. W., Day, J., Greenwood, A., & McPherson, A. (1992). The three-dimensional structure of an intact monoclonal antibody for canine lymphoma. *Nature*, *360*(6402), 6402. https://doi.org/10.1038/360369a0

Harris, L. J., Larson, S. B., Hasel, K. W., & McPherson, A. (1997). Refined structure of an intact IgG2a monoclonal antibody. *Biochemistry*, *36*(7), 1581–1597. https://doi.org/10.1021/bi962514+

Harris, L. J., Skaletsky, E., & McPherson, A. (1998). Crystallographic structure of an intact IgG1 monoclonal antibody11Edited by I. A. Wilson. *J Mol Biol*, *275*(5), 861–872. https://doi.org/10.1006/jmbi.1997.1508

Hopkins, J. B., Gillilan, R. E., & Skou, S. (2017). BioXTAS RAW: Improvements to a free open-source program for small-angle X-ray scattering data reduction and analysis. *J of Appl Crystallogr*, *50*(5), 5. https://doi.org/10.1107/S1600576717011438

Houde, D., Arndt, J., Domeier, W., Berkowitz, S., & Engen, J. R. (2009). Rapid characterization of IgG1 conformation and conformational dynamics by hydrogen/deuterium exchange mass spectrometry. *Anal Chem*, *81*(7), 2644–2651. https://doi.org/10.1021/ac802575y

Houde, D., & Engen, J. R. (2013). Conformational Analysis of Recombinant Monoclonal Antibodies with Hydrogen/Deuterium Exchange Mass Spectrometry. *Methods in Molecular Biology (Clifton, N.J.)*, *988*, 269. https://doi.org/10.1007/978-1-62703-327-5_17

Huang, R. Y.-C., & Chen, G. (2014). Higher order structure characterization of protein therapeutics by hydrogen/deuterium exchange mass spectrometry. *Anal Bioanal Chem*, *406*(26), 6541–6558. https://doi.org/10.1007/s00216-014-7924-3

Hui, G. K., Gardener, A. D., Begum, H., Eldrid, C., Thalassinos, K., Gor, J., & Perkins, S. J. (2019). The solution structure of the human IgG2 subclass is distinct from those for human IgG1 and IgG4 providing an explanation for their discrete functions. *J Biol Chem*, *294*(28), 10789–10806. https://doi.org/10.1074/jbc.RA118.007134

Hui, G. K., Wright, D. W., Vennard, O. L., Rayner, L. E., Pang, M., Yeo, S. C., Gor, J., Molyneux, K., Barratt, J., & Perkins, S. J. (2015). The solution structures of native and patient monomeric human IgA1 reveal asymmetric extended structures: Implications for function and IgAN disease. *Biochem J*, *471*(2), 167–185. https://doi.org/10.1042/bj20150612

Izadi, A., Hailu, A., Godzwon, M., Wrighton, S., Olofsson, B., Schmidt, T., Söderlund-Strand, A., Elder, E., Appelberg, S., Valsjö, M., Larsson, O., Wendel-Hansen, V., Ohlin, M., Bahnan, W., & Nordenfelt, P. (2023). Subclass-switched anti-spike IgG3 oligoclonal cocktails strongly enhance Fc-mediated opsonization. *PNAS*, *120*(15), e2217590120. https://doi.org/10.1073/pnas.2217590120

Kallolimath, S., Sun, L., Palt, R., Stiasny, K., Mayrhofer, P., Gruber, C., Kogelmann, B., Chen, Q., & Steinkellner, H. (2021). Highly active engineered IgG3 antibodies against SARS-CoV-2. *PNAS*, *118*(42). https://doi.org/10.1073/pnas.2107249118

Kaplon, H., Chenoweth, A., Crescioli, S., & Reichert, J. M. (2022). Antibodies to watch in 2022. *MAbs*, *14*(1), 2014296. https://doi.org/10.1080/19420862.2021.2014296

Khatri, I., Berkowska, M. A., van den Akker, E. B., Teodosio, C., Reinders, M. J. T., & van Dongen, J. J. M. (2021). Population matched (pm) germline allelic variants of immunoglobulin (IG) loci: Relevance in infectious diseases and vaccination studies in human populations. *Genes Immun*, *22*(3), 172–186. https://doi.org/10.1038/s41435-021-00143-7

Kikhney, A. G., & Svergun, D. I. (2015). A practical guide to small angle X-ray scattering (SAXS) of flexible and intrinsically disordered proteins. *FEBS Lett*, *589*(19PartA), 2570–2577. https://doi.org/10.1016/j.febslet.2015.08.027

Kober, C., Manni, S., Wolff, S., Barnes, T., Mukherjee, S., Vogel, T., Hoenig, L., Vogel, P., Hahn, A., Gerlach, M., Vey, M., Widmer, E., Keiner, B., Schuetz, P., Roth, N., & Kalina, U. (2022). IgG3 and IgM Identified as Key to SARS-CoV-2 Neutralization in Convalescent Plasma Pools. *PLOS ONE*, *17*(1), e0262162. https://doi.org/10.1371/journal.pone.0262162

Kozin, M. B., & Svergun, D. I. (2001). Automated matching of high- and low-resolution structural models. *J Appl Crystallog*, *34*(1), 1. https://doi.org/10.1107/S0021889800014126

Kralj, S., Hodošček, M., Podobnik, B., Kunej, T., Bren, U., Janežič, D., & Konc, J. (2021). Molecular Dynamics Simulations Reveal Interactions of an IgG1 Antibody With Selected Fc Receptors. *Front Chem*, *9*. https://www.frontiersin.org/articles/10.3389/fchem.2021.705931

Krapp, S., Mimura, Y., Jefferis, R., Huber, R., & Sondermann, P. (2003). Structural Analysis of Human IgG-Fc Glycoforms Reveals a Correlation Between Glycosylation and Structural Integrity. *J Mol Biol*, *325*(5), 979–989. https://doi.org/10.1016/S0022-2836(02)01250-0

Kyei-Baafour, E., Kusi, K. A., Arthur, F. K. N., Sarkodie-Addo, T., Theisen, M., Dodoo, D., & Adu, B. (2022). Association of Immunoglobulin G3 Hinge Region Length Polymorphism With Cerebral Malaria in Ghanaian Children. *J Infect Dis*, *225*(10), 1786–1790. https://doi.org/10.1093/infdis/jiab548

Larson, S., Day, J., Greenwood, A., Skaletsky, E., & McPherson, A. (1991). Characterization of crystals of an intact monoclonal antibody for canine lymphoma. *J Mol Biol*, *222*(1), 17–19. https://doi.org/10.1016/0022-2836(91)90731-K

Lefranc, M.-P., & Lefranc, G. (2019). IMGT(®) and 30 years of immunoinformatics insight in antibody V and C domain structure and function. *Antibodies (Basel)*, *8*(2), 29. https://doi.org/10.3390/antib8020029

Liu, H., & May, K. (2012). Disulfide bond structures of IgG molecules. *MAbs*, *4*(1), 17–23. https://doi.org/10.4161/mabs.4.1.18347

Liu, X., Zhao, Y., Shi, H., Zhang, Y., Yin, X., Liu, M., Zhang, H., He, Y., Lu, B., Jin, T., & Li, F. (2019). Human immunoglobulin G hinge regulates agonistic anti-CD40 immunostimulatory and antitumour activities through biophysical flexibility. *Nature Comm*, *10*(1), 1. https://doi.org/10.1038/s41467-019-12097-6

López-Martínez, R., Albaiceta, G. M., Amado-Rodríguez, L., Gómez, J., Cuesta-Llavona, E., García-Clemente, M., Hermida-Valverde, T., Enríquez-Rodriguez, A. I., Hernández-González, C., Martínez-Borra, J., López-Larrea, C., Gil-Peña, H., Alvarez, V., & Coto, E. (2022). IGHG3 hinge length variation was associated with the risk of critical disease and death in a Spanish COVID-19 cohort. *Genes Immun*, *23*(6), 205–208. https://doi.org/10.1038/s41435-022-00179-3

Lu, Y., Harding, S. E., Michaelsen, T. E., Longman, E., Davis, K. G., Ortega, Á., Grossmann, J. G., Sandlie, I., & García de la Torre, J. (2007). Solution Conformation of Wild-Type and Mutant IgG3 and IgG4 Immunoglobulins Using Crystallohydrodynamics: Possible Implications for Complement Activation. *Biophys J*, *93*(11), 3733–3744. https://doi.org/10.1529/biophysj.107.108993

Makowski, L., Berkowitz, S. A., & Houde, D. J. (2020). Chapter 8—Scattering techniques for the characterization of biopharmaceuticals. In D. J. Houde & S. A. Berkowitz (Eds.), *Biophysical Characterization of Proteins in Developing Biopharmaceuticals (Second Edition)* (pp. 185–223). Elsevier. https://doi.org/10.1016/B978-0-444-64173-1.00008-1

Manalastas-Cantos, K., Konarev, P. V., Hajizadeh, N. R., Kikhney, A. G., Petoukhov, M. V., Molodenskiy, D. S., Panjkovich, A., Mertens, H. D. T., Gruzinov, A., Borges, C., Jeffries, C. M., Svergun, D. I., & Franke, D. (2021). ATSAS 3.0: Expanded functionality and new tools for small-angle scattering data analysis. *J Appl Crystallog*, *54*(1), 343–355. https://doi.org/10.1107/S1600576720013412

Morell, A., Terry, W. D., & Waldmann, T. A. (1970). Metabolic properties of IgG subclasses in man. *J Clin Invest*, *49*(4), 673–680.

Padlan, E. A. (1996). X-ray crystallography of antibodies. *Adv Protein Chem*, *49*, 57–133. https://doi.org/10.1016/s0065-3233(08)60488-x

Panjkovich, A., & Svergun, D. I. (2018). CHROMIXS: Automatic and interactive analysis of chromatography-coupled small-angle X-ray scattering data. *Bioinformatics (Oxford, England)*, *34*(11), 1944–1946. https://doi.org/10.1093/bioinformatics/btx846

Perkins, S. J., Wright, D. W., Zhang, H., Brookes, E. H., Chen, J., Irving, T. C., Krueger, S., Barlow, D. J., Edler, K. J., Scott, D. J., Terrill, N. J., King, S. M., Butler, P. D., & Curtis, J. E. (2016). Atomistic modelling of scattering data in the ollaborative Computational Project for Small Angle Scattering (CCP-SAS). *J Appl Crystallog*, *49*(6), 1861–1875. Scopus. https://doi.org/10.1107/S160057671601517X

Petoukhov, M. V., Franke, D., Shkumatov, A. V., Tria, G., Kikhney, A. G., Gajda, M., Gorba, C., Mertens, H. D. T., Konarev, P. V., & Svergun, D. I. (2012). New developments in the ATSAS program package

for small-angle scattering data analysis. *J Appl Crystallog*, *45*(Pt 2), 342–350. https://doi.org/10.1107/S0021889812007662

Putnam, C. D. (2016). Guinier peak analysis for visual and automated inspection of small-angle X-ray scattering data. *J Appl Crystallog*, *49*(Pt 5), 1412–1419. https://doi.org/10.1107/S1600576716010906

Rambo, R. P., & Tainer, J. A. (2011). Characterizing flexible and intrinsically unstructured biological macromolecules by SAS using the Porod-Debye law. *Biopolymers*, *95*(8), 559–571. https://doi.org/10.1002/bip.21638

Rayner, L. E., Hui, G. K., Gor, J., Heenan, R. K., Dalby, P. A., & Perkins, S. J. (2015). The Solution Structures of Two Human IgG1 Antibodies Show Conformational Stability and Accommodate Their C1q and FcγR Ligands. *J Biol Chem*, *290*(13), 8420–8438. https://doi.org/10.1074/jbc.M114.631002

Receveur-Bréchot, V., & Durand, D. (2012). How Random are Intrinsically Disordered Proteins? A Small Angle Scattering Perspective. *Curr Protein Pept Sci*, *13*(1), 55–75. https://doi.org/10.2174/138920312799277901

Richardson, S. I., Lambson, B. E., Crowley, A. R., Bashirova, A., Scheepers, C., Garrett, N., Karim, S. A., Mkhize, N. N., Carrington, M., Ackerman, M. E., Moore, P. L., & Morris, L. (2019). IgG3 enhances neutralization potency and Fc effector function of an HIV V2-specific broadly neutralizing antibody. *PLOS Pathogens*, *15*(12), e1008064. https://doi.org/10.1371/journal.ppat.1008064

Roux, K. H., Strelets, L., Brekke, O. H., Sandlie, I., & Michaelsen, T. E. (1998). Comparisons of the Ability of Human IgG3 Hinge Mutants, IgM, IgE, and IgA2, to Form Small Immune Complexes: A Role for Flexibility and Geometry. *J Immunol*, *161*(8), 4083–4090.

Roux, K. H., Strelets, L., & Michaelsen, T. E. (1997). Flexibility of human IgG subclasses. *J Immunol (Baltimore, Md.: 1950)*, *159*(7), 3372–3382.

Ryazantsev, S., Tishchenko, V., Vasiliev, V., Zav'yalov, V., & Abramov, V. (1990). Structure of human myeloma IgG3 Kuc. *Eur J Biochem*, *190*(2), 393–399. https://doi.org/10.1111/j.1432-1033.1990.tb15588.x

Saphire, E. O., Parren, P. W. H. I., Barbas, C. F., Burton, D. R., & Wilson, I. A. (2001). Crystallization and preliminary structure determination of an intact human immunoglobulin, b12: An antibody that broadly neutralizes primary isolates of HIV-1. *Acta Crystallogr, Sect D: Biol Crystallogr*, *57*(1), 1. https://doi.org/10.1107/S0907444900017376

Saphire, E. O., Parren, P. W. H. I., Pantophlet, R., Zwick, M. B., Morris, G. M., Rudd, P. M., Dwek, R. A., Stanfield, R. L., Burton, D. R., & Wilson, I. A. (2001). Crystal Structure of a Neutralizing Human IgG Against HIV-1: A Template for Vaccine Design. *Science*, *293*(5532), 1155–1159. https://doi.org/10.1126/science.1061692

Saphire, E. O., Stanfield, R. L., Max Crispin, M. D., Parren, P. W. H. I., Rudd, P. M., Dwek, R. A., Burton, D. R., & Wilson, I. A. (2002). Contrasting IgG Structures Reveal Extreme Asymmetry and Flexibility. *J Mol Biol*, *319*(1), 9–18. https://doi.org/10.1016/S0022-2836(02)00244-9

Scharf, O., Golding, H., King, L. R., Eller, N., Frazier, D., Golding, B., & Scott, D. E. (2001). Immunoglobulin G3 from Polyclonal Human Immunodeficiency Virus (HIV) Immune Globulin Is More Potent than Other Subclasses in Neutralizing HIV Type 1. *J Virol*, *75*(14), 6558–6565. https://doi.org/10.1128/JVI.75.14.6558-6565.2001

Shah, I. S., Lovell, S., Mehzabeen, N., Battaile, K. P., & Tolbert, T. J. (2017). Structural characterization of the Man5 glycoform of human IgG3 Fc. *Mol Immunol*, *92*, 28–37. https://doi.org/10.1016/j.molimm.2017.10.001

Shaw, A., Hoffecker, I. T., Smyrlaki, I., Rosa, J., Grevys, A., Bratlie, D., Sandlie, I., Michaelsen, T. E., Andersen, J. T., & Högberg, B. (2019). Binding to Nanopatterned Antigens is Dominated by the Spatial Tolerance of Antibodies. *Nat Nanotechnol*, *14*(2), 184–190. https://doi.org/10.1038/s41565-018-0336-3

Spiteri, V. A., Doutch, J., Rambo, R. P., Gor, J., Dalby, P. A., & Perkins, S. J. (2021). Solution structure of deglycosylated human IgG1 shows the role of CH2 glycans in its conformation. *Biophys J*, *120*(9), 1814–1834. https://doi.org/10.1016/j.bpj.2021.02.038

Spiteri, V. A., Goodall, M., Doutch, J., Rambo, R. P., Gor, J., & Perkins, S. J. (2021). Solution structures of human myeloma IgG3 antibody reveal extended Fab and Fc regions relative to the other IgG subclasses. *J Biol Chem*, *297*(3). https://doi.org/10.1016/j.jbc.2021.100995

Svergun, D. I. (1992). Determination of the regularization parameter in indirect-transform methods using perceptual criteria. *J Appl Crystallogr*, *25*(4), 4. https://doi.org/10.1107/S0021889892001663

Svergun, D. I., Petoukhov, M. V., & Koch, M. H. J. (2001). Determination of Domain Structure of Proteins from X-Ray Solution Scattering. *Biophys J*, *80*(6), 2946–2953. https://doi.org/10.1016/S0006-3495(01)76260-1

Tan, L. K., Shopes, R. J., Oi, V. T., & Morrison, S. L. (1990). Influence of the hinge region on complement activation, C1q binding, and segmental flexibility in chimeric human immunoglobulins. *PNAS USA*, *87*(1), 162–166. https://doi.org/10.1073/pnas.87.1.162

Teplyakov, A., Zhao, Y., Malia, T. J., Obmolova, G., & Gilliland, G. L. (2013). IgG2 Fc structure and the dynamic features of the IgG CH2–CH3 interface. *Mol Immunol*, *56*(1), 131–139. https://doi.org/10.1016/j.molimm.2013.03.018

Tian, X., Langkilde, A. E., Thorolfsson, M., Rasmussen, H. B., & Vestergaard, B. (2014). Small-Angle X-ray Scattering Screening Complements Conventional Biophys Analysis: Comparative Structural and Biophys Analysis of Monoclonal Antibodies IgG1, IgG2, and IgG4. *J Pharm Sci*, *103*(6), 1701–1710. https://doi.org/10.1002/jps.23964

Tian, X., Vestergaard, B., Thorolfsson, M., Yang, Z., Rasmussen, H. B., & Langkilde, A. E. (2015). In-depth analysis of subclass-specific conformational preferences of IgG antibodies. *IUCrJ*, *2*(1), 1. https://doi.org/10.1107/S205225251402209X

Tian, Y., Huang, L., Ruotolo, B. T., & Wang, N. (2019). Hydrogen/deuterium exchange-mass spectrometry analysis of high concentration biotherapeutics: Application to phase-separated antibody formulations. *MAbs*, *11*(4), 779–788. https://doi.org/10.1080/19420862.2019.1589850

Wales, T. E., & Engen, J. R. (2006). Hydrogen exchange mass spectrometry for the analysis of protein dynamics. *Mass Spectrom Rev*, *25*(1), 158–170. https://doi.org/10.1002/mas.20064

Warrender, A. K., Pan, J., Pudney, C. R., Arcus, V. L., & Kelton, W. (2023). Constant domain polymorphisms influence monoclonal antibody stability and dynamics. *Prot Sci*, *32*(3), e4589. https://doi.org/10.1002/pro.4589

Wei, H., Mo, J., Tao, L., Russell, R. J., Tymiak, A. A., Chen, G., Iacob, R. E., & Engen, J. R. (2014). Hydrogen/deuterium exchange mass spectrometry for probing higher order structure of protein therapeutics: Methodology and applications. *Drug Discovery Today*, *19*(1), 95–102. https://doi.org/10.1016/j.drudis.2013.07.019

Zhang, A., Fang, J., Chou, R. Y.-T., Bondarenko, P. V., & Zhang, Z. (2015). Conformational Difference in Human IgG2 Disulfide Isoforms Revealed by Hydrogen/Deuterium Exchange Mass Spectrometry. *Biochemistry*, *54*(10), 1956–1962. https://doi.org/10.1021/bi5015216

Zhang, X., Zhang, L., Tong, H., Peng, B., Rames, M. J., Zhang, S., & Ren, G. (2015). 3D Structural Fluctuation of IgG1 Antibody Revealed by Individual Particle Electron Tomography. *Scientific Reports*, *5*(1), 1. https://doi.org/10.1038/srep09803

Chapter Six

Conclusions and Future Perspectives

6.1 Thesis Summary

The immune system has evolved over long timescales to provide host organisms with strong protection against infection. Antibodies form part of this protective layering as integral components of the adaptive immune system, where they can directly eliminate pathogens via direct neutralisation or via Fc-mediated effector functions. Their remarkable effectiveness has led to widespread adoption as therapeutics, culminating in the recent approval of the 100th monoclonal antibody drug (Mullard, 2021). Despite the name given to the constant region of antibody molecules, it is perhaps unsurprising to find evolutionary pressures have also acted upon the protein sequence of this antibody region. Within the last five years, several studies have begun to reveal links between amino acid polymorphisms and the binding affinity to Fc receptors, as well as to disease susceptibility and mortality. However, there is a clear gap in the literature exploring how these polymorphisms might influence fundamental structural dynamics that contribute to antibody stability and flexibility.

To tackle this question, I expressed a large panel of 35 unique antibody variants belonging to subclasses IgG1, IgG2 and IgG3. Each variant encoded naturally occurring amino acid variation in the constant region and invariant trastuzumab variable regions. First, the thermal stability of a subset of 32 antibodies containing equal tryptophan content was compared using red edge excitation shift (REES) spectroscopy. As the IgG antibody variants share many sequence and structural similarities, simple laboratory techniques for measuring protein stability, such as differential scanning fluorimetry, were not sensitive enough to resolve differences between the variants. Using REES, I resolved notable differences in stability between the subclasses, finding that IgG3 exhibited the lowest overall stability while IgG1 had the highest stability. Differences were also apparent between variants within each subclass. Variants belonging to the IgG3 subclass showed the greatest variation in stability, possibly owing to increased sequence diversity between alleles compared to IgG1 and IgG2 variants. I identified select amino acid polymorphisms that were linked to high stability within the IgG3 variant pool. These polymorphisms tended to be located at the interface between heavy chain CH2 and CH3 domains suggesting mutations at these positions strengthen interdomain interactions to prevent the

unfolding of the antibody structure at high temperatures. It was also confirmed that glycans appended to the constant domains of the antibodies did not significantly contribute to observed stability differences. Heterogeneous glycan profiles were resolved by High-Performance Liquid Chromatography and Mass Spectrometry and the relative abundance of each glycan species was very similar among all of the variants.

Within the 21 IgG3 subclass alleles expressed, three have arginine to tryptophan polymorphisms at position 292 which result in two extra tryptophan residues per assembled antibody. As REES uses the intrinsic fluorescence of tryptophan residues to detect changes in protein structural dynamics, these variants were excluded from the comparative analysis presented in Chapter Three. Instead, these naturally occurring variants offered a unique dataset to experimentally demonstrate the link between the tryptophan microenvironment and REES predictions of stability. I confirmed that REES was highly sensitive to the tryptophan microenvironments and the magnitude of parameters derived from the fluorescent profiles were directly correlated to tryptophan solvent exposure. These results validated suggestions made by other groups that tryptophan composition is an important prerequisite for using REES to compare stability between proteins.

In addition to stability, the flexibility of full-length antibody structures is known to have important implications for antigen and Fc-receptor binding. The hinge region, connecting the Fab domains to the Fc domain, is an essential mediator of this flexibility. I was, therefore, interested in investigating the effects of naturally occurring hinge length polymorphisms present in the IgG3 subclass. The solution structures of a subset of IgG3 allelic variants were analysed using size-exclusion coupled small angle X-ray scattering. Distinct X-ray scattering behaviour was consistently observed for variants with different hinge lengths, which translated to differences in the overall dimensions and flexibility of the antibody structures. *Ab initio* models generated from the scattering data revealed a relationship between hinge length and structural compactness, in which a longer hinge correlated with a more elongated structure. The findings from this study provide strong precedence to proceed with more in-depth analyses of the genetic variants which will have important implications for understanding the structural mechanisms underlying functionality differences.

Beyond the findings presented here, a further key outcome of this work is the production of a large panel of IgG antibodies which will be an important resource for future studies in this area. The antibody expression vectors are specially designed in a modular format

with restriction enzyme recognition sites for the easy exchange of variable domains and constant region sequences. This provides a cost-effective means of producing a diverse range of antibodies with different antigen specificities (variable domains) and alternate constant region sequences, such as novel IgG allele sequences. The vectors are designed for mammalian expression using HEK293 cell lines to enable the production of well-assembled, low-endotoxin antibody preparations in future work.

6.2 Future Perspectives

6.2.1 Assess the influence of IgG allelic variation on anti-viral neutralisation via intracellular receptor, Tripartite Motif 21

Having resolved key aspects of how IgG genetic diversity influences fundamental antibody properties, further investigations into the influence on effector functions will contribute to a more comprehensive understanding of polymorphic effects. The binding to canonical Fc receptors by IgG allelic variants has been analysed previously (Crowley et al., 2022; de Taeye et al., 2020). Specific polymorphisms present in IgG3 alleles have been linked to enhanced binding affinities to FcγRIIa and FcγRIIIa receptors and stronger antibody dependent cellular cytotoxicity activity (de Taeye et al., 2020). While single amino acid mutations do not appear to affect antibody mediated phagocytosis (Crowley et al., 2022), variation in hinge length has been correlated with phagocytic activity (Chu et al., 2020).

Outside of the canonical Fc receptors there is a large array of other ligands that can bind to the Fc domain to mediate immune functions (e.g., Fc receptor-like molecules, and complement component C1q). In light of the recent SARS-CoV-2 pandemic, it would be of particular interest to investigate the binding of IgG alleles to the intracellular receptor Tripartite Motif 21 (TRIM21) (Mallery et al., 2010; McEwan et al., 2012). TRIM21 is located inside the cytoplasm of the cell and triggers antibody-dependent intracellular neutralisation (ADIN) by interacting with antibodies coating cytosolic viruses (Foss et al., 2016). While TRIM21 binds to a range of antibody isotypes (IgA, IgM, and IgG), the interactions are strongest with IgG (Foss et al., 2015; Mallery et al., 2010). Differences in binding affinity have been attributed to sequence variation in the CH3-loop (positions 429 to 436) of the IgG-TRIM21 binding site (Foss et al., 2015). The binding site also overlaps with that of Protein A, which is well established to only bind to IgG antibodies with a histidine polymorphism at position 435 (Saito et al., 2019; Shah et al., 2017). It is therefore possible that TRIM21 binding may also be dependent on constant region amino

acid polymorphisms considering the location of these polymorphic residues in the Fc binding pocket of the PRYSPRY TRIM21 subdomain (McEwan, 2016). Interestingly, the flexibility of the longest IgG3 hinge domain has been shown to enhance TRIM21 mediated neutralisation capacity (Foss et al., 2022). Characterising the interaction between TRIM21 and IgG allelic variants would contribute to our understanding of intracellular immunity and inform development of novel antibody-based therapeutics, particularly against viruses where antibody-mediated neutralisation is difficult.

I have conducted preliminary experiments to assess the binding kinetics of IgG allelic variants with TRIM21 (Unpublished data). These experiments were performed in the Laboratory of Systems and Synthetic Immunology led by Prof. Sai Reddy at ETH Zurich, Switzerland. The kinetics of IgG-TRIM21 binding were determined using Biolayer Interferometry (BLI) technology on an Octet Red 96e system. This equipment enabled the accurate determination of association and dissociation rates for a subset of IgG genetic variants in high throughput. The experimental conditions (e.g., ligand concentration, analyte concentration, and surface regeneration conditions) were optimised for our panel of antibodies with purified, full-length TRIM21 (Appendix D.1). Kinetic data was collected for nine IgG3 antibody variants with surface bound TRIM21 (Figure 6-1A). The association rates (k_{on}), dissociation rates (k_{off}), and equilibrium constant (K_D) were determined by fitting the curves with a 1:1 binding model. The association and dissociation rates were similar for most of the variants, except for IgG3*17 which had substantially slower rates for both steps (Figure 6-1B). Disparities in the overall binding affinities (as determined by the K_D values) (Figure 6-1C) suggest polymorphic diversity may influence this interaction, however a direct correlation with specific amino acid polymorphisms is yet to be determined and will require further experimentation. It should be noted that TRIM21 neutralisation potency is not necessarily correlated to the binding affinity (Bottermann et al., 2016; Foss et al., 2016, 2022). Therefore, *in vitro* experiments to test allelic variation with viral neutralisation would also be of value to this line of investigation.

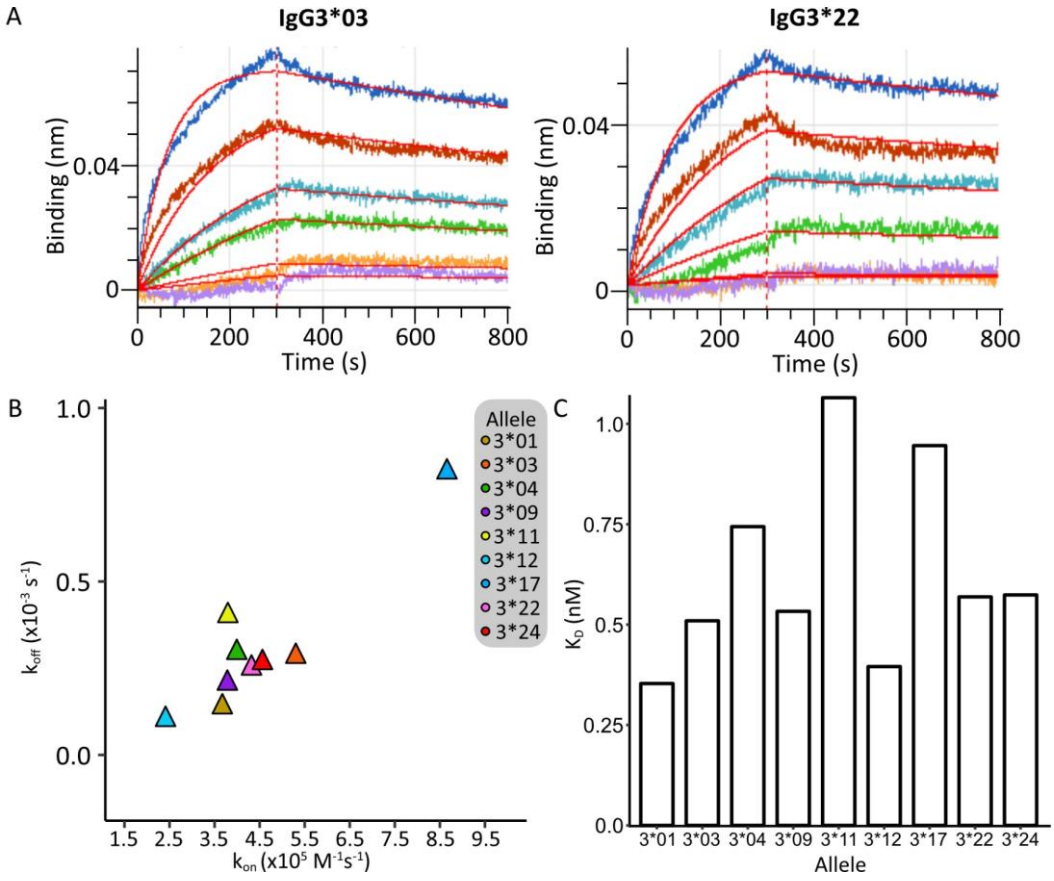

Figure 6-1. Octet data measuring IgG-TRIM21 binding kinetics. (A) Example kinetic curves of IgG3*03 and IgG3*22 antibodies at various concentrations. The binding signal shows the association of IgG to TRIM21 for the first 300 s, followed by the signal change as the antibody dissociates. Data is fit with a 1:1 kinetic model (red line). (B) The calculated association (k_{on}) and dissociation (k_{off}) rates from the 1:1 kinetic model for nine IgG3 allelic variants. (C) Dissociation constants of the nine IgG3 allelic variants.

6.2.2 Expanding the panel of purified IgG variants to include new genetic variants and alternative epitope specificities

Since commencing this thesis work, full length allele sequences of IgG4 have been resolved, along with more non-synonymous polymorphisms within allelic sequences across all the IgG subclasses. To continue to build on our understanding of how IgG polymorphisms influence antibody properties, our plasmid system for antibody production will enable the rapid expression of these newer variants for functional characterisation. Comparing the thermal stability properties of these new variants could be undertaken using the high-throughput REES technique, especially since the experimental procedures and data processing methods have already been optimised.

To further elaborate on the studies performed as part of this PhD thesis, new antibodies can be generated with the same IgG allelic variation in the constant region but with

alternative variable domains (rather than the anti-HER2 trastuzumab format used here). I have already begun to generate IgG antibodies with anti-9C12 and anti-CD20 variable domains, using the modular design of the expression vectors to "swap-in" the new variable domains. IgG variants with different epitope specificities will be useful to establish whether the results seen in this thesis are specific to anti-HER2 IgG antibodies or if the results are universal across other variable domain sequences. Furthermore, new epitope specificities will enable an expansion of experimental capabilities to further test the effects of constant domain diversity on immune effector functions. For example, anti-9C12 can be used to test TRIM21 neutralisation potencies of adeno-associated virus vectors. Similarly, anti-CD20 IgG can be used for *in vitro* analysis of complement deposition and cytotoxicity screening.

6.2.3 Combining IgG allelic diversity with FcγR allelic diversity

In addition to the constant domains of IgG, the sequence of Fc gamma receptors (FcγRs) are important in determining the strength of effector functions. Given the vast amount of diversity now known to be present within the IgG constant domain sequences, it is unsurprising that genetic diversity is also prevalent among the FcγR genes. Some polymorphisms are well-characterised and the functional effects of these have been clearly established. Notably, FcγRIIa and FcγRIIIa have allelic polymorphisms (R131H and V158F, respectively) that alter IgG binding affinities (Bruhns et al., 2009; Nagelkerke et al., 2019; Sanders et al., 1995; Wu et al., 1997). The low affinity variant FcγRIIa-R131 has been correlated to increased susceptibility to streptococcal and pneumococcal bacterial infections due to an impaired ability to induce IgG2-mediated phagocytosis (Sanders et al., 1995). The high affinity variant of FcγRIIIa (V158) is able to produce an enhanced antibody-dependent cellular cytotoxicity (ADCC) response (Nagelkerke et al., 2019). Other genetic variants are present among the human FcγR genes but have been considerably under characterised despite strong links with disease (Geraghty et al., 2019). FcγRIIb has a polymorphism from isoleucine to threonine which has been linked to disease susceptibility of systemic lupus erythematosus (Kono et al., 2005) and another variant of FcγRIIa (Q27W) shows potential links to common variable immunodeficiency (Flinsenberg et al., 2014).

Combining the full extent of FcγR genetic diversity in binding studies with IgG genetic variants would provide a more comprehensive analysis of antibody function than previously achieved and be more representative of the allelic combinations in human populations. Additionally, analysing the population frequencies of both IgG and FcγRs

alleles may provide insight into evolutionary selection pressures driving this diversity. Expanding our understanding of the role genetic diversity plays in immune function will have positive implications for many avenues of biomedical research to further advance immune-based therapies and potentially provide insight for personalised medicine.

6.3 References

Bottermann, M., Lode, H. E., Watkinson, R. E., Foss, S., Sandlie, I., Andersen, J. T., & James, L. C. (2016). Antibody-antigen kinetics constrain intracellular humoral immunity. *Scientific Reports*, *6*, 37457. https://doi.org/10.1038/srep37457

Bruhns, P., Iannascoli, B., England, P., Mancardi, D. A., Fernandez, N., Jorieux, S., & Daëron, M. (2009). Specificity and affinity of human Fcγ receptors and their polymorphic variants for human IgG subclasses. *Blood*, *113*(16), 3716–3725. https://doi.org/10.1182/blood-2008-09-179754

Chu, T. H., Crowley, A. R., Backes, I., Chang, C., Tay, M., Broge, T., Tuyishime, M., Ferrari, G., Seaman, M. S., Richardson, S. I., Tomaras, G. D., Alter, G., Leib, D., & Ackerman, M. E. (2020). Hinge length contributes to the phagocytic activity of HIV-specific IgG1 and IgG3 antibodies. *PLOS Pathogens*, *16*(2), e1008083. https://doi.org/10.1371/journal.ppat.1008083

Crowley, A. R., Richardson, S. I., Tuyishime, M., Jennewein, M., Bailey, M. J., Lee, J., Alter, G., Ferrari, G., Morris, L., & Ackerman, M. E. (2022). Functional consequences of allotypic polymorphisms in human immunoglobulin G subclasses. *Immunogenetics*. https://doi.org/10.1007/s00251-022-01272-7

de Taeye, S. W., Bentlage, A. E. H., Mebius, M. M., Meesters, J. I., Lissenberg-Thunnissen, S., Falck, D., Sénard, T., Salehi, N., Wuhrer, M., Schuurman, J., Labrijn, A. F., Rispens, T., & Vidarsson, G. (2020). FcγR binding and ADCC activity of human IgG allotypes. *Front Immunol*, *11*(740). https://doi.org/10.3389/fimmu.2020.00740

Flinsenberg, T. W. H., Janssen, W. J., Herczenik, E., Boross, P., Nederend, M., Jongeneel, L. H., Scholman, R. C., Boelens, J.-J., Maas, C., van Gijn, M. E., van Montfrans, J. M., Leusen, J. H., & Boes, M. (2014). A novel FcγRIIa Q27W gene variant is associated with common variable immune deficiency through defective FcγRIIa downstream signaling. *Clinical Immunology*, *155*(1), 108–117. https://doi.org/10.1016/j.clim.2014.09.006

Foss, S., Jonsson, A., Bottermann, M., Watkinson, R., Lode, H. E., McAdam, M. B., Michaelsen, T. E., Sandlie, I., James, L. C., & Andersen, J. T. (2022). Potent TRIM21 and complement-dependent intracellular antiviral immunity requires the IgG3 hinge. *Science Immunology*, *7*(70), eabj1640. https://doi.org/10.1126/sciimmunol.abj1640

Foss, S., Watkinson, R. E., Grevys, A., McAdam, M. B., Bern, M., Høydahl, L. S., Dalhus, B., Michaelsen, T. E., Sandlie, I., James, L. C., & Andersen, J. T. (2016). TRIM21 Immune Signaling Is More Sensitive to Antibody Affinity Than Its Neutralization Activity. *J of Immunology (Baltimore, Md. : 1950)*, *196*(8), 3452–3459. https://doi.org/10.4049/jimmunol.1502601

Foss, S., Watkinson, R., Sandlie, I., James, L. C., & Andersen, J. T. (2015). TRIM21: A cytosolic Fc receptor with broad antibody isotype specificity. *Immunol Rev*, *268*(1), 328–339. https://doi.org/10.1111/imr.12363

Geraghty, D. E., Thorball, C. W., Fellay, J., & Thomas, R. (2019). Effect of Fc Receptor Genetic Diversity on HIV-1 Disease Pathogenesis. *Frontiers in Immunology*, *10*. https://www.frontiersin.org/articles/10.3389/fimmu.2019.00970

Kono, H., Kyogoku, C., Suzuki, T., Tsuchiya, N., Honda, H., Yamamoto, K., Tokunaga, K., & Honda, Z.-I. (2005). FcγRIIB Ile232Thr transmembrane polymorphism associated with human systemic lupus erythematosus decreases affinity to lipid rafts and attenuates inhibitory effects on B cell receptor signaling. *Human Mol Genetics*, *14*(19), 2881–2892. https://doi.org/10.1093/hmg/ddi320

Mallery, D. L., McEwan, W. A., Bidgood, S. R., Towers, G. J., Johnson, C. M., & James, L. C. (2010). Antibodies mediate intracellular immunity through tripartite motif-containing 21 (TRIM21). *Proc Natl Acad Sci U S A*, *107*(46), 19985–19990. https://doi.org/10.1073/pnas.1014074107

McEwan, W. A. (2016). Surveillance for Intracellular Antibody by Cytosolic Fc Receptor TRIM21. *Antibodies*, *5*(4), 21. https://doi.org/10.3390/antib5040021

McEwan, W. A., Hauler, F., Williams, C. R., Bidgood, S. R., Mallery, D. L., Crowther, R. A., & James, L. C. (2012). Regulation of Virus Neutralization and the Persistent Fraction by TRIM21. *J of Virology*, *86*(16), 8482–8491. https://doi.org/10.1128/JVI.00728-12

Mullard, A. (2021). FDA approves 100th monoclonal antibody product. *Nature Reviews Drug Discovery*, *20*(7), 491–495. https://doi.org/10.1038/d41573-021-00079-7

Nagelkerke, S. Q., Schmidt, D. E., de Haas, M., & Kuijpers, T. W. (2019). Genetic variation in low-to-medium-affinity Fcγ receptors: Functional consequences, disease associations, and opportunities for personalized medicine. *Front Immunol*, *10*(2237). https://doi.org/10.3389/fimmu.2019.02237

Saito, S., Namisaki, H., Hiraishi, K., Takahashi, N., & Iida, S. (2019). A stable engineered human IgG3 antibody with decreased aggregation during antibody expression and low pH stress. *Protein Science*, *28*(5), 900–909. https://doi.org/10.1002/pro.3598

Sanders, L. A., Feldman, R. G., Voorhorst-Ogink, M. M., de Haas, M., Rijkers, G. T., Capel, P. J., Zegers, B. J., & van de Winkel, J. G. (1995). Human immunoglobulin G (IgG) Fc receptor IIA (CD32) polymorphism and IgG2-mediated bacterial phagocytosis by neutrophils. *Infection and Immunity*, *63*(1), 73–81.

Shah, I. S., Lovell, S., Mehzabeen, N., Battaile, K. P., & Tolbert, T. J. (2017). Structural characterization of the Man5 glycoform of human IgG3 Fc. *Mol Immunology*, *92*, 28–37. https://doi.org/10.1016/j.molimm.2017.10.001

Wu, J., Edberg, J. C., Redecha, P. B., Bansal, V., Guyre, P. M., Coleman, K., Salmon, J. E., & Kimberly, R. P. (1997). A novel polymorphism of FcgammaRIIIa (CD16) alters receptor function and predisposes to autoimmune disease. *The J of Clinical Investigation*, *100*(5), 1059–1070. https://doi.org/10.1172/JCI119616

Appendix A:

Supplementary Material for Chapter Three

A.1 Supplementary tables

Table A-1. Amino acid sequences for antibody variants used in this study

>Herceptin_VL	EMADIQMTQSPSSLSASVGDRVTITCRASQDVNTAVAWYQQKPGKAPKLLIYSASFLYSGVPSRFSGSRSGTDFTLTISSLQPEDFATYYCQQHYTTPPTFGQGTKVEIKR
>IGKC_CL	EMADIQMTQSPSSLSASVGDRVTITCRASQDVNTAVAWYQQKPGKAPKLLIYSASFLYSGVPSRFSGSRSGTDFTLTISSLQPEDFATYYCQQHYTTPPTFGQGTKVEIKRTAAAPSVFIFPPSDEQLKSGTASVVCLLNNFYPREAKVQWKVDNALQSGNSQESVTEQDSKDSTYSLSSTLTLSKADYEKHKVYACEVTHQGLSSPVTKSFNRGEC
>Herceptin_VH	EMAEVQLVESGGGLVQPGGSLRLSCAASGFNIKDTYIHWVRQAPGKGLEWVARIYPTNGYTRYADSVKGRFTISADTSKNTAYLQMNSLRAEDTAVYYCSRWGGDGFYAMDYWGQGTLVTVSS
>IGHG1_01	ASTKGPSVFPLAPSSKSTSGGTAALGCLVKDYFPEPVTVSWNSGALTSGVHTFPAVLQSSGLYSLSSVVTVPSSSLGTQTYICNVNHKPSNTKVDKKVEPKSCDKTHTCPPCPAPELLGGPSVFLFPPKPKDTLMISRTPEVTCVVVDVSHEDPEVKFNWYVDGVEVHNAKTKPREEQYNSTYRVVSVLTVLHQDWLNGKEYKCKVSNKALPAPIEKTISKAKGQPREPQVYTLPPSRDELTKNQVSLTCLVKGFYPSDIAVEWESNGQPENNYKTTPPVLDSDGSFFLYSKLTVDKSRWQQGNVFSCSVMHEALHNHYTQKSLSLSPGK
>IGHG1_03	ASTKGPSVFPLAPSSKSTSGGTAALGCLVKDYFPEPVTVSWNSGALTSGVHTFPAVLQSSGLYSLSSVVTVPSSSLGTQTYICNVNHKPSNTKVDKRVEPKSCDKTHTCPPCPAPELLGGPSVFLFPPKPKDTLMISRTPEVTCVVVDVSHEDPEVKFNWYVDGVEVHNAKTKPREEQYNSTYRVVSVLTVLHQDWLNGKEYKCKVSNKALPAPIEKTISKAKGQPREPQVYTLPPSREEMTKNQVSLTCLVKGFYPSDIAVEWESNGQPENNYKTTPPVLDSDGSFFLYSKLTVDKSRWQQGNVFSCSVMHEALHNHYTQKSLSLSPGK
>IGHG1_04	ASTKGPSVFPLAPSSKSTSGGTAALGCLVKDYFPEPVTVSWNSGALTSGVHTFPAVLQSSGLYSLSSVVTVPSSSLGTQTYICNVNHKPSNTKVDKKVEPKSCDKTHTCPPCPAPELLGGPSVFLFPPKPKDTLMISRTPEVTCVVVDVSHEDPEVKFNWYVDGVEVHNAKTKPREEQYNSTYRVVSVLTVLHQDWLNGKEYKCKVSNKALPAPIEKTISKAKGQPREPQVYTLPPSRDELTKNQVSLTCLVKGFYPSDIAVEWESNGQPENNYKTTPPVLDSDGSFFLYSKLTVDKSRWQQGNIFSCSVMHEALHNHYTQKSLSLSPGK
>IGHG1_07	ASTKGPSVFPLAPSSKSTSGGTAALGCLVKDYFPEPVTVSWNSGALTSGVHTFPAVLQSSGLYSLSSVVTVPSSSLGTQTYICNVNHKPSNTKVDKKVEPKSCDKTHTCPPCPAPELLGGPSVFLFPPKPKDTLMISRTPEVTCVVVDVSHEDPEVKFNWYVDGVEVHNAKTKPREEQYNSTYRVVSVLTVLHQDWLNGKEYKCKVSNKALPAPIEKTISKAKGQPREPQVYTLPPSRDELTKNQVSLTCLVKGFYPSDI

	AVEWESNGQPENNYKTTPPVLDSDGSFFLYSKLTVDKSRWQQGNVFSCSVM HEGLHNHYTQKSLSLSPGK
>IGHG1_08	ASTKGPSVFPLAPSSKSTSGGTAALGCLVKDYFPEPVTVSWNSGALTSGVHT FPAVLQSSGLYSLSSVVTVPSSSLGTQTYICNVNHKPSNTKVDKRVEPKSCDK THTCPPCPAPELLGGPSVFLFPPKPKDTLMISRTPEVTCVVVDVSHEDPEVKF NWYVDGVEVHNAKTKPREEQYNSTYRVVSVLTVLHQDWLNGKEYKCKVS NKALPAPIEKTISKAKGQPREPQVYTLPPSRDELTKNQVSLTCLVKGFYPSDI AVEWESNGQPENNYKTTPPVLDSDGSFFLYSKLTVDKSRWQQGNVFSCSVM HEALHNHYTQKSLSLSPGK
>IGHG1_11	ASTKGPSVFPLAPSSKSTSGGTAALGCLVKDYFPEPVTVSWNSGALTSGVHT FPAVLQSSGLYSLSSVVTVPSSSLGTQTYICNVNHKPSNTKVDKKVEPKSCD KTHTCPPCPAPELLGGPSVFLFPPKPKDTLMISRTPEVTCVVVDVSHEDPEVK FNWYVDGVEVHNAKTKPREEQYNSTYRVVSVLTVVHQDWLNGKEYKCKV SNKALPAPIEKTISKAKGQPREPQVYTLPPSRDELTKNQVSLTCLVKGFYPSDI AVEWESNGQPENNYKTTPPVLDSDGSFFLYSKLTVDKSRWQQGNVFSCSVM HEALHNHYTQKSLSLSPGK
>IGHG1_13	ASTKGPSVFPLAPSSKSTSGGTAALGCLVKDYFPEPVTVSWNSGALTSGVHT FPAVLQSSGLYSLSSVVTVPSSSLGTQTYICNVNHKPSNTKVDKKVEPKSCD KTHTCPPCPAPELLGGPSVFLFPPKPKDTLMISRTPEVTCVVVDVSHEDPEVK FNWYVDGVEVHNAKTKPREEQFNSTYRVVSVLTVLHQDWLNGKEYKCKV SNKALPAPIEKTISKAKGQPREPQVYTLPPSRDELTKNQVSLTCLVKGFYPSDI AVEWESNGQPENNYKTTPPVLDSDGSFFLYSKLTVDKSRWQQGNVFSCSVM HEALHNHYTQKSLSLSPGK
>IGHG2_01	ASTKGPSVFPLAPCSRSTSESTAALGCLVKDYFPEPVTVSWNSGALTSGVHTF PAVLQSSGLYSLSSVVTVPSSNFGTQTYTCNVDHKPSNTKVDKTVERKCCVE CPPCPAPPVAGPSVFLFPPKPKDTLMISRTPEVTCVVVDVSHEDPEVQFNWY VDGVEVHNAKTKPREEQFNSTFRVVSVLTVVHQDWLNGKEYKCKVSNKGL PAPIEKTISKTKGQPREPQVYTLPPSREEMTKNQVSLTCLVKGFYPSDIAVEW ESNGQPENNYKTTPPMLDSDGSFFLYSKLTVDKSRWQQGNVFSCSVMHEAL HNHYTQKSLSLSPGK
>IGHG2_02	ASTKGPSVFPLAPCSRSTSESTAALGCLVKDYFPEPVTVSWNSGALTSGVHTF PAVLQSSGLYSLSSVVTVTSSNFGTQTYTCNVDHKPSNTKVDKTVERKCCVE CPPCPAPPVAGPSVFLFPPKPKDTLMISRTPEVTCVVVDVSHEDPEVQFNWY VDGMEVHNAKTKPREEQFNSTFRVVSVLTVVHQDWLNGKEYKCKVSNKGL PAPIEKTISKTKGQPREPQVYTLPPSREEMTKNQVSLTCLVKGFYPSDIAVEW ESNGQPENNYKTTPPMLDSDGSFFLYSKLTVDKSRWQQGNVFSCSVMHEAL HNHYTQKSLSLSPGK
>IGHG2_04	ASTKGPSVFPLAPCSRSTSESTAALGCLVKDYFPEPVTVSWNSGALTSGVHTF PAVLQSSGLYSLSSVVTVPSSSLGTQTYTCNVDHKPSNTKVDKTVERKCCVE CPPCPAPPVAGPSVFLFPPKPKDTLMISRTPEVTCVVVDVSHEDPEVQFNWY VDGVEVHNAKTKPREEQFNSTFRVVSVLTVVHQDWLNGKEYKCKVSNKGL PAPIEKTISKTKGQPREPQVYTLPPSREEMTKNQVSLTCLVKGFYPSDIAVEW ESNGQPENNYKTTPPMLDSDGSFFLYSKLTVDKSRWQQGNVFSCSVMHEAL HNHYTQKSLSLSPGK
>IGHG2_06	ASTKGPSVFPLAPCSRSTSESTAALGCLVKDYFPEPVTVSWNSGALTSGVHTF PAVLQSSGLYSLSSVVTVPSSNFGTQTYTCNVDHKPSNTKVDKTVERKCCVE CPPCPAPPVAGPSVFLFPPKPKDTLMISRTPEVTCVVVDVSHEDPEVQFNWY VDGVEVHNAKTKPREEQFNSTFRVVSVLTVVHQDWLNGKEYKCKVSNKGL

	PAPIEKTISKTKGQPREPQVYTLPPSREEMTKNQVSLTCLVKGFYPSDISVEW ESNGQPENNYKTTPPMLDSDGSFFLYSKLTVDKSRWQQGNVFSCSVMHEAL HNHYTQKSLSLSPGK
>IGHG2_09	ASTKGPSVFPLAPCSRSTSGGTAALGCLVKDYFPEPVTVSWNSGALTSGVHT FPAVLQSSGLYSLSSVVTVPSSNFGTQTYTCNVDHKPSNTKVDKTVERKCCV ECPPCPAPPVAGPSVFLFPPKPKDTLMISRTPEVTCVVVDVSHEDPEVQFNWY VDGVEVHNAKTKPREEQFNSTFRVVSVLTVVHQDWLNGKEYKCKVSNKGL PAPIEKTISKTKGQPREPQVYTLPPSREEMTKNQVSLTCLVKGFYPSDIAVEW ESNGQPENNYKTTPPMLDSDGSFFLYSKLTVDKSRWQQGNVFSCSVMHEAL HNHYTQKSLSLSPGK
>IGHG2_11	ASTKGPSVFPLAPCSRSTSESTAALGCLVKDYFPEPVTVSWNSGALTSGVHTF PAVLQSSGLYSLSSVVTVPSSNFGTQTYTCNVDHKPSNTKVDKTVERKCCVE CPPCPAPPVAGPSVFLFPPKPKDTLMISRTPEVTCVVVDVSHEDPEVQFNWY VDGVEVHNAKTKPREEQFNSTFRVVSVLTVLHQDWLNGKEYKCKVSNKGL PAPIEKTISKTKGQPREPQVYTLPPSREEMTKNQVSLTCLVKGFYPSDIAVEW ESNGQPENNYKTTPPMLDSDGSFFLYSKLTVDKSRWQQGNVFSCSVMHEAL HNHYTQKSLSLSPGK
>IGHG2_15	ASTKGPSVFPLAPCSRSTSESTAALGCLVKDYFPEPVTVSWNSGALTSGVHTF PAVLQSSGLYSLSSVVTVPSSNFGTQTYTCNVDHKPSNTKVDKTVERKCCVE CPPCPAPPVAGPSVFLFPPKPKDTLMISRTPEVTCVVVDVSHEDPEVQFNWY VDGVEVHNAKTKPREEQFNSTFRVVSVLTVVHQDWLNGKEYKCKVSNKGL PAPIEKTISKTKGQPREPQVYTLPPSREEMTKNQVSLTCLVKGFYPSDIAVEW ESNGQPENNYNTTPPMLDSDGSFFLYSKLTVDKSRWQQGNVFSCSVMHEAL HNHYTQKSLSLSPGK
>IGHG3_01	ASTKGPSVFPLAPCSRSTSGGTAALGCLVKDYFPEPVTVSWNSGALTSGVHT FPAVLQSSGLYSLSSVVTVPSSSLGTQTYTCNVNHKPSNTKVDKRVELKTPL GDTTHTCPRCPEPKSCDTPPPCPRCPEPKSCDTPPPCPRCPEPKSCDTPPPCPRC PAPELLGGPSVFLFPPKPKDTLMISRTPEVTCVVVDVSHEDPEVQFKWYVDG VEVHNAKTKPREEQYNSTFRVVSVLTVLHQDWLNGKEYKCKVSNKALPAPI EKTISKTKGQPREPQVYTLPPSREEMTKNQVSLTCLVKGFYPSDIAVEWESSG QPENNYNTTPPMLDSDGSFFLYSKLTVDKSRWQQGNIFSCSVMHEALHNRF TQKSLSLSPGK
>IGHG3_03	ASTKGPSVFPLAPCSRSTSGGTAALGCLVKDYFPEPVTVSWNSGALTSGVHT FPAVLQSSGLYSLSSVVTVPSSSLGTQTYTCNVNHKPSNTKVDKRVELKTPL GDTTHTCPRCPEPKSCDTPPPCPRCPEPKSCDTPPPCPRCPAPELLGGPSVFLFP PKPKDTLMISRTPEVTCVVVDVSHEDPEVQFKWYVDGVEVHNAKTKPREEQ YNSTFRVVSVLTVLHQDWLNGKEYKCKVSNKALPAPIEKTISKTKGQPREPQ VYTLPPSREEMTKNQVSLTCLVKGFYPSDIAVEWESSGQPENNYNTTPPVLD SDGSFFLYSRLTVDKSRWQEGNVFSCSVMHEALHNRFTQKSLSLSPGK
>IGHG3_04	ASTKGPSVFPLAPCSRSTSGGTAALGCLVKDYFPEPVTVSWNSGALTSGVHT FPAVLQSSGLYSLSSVVTVPSSSLGTQTYTCNVNHKPSNTKVDKRVELKTPL GDTTHTCPRCPEPKSCDTPPPCPRCPAPELLGGPSVFLFPPKPKDTLMISRTPE VTCVVVDVSHEDPEVQFKWYVDGVEVHNAKTKPREEQYNSTFRVVSVLTV LHQDWLNGKEYKCKVSNKALPAPIEKTISKTKGQPREPQVYTLPPSREEMTK NQVSLTCLVKGFYPSDIAVEWESSGQPENNYNTTPPMLDSDGSFFLYSKLTV DKSRWQQGNIFSCSVMHEALHNRFTQKSLSLSPGK
>IGHG3_06	ASTKGPSVFPLAPCSRSTSGGTAALGCLVKDYFPEPVTVSWNSGALTSGVHT FPAVLQSSGLYSLSSVVTVPSSSLGTQTYTCNVNHKPSNTKVDKRVELKTPL

	GDTTHTCPRCPEPKSCDTPPPCPRCPEPKSCDTPPPCPRCPEPKSCDTPPPCPRC PAPELLGGPSVFLFPPKPKDTLMISRTPEVTCVVVDVSHEDPEVQFKWYVDG VEVHNAKTKPREEQYNSTFRVVSVLTVLHQDWLNGKEYKCKVSNKALPAPI EKTISKTKGQPREPQVYTLPPSREEMTKNQVSLTCLVKGFYPSDIAVEWESSG QPENNYKTTPPMLDSDGSFFLYSKLTVDKSRWQQGNIFSCSVMHEALHNRF TQKSLSLSPGK
>IGHG3_08	ASTKGPSVFPLAPCSRSTSGGTAALGCLVKDYFPEPVTVSWNSGALTSGVHT FPAVLQSSGLYSLSSVVTVPSSSLGTQTYTCNVNHKPSNTKVDKRVELKTPL GDTTHTCPRCPEPKSCDTPPPCPRCPEPKSCDTPPPCPRCPEPKSCDTPPPCPRC PAPELLGGPSVFLFPPKPKDTLMISRTPEVTCVVVDVSHEDPEVQFKWYVDG VEVHNAKTKPREEQYNSTFRVVSVLTVLHQDWLNGKEYKCKVSNKALPAPI EKTISKTKGQPREPQVYTLPPSREEMTKNQVSLTCLVKGFYPSDIAVEWESN GQPENNYNTTPPMLDSDGSFFLYSKLTVDKSRWQQGNIFSCSVMHEALHNR FTQKSLSLSPGK
>IGHG3_09	ASTKGPSVFPLAPCSRSTSGGTAALGCLVKDYFPEPVTVSWNSGALTSGVHT FPAVLQSSGLYSLSSVVTVPSSSLGTQTYTCNVNHKPSNTKVDKRVELKTPL GDTTHTCPRCPEPKSCDTPPPCPRCPEPKSCDTPPPCPRCPEPKSCDTPPPCPRC PAPELLGGPSVFLFPPKPKDTLMISRTPEVTCVVVDVSHEDPEVQFKWYVDG VEVHNAKTKPREEQYNSTFRVVSVLTVVHQDWLNGKEYKCKVSNKALPAPI EKTISKTKGQPREPQVYTLPPSREEMTKNQVSLTCLVKGFYPSDIAVEWESSG QPENNYNTTPPMLDSDGSFFLYSKLTVDKSRWQQGNIFSCSVMHEALHNRF TQKSLSLSPGK
>IGHG3_11	ASTKGPSVFPLAPCSRSTSGGTAALGCLVKDYFPEPVTVSWNSGALTSGVHT FPAVLQSSGLYSLSSVVTVPSSSLGTQTYTCNVNHKPSNTKVDKRVELKTPL GDTTHTCPRCPEPKSCDTPPPCPRCPEPKSCDTPPPCPRCPEPKSCDTPPPCPRC PAPELLGGPSVFLFPPKPKDTLMISRTPEVTCVVVDVSHEDPEVQFKWYVDG VEVHNAKTKPREEQFNSTFRVVSVLTVLHQDWLNGKEYKCKVSNKALPAPI EKTISKTKGQPREPQVYTLPPSREEMTKNQVSLTCLVKGFYPSDIAVEWESSG QPENNYNTTPPMLDSDGSFFLYSKLTVDKSRWQQGNIFSCSVMHEALHNRF TQKSLSLSPGK
>IGHG3_12	ASTKGPSVFPLAPCSRSTSGGTAALGCLVKDYFPEPVTVSWNSGALTSGVHT FPAVLQSSGLYSLSSVVTVPSSSLGTQTYTCNVNHKPSNTKVDKRVELKTPL GDTTHTCPRCPEPKSCDTPPPCPRCPEPKSCDTPPPCPRCPAPELLGGPSVFLFP PKPKDTLMISRTPEVTCVVVDVSHEDPEVQFKWYVDGVEVHNAKTKPREEQ FNSTFRVVSVLTVLHQDWLNGKEYKCKVSNKALPAPIEKTISKTKGQPREPQ VYTLPPSREEMTKNQVSLTCLVKGFYPSDIAVEWESSGQPENNYNTTPPMLD SDGSFFLYSKLTVDKSRWQQGNIFSCSVMHEALHNRFTQKSLSLSPGK
>IGHG3_13	ASTKGPSVFPLAPCSRSTSGGTAALGCLVKDYFPEPVTVSWNSGALTSGVHT FPAVLQSSGLYSLSSVVTVPSSSLGTQTYTCNVNHKPSNTKVDKRVELKTPL GDTTHTCPRCPEPKSCDTPPPCPRCPEPKSCDTPPPCPRCPEPKSCDTPPPCPRC PAPELLGGPSVFLFPPKPKDTLMISRTPEVTCVVVDVSHEDPEVQFKWYVDG VEVHNAKTKPREEQYNSTFRVVSVLTVLHQDWLNGKEYKCKVSNKALPAPI EKTISKTKGQPREPQVYTLPPSREEMTKNQVSLTCLVKGFYPSDIAVEWESSG QPENNYKTTPPMLDSDGSFFLYSKLTVDKSRWQEGNIFSCSVMHEALHNRFT QKSLSLSPGK
>IGHG3_14	ASTKGPSVFPLAPCSRSTSGGTAALGCLVKDYFPEPVTVSWNSGALTSGVHT FPAVLQSSGLYSLSSVVTVPSSSLGTQTYTCNVNHKPSNTKVDKRVELKTPL GDTTHTCPRCPEPKSCDTPPPCPRCPEPKSCDTPPPCPRCPEPKSCDTPPPCPRC PAPELLGGPSVFLFPPKPKDTLMISRTPEVTCVVVDVSHEDPEVQFKWYVDG

	VEVHNAKTKLREEQYNSTFRVVSVLTVLHQDWLNGKEYKCKVSNKALPAPI EKTISKTKGQPREPQVYTLPPSREEMTKNQVSLTCLVKGFYPSDIAVEWESN GQPENNYNTTPPMLDSDGSFFLYSKLTVDKSRWQQGNIFSCSVMHEALHNR YTQKSLSLSPGK
>IGHG3_15	ASTKGPSVFPLAPCSRSTSGGTAALGCLVKDYFPEPVTVSWNSGALTSGVHT FPAVLQSSGLYSLSSVVTVPSSSLGTQTYTCNVNHKPSNTKVDKRVELKTPL GDTTHTCPRCPEPKSCDTPPPCPRCPEPKSCDTPPPCPRCPEPKSCDTPPPCPRC PAPELLGGPSVFLFPPKPKDTLMISRTPEVTCVVVDVSHEDPEVQFKWYVDG VEVHNAKTKLREEQYNSTFRVVSVLTVLHQDWLNGKEYKCKVSNKALPAPI EKTISKTKGQPREPQVYTLPPSREEMTKNQVSLTCLVKGFYPSDIAVEWESN GQPENNYKTTPPMLDSDGSFFLYSKLTVDKSRWQQGNIFSCSVMHEALHNR YTQKSLSLSPGK
>IGHG3_16	ASTKGPSVFPLAPCSRSTSGGTAALGCLVKDYFPEPVTVSWNSGALTSGVHT FPAVLQSSGLYSLSSVVTVPSSSLGTQTYTCNVNHKPSNTKVDKRVELKTPL GDTTHTCPRCPEPKSCDTPPPCPRCPEPKSCDTPPPCPRCPEPKSCDTPPPCPRC PAPELLGGPSVFLFPPKPKDTLMISRTPEVTCVVVDVSHEDPEVQFKWYVDG VEVHNAKTKLREEQYNSTFRVVSVLTVLHQDWLNGKEYKCKVSNKALPAPI EKTISKAKGQPREPQVYTLPPSREEMTKNQVSLTCLVKGFYPSDIAVEWESN GQPENNYNTTPPMLDSDGSFFLYSKLTVDKSRWQQGNIFSCSVMHEALHNR YTQKSLSLSPGK
>IGHG3_17	ASTKGPSVFPLAPCSRSTSGGTAALGCLVKDYFPEPVTVSWNSGALTSGVHT FPAVLQSSGLYSLSSVVTVPSSNFGTQTYTCNVNHKPSNTKVDKRVELKTPL GDTTHTCPRCPEPKSCDTPPPCPRCPEPKSCDTPPPCPRCPAPELLGGPSVFLFP PKPKDTLMISRTPEVTCVVVDVSHEDPEVQFKWYVDGVEVHNAKTKPREEQ YNSTFRVVSVLTVLHQDWLNGKEYKCKVSNKALPAPIEKTISKTKGQPREPQ VYTLPPSREEMTKNQVSLTCLVKGFYPSDIAMEWESSGQPENNYKTTPPVLD SDGSFFLYSKLTVDKSRWQQGNIFSCSVMHEALHNHYTQKSLSLSPGK
>IGHG3_20	ASTKGPSVFPLAPCSRSTSGGTAALGCLVKDYFPEPVTVSWNSGALTSGVHT FPAVLQSSGLYSLSSVVTVPSSSLGTQTYTCNVNHKPSNTKVDKRVELKTPL GDTTHTCPRCPEPKSCDTPPPCPRCPEPKSCDTPPPCPRCPEPKSCDTPPPCPRC PAPELLGGPSVFLFPPKPKDTLMISRTPEVTCVVVDVSHEDPEVQFKWYVDG VEVHNAKTKLREEQYNSTFRVVSVLTVLHQDWLNGKEYKCKVSNKALPAPI EKTISKTKGQPREPQVYTLPPSREEMTKNQVSLTCLVKGFYPSDIAVEWESN GQRENNYNTTPPMLDSDGSFFLYSKLTVDKSRWQQGNIFSCSVMHEALHNR YTQKSLSLSPGK
>IGHG3_22	ASTKGPSVFPLAPCSRSTSGGTAALGCLVKDYFPEPVTVSWNSGALTSGVHT FPAVLQSSGLYSLSSVVTVPSSSLGTQTYTCNVNHKPSNTKVDKRVELKTPL GDTTHTCPRCPEPKSCDTPPPCPRCPEPKSCDTPPPCPRCPEPKSCDTPPPCPRC PAPELLGGPSVFLFPPKPKDTLMISRTPEVTCVVVDVSHEDPEVQFKWYVDG VEVHNAKTKLREEQYNSTFRVVSVLTVLHQDWLNGKEYKCKVSNKALPAPI EKTISKTKGQPREPQVYTLPPSREEMTKNQVSLTCLVKGFYPSDIAVEWESN GQPENNYNTTPPMLDSDGSFFLYSKLTVDKSRWQQGNIFSCSVMHEALHNH YTQKSLSLSPGK
>IGHG3_24	ASTKGPSVFPLAPCSRSTSGGTAALGCLVKDYFPEPVTVSWNSGALTSGVHT FPAVLQSSGLYSLSSVVTVPSSSLGTQTYTCNVNHKPSNTKVDKRVELKTPL GDTTHTCPRCPEPKSCDTPPPCPRCPEPKSCDTPPPCPRCPEPKSCDTPPPCPRC PAPELLGGPSVFLFPPKPKDTLMISRTPEVTCVVVDVSHEDPEVQFKWYVDG VEVHNAKTKPREEQYNSTFRVVSVLTVLHQDWLNGKEYKCKVSNKALPAPI EKTISKTKGQPREPQVYTLPPSREEMTKNQVSLTCLVKGFYPSDIAVEWESN

	GQPENNYKTTPPMLDSDGSFFLYSKLTVDKSRWQQGNIFSCSVMHEALHNR YTQKSLSLSPGK
>IGHG3_25	ASTKGPSVFPLAPCSRSTSGGTAALGCLVKDYFPEPVTVSWNSGALTSGVHT FPAVLQSSGLYSLSSVVTVPSSSLGTQTYTCNVNHKPSNTKVDKRVELKTPL GDTTHTCPRCPEPKSCDTPPPCPRCPEPKSCDTPPPCPRCPEPKSCDTPPPCPRC PAPELLGGPSVFLFPPKPKDTLMISRTPEVTCVVVDVSHEDPEVKFKWYVDG VEVHNAKTKLREEQYNSTFRVVSVLTVLHQDWLNGKEYKCKVSNKALPAPI EKTISKTKGQPREPQVYTLPPSREEMTKNQVSLTCLVKGFYPSDIAVEWESN GQPENNYNTTPPMLDSDGSFFLYSKLTVDKSRWQQGNIFSCSVMHEALHNR YTQKSLSLSPGK
>IGHG3_26	ASTKGPSVFPLAPCSRSTSGGTAALGCLVKDYFPEPVTVSWNSGALTSGVHT FPAVLQSSGLYSLSSVVTVPSSSLGTQTYTCNVNHKPSNTKVDKRVELKTPL GDTTHTCPRCPEPKSCDTPPPCPRCPEPKSCDTPPPCPRCPEPKSCDTPPPCPRC PAPELLGGPSVFLFPPKPKDTLMISRTPEVTCVVVDVSHEDPEVQFKWYVDG VEVHNAKTKPREEQFNSTFRVVSVLTVLHQDWLNGKEYKCKVSNKGLPAPI EKTISKTKGQPREPQVYTLPPSREEMTKNQVSLTCLVKGFYPSDIAVEWESSG QPENNYNTTPPMLDSDGSFFLYSKLTVDKSRWQQGNIFSCSVMHEALHNRF TQKSLSLSPGK

Table A-2. Root mean square deviation (RMSD) scores for the alignment of IgG1 structural homology models to 1hzh in PyMOL

Allele	RMSD score	Atoms aligned
1*01	0.707	1195
1*03	1.634	1271
1*04	1.248	1264
1*07	1.054	1264
1*08	0.600	1082
1*11	0.865	1237
1*13	1.856	1288

Table A-3. Relative glycan species abundance as a percentage for each antibody variant determined by HPLC-MS. Blank cells indicate the glycan species was not detected.

		IgG1						
Glycoforms	**Theoretical mass [M+2H][1]**	***01**	***03**	***04**	***07**	***08**	***11**	***13**
G0-2GlcNAc	911.34						4.47	0.09
G0-GlcNAc	1114.42	0.30	0.53	0.30	0.15	0.23	1.12	0.76
G0 F-GlcNAc	1260.47	4.69	3.34	3.59	3.45	4.93	7.01	3.88
G0	1317.49		0.10		0.11		0.35	0.35
G1 + GlcNac	1682.63							
G1 F-GlcNAc a	1421.53	0.43	0.41	0.45		0.21	0.63	
G1-GlcNAc	1276.47	0.00	0.31	0.45	0.19			0.24
G0 F	1463.55	46.40	35.55	35.56	31.59	29.71	36.15	44.73
M5 F	1380.50	0.00	0.28	0.38	0.25	0.22	0.33	0.08
M5	1235.44	8.18	8.97	10.72	7.87	12.42	15.88	7.94
G1 F-GlcNAc b	1421.53	1.13	1.35	1.39	1.60	0.87	0.53	1.97
G1	1479.55				0.38			0.07
G0 F+ GlcNac	1666.63							0.09
G1 Fa	1625.61	16.67	20.63	19.55	20.84	16.47	13.13	10.40
G1 Fb	1625.61	6.53	7.15	6.60	7.18	4.80	3.96	10.75
G1 F+ GlcNAc a	1828.68						2.18	
M6	1397.49	0.80	2.68	3.38	2.46	2.89	0.72	1.43
G0 F- GlcNac+SA	1713.62			0.20				0.20
G1-GlcNac+SA	1566.56	0.21	0.24	0.22			2.48	
G1 F+ GlcNAc b	1828.68				0.49	0.66	0.52	0.17
G2 F	1787.66	3.36	5.68	5.18	6.31	4.49	1.98	2.57
G1 +SA+M1	1729.62							
M7	1559.55	0.31	1.41	1.66	1.18	2.78	0.25	1.07
G1 F+ SA	1916.70							
G2 + SA	1932.69						1.08	
M8	1721.60					2.14		0.56
G2 F+ SA	2078.75				0.16		0.13	0.07
G1 F+ SA+M2	2037.73							0.16

[1]Bereman, M. S., Young, D. D., Deiters, A., & Muddiman, D. C. (2009). Development of a robust and high throughput method for profiling N-linked Glycans derived from plasma glycoproteins by NanoLC− FTICR mass spectrometry. *Journal of proteome research*, *8*(7), 3764-3770.

Table A-3. (continued) Relative glycan species abundance as a percentage for each antibody variant determined by HPLC-MS. Blank cells indicate the glycan species was not detected.

				IgG2			
Glycoforms	***01**	***02**	***04**	***06**	***09**	***11**	***15**
G0-2GlcNAc					3.59		
G0-GlcNAc		0.75	0.53	0.43	0.67		0.88
G0 F-GlcNAc	4.34	7.04	4.55	5.17	6.54	3.93	4.57
G0				0.31			
G1 + GlcNac							
G1 F-GlcNAc a	1.42	0.39	0.60	0.46			
G1-GlcNAc	0.44				0.41	0.15	0.13
G0 F	32.57	36.10	31.84	29.15	34.44	28.93	35.75
M5 F	0.05	0.37					
M5	13.66	17.72	16.19	12.62	14.66	15.62	12.25
G1 F-GlcNAc b	1.91	0.91	1.58	2.26	2.72	1.93	1.10
G1							
G0 F+ GlcNac							
G1 Fa	6.46	6.15	7.06	6.11	5.94	5.61	6.97
G1 Fb	7.51	6.59	7.39	5.83	7.37	6.78	7.02
G1 F+ GlcNAc a	0.05						
M6	3.26	0.59	0.52	0.94	1.04	0.11	4.08
G0 F- GlcNac+SA							
G1-GlcNac+SA							
G1 F+ GlcNAc b	0.23						
G2 F	1.86	2.03	2.57	2.17	1.18	1.08	2.22
G1+ SA+M1							
M7	2.07	1.91	3.40	1.32	1.59	0.39	1.96
G1 F+ SA							
G2 + SA							
M8	1.99	1.35	3.07	1.04	1.60	3.07	1.17
G2 F +SA							
G1F+SA+M2							

[1]Bereman, M. S., Young, D. D., Deiters, A., & Muddiman, D. C. (2009). Development of a robust and high throughput method for profiling N-linked Glycans derived from plasma glycoproteins by NanoLC− FTICR mass spectrometry. *Journal of proteome research*, *8*(7), 3764-3770.

Table A-3. (continued) Relative glycan species abundance as a percentage for each antibody variant determined by HPLC-MS. Blank cells indicate the glycan species was not detected.

						IgG3					
Glycoforms	***01**	***03**	***04**	***06**	***08**	***09**	***11**	***12**	***13**	***14**	***15**
G0-2GlcNAc	0.29										
G0-GlcNAc	0.55	0.59	0.44	0.60	0.74	0.18		0.13		0.29	0.28
G0 F-GlcNAc	2.22	2.49	2.19	3.41	3.88	2.03	1.35	2.68	1.52	4.89	2.23
G0	1.62	0.42	0.08	0.18			0.21	0.10	0.23	1.64	0.17
G1 + GlcNac	0.39	0.28									
G1 F-GlcNAc a					0.25	0.12			0.25		
G1-GlcNAc	0.26	0.18					0.71	0.59			
G0 F	40.55	39.47	46.60	40.42	40.64	33.32	42.84	57.57	45.15	40.48	44.37
M5 F											
M5	9.76	9.17	7.88	8.41	10.86	9.30	9.21	6.69	6.07	6.91	5.69
G1 F-GlcNAc b	0.43	0.09	0.29	1.16	0.09	0.32	0.69	0.36	0.33		0.37
G1		0.29	0.18	0.14						0.29	
G0 F+ GlcNac											
G1 Fa	15.32	17.97	17.20	16.45	15.61	15.88	9.57	9.27	13.38	17.22	17.52
G1 Fb	6.07	7.66	7.72	8.48	6.08	6.48	10.26	11.09	7.26	8.81	10.51
G1 F+ GlcNAc a		0.43									
M6	1.78	3.85	1.83	1.53	2.31	2.89	4.20	1.17	0.75	1.37	0.36
G0 F- GlcNac+SA											
G1-GlcNac+SA		0.13									
G1 F+ GlcNAc b		0.36					0.18	0.14	0.28	0.59	0.77
G2 F	3.60	5.09	3.86	5.08	3.47	5.08	3.55	2.82	3.68	5.29	6.17
G1+ SA+M1		0.36									
M7		1.43									0.42
G1 F+ SA								0.73			
G2 + SA		0.38						0.25			
M8	0.70	0.82	0.25	1.22	0.91	0.64	2.26		0.75	0.32	0.40
G2 F +SA								0.18			
G1F+SA+M2											

[1]Bereman, M. S., Young, D. D., Deiters, A., & Muddiman, D. C. (2009). Development of a robust and high throughput method for profiling N-linked Glycans derived from plasma glycoproteins by NanoLC− FTICR mass spectrometry. *Journal of proteome research*, *8*(7), 3764-3770.

Table A-3. (continued) Relative glycan species abundance as a percentage for each antibody variant determined by HPLC-MS. Blank cells indicate the glycan species was not detected.

	IgG3 (continued)									
Glycoforms	***16**	***17**	***18**	***19**	***20**	***22**	***23**	***24**	***25**	***26**
G0-2GlcNAc										
G0-GlcNAc		0.38	0.36	1.76	0.37		0.22	0.59	0.10	2.52
G0 F-GlcNAc	1.48	3.41	1.71	1.63	1.81	1.74	2.01	3.36	1.68	1.90
G0	0.11	0.17	0.27		0.26	0.31	0.09	0.32	0.16	
G1 + GlcNac										
G1 F-GlcNAc a	0.33									
G1-GlcNAc		0.26	1.12							
G0 F	41.93	48.37	40.56	38.02	39.26	40.43	42.84	44.53	37.46	49.66
M5 F										
M5	7.89	7.24	1.76	2.24	8.53	6.97	4.59	7.84	8.32	9.36
G1 F-GlcNAc b		0.60	0.23	0.14	0.27			0.43		0.19
G1	0.16									
G0 F+ GlcNac			0.30		0.37	0.23	0.35	0.25	0.35	0.34
G1 Fa	19.20	16.59	22.32	25.01	18.57	19.71	23.01	15.28	16.67	8.57
G1 Fb	8.27	7.71	8.79	9.28	9.09	8.69	9.10	7.99	8.54	10.20
G1 F+ GlcNAc a						0.15	0.11		0.07	
M6	2.57	0.51	0.09	0.13	1.92	2.88	0.38	0.83	1.46	1.99
G0 F- GlcNac+SA										
G1-GlcNac+SA			1.18							
G1 F+ GlcNAc b	0.74	0.35		1.41		0.69	1.40	0.45	0.89	0.26
G2 F	6.45	3.95	7.92	10.43	6.97	6.24	8.22	4.26	6.50	2.94
G1+ SA+M1										
M7	0.97					1.09			0.70	1.19
G1 F+ SA					1.15					
G2 + SA										
M8	0.35	0.21	0.52	0.60	0.44	0.64	0.49	0.84		0.49
G2 F +SA	0.54								0.40	
G1F+SA+M2										

[1]Bereman, M. S., Young, D. D., Deiters, A., & Muddiman, D. C. (2009). Development of a robust and high throughput method for profiling N-linked Glycans derived from plasma glycoproteins by NanoLC− FTICR mass spectrometry. *Journal of proteome research*, *8*(7), 3764-3770.

Table A-4. Correlation coefficient (R) of the relative abundance of glycoforms versus the change in CSM(λ_{Ex}^{Fc}) and ΔG*m*

		IgG1		IgG2		IgG3	
Glycoform	**Measurement**	**R**	**p-value**	**R**	**p-value**	**R**	**p-value**
G0 F	ΔCSM(λ_{Ex}^{Fc})	-0.66	0.10	0.77	0.04	0.07	0.77
	$\Delta\Delta G_m$	-0.14	0.76	0.02	0.97	0.22	0.38
G1 Fa	ΔCSM(λ_{Ex}^{Fc})	0.12	0.80	0.59	0.17	-0.32	0.19
	$\Delta\Delta G_m$	0.29	0.53	-0.47	0.29	-0.35	0.16
G1 Fb	ΔCSM(λ_{Ex}^{Fc})	0.02	0.97	-0.06	0.90	-0.25	0.32
	$\Delta\Delta G_m$	-0.30	0.51	0.04	0.93	0.13	0.60
M5	ΔCSM(λ_{Ex}^{Fc})	0.26	0.57	-0.04	0.94	0.25	0.31
	$\Delta\Delta G_m$	0.04	0.93	-0.18	0.70	0.15	0.55

A.2 Supplementary Figures

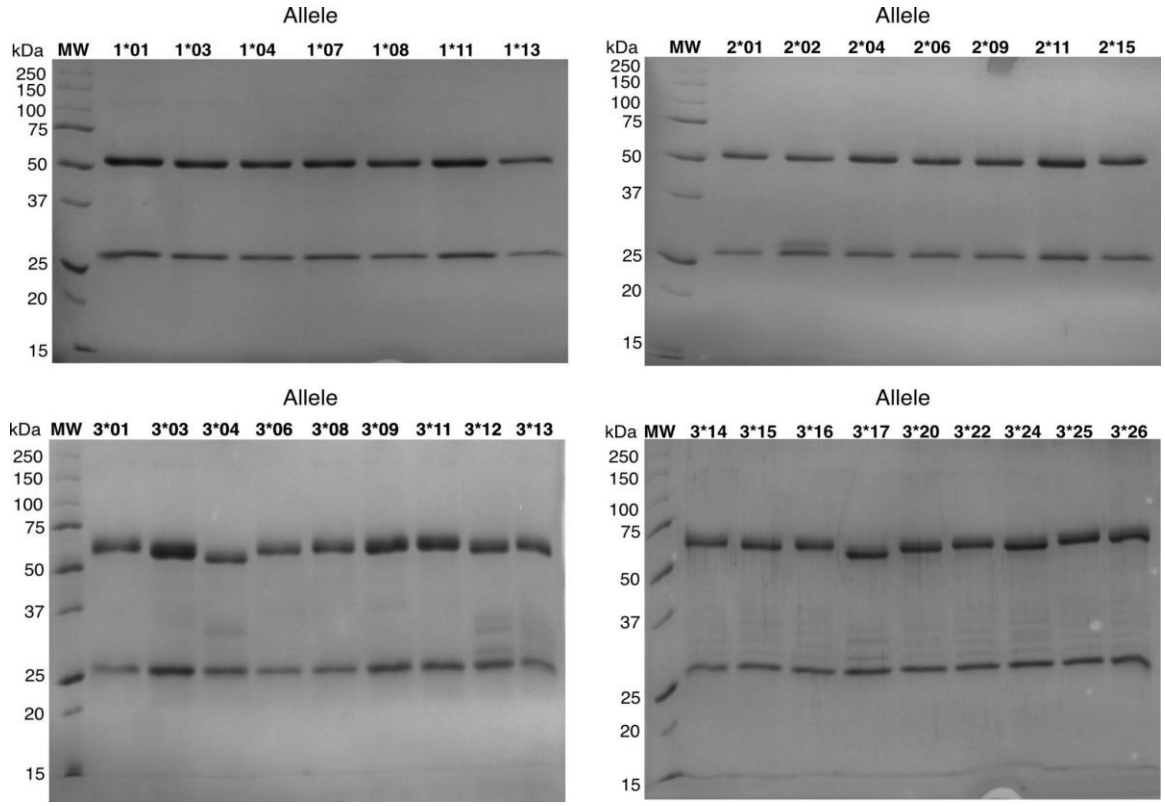

Figure A-1. SDS-PAGE gels showing >95% purity of antibody samples following expression and purification. The gels were prepared with 12% cross-linked acrylamide and run under reducing conditions. Expected band size for antibody heavy chain is 50-65 kDa depending on the variant and 25 kDa for the light chain.

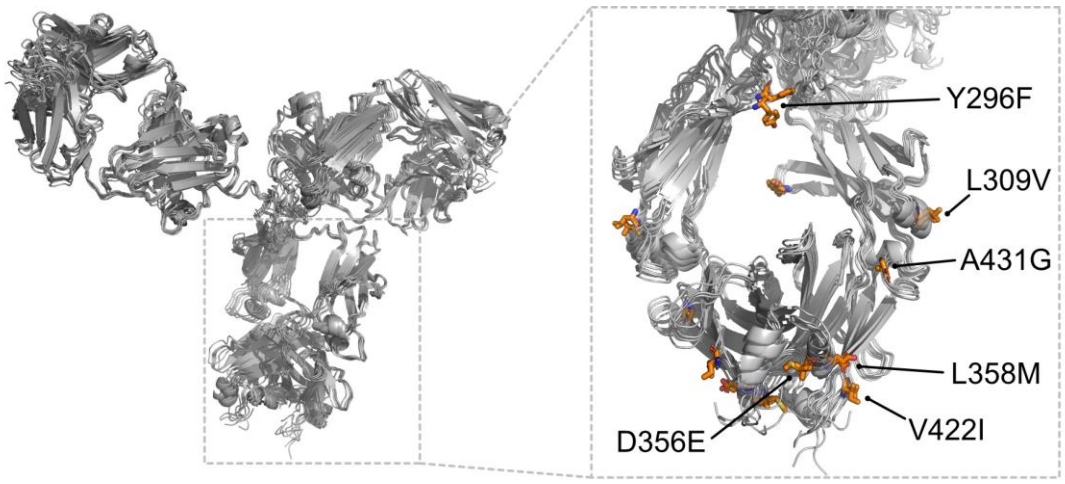

Figure A-2. Structural homology models of IgG1 produced using Rosetta software. Amino acid sequences were threaded onto PDB structure 1hzh and alignment was analysed in PyMOL. Aside from differences in the rotation of side chains, there are few differences in the structure of the antibody backbone.

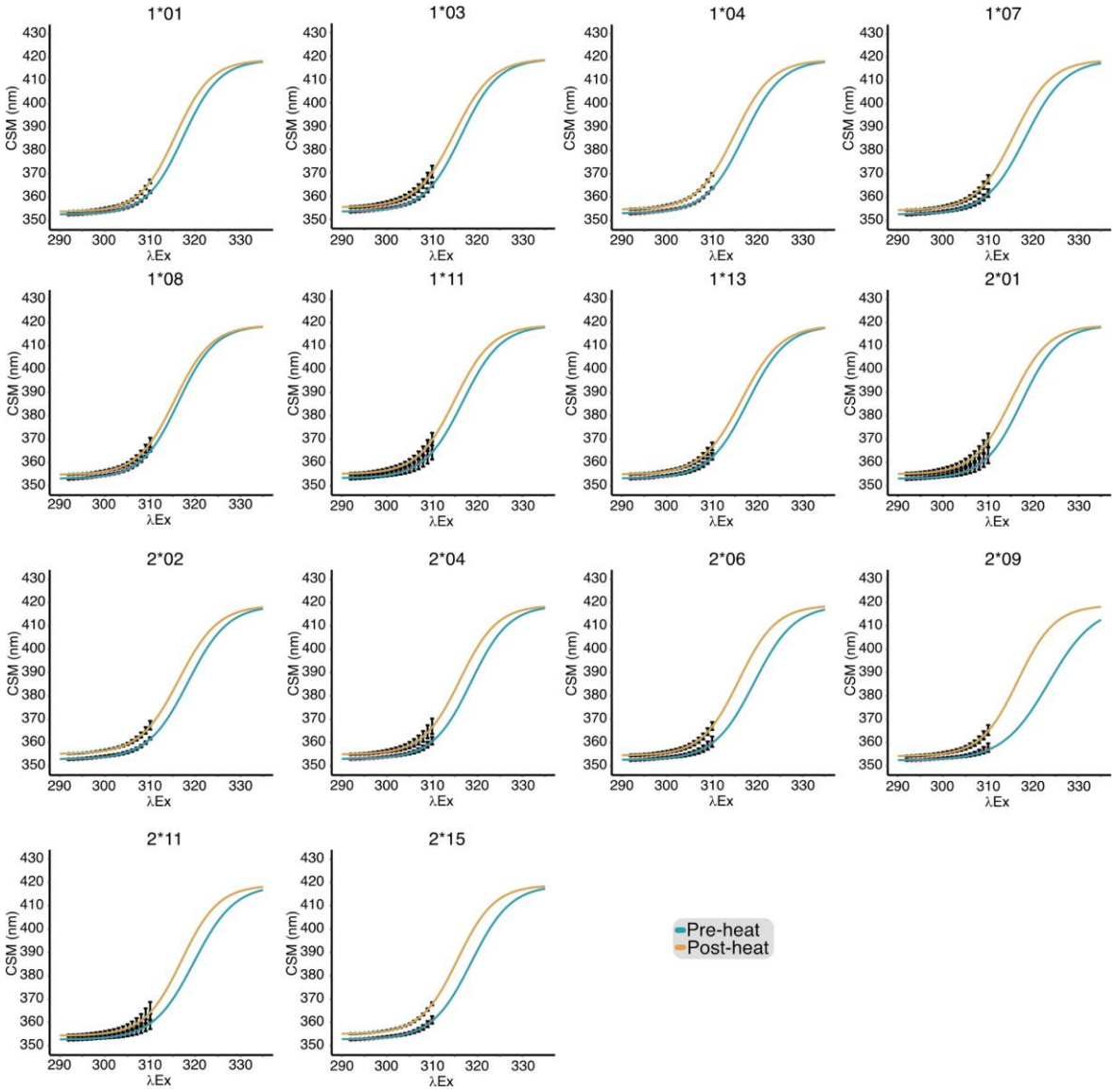

Figure A-3. CSM data for each antibody variant before (pre-heat) and after (post-heat) heating. Data was collected in triplicate. The average CSM values are plotted with error bars showing the standard deviation. The solid lines are the fits of Equation 2 to the CSM data.

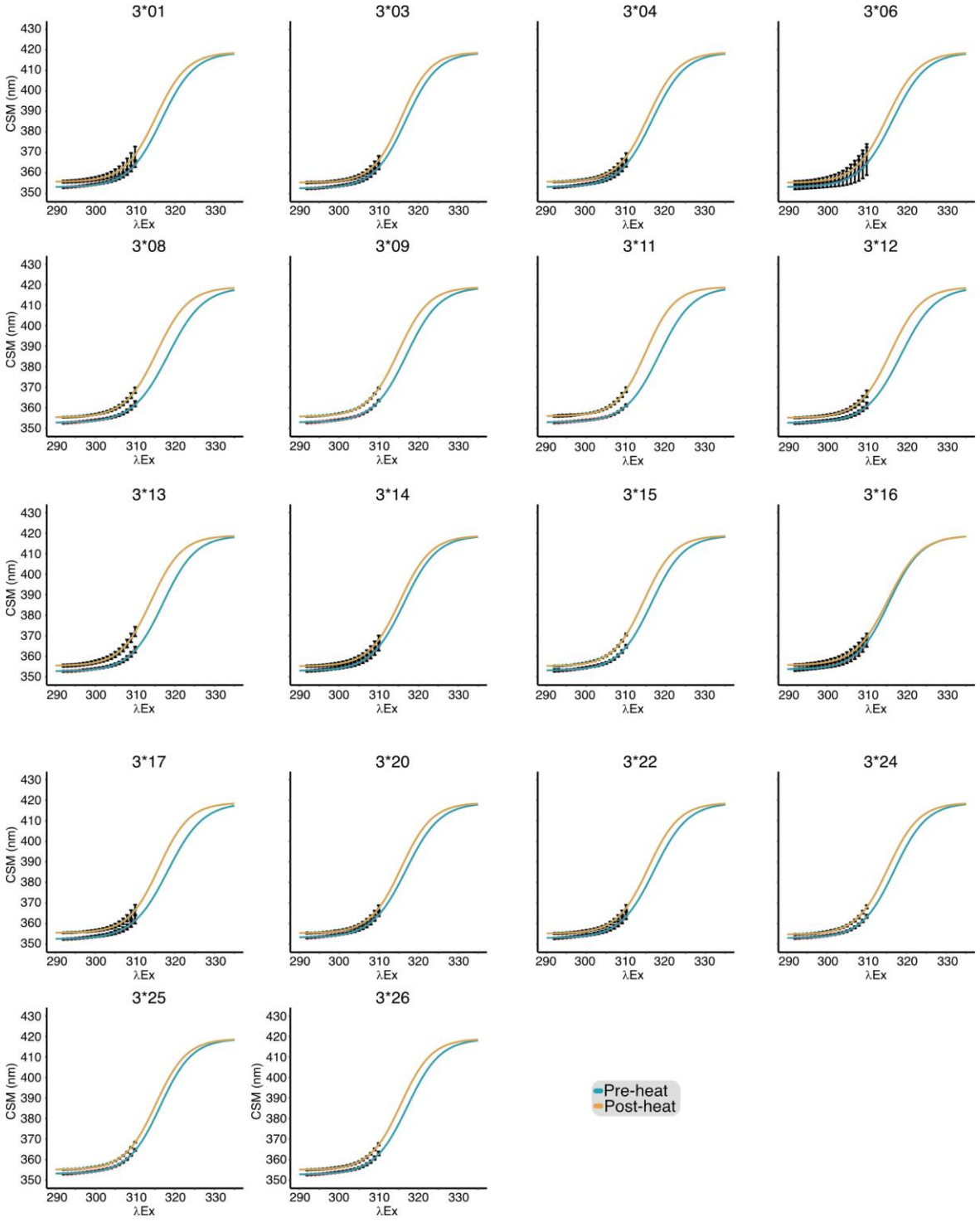

Figure A-3. (continued) CSM data for each antibody variant before (pre-heat) and after (post-heat) heating. Data was collected in triplicate. The average CSM values are plotted with error bars showing the standard deviation. The solid lines are the fits of Equation 2 to the CSM data.

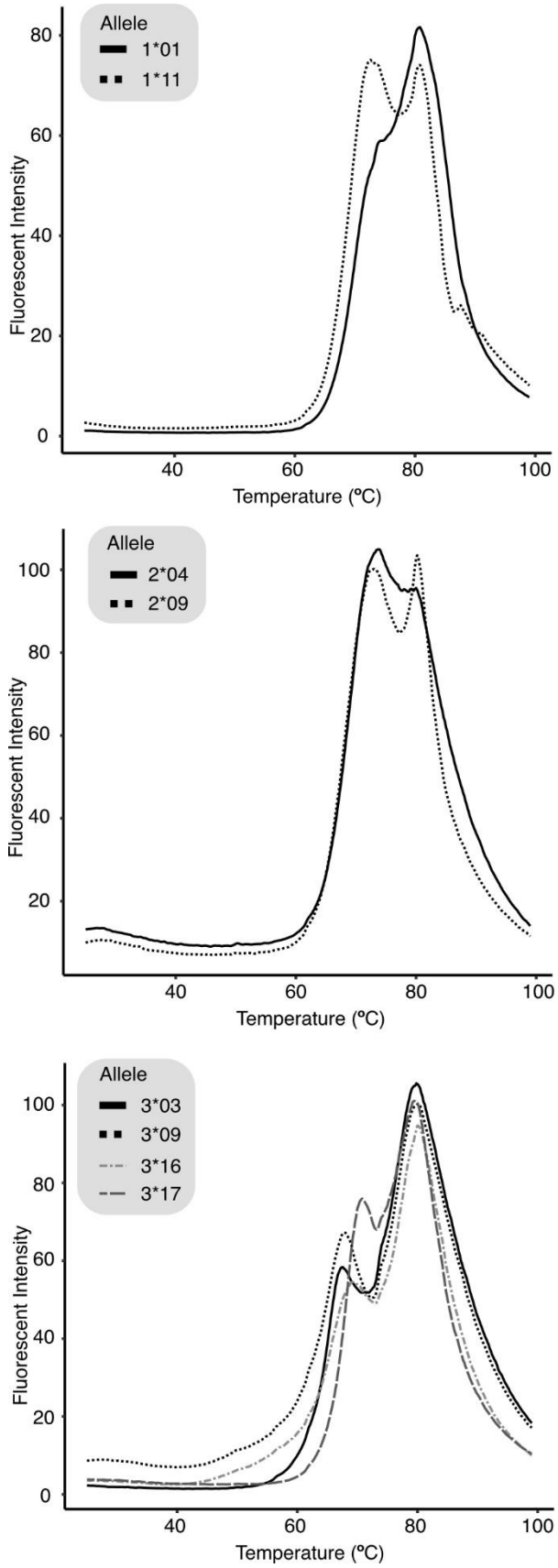

Figure A-4. Thermal unfolding (melt) curves measured by differential scanning fluorimetry using SYPRO orange dye.

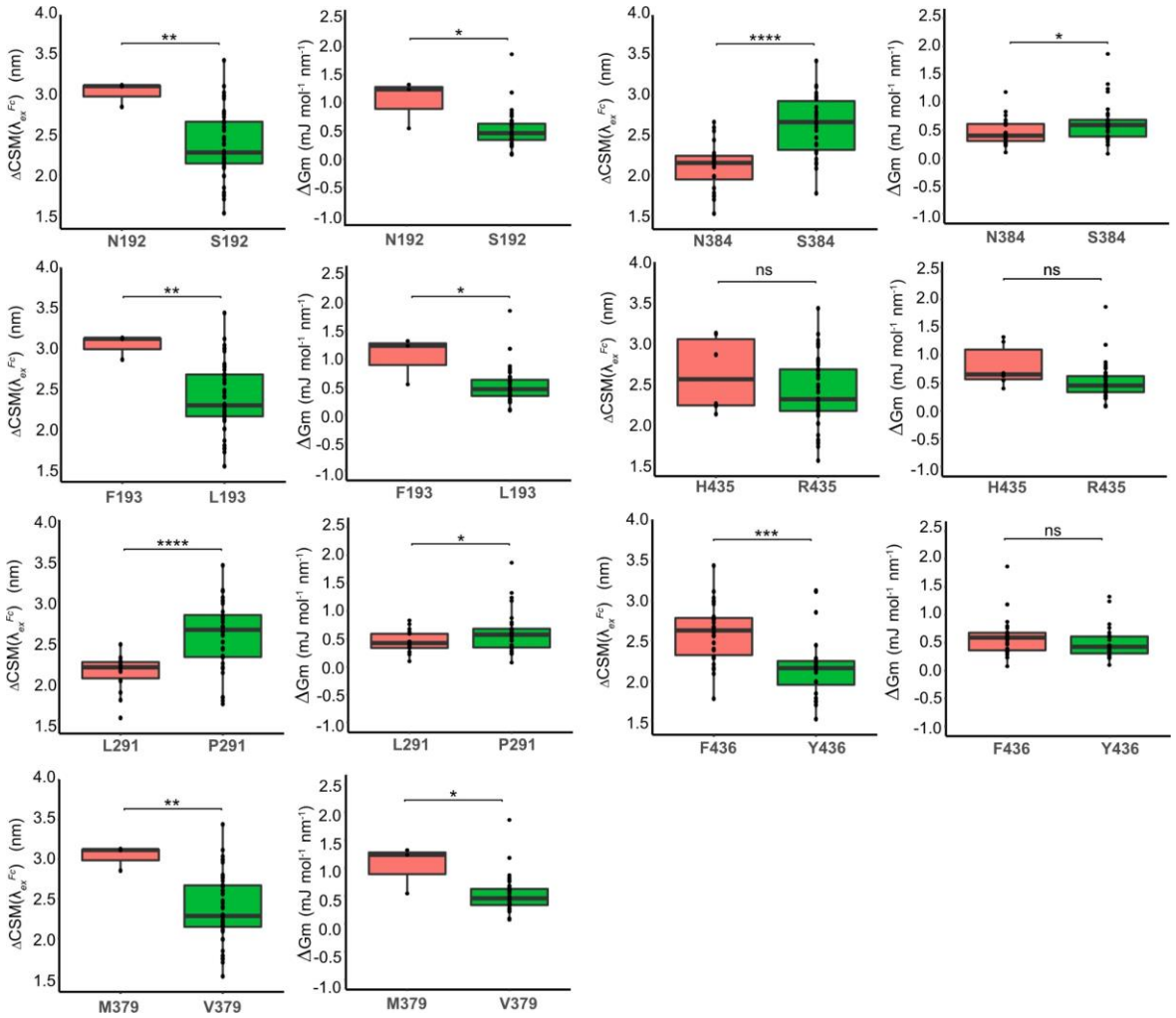

Figure A-5. Allelic mutations show trends in REES stability measurements. Boxplots showing the magnitude of change in $\boldsymbol{CSM}(\boldsymbol{\lambda}_{\boldsymbol{Ex}}^{\boldsymbol{Fc}})$ and Δ*Gm* for several amino acid polymorphisms. Data is of IgG3 alleles only. Data for polymorphisms at position 435 is included, despite no statistical significance, to complement the analysis of collective polymorphisms at 435 and 436 together. Statistical significance was tested by one-way ANOVA with Tukey PostHoc multiple comparison testing. * $p < 0.05$, ** $p < 0.01$, *** $p < 0.001$, **** $p < 0.0001$.

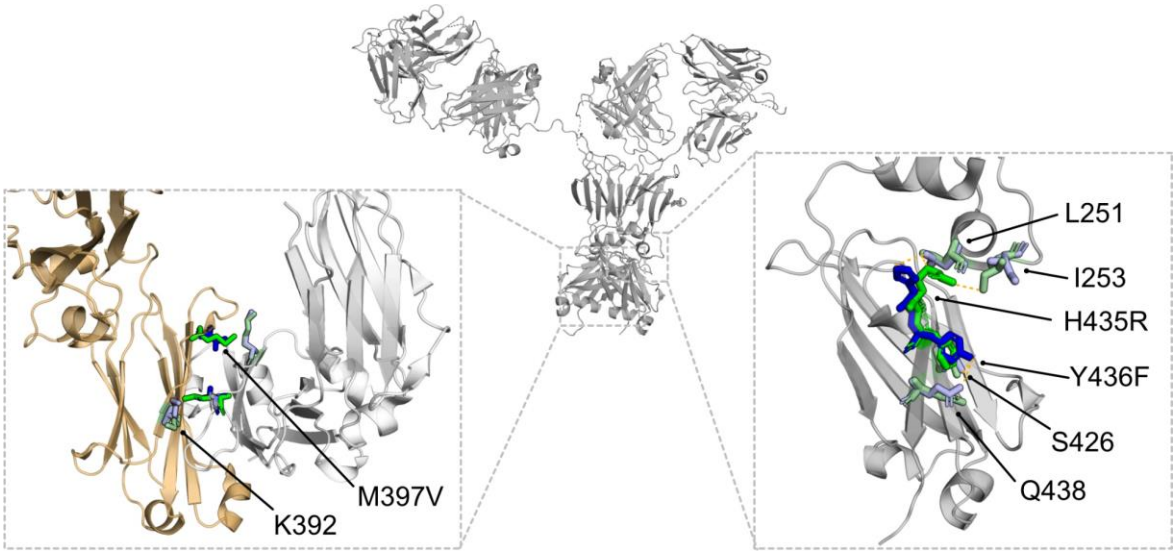

Figure A-6. Structural alignment of amino acid mutations with significant differences in stability. Left panel: Met-397 (green) vs Val-397 (blue) at the interface of the CH3 domains. Lys-392 is also shown as this is suggested to have a role in stability in combination with 397. One half of the CH3 domain dimer is coloured gold. Right panel: His-435 (blue) vs Arg-435 (green) and Tyr-436 (blue) vs Phe-436 (green). The interactions of key residues and surrounding side chains are indicated by the yellow dotted lines.

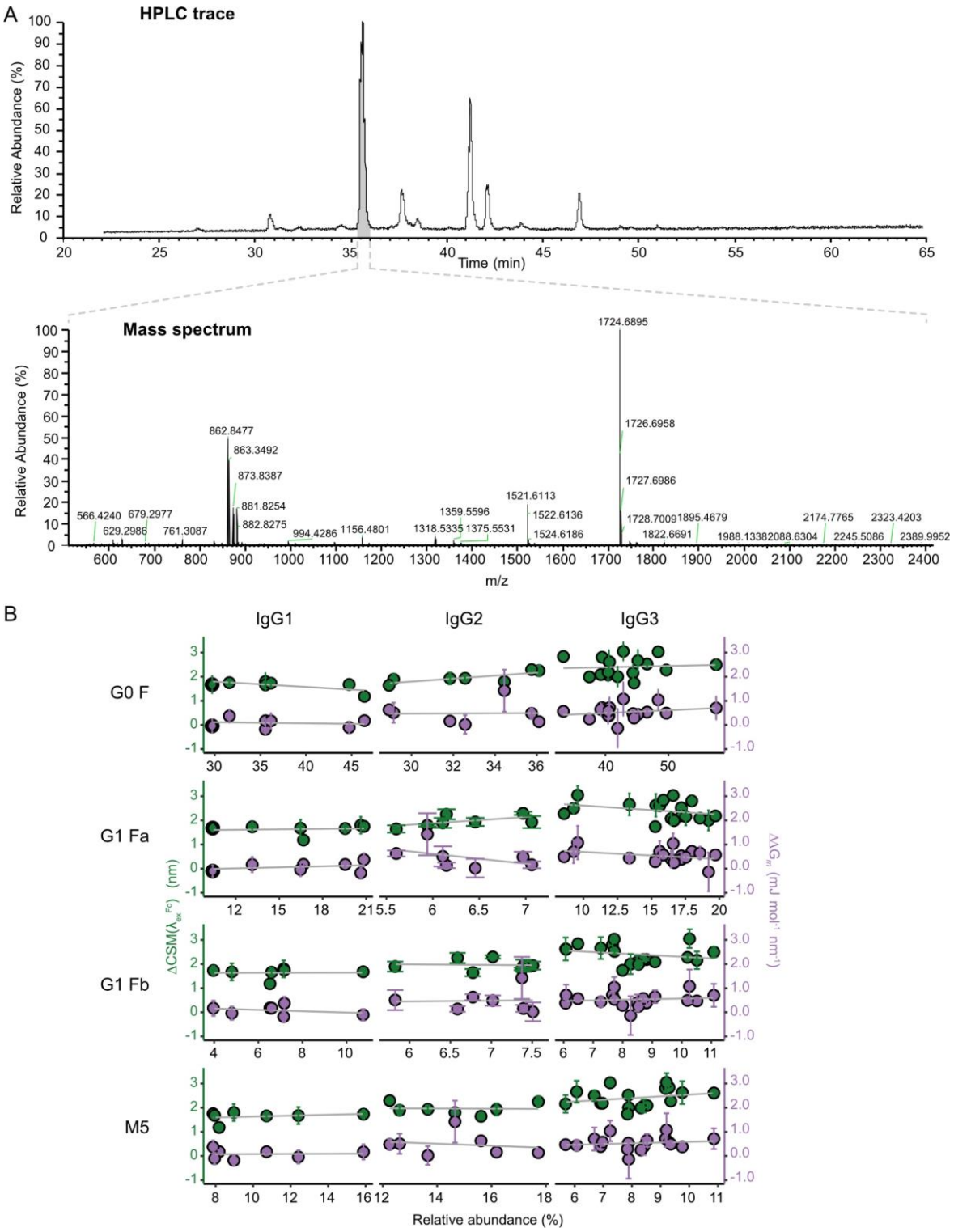

Figure A-7. Effects of glycans on stability. (A) High-performance liquid chromatography chromatogram of free glycans released from antibody IgG1*07 and labelled with InstantPC dye. Example of mass spectrum for elution peak at approximately 35 min showing mass-to-charge ratios of glycoform, G0 F. (B) Correlation analysis of the abundance percentage of the four most abundant glycans with the change in $\boldsymbol{CSM}(\boldsymbol{\lambda_{Ex}^{Fc}})$ (green, left y axis) and the change in ΔG*m* (purple, right y axis) per subclass. Correlation coefficients and the p-value for each correlation are given in Table S4.

Appendix B:

Supplementary Material for Chapter Four

B.1 Supplementary Tables

Table B-1. Amino acid sequences for antibody variants used in this study. VL – Variable domain light chain. VH – Variable domain heavy chain. IGKC-CL – Ig kappa constant domain light chain. IGHG – IgG constant domain heavy chain with allele identity. Adapted from Warrender, A. K., Pan, J., Pudney, C. R., Arcus, V. L., & Kelton, W. (2023). *Protein Science*, 32(3), e4589.

>Herceptin_VL	EMADIQMTQSPSSLSASVGDRVTITCRASQDVNTAVAWYQQKPGKAPKLLIYSASFLY SGVPSRFSGSRSGTDFTLTISSLQPEDFATYYCQQHYTTPPTFGQGTKVEIKR
>IGKC_CL	TAAAPSVFIFPPSDEQLKSGTASVVCLLNNFYPREAKVQWKVDNALQSGNSQESVTEQ DSKDSTYSLSSTLTLSKADYEKHKVYACEVTHQGLSSPVTKSFNRGEC
>Herceptin_VH	EMAEVQLVESGGGLVQPGGSLRLSCAASGFNIKDTYIHWVRQAPGKGLEWVARIYPT NGYTRYADSVKGRFTISADTSKNTAYLQMNSLRAEDTAVYYCSRWGGDGFYAMDY WGQGTLVTVSS
>IGHG3_01	ASTKGPSVFPLAPCSRSTSGGTAALGCLVKDYFPEPVTVSWNSGALTSGVHTFPAVLQ SSGLYSLSSVVTVPSSSLGTQTYTCNVNHKPSNTKVDKRVELKTPLGDTTHTCPRCPEP KSCDTPPPCPRCPEPKSCDTPPPCPRCPEPKSCDTPPPCPRCPAPELLGGPSVFLFPPKPK DTLMISRTPEVTCVVVDVSHEDPEVQFKWYVDGVEVHNAKTKPREEQYNSTFRVVSV LTVLHQDWLNGKEYKCKVSNKALPAPIEKTISKTKGQPREPQVYTLPPSREEMTKNQV SLTCLVKGFYPSDIAVEWESSGQPENNYNTTPPMLDSDGSFFLYSKLTVDKSRWQQGN IFSCSVMHEALHNRFTQKSLSLSPGK
>IGHG3_03	ASTKGPSVFPLAPCSRSTSGGTAALGCLVKDYFPEPVTVSWNSGALTSGVHTFPAVLQ SSGLYSLSSVVTVPSSSLGTQTYTCNVNHKPSNTKVDKRVELKTPLGDTTHTCPRCPEP KSCDTPPPCPRCPEPKSCDTPPPCPRCPAPELLGGPSVFLFPPKPKDTLMISRTPEVTCVV VDVSHEDPEVQFKWYVDGVEVHNAKTKPREEQYNSTFRVVSVLTVLHQDWLNGKE YKCKVSNKALPAPIEKTISKTKGQPREPQVYTLPPSREEMTKNQVSLTCLVKGFYPSDI AVEWESSGQPENNYNTTPPVLDSDGSFFLYSRLTVDKSRWQEGNVFSCSVMHEALHN RFTQKSLSLSPGK
>IGHG3_04	ASTKGPSVFPLAPCSRSTSGGTAALGCLVKDYFPEPVTVSWNSGALTSGVHTFPAVLQ SSGLYSLSSVVTVPSSSLGTQTYTCNVNHKPSNTKVDKRVELKTPLGDTTHTCPRCPEP KSCDTPPPCPRCPAPELLGGPSVFLFPPKPKDTLMISRTPEVTCVVVDVSHEDPEVQFK WYVDGVEVHNAKTKPREEQYNSTFRVVSVLTVLHQDWLNGKEYKCKVSNKALPAPI EKTISKTKGQPREPQVYTLPPSREEMTKNQVSLTCLVKGFYPSDIAVEWESSGQPENNY NTTPPMLDSDGSFFLYSKLTVDKSRWQQGNIFSCSVMHEALHNRFTQKSLSLSPGK
>IGHG3_06	ASTKGPSVFPLAPCSRSTSGGTAALGCLVKDYFPEPVTVSWNSGALTSGVHTFPAVLQ SSGLYSLSSVVTVPSSSLGTQTYTCNVNHKPSNTKVDKRVELKTPLGDTTHTCPRCPEP KSCDTPPPCPRCPEPKSCDTPPPCPRCPEPKSCDTPPPCPRCPAPELLGGPSVFLFPPKPK DTLMISRTPEVTCVVVDVSHEDPEVQFKWYVDGVEVHNAKTKPREEQYNSTFRVVSV LTVLHQDWLNGKEYKCKVSNKALPAPIEKTISKTKGQPREPQVYTLPPSREEMTKNQV

	SLTCLVKGFYPSDIAVEWESSGQPENNYKTTPPMLDSDGSFFLYSKLTVDKSRWQQGN IFSCSVMHEALHNRFTQKSLSLSPGK
>IGHG3_08	ASTKGPSVFPLAPCSRSTSGGTAALGCLVKDYFPEPVTVSWNSGALTSGVHTFPAVLQ SSGLYSLSSVVTVPSSSLGTQTYTCNVNHKPSNTKVDKRVELKTPLGDTTHTCPRCPEP KSCDTPPPCPRCPEPKSCDTPPPCPRCPEPKSCDTPPPCPRCPAPELLGGPSVFLFPPKPK DTLMISRTPEVTCVVVDVSHEDPEVQFKWYVDGVEVHNAKTKPREEQYNSTFRVVSV LTVLHQDWLNGKEYKCKVSNKALPAPIEKTISKTKGQPREPQVYTLPPSREEMTKNQV SLTCLVKGFYPSDIAVEWESNGQPENNYNTTPPMLDSDGSFFLYSKLTVDKSRWQQG NIFSCSVMHEALHNRFTQKSLSLSPGK
>IGHG3_09	ASTKGPSVFPLAPCSRSTSGGTAALGCLVKDYFPEPVTVSWNSGALTSGVHTFPAVLQ SSGLYSLSSVVTVPSSSLGTQTYTCNVNHKPSNTKVDKRVELKTPLGDTTHTCPRCPEP KSCDTPPPCPRCPEPKSCDTPPPCPRCPEPKSCDTPPPCPRCPAPELLGGPSVFLFPPKPK DTLMISRTPEVTCVVVDVSHEDPEVQFKWYVDGVEVHNAKTKPREEQYNSTFRVVSV LTVVHQDWLNGKEYKCKVSNKALPAPIEKTISKTKGQPREPQVYTLPPSREEMTKNQ VSLTCLVKGFYPSDIAVEWESSGQPENNYNTTPPMLDSDGSFFLYSKLTVDKSRWQQG NIFSCSVMHEALHNRFTQKSLSLSPGK
>IGHG3_11	ASTKGPSVFPLAPCSRSTSGGTAALGCLVKDYFPEPVTVSWNSGALTSGVHTFPAVLQ SSGLYSLSSVVTVPSSSLGTQTYTCNVNHKPSNTKVDKRVELKTPLGDTTHTCPRCPEP KSCDTPPPCPRCPEPKSCDTPPPCPRCPEPKSCDTPPPCPRCPAPELLGGPSVFLFPPKPK DTLMISRTPEVTCVVVDVSHEDPEVQFKWYVDGVEVHNAKTKPREEQFNSTFRVVSV LTVLHQDWLNGKEYKCKVSNKALPAPIEKTISKTKGQPREPQVYTLPPSREEMTKNQV SLTCLVKGFYPSDIAVEWESSGQPENNYNTTPPMLDSDGSFFLYSKLTVDKSRWQQGN IFSCSVMHEALHNRFTQKSLSLSPGK
>IGHG3_12	ASTKGPSVFPLAPCSRSTSGGTAALGCLVKDYFPEPVTVSWNSGALTSGVHTFPAVLQ SSGLYSLSSVVTVPSSSLGTQTYTCNVNHKPSNTKVDKRVELKTPLGDTTHTCPRCPEP KSCDTPPPCPRCPEPKSCDTPPPCPRCPAPELLGGPSVFLFPPKPKDTLMISRTPEVTCVV VDVSHEDPEVQFKWYVDGVEVHNAKTKPREEQFNSTFRVVSVLTVLHQDWLNGKEY KCKVSNKALPAPIEKTISKTKGQPREPQVYTLPPSREEMTKNQVSLTCLVKGFYPSDIA VEWESSGQPENNYNTTPPMLDSDGSFFLYSKLTVDKSRWQQGNIFSCSVMHEALHNR FTQKSLSLSPGK
>IGHG3_13	ASTKGPSVFPLAPCSRSTSGGTAALGCLVKDYFPEPVTVSWNSGALTSGVHTFPAVLQ SSGLYSLSSVVTVPSSSLGTQTYTCNVNHKPSNTKVDKRVELKTPLGDTTHTCPRCPEP KSCDTPPPCPRCPEPKSCDTPPPCPRCPEPKSCDTPPPCPRCPAPELLGGPSVFLFPPKPK DTLMISRTPEVTCVVVDVSHEDPEVQFKWYVDGVEVHNAKTKPREEQYNSTFRVVSV LTVLHQDWLNGKEYKCKVSNKALPAPIEKTISKTKGQPREPQVYTLPPSREEMTKNQV SLTCLVKGFYPSDIAVEWESSGQPENNYKTTPPMLDSDGSFFLYSKLTVDKSRWQEGN IFSCSVMHEALHNRFTQKSLSLSPGK
>IGHG3_14	ASTKGPSVFPLAPCSRSTSGGTAALGCLVKDYFPEPVTVSWNSGALTSGVHTFPAVLQ SSGLYSLSSVVTVPSSSLGTQTYTCNVNHKPSNTKVDKRVELKTPLGDTTHTCPRCPEP KSCDTPPPCPRCPEPKSCDTPPPCPRCPEPKSCDTPPPCPRCPAPELLGGPSVFLFPPKPK DTLMISRTPEVTCVVVDVSHEDPEVQFKWYVDGVEVHNAKTKLREEQYNSTFRVVSV LTVLHQDWLNGKEYKCKVSNKALPAPIEKTISKTKGQPREPQVYTLPPSREEMTKNQV SLTCLVKGFYPSDIAVEWESNGQPENNYNTTPPMLDSDGSFFLYSKLTVDKSRWQQG NIFSCSVMHEALHNRYTQKSLSLSPGK
>IGHG3_15	ASTKGPSVFPLAPCSRSTSGGTAALGCLVKDYFPEPVTVSWNSGALTSGVHTFPAVLQ SSGLYSLSSVVTVPSSSLGTQTYTCNVNHKPSNTKVDKRVELKTPLGDTTHTCPRCPEP

	KSCDTPPPCPRCPEPKSCDTPPPCPRCPEPKSCDTPPPCPRCPAPELLGGPSVFLFPPKPK DTLMISRTPEVTCVVVDVSHEDPEVQFKWYVDGVEVHNAKTKLREEQYNSTFRVVSV LTVLHQDWLNGKEYKCKVSNKALPAPIEKTISKTKGQPREPQVYTLPPSREEMTKNQV SLTCLVKGFYPSDIAVEWESNGQPENNYKTTPPMLDSDGSFFLYSKLTVDKSRWQQG NIFSCSVMHEALHNRYTQKSLSLSPGK
>IGHG3_16	ASTKGPSVFPLAPCSRSTSGGTAALGCLVKDYFPEPVTVSWNSGALTSGVHTFPAVLQ SSGLYSLSSVVTVPSSSLGTQTYTCNVNHKPSNTKVDKRVELKTPLGDTTHTCPRCPEP KSCDTPPPCPRCPEPKSCDTPPPCPRCPEPKSCDTPPPCPRCPAPELLGGPSVFLFPPKPK DTLMISRTPEVTCVVVDVSHEDPEVQFKWYVDGVEVHNAKTKLREEQYNSTFRVVSV LTVLHQDWLNGKEYKCKVSNKALPAPIEKTISKAKGQPREPQVYTLPPSREEMTKNQ VSLTCLVKGFYPSDIAVEWESNGQPENNYNTTPPMLDSDGSFFLYSKLTVDKSRWQQ GNIFSCSVMHEALHNRYTQKSLSLSPGK
>IGHG3_17	ASTKGPSVFPLAPCSRSTSGGTAALGCLVKDYFPEPVTVSWNSGALTSGVHTFPAVLQ SSGLYSLSSVVTVPSSNFGTQTYTCNVNHKPSNTKVDKRVELKTPLGDTTHTCPRCPEP KSCDTPPPCPRCPEPKSCDTPPPCPRCPAPELLGGPSVFLFPPKPKDTLMISRTPEVTCVV VDVSHEDPEVQFKWYVDGVEVHNAKTKPREEQYNSTFRVVSVLTVLHQDWLNGKE YKCKVSNKALPAPIEKTISKTKGQPREPQVYTLPPSREEMTKNQVSLTCLVKGFYPSDI AMEWESSGQPENNYKTTPPVLDSDGSFFLYSKLTVDKSRWQQGNIFSCSVMHEALHN HYTQKSLSLSPGK
>IGHG3_18	ASTKGPSVFPLAPCSRSTSGGTAALGCLVKDYFPEPVTVSWNSGALTSGVHTFPAVLQ YSGLYSLSSVVTVPSSSLGTQTYTCNVNHKPSNTKVDKRVELKTPLGDTTHTCPRCPE PKSCDTPPPCPRCPEPKSCDTPPPCPRCPAPELLGGPSVFLFPPKPKDTLMISRTPEVTCV VVDVSHEDPEVQFKWYVDGVEVHNAKTKPWEEQYNSTFRVVSVLTVLHQDWLNGK EYKCKVSNKALPAPIEKTISKTKGQPREPQVYTLPPSREEMTKNQVSLTCLVKGFYPSD IAMEWESSGQPENNYKTTPPVLDSDGSFFLYSKLTVDKSRWQQGNIFSCSVMHEALH NHYTQKSLSLSPGK
>IGHG3_19	ASTKGPSVFPLAPCSRSTSGGTAALGCLVKDYFPEPVTVSWNSGALTSGVHTFPAVLQ SSGLYSLSSVVTVPSSSLGTQTYTCNVNHKPSNTKVDKRVELKTPLGDTTHTCPRCPEP KSCDTPPPCPRCPEPKSCDTPPPCPRCPAPELLGGPSVFLFPPKPKDTLMISRTPEVTCVV VDVSHEDPEVQFKWYVDGVEVHNAKTKPWEEQYNSTFRVVSVLTVLHQDWLNGKE YKCKVSNKALPAPIEKTISKTKGQPREPQVYTLPPSREEMTKNQVSLTCLVKGFYPSDI AMEWESSGQPENNYKTTPPVLDSDGSFFLYSKLTVDKSRWQQGNIFSCSVMHEALHN HYTQKSLSLSPGK
>IGHG3_20	ASTKGPSVFPLAPCSRSTSGGTAALGCLVKDYFPEPVTVSWNSGALTSGVHTFPAVLQ SSGLYSLSSVVTVPSSSLGTQTYTCNVNHKPSNTKVDKRVELKTPLGDTTHTCPRCPEP KSCDTPPPCPRCPEPKSCDTPPPCPRCPEPKSCDTPPPCPRCPAPELLGGPSVFLFPPKPK DTLMISRTPEVTCVVVDVSHEDPEVQFKWYVDGVEVHNAKTKLREEQYNSTFRVVSV LTVLHQDWLNGKEYKCKVSNKALPAPIEKTISKTKGQPREPQVYTLPPSREEMTKNQV SLTCLVKGFYPSDIAVEWESNGQRENNYNTTPPMLDSDGSFFLYSKLTVDKSRWQQG NIFSCSVMHEALHNRYTQKSLSLSPGK
>IGHG3_22	ASTKGPSVFPLAPCSRSTSGGTAALGCLVKDYFPEPVTVSWNSGALTSGVHTFPAVLQ SSGLYSLSSVVTVPSSSLGTQTYTCNVNHKPSNTKVDKRVELKTPLGDTTHTCPRCPEP KSCDTPPPCPRCPEPKSCDTPPPCPRCPEPKSCDTPPPCPRCPAPELLGGPSVFLFPPKPK DTLMISRTPEVTCVVVDVSHEDPEVQFKWYVDGVEVHNAKTKLREEQYNSTFRVVSV LTVLHQDWLNGKEYKCKVSNKALPAPIEKTISKTKGQPREPQVYTLPPSREEMTKNQV SLTCLVKGFYPSDIAVEWESNGQPENNYNTTPPMLDSDGSFFLYSKLTVDKSRWQQG NIFSCSVMHEALHNHYTQKSLSLSPGK

>IGHG3_23	ASTKGPSVFPLAPCSRSTSGGTAALGCLVKDYFPEPVTVSWNSGALTSGVHTFPAVLQ SSGLYSLSSVVTVPSSSLGTQTYTCNVNHKPSNTKVDKRVELKTPLGDTTHTCPRCPEP KSCDTPPPCPRCPEPKSCDTPPPCPRCPAPELLGGPSVFLFPPKPKDTLMISRTPEVTCVV VDVSHEDPEVQFKWYVDGVEVHNAKTKPWEEQYNSTFRVVSVLTVLHQDWLNGKE YKCKVSNKALPAPIEKTISKTKGQPREPQVYTLPPSREEMTKNQVSLTCLVKGFYPSDI AVEWESSGQPENNYKTTPPVLDSDGSFFLYSKLTVDKSRWQQGNIFSCSVMHEALHN HYTQKSLSLSPGK
>IGHG3_24	ASTKGPSVFPLAPCSRSTSGGTAALGCLVKDYFPEPVTVSWNSGALTSGVHTFPAVLQ SSGLYSLSSVVTVPSSSLGTQTYTCNVNHKPSNTKVDKRVELKTPLGDTTHTCPRCPEP KSCDTPPPCPRCPEPKSCDTPPPCPRCPEPKSCDTPPPCPRCPAPELLGGPSVFLFPPKPK DTLMISRTPEVTCVVVDVSHEDPEVQFKWYVDGVEVHNAKTKPREEQYNSTFRVVSV LTVLHQDWLNGKEYKCKVSNKALPAPIEKTISKTKGQPREPQVYTLPPSREEMTKNQV SLTCLVKGFYPSDIAVEWESNGQPENNYKTTPPMLDSDGSFFLYSKLTVDKSRWQQG NIFSCSVMHEALHNRYTQKSLSLSPGK
>IGHG3_25	ASTKGPSVFPLAPCSRSTSGGTAALGCLVKDYFPEPVTVSWNSGALTSGVHTFPAVLQ SSGLYSLSSVVTVPSSSLGTQTYTCNVNHKPSNTKVDKRVELKTPLGDTTHTCPRCPEP KSCDTPPPCPRCPEPKSCDTPPPCPRCPEPKSCDTPPPCPRCPAPELLGGPSVFLFPPKPK DTLMISRTPEVTCVVVDVSHEDPEVKFKWYVDGVEVHNAKTKLREEQYNSTFRVVSV LTVLHQDWLNGKEYKCKVSNKALPAPIEKTISKTKGQPREPQVYTLPPSREEMTKNQV SLTCLVKGFYPSDIAVEWESNGQPENNYNTTPPMLDSDGSFFLYSKLTVDKSRWQQG NIFSCSVMHEALHNRYTQKSLSLSPGK
>IGHG3_26	ASTKGPSVFPLAPCSRSTSGGTAALGCLVKDYFPEPVTVSWNSGALTSGVHTFPAVLQ SSGLYSLSSVVTVPSSSLGTQTYTCNVNHKPSNTKVDKRVELKTPLGDTTHTCPRCPEP KSCDTPPPCPRCPEPKSCDTPPPCPRCPEPKSCDTPPPCPRCPAPELLGGPSVFLFPPKPK DTLMISRTPEVTCVVVDVSHEDPEVQFKWYVDGVEVHNAKTKPREEQFNSTFRVVSV LTVLHQDWLNGKEYKCKVSNKGLPAPIEKTISKTKGQPREPQVYTLPPSREEMTKNQV SLTCLVKGFYPSDIAVEWESSGQPENNYNTTPPMLDSDGSFFLYSKLTVDKSRWQQGN IFSCSVMHEALHNRFTQKSLSLSPGK

Table B-2. Relative percentage of solvent accessible surface area of each tryptophan (Trp) in each IgG3 variant. The allele number is listed across the top and grouped based on Trp content (IgG3-Arg292 and IgG3-Trp292). Values given are percentages calculated using PyMOL, where 0% is no solvent exposure and 100% is completely solvent exposed. For IgG3-Arg292 variants, no Trp is present at position 292.

Domain	Trp Sequence Position (Eu #)	IgG3-Arg292										
		3*01	**3*03**	**3*04**	**3*06**	**3*08**	**3*09**	**3*11**	**3*12**	**3*13**	**3*14**	**3*15**
anti-HER2 LC (A)	38	0	1	0	0	0	0	0	0	0	0	0
IGK LC (A)	41	2	1	1	1	4	1	1	2	2	1	0
anti-HER2 LC (B)	38	0	0	0	0	0	0	0	0	0	0	0
IGK LC (B)	41	1	2	2	1	4	2	3	1	2	1	4
anti-HER2 HC (A)	39	0	0	0	0	0	0	0	0	0	0	0
	50	5	8	3	4	3	8	10	6	6	8	11
	102	1	2	6	7	17	24	9	12	22	26	29
	113	7	2	8	6	12	9	6	9	12	12	4
IGHG HC (A)	158	0	0	0	0	0	0	0	0	0	0	0
	277	1	1	1	1	1	1	1	1	1	1	1
	292	-	-	-	-	-	-	-	-	-	-	-
	313	3	4	3	2	4	3	3	3	3	4	3
	381	0	0	0	0	1	0	1	0	0	0	0
	417	0	1	5	0	1	3	1	0	1	1	1
anti-HER2 HC (B)	39	0	0	0	0	1	0	0	0	1	0	0
	50	3	4	6	5	5	10	3	7	5	8	7
	102	6	5	16	18	3	11	9	3	23	6	7
	113	7	7	4	4	1	5	6	8	6	2	7
IGHG HC (B)	158	0	0	0	2	0	0	1	0	0	0	1
	277	1	1	1	1	1	1	1	1	1	1	1
	292	-	-	-	-	-	-	-	-	-	-	-
	313	3	1	3	2	1	2	2	2	1	1	1
	381	0	0	0	0	0	0	0	0	0	0	0
	417	1	0	3	1	1	8	0	13	1	1	0

HC – Heavy Chain. LC – Light Chain. Each chain has two copies - (A) and (B). IGHG – IgG constant domain. IGK – Ig kappa constant domain.

Table B-2. (continued) Relative percentage of solvent accessible surface area of each tryptophan (Trp) in each IgG3 variant.

Domain	Trp Sequence Position	IgG3-Arg292							IgG3-Trp292		
		3*16	3*17	3*20	3*22	3*24	3*25	3*26	3*18	3*19	3*23
anti-HER2 LC (A)	38	0	0	0	0	0	0	0	0	0	0
IGK LC (A)	41	2	2	2	1	1	3	2	2	2	1
anti-HER2 LC (B)	38	0	0	0	0	0	0	0	0	0	0
IGK LC (B)	41	3	3	3	2	1	2	3	2	2	2
anti-HER2 HC (A)	39	0	0	0	0	0	0	0	0	0	0
	50	7	5	7	6	7	6	7	7	5	6
	102	20	10	24	7	19	9	25	22	20	15
	113	12	7	10	11	6	10	12	10	14	10
IGHG HC (A)	158	0	0	0	0	0	0	0	0	0	0
	277	1	1	1	0	1	1	1	1	1	1
	292	-	-	-	-	-	-	-	39	40	44
	313	3	4	4	3	4	3	5	4	4	5
	381	0	1	0	0	0	0	0	0	0	0
	417	15	2	1	0	0	2	1	4	1	4
anti-HER2 HC (B)	39	0	1	0	0	0	0	0	0	0	0
	50	4	8	3	7	4	5	6	5	5	8
	102	21	22	12	7	5	13	0	23	9	6
	113	4	8	1	8	8	10	7	10	9	8
IGHG HC (B)	158	1	0	1	1	0	0	0	0	0	0
	277	1	1	1	1	1	1	1	1	1	1
	292	-	-	-	-	-	-	-	62	33	53
	313	1	2	2	3	1	2	2	2	2	2
	381	0	0	0	0	0	0	0	0	0	0
	417	0	1	0	0	0	0	5	5	1	6

HC – Heavy Chain. LC – Light Chain. Each chain has two copies - (A) and (B). IGHG – IgG constant domain. IGK – Ig kappa constant domain.

B.2 Supplementary Figures

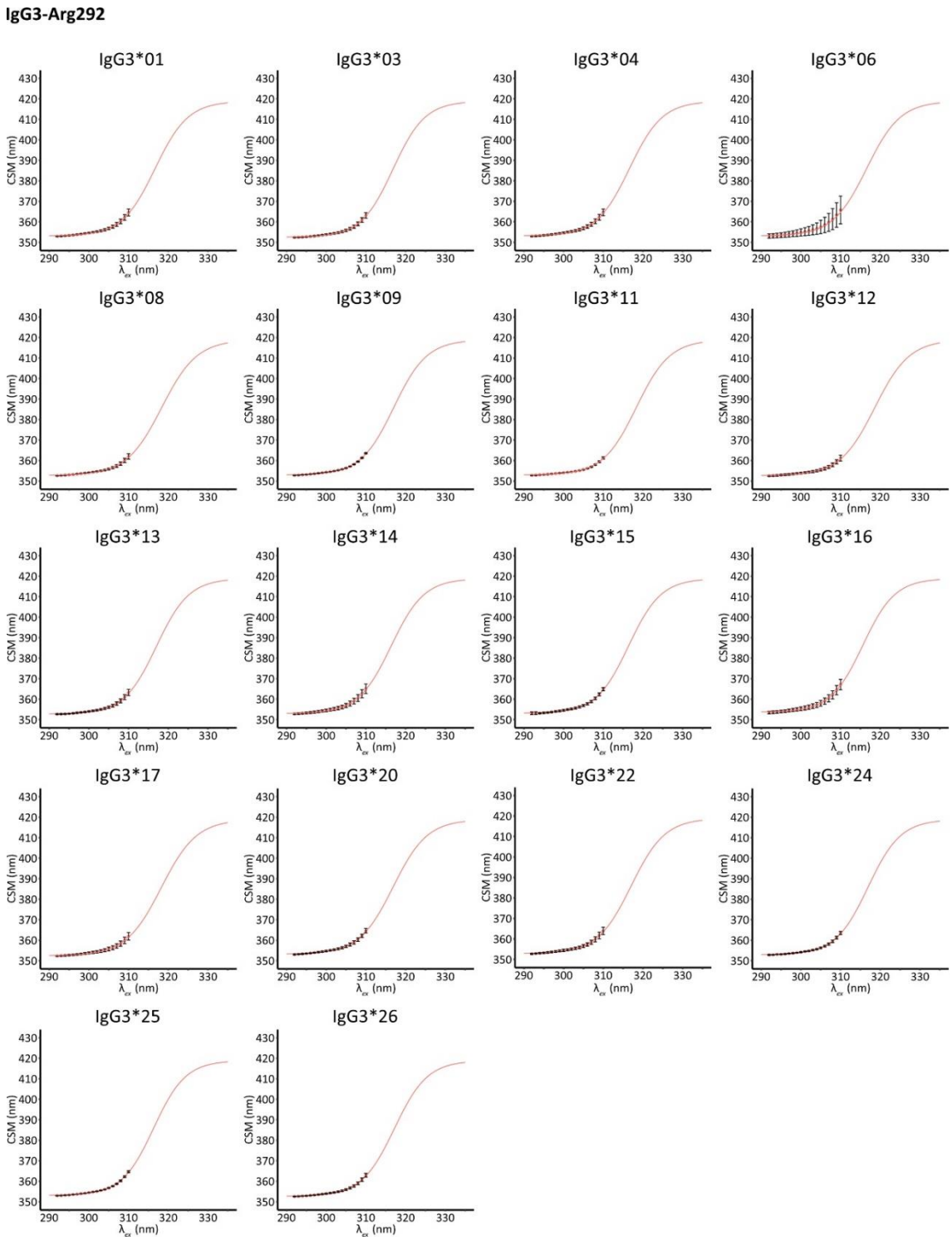

Figure B-1. Fluorescence emission centre of spectral mass (CSM) data for all the IgG3 variants included in this study. Data points show the average of triplicate measurements with error bars showing standard deviation. The solid line shows the fit of the sigmoidal REES model. Figure adapted from Warrender, A. K., Pan, J., Pudney, C. R., Arcus, V. L., & Kelton, W. (2023). *Protein Science*, 32(3), e4589.

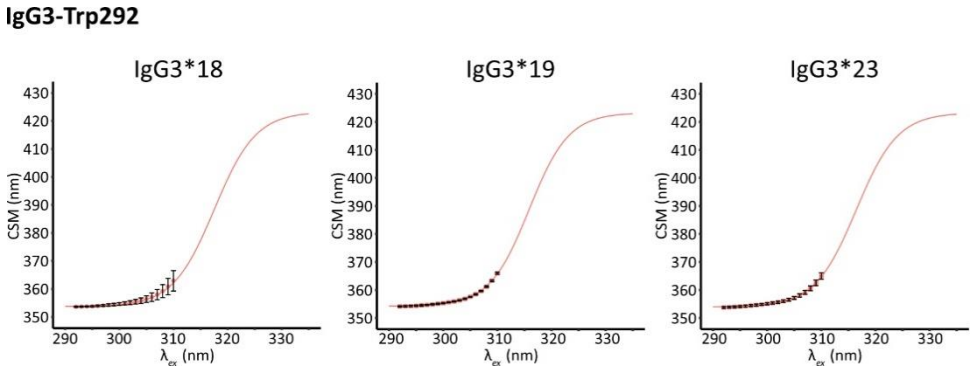

Figure B-1. (continued) Fluorescence emission centre of spectral mass (CSM) data for all the IgG3 variants included in this study. Data points show the average of triplicate measurements with error bars showing standard deviation. The solid line shows the fit of the sigmoidal REES model. Figure adapted from Warrender, A. K., Pan, J., Pudney, C. R., Arcus, V. L., & Kelton, W. (2023). *Protein Science*, 32(3), e4589.

Appendix C: Supplementary Material for Chapter Five

C.1 Supplementary Tables

Table C-1. Calculated SAXS parameters for high concentration samples

	IgG1*01	IgG2*02	IgG3*01	IgG3*03	IgG3*04	IgG3*08	IgG3*12
Concentration (mg ml^{-1})	6	6	7.5	6	7.5	7.5	7.5
Hinge length (amino acids)	15	12	62	47	32	62	47
Radius of gyration analysis							
Data point range	5 – 48	2 – 51	3 – 17	5 – 34	4 – 27	3 – 18	5 – 21
I(0) (cm-1) [from Guinier]	0.057 ± 0.0003	0.051 ± 0.0002	0.47 ± 0.0039	0.041 ± 0.0004	0.22 ± 0.0015	0.36 ± 0.0032	0.24 ± 0.0023
Rg (Å) [from Guinier]	50.41 ± 0.42	48.37 ± 0.37	77.58 ± 1.03	66.19 ± 1.09	57.45 ± 0.58	76.62 ± 1.05	66.92 ± 1.01
*q*Rg limits	0.37 – 1.28	0.29 – 1.29	0.46 – 1.22	0.49 – 1.29	0.38 – 1.3	0.45 – 1.26	0.49 – 1.24
Fidelity	1	1	1	1	1	1	1
Distance distribution analysis							
q range ($Å^{-1}$)	0.0074 – 0.2018	0.0061 – 0.2013	0.0073 – 0.2011	0.0074 – 0.203	0.0066 – 0.1983	0.0066 – 0.2032	0.0073 – 0.2004
P(r) total quality estimate	0.84	0.84	0.63	0.64	0.7965	0.58	0.71
Rg (Å) [from Guinier]	50.83	48.97	78.01	68.54	58.47	77.41	67.69
I(0) (cm^{-1}) [from Guinier]	0.057	0.051	0.461	0.042	0.219	0.358	0.235
Rg (Å) [from P(r)]	50.85 ± 0.189	48.98 ± 0.199	78.37 ± 0.5122	67.72 ± 0.6583	58.53 ± 0.3545	77.66 ± 0.4356	67.86 ± 0.5122
I(0) (cm^{-1}) [from P(r)]	0.0572 ± 0.0002	0.0512 ± 0.0002	0.4612 ± 0.0028	0.0419 ± 0.0004	0.2191 ± 0.0012	0.3579 ± 0.0023	0.2352 ± 0.0016
D_{max} (Å)	151.15	147.32	243.72	211.5	181.96	231	208.3
Points	152	155	93	131	110	94	101
Alpha	6.785	5.64	2.443	0.5396	4.301	2.996	1.829

C.2 Supplementary Figures

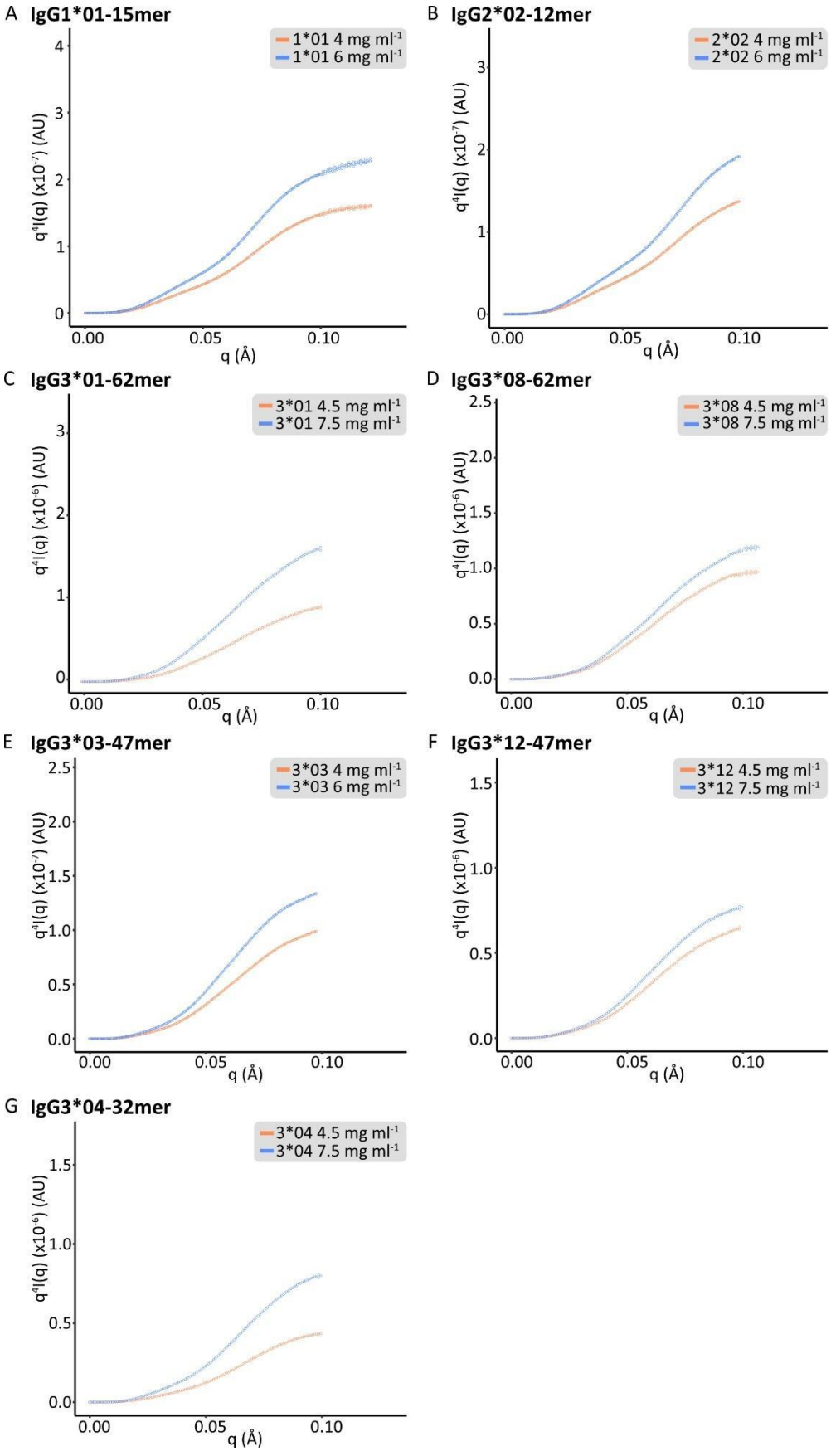

Figure C-1. Porod plot defining the *q* range used for Porod volume (V_p) determination

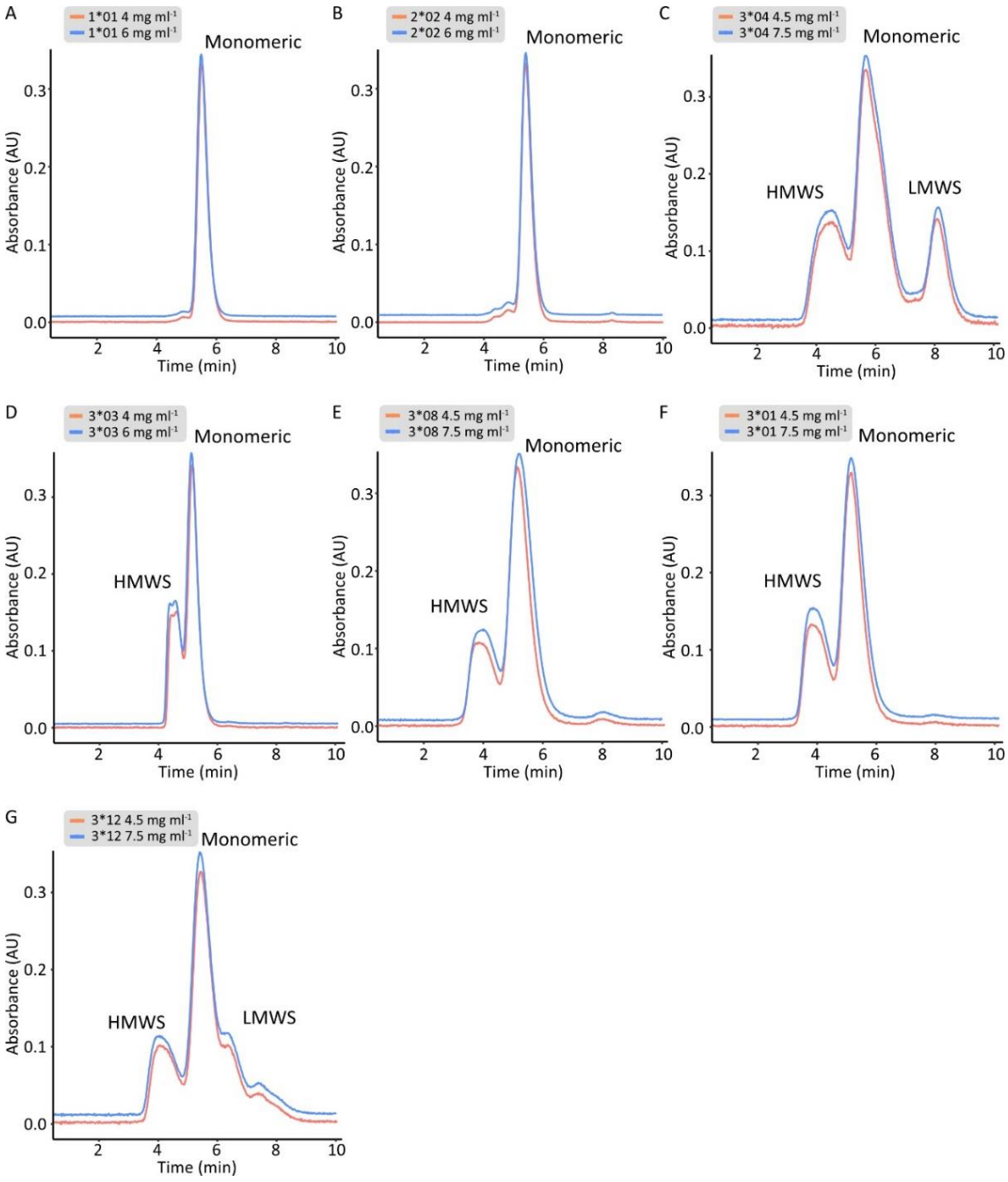

Figure C-2. Size exclusion chromatograms for each sample

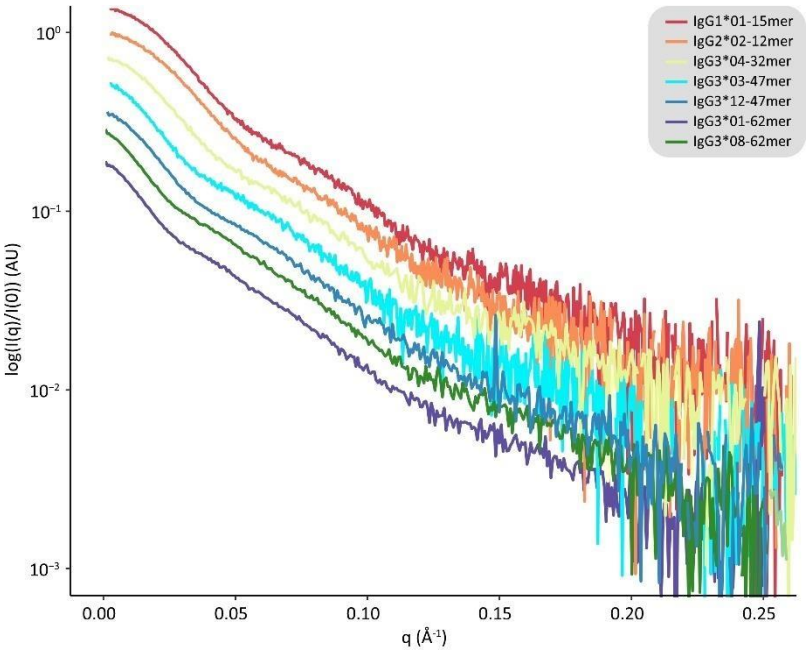

Figure C-3. Scattering profiles scaled by the relative intensity and arbitrarily separated for ease of comparison

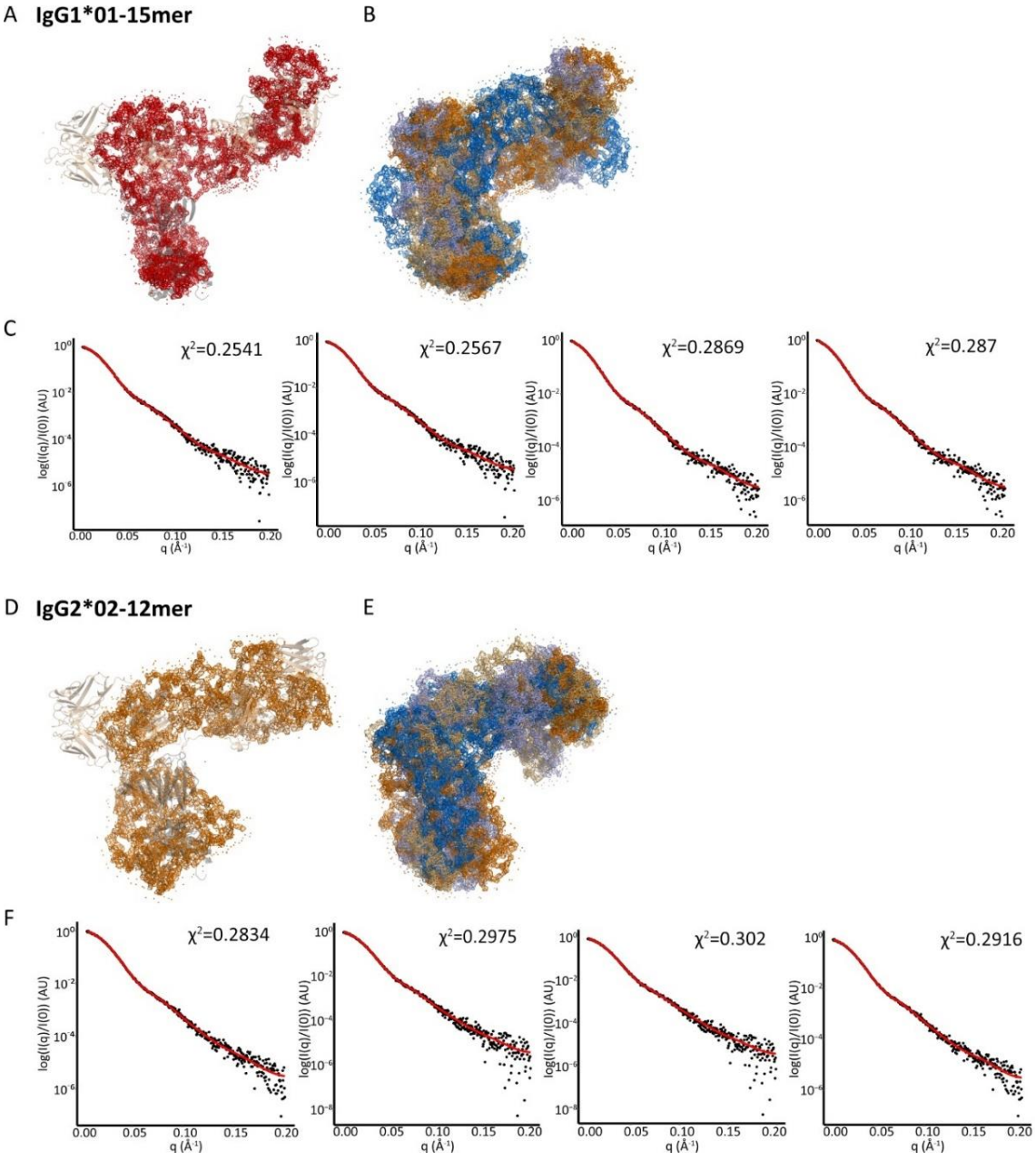

Figure C-4. *Ab initio* model analysis of IgG1*01-15mer (A-C) and IgG2*02-12mer (D-F). (A) alignment of IgG1*01-15mer with crystal structure anti-gp120 IgG1 (PDB: 1hzh). (D) alignment of IgG2*02-15mer with crystal structure of murine IgG2a (PDB: 1igt). (B, E) Superimposition of all predicted ab initio models from the SAXS data of both sample concentrations. (C, F) Scattering data of the predicted models (red line) aligned to the experimental scattering data (black dots). Chi-squared values to quantify the quality of fit.

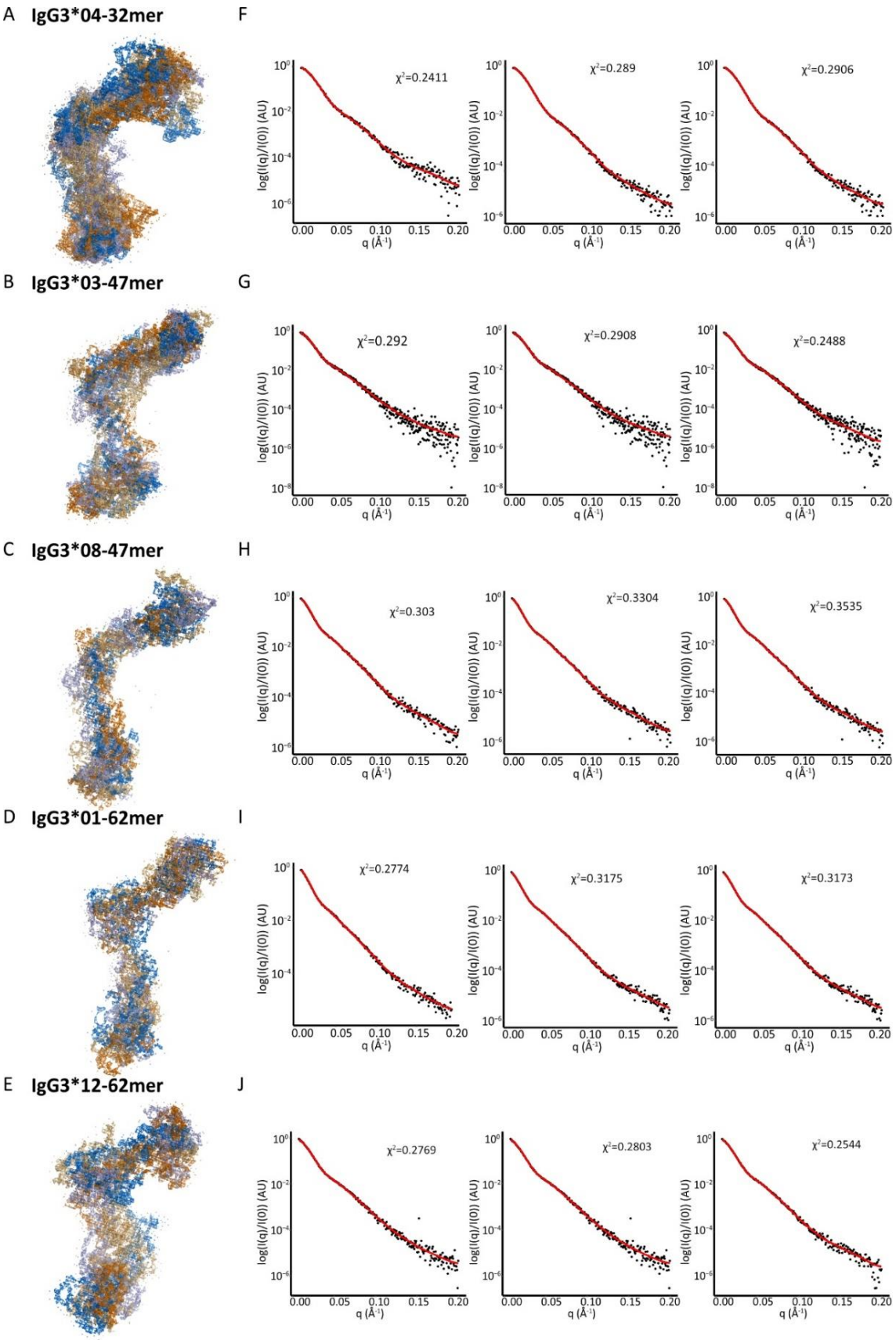

Figure C-5. *Ab initio* model analysis of IgG3 variants. (A-E) Superimposition of all predicted ab initio models from the SAXS data of both sample concentrations for each variant. (F-J) Scattering data of the predicted models (red line) aligned to the experimental scattering data (black dots). Chi-squared values to quantify the quality of fit.

Appendix D:

Supplementary Material for Chapter Six

D.1 Methods of TRIM21 expression and kinetic analyses

Full-length, human TRIM21 protein was expressed with an N-terminal His-Lipoyl tag (HLTV-hTRIM21, referred to as TRIM21). The TRIM21 expression plasmid (Clift et al., 2017) was ordered from Addgene (plasmid #104973), transformed into E. coli BL21 (DE3) cells and expressed according to the methods described previously (Clift et al., 2017). TRIM21 expression was induced with 1 mM IPTG overnight at 18°C. Cell pellets were sonicated in 50 mM Tris pH 8, 150 mM NaCl, 1 mM DTT, 5 mM imidazole pH 8, 20% BugBuster® (Novagen) and cOmplete protease inhibitor (Roche) and centrifuged at 16,000 x *g* for 1 h at 4°C. TRIM21 was purified from the clear lysate first by nickel affinity chromatography using a 5 mL Ni-NTA column and eluting with 300 mM Imidazole, followed by size-exclusion with an S200 16/60 column in 1 X PBS buffer.

Kinetic analysis was conducted on an Octet Red 96e BLI system with a Ni-NTA Biosensor (ForteBio). The Octet Kinetics Buffer (Sartorius) was used for all kinetic experiments at pH 7.4. HLTV-TRIM21 was prepared at 150 nM in 1 X Kinetics buffer and coated onto the biosensors for 1500 s. Immediately following ligand loading, TRIM21 was cross-linked onto the Biosensor surface with 0.1 M EDC and 0.025 M NHS prepared in water. The cross-linking reagents were quenched using 1 M ethanolamine, pH 8.5. The biosensors were washed and equilibrated with 1X Kinetics Buffer. Kinetic analysis was performed using a concentration series (0 – 25 nM) of IgG antibodies prepared in 1X Kinetics buffer, with each concentration measured in triplicate. Antibodies were allowed to associate for 300 s followed by 500 s of dissociation. Between replicates, the surface of the biosensors was regenerated using 10 mM Glycine pH 1.7 for 5 s, followed by 5 s of Kinetics Buffer. The surface was recharged with 10 mM NiCl2 and equilibrated to baseline with Kinetics Buffer. Kinetic data was collected and analysed using the Octet Data Analysis High Throughput software.

References

Clift, D., McEwan, W. A., Labzin, L. I., Konieczny, V., Mogessie, B., James, L. C., & Schuh, M. (2017). A Method for the Acute and Rapid Degradation of Endogenous Proteins. *Cell*, *171*(7), 1692-1706.e18. https://doi.org/10.1016/j.cell.2017.10.03

Appendix E:

Co-Authorship Forms

E.1 Co-Authorship Form for Chapter Two: Beyond Allotypes: The Influence of Allelic Diversity in Antibody Constant Domains.

THE UNIVERSITY OF WAIKATO

Co-Authorship Form

Postgraduate Studies Office
Student and Academic Services Division
Wahanga Ratonga Matauranga Akonga
The University of Waikato
Private Bag 3105
Hamilton 3240, New Zealand
Phone +64 7 838 4439
Website: http://www.waikato.ac.nz/sasd/postgraduate/

This form is to accompany the submission of any PhD that contains research reported in published or unpublished co-authored work. **Please include one copy of this form for each co-authored work.** Completed forms should be included in your appendices for all the copies of your thesis submitted for examination and library deposit (including digital deposit).

Please indicate the chapter/section/pages of this thesis that are extracted from a co-authored work and give the title and publication details or details of submission of the co-authored work.

Chapter Two | Beyond Allotypes: The Influence of Allelic Diversity in Antibody Constant Domains. | Published in *Frontiers in Immunology* (2020) Volume 11, Issue 2016 | DOI: 10.3389/fimmu.2020.02016

Nature of contribution by PhD candidate	Analysis of literature, manuscript writing and editing
Extent of contribution by PhD candidate (%)	75

CO-AUTHORS

Name	Nature of Contribution
William Kelton	Analysis of literature, manuscript writing and editing

Certification by Co-Authors

The undersigned hereby certify that:

- the above statement correctly reflects the nature and extent of the PhD candidate's contribution to this work, and the nature of the contribution of each of the co-authors; and

Name	Signature	Date
William Kelton	wjkelton	21/06/2023

July 2015

E.2 Co-Authorship Form for Chapter Three: Constant Domain Polymorphisms Influence Monoclonal Antibody Stability and Dynamics

THE UNIVERSITY OF WAIKATO
Te Whare Wānanga o Waikato

Co-Authorship Form

Postgraduate Studies Office
Student and Academic Services Division
Wahanga Ratonga Matauranga Akonga
The University of Waikato
Private Bag 3105
Hamilton 3240, New Zealand
Phone +64 7 838 4439
Website: http://www.waikato.ac.nz/sasd/postgraduate/

This form is to accompany the submission of any PhD that contains research reported in published or unpublished co-authored work. **Please include one copy of this form for each co-authored work.** Completed forms should be included in your appendices for all the copies of your thesis submitted for examination and library deposit (including digital deposit).

Please indicate the chapter/section/pages of this thesis that are extracted from a co-authored work and give the title and publication details or details of submission of the co-authored work.

Chapter Three | Constant domain polymorphisms influence monoclonal antibody stability and dynamics.
Published in *Protein Science* (2023) Volume 32, Issue 3 | DOI: 10.1002/pro.4589

Nature of contribution by PhD candidate	Experimental design, experimental processing, data analysis, manuscript writing and editting
Extent of contribution by PhD candidate (%)	85

CO-AUTHORS

Name	Nature of Contribution
Jolyn Pan	Antibody production
Christopher Pudney	Supported experimental design and data analysis, manuscript editting
Vickery Arcus	Supported experimental design and data analysis, manuscript editting
William Kelton	Experimental design, experimental processing supported data analysis, manuscript writing and editting

Certification by Co-Authors

The undersigned hereby certify that:

- the above statement correctly reflects the nature and extent of the PhD candidate's contribution to this work, and the nature of the contribution of each of the co-authors; and

Name	Signature	Date
Jolyn Pan		21/6/23
Christopher Pudney		21-06-23
Vickery Arcus	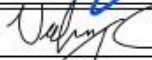	27/6/23
William Kelton	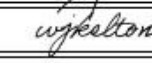	21/06/2023

July 2015

E.3 Co-Authorship Form for Chapter Four: Red Edge Excitation Shift Spectroscopy is Highly Sensitive to Tryptophan Composition

THE UNIVERSITY OF WAIKATO
Te Whare Wānanga o Waikato

Co-Authorship Form

Postgraduate Studies Office
Student and Academic Services Division
Waharanga Ratonga Matauranga Akonga
The University of Waikato
Private Bag 3105
Hamilton 3240, New Zealand
Phone +64 7 838 4439
Website: http://www.waikato.ac.nz/sasd/postgraduate/

This form is to accompany the submission of any PhD that contains research reported in published or unpublished co-authored work. **Please include one copy of this form for each co-authored work.** Completed forms should be included in your appendices for all the copies of your thesis submitted for examination and library deposit (including digital deposit).

Please indicate the chapter/section/pages of this thesis that are extracted from a co-authored work and give the title and publication details or details of submission of the co-authored work.

Chapter Four | Red Edge Excitation Shift Spectroscopy is Highly Sensitive to Tryptophan Composition. Submitted to the *Journal of the Royal Society Interface* (2023)

Nature of contribution by PhD candidate	Experimental design, experimental processing, data analysis, manuscript writing and editting
Extent of contribution by PhD candidate (%)	90

CO-AUTHORS

Name	Nature of Contribution
Jolyn Pan	Antibody production
Christopher Pudney	Supported experimental design and data analysis, manuscript editting
Vickery Arcus	Supported experimental design and data analysis, manuscript editting
William Kelton	Experimental design, supported data analysis, manuscript writing and editting

Certification by Co-Authors

The undersigned hereby certify that:

- the above statement correctly reflects the nature and extent of the PhD candidate's contribution to this work, and the nature of the contribution of each of the co-authors; and

Name	Signature	Date
Jolyn Pan	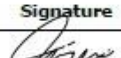	21/6/23
Christopher Pudney		21-06-23
Vickery Arcus	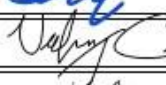	27/6/23
William Kelton	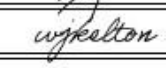	21/06/2023

July 2015

E.4 Co-Authorship Form for Chapter Five: Antibody Hinge Length Governs Conformational Flexibility of IgG3 Allelic Variants

THE UNIVERSITY OF WAIKATO
Te Whare Wānanga o Waikato

Co-Authorship Form

Postgraduate Studies Office
Student and Academic Services Division
Waharoa Ratonga Mataurauga Akonga
The University of Waikato
Private Bag 3105
Hamilton 3240, New Zealand
Phone +64 7 838 4439
Website: http://www.waikato.ac.nz/sasd/postgraduate/

This form is to accompany the submission of any PhD that contains research reported in published or unpublished co-authored work. **Please include one copy of this form for each co-authored work.** Completed forms should be included in your appendices for all the copies of your thesis submitted for examination and library deposit (including digital deposit).

Please indicate the chapter/section/pages of this thesis that are extracted from a co-authored work and give the title and publication details or details of submission of the co-authored work.

Chapter Five | Antibody Hinge Length Governs Conformational Flexibility of IgG3 Allelic Variants
To be submitted

Nature of contribution by PhD candidate	Experimental design, experimental processing, data analysis, manuscript writing and editing
Extent of contribution by PhD candidate (%)	90

CO-AUTHORS

Name	Nature of Contribution
Jolyn Pan	Antibody production, sample preparation
Ashish Sethi	Supported experimental design and data analysis
William Kelton	Experimental design, experimental processing, manuscript writing and editing

Certification by Co-Authors

The undersigned hereby certify that:
the above statement correctly reflects the nature and extent of the PhD candidate's contribution to this work, and the nature of the contribution of each of the co-authors; and

Name	Signature	Date
Jolyn Pan	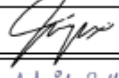	21/6/23
Ashish Sethi	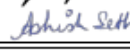	21/06/23
William Kelton		21/06/2023

July 2015